ASPECTS OF CATALYSIS IN TRIMETHYLAMINE DEHYDROGENASE: SUBSTRATE INHIBITION, H-TUNNELLING AND SUBSTRATE REDESIGN

Thesis submitted for the degree of
Doctor of Philosophy
at the University of Leicester

by

Peter Roberts BSc (Wales)
Department of Biochemistry
University of Leicester

June 2000

ProQuest LLC
789 East Eisenhower Parkway
P.O. Box 1346
Ann Arbor, MI 48106-1346

Acknowledgements

The work presented in this thesis was carried out in the laboratory of Professor N. Scrutton in the Department of Biochemistry, University of Leicester.

My family have been especially supportive, in terms of both morale and financially, throughout my education.

Thanks to Nigel for his advice throughout my research and the writing of this thesis. Big thanks to all the members of his laboratory at Leicester, past and present for either help, advice, or both and making our lab a fun place to work.

I was very lucky to have a great group of friends at Leicester. Wednesday nights will never be the same, except when we meet up again.

The BBSRC paid me and gave me some travel money.

Finally, I would like to thank Annemarie for making it worthwhile.

Abstract

Aspects of Catalysis in TMADH: Substrate Inhibition, H-Tunnelling and Substrate Redesign.

Peter Roberts

Trimethylamine dehydrogenase (TMADH) is an iron-sulphur flavoprotein that catalyses the demethylation of trimethylamine (TMA) to dimethylamine and formaldeyde. In this thesis, three aspects of TMADH enzymology have been addressed: the effect of substrate on the redox state of the enzyme, the quantum mechanical tunnelling of hydrogen during substrate C-H bond cleavage, and an attempt to improve specificity for the secondary amine DMA by rational protein engineering.

Substrate inhibition in TMADH has been studied using the native enzyme and active site mutants that show different degrees of substrate inhibition. Use of Fc^+ and a photodiode array to directly observe the redox state of the enzyme during steady-state turnover has demonstrated that TMADH participates in two different redox cycles. At low TMA concentrations, the enzyme undergoes a 0/2 cycle, in which enzyme bound flavin is reduced by a maximum of two reducing equivalents; when inhibited at high TMA concentrations the enzyme undergoes a 1/3 cycle, in which enzyme bound flavin is reduced by either one or three reducing equivalents. Increasing the concentration of the electron acceptor Fc^+ decreases the extent of inhibition. Excess substrate binding at the active site of 1-electron reduced enzyme stabilises the semiquinone form of enzyme bound 6-S-cysteinyl FMN, preventing further reduction by substrate, causing excess substrate inhibition.

C-H bond cleavage in TMADH has been investigated with regard to determining the importance of H-tunnelling mediated by protein dynamics during catalysis. The rate of flavin reduction with normal and perdeuterated TMA was measured by stopped-flow spectroscopy to produce temperature dependence data for native TMADH and two mutant enzymes, Y169F and H172Q, between pH 6.5 and 8.5. The results of this preliminary study are highly suggestive of H-tunnelling during catalysis by TMADH. The extent of protium and deuterium tunnelling increases with pH, suggesting a pH-dependent effect on reaction barrier width. The results also indicate that barrier width is increased by introducing the mutations Y169F and H172Q.

An attempt has been made to rationally engineer the substrate specificity of TMADH for DMA, following the construction of a homology model for DMADH. Building on earlier work, three new mutant variants of TMADH were generated. Of these, the TMADH Quad-mutant maintained a 10 000-fold switch in specificity for DMA over TMA, when compared to wild-type enzyme. In an attempt to engineer a H-bonding network in TMADH, additional mutations caused unforeseen changes, which meant that the new variants of TMADH had little or no bound FMN and only residual enzyme activity.

Abbreviations

In addition to the accepted abbreviations stated in *Biochemical Journal* (1986) **233**, 1-24, the following abbreviations have been adopted, in some cases without previous definition:

ADP	Adenosine diphosphate
ATP	Adenosine triphosphate
DCPIP	2, 6-dichlorophenol-indophenol
DEMA	Diethylmethylamine
DMA	Dimethylamine
DMADH	Dimethylamine dehydrogenase
DMButA	Dimethylbutylamine
DNA	Deoxyribonucleic acid
EDMA	Ethyldimethylamine
ETF	Electron transferring flavoprotein
FAD	Flavin adenine nucleotide
FBP	D-fructose, 1-6 bisphosphate
Fc^+	Ferricenium hexafluorophosphate
FMN	Flavin mononucleotide
FMN_{sq}	Semiquinone flavin mononucleotide
MalNEt	N-ethylmaleimide
PAGE	Polyacrylamide gel electrophoresis
PMS	Phenazine methosulphate
SAXS	Single angle X-ray scattering
SDS	Sodium dodecyl sulphate
TEA	Triethlamine
TEMED	N, N, N', N'-tetramethylethylenediamine
TMA	Trimethylamine
TMAC	Tetramethylammonium chloride
TMADH	Trimethylamine dehydrogenase
TTQ	Tryptophan tryptophylquinone
UV	Ultraviolet

Table of Contents

1.1 Trimethylamine Dehydrogenase

1.1.1 Overview

Trimethylamine dehydrogenase (TMADH, EC 1.5.99.7) is an iron-sulphur flavoprotein that catalyses the oxidative *N*-demethylation of trimethylamine (TMA), to yield dimethylamine (DMA) and formaldehyde (Steenkamp & Mallinson, 1976):

$$(CH_3)_3N + H_2O \rightarrow (CH_3)_2NH + HCHO + 2\ H^+ + 2\ e^-$$

TMADH is a homodimer; each subunit consists of 729 amino acids (Boyd *et al.*, 1992) and the assembled dimer has a molecular weight of about 166 kD (Kasprzak *et al.*, 1983; Lim *et al.*, 1984). Within each subunit is a covalently bound flavin mononucleotide (FMN, Figure 1.1) (Steenkamp *et al.*, 1978b; Kenney *et al.*, 1978) and a 4Fe-4S cluster (Hill *et al.*, 1977), both of which are essential for the activity of the enzyme, and a non-covalently bound molecule of ADP (Lim *et al.*, 1988).

TMADH belongs to the minority of flavoproteins that covalently bind their flavin prosthetic group (Mewies *et al.*, 1998). The FMN moiety is attached to the protein through the cysteinyl sulphur of Cys-30 at C-6 of the isoalloxazine ring: a 6-*S*-cysteinyl linkage (Steenkamp et al., 1978b; Barber *et al.*, 1992). Dimethylamine dehydrogenase (DMADH), an evolutionary relative of TMADH also has a C-6 linkage to FMN (Meiberg & Harder, 1979; Yang *et al.*, 1995). This particular mode of flavin attachment is unusual; covalent linkage of flavin to protein usually occurs through the 8α-methyl of the flavin (Mewies et al., 1998).

The iron-sulphur centre of TMADH is a ferredoxin-like 4Fe-4S cluster (Hill *et al.*, 1977; Lim *et al.*, 1986), while the function of the ADP molecule is unknown; it plays no role in catalysis and is bound as part of a vestigial nucleotide binding domain recruited during the evolution of TMADH (Lim *et al.*, 1988). However, it is bound very tightly and is probably required for the structural integrity of the enzyme.

As with all redox enzymes, the reaction catalysed by TMADH can be expressed as reductive and oxidative half-reactions. During the reductive half-reaction, two electrons derived from the oxidation of TMA are transferred to the 6-*S*-cysteinyl FMN, producing hydroquinone (Steenkamp & Beinert, 1982a). The 4Fe-4S centre of the enzyme is only capable of accepting one electron at a time, so single

A.

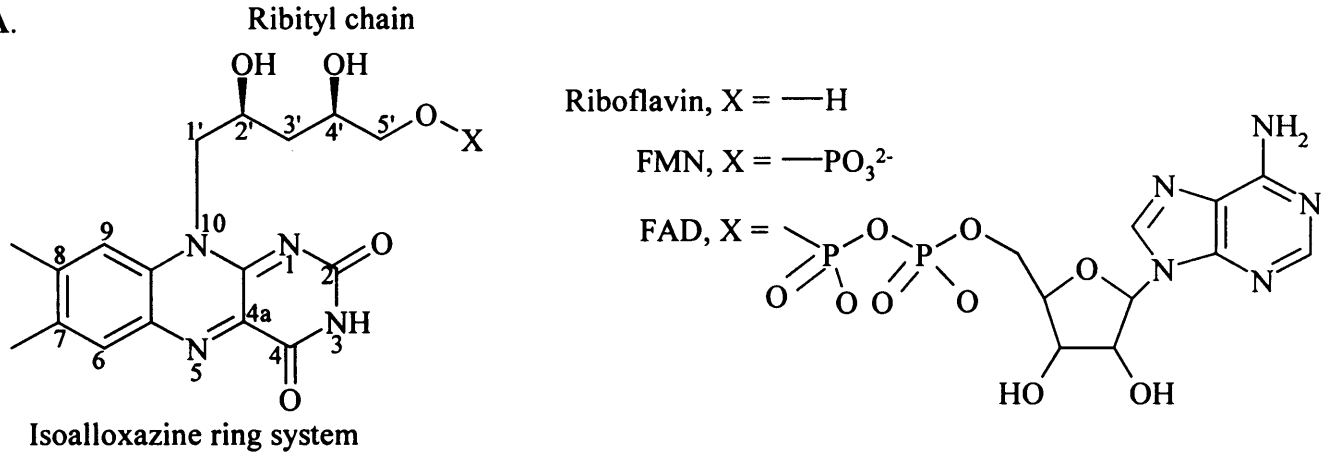

B

Oxidised

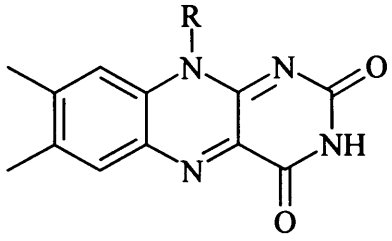

1-Electron reduced (semiquinone)

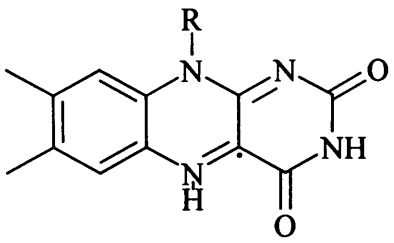
Neutral (blue)

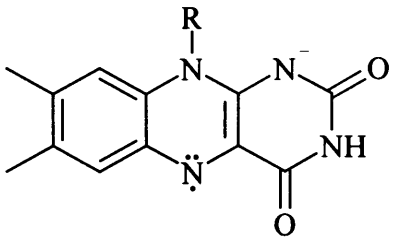
Anion (red)

2-Electron reduced (hydroquinone)

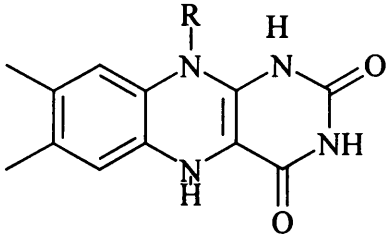

Figure 1.1: Structure and oxidation-reduction properties of flavins. A. Structure and derivatives of riboflavin, FMN and FAD. B. Stages and relevant structures in flavin reduction.

electrons are passed sequentially to it from flavin (Steenkamp & Beinert, 1982b). In the oxidative half -reaction, electrons travel from the 4Fe-4S centre to an external one-electron acceptor (Colby & Zatman, 1974). *In vivo*, this electron acceptor is a 62 kD FAD-containing electron transferring flavoprotein (ETF) (Steenkamp & Gallup, 1978; DuPlessis *et al.*, 1994), and the energy of these electrons is harnessed within the host bacterium by being passed to a membrane bound electron transfer chain (Anthony, 1982). *In vitro* electron acceptors, used to assay TMADH, include phenazine methosulphate (PMS) (Colby & Zatman, 1974) and ferricenium hexafluorophosphate (Fc^+) (Rohlfs & Hille, 1994).

Steady-state assays of TMADH show that the enzyme is partially inhibited at high substrate concentrations (Steenkamp *et al.*, 1978c). The enzyme possesses optimum catalytic activity at pH 8.5 (Colby & Zatman, 1974), and is moderately promiscuous in its use of amines, being able to oxidise a number of secondary and tertiary amines including diethylmethylamine, ethylmethylamine, triethlyamine and dimethylamine; TMADH does not oxidise primary amines, diamines or polyamines; quaternary ammonium salts have been found to inhibit activity (Colby & Zatman, 1974).

1.1.2 In Context: TMADH as a Flavoprotein

Flavoproteins are proteins that contain a bound flavin prosthetic group (Singer & Edmondson, 1978). They are electron-transferring enzymes that catalyse redox reactions in which the flavin moiety, which can be bound to the protein covalently, or more usually, non-covalently, accepts one or two electrons from the reducing substrate and donates one or two electrons to the oxidised substrate or electron acceptor. The possession of a flavin cofactor by TMADH confers certain properties, and allows certain methods of study, which are common to most flavoproteins.

The flavin coenzymes, flavin adenine nucleotide (FAD) and flavin mononucleotide (FMN) are derived from riboflavin (vitamin B_2) (Figure 1.1) (Macheroux, 1999). The functional part of both coenzymes is the isoalloxazine ring, which is attached to ribitol, an open-chain version of ribose with the aldehyde carbon reduced to the hydroxymethyl level (Mathews & van Holde, 1990). In FMN the 5' carbon of ribitol is linked to phosphate, while FAD is a adenylylated derivative of FMN. FMN and FAD undergo virtually identical electron transfer reactions, and the

use of one or the other coenzyme is largely a matter of structural moieties involved in binding the coenzyme to the apoenzyme (Singer & Edmondson, 1978).

Flavin has a bright yellow colour, and is usually bound tightly so that a protein with bound flavin can be purified by monitoring this colour (Palfrey & Massey, 1998). More importantly, observable spectral changes occurring during flavo-enzymatic reactions yield important information about reaction mechanisms and are particularly suited to observation using rapid reaction kinetic instruments such as stopped-flow devices (Palfrey & Massey, 1998; Macheroux, 1999). The yellow appearance of oxidised flavin and of flavoproteins is due to a major absorbance band at about 450 nm, with smaller maxima at about 370 nm and 260 nm. Excitation of the 450 nm band, either directly or by energy transfer from the short wavelength bands, gives green fluorescence maximal at 540 nm (Siegel, 1978).

Like the nicotinamide coenzymes, the flavins undergo two-electron oxidation and reduction reactions (Singer & Edmondson, 1978). The flavins are distinct, however, in having a stable one-electron-reduced species, the semiquinone free radical (Palfrey & Massey, 1998) (Figure 1.1). The stability of this intermediate gives flavins a catalytic versatility lacked by nicotinamide coenzymes, in that they can interact with two-electron or one-electron donor-acceptor pairs (Massey & Hemmerich, 1980). Flavoproteins can also interact directly with oxygen. One-electron reduced semiquinone flavin exists as one of two forms, depending on pH: it can either be protonated to give the neutral 'blue' semiquinone, or monodeprotonated to give the anionic 'red' semiquinone (Mathews & van Holde, 1990). The different reduction states of flavin have characteristic spectra (Macheroux, 1999). The neutral semiquinone has a characteristic long wavelength absorbance at 580-620 nm, whereas the anionic semiquinone radical has a strong absorbance at about 380 nm. Reduction to the hydroquinone form leads to bleaching of flavins that is featureless in the visible and near UV region (Figure 1.2). Some flavoproteins form charge transfer complexes that have strong long-wavelength absorbance bands, for example during the interaction between a flavin and nicotinamide, that are produced by the interaction between the π-bonds of the flavin isoalloaxazine ring and the π-bonds of a nearby molecule (Shieh *et al.*, 1981; Palfrey & Massey, 1998).

The majority of flavoproteins contain flavin that is non-covalently bound, although such flavin is usually bound tightly enough so that under normal conditions it does not dissociate from the protein (Palfrey & Massey, 1998). Where covalent linkage to an amino acid residue occurs, it is at the 8α methyl or C-6 position of the flavin isoalloxazine ring, with linkage occuring through either histidine, tyrosine or

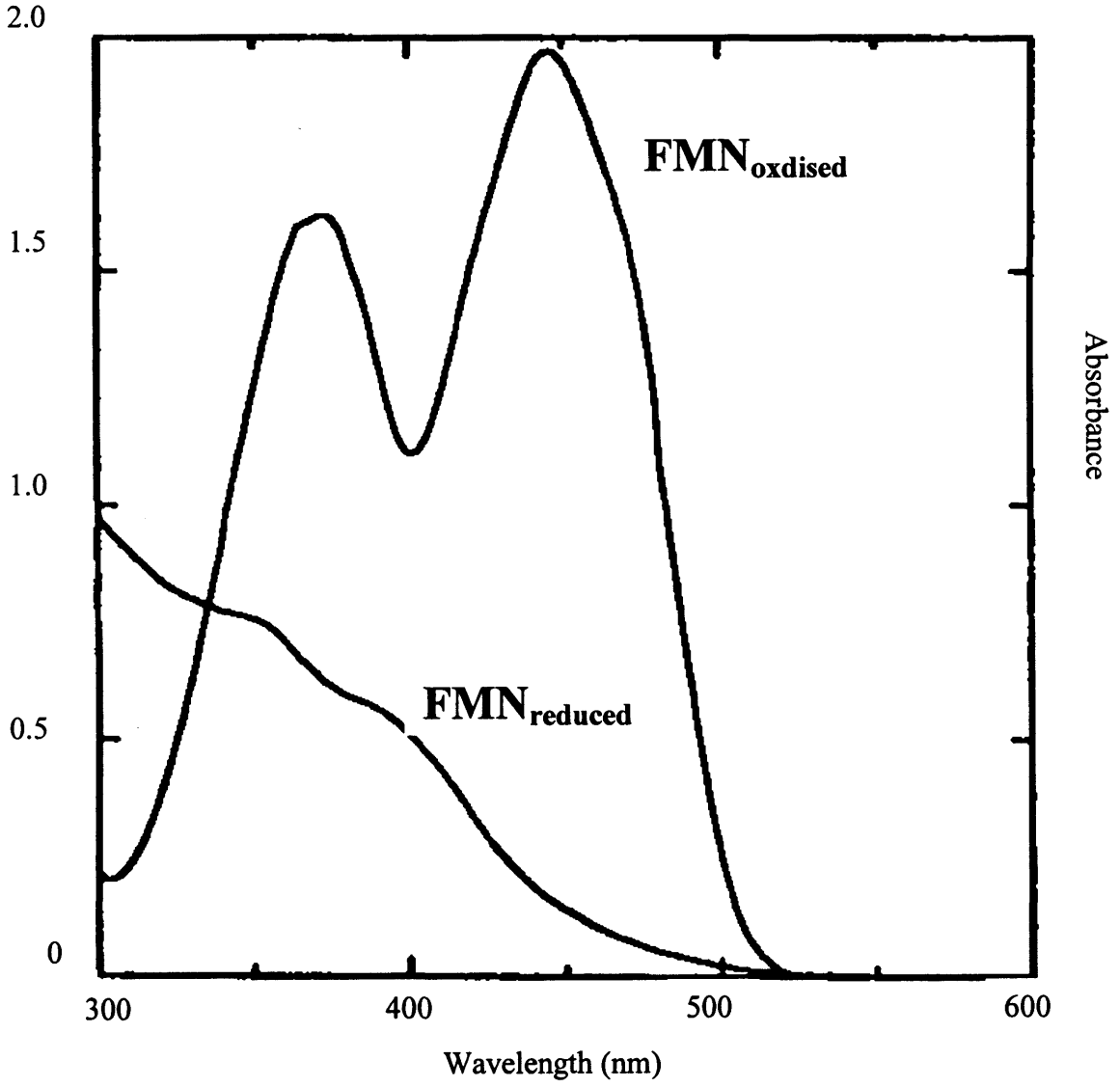

Figure 1.2. Oxidised and reduced absorption spectrum of FMN. Taken from Macheroux (Macheroux, 1999).

cysteine residues (Mewies et al., 1998). The binding of flavin to a protein often changes the spectral properties of the cofactor. Absorption of the flavin can become more or less intense, or there can be a 'resolution' of the 450 nm band producing shoulders and often a shift in the wavelength of maximum absorbance. These variations are thought to reflect the different environments of the flavin binding site, which can effect the spectral properties of bound flavin in much the same way as those of free flavin are affected by polarity and pH.

FAD and FMN are extremely versatile coenzymes, taking part in radical, carbanion, or hydride-transfer mechanisms, occupying an important position in enzyme-catalysed redox reactions and are responsible for catalysing the dehydrogenation of many different types of compounds, including dithiols, reduced nicotinamide nucleotides, alcohols and α-hydroxy acids, amines and α-amino acids, and even saturated C-C bonds (Massey & Hemmerich, 1980). In addition, they can fulfill structural and regulatory roles (Edmondson & Ghisla, 1999; Palfrey & Massey, 1998). In the process of catalysing these dehydrogenation reactions, the flavin moiety is itself reduced and in order to function catalytically, the oxidised form must be regenerated at the expense of reduction of some acceptor. The acceptor may in some cases be the oxidised form of the same type of compound that serves as reducing substrate, e.g. it might be a disulphide, an oxidised nicotinamide nucleotide or an unsaturated compound such as fumarate or crotonyl-CoA. In most cases however, the acceptor molecule will be molecular O_2 or another redox protein, such as an iron-sulphur protein or cytochrome (Singer & Edmondson, 1978; Palfrey & Massey, 1998). In the latter cases the flavoprotein necessarily acts as a mediator between one- and two-electron transfers (Massey & Hemmerich, 1980; Massey, 1995), requiring formation and stabilisation of the flavin semiquinone. Flavoproteins fill a unique spot in biochemistry with this capacity. All biological redox chains contain at least one such flavoprotein, since no redox transfer between the strictly two-electron reacting nicotinamide nucleotides and the strictly one-electron reacting haem proteins and iron-sulphur proteins is carried out without the aid of flavoproteins.

The 2-electron reduction potential of free flavin is –207 mV, while the semiquinone state is thermodynamically unstable. This behaviour is altered markedly in many flavoproteins (Brunori *et al.*, 1971; Mayhew *et al.*, 1969; Palfrey & Massey, 1998). Thus, flavoproteins having redox potentials as low as -495 mV for the semiquinone/reduced couple and as high as +40mV for the oxidised/reduced couple are known, and many form stable semiquinones (Massey, 1995; Singer & Edmondson, 1978).

Flavoenzymes are classified according to the reaction they catalyse, their ability to use molecular oxygen as an electron acceptor, and the nature of auxiliary redox centres. On these criteria flavoproteins are classified as oxidases, disulfide reductases, monooxygenases, reductases, dehydrogenases or electron transferases (Singer & Edmondson, 1978; Massey & Hemmerich, 1980; Hemmerich & Massey, 1982; Palfrey & Massey, 1998). Flavoenzymes in which flavin is the only active group are usually classified as 'simple' flavoproteins, and those like TMADH, which contain additional electron carriers, are classified as 'complex' flavoproteins.

1.1.3 The Role of Trimethylamine Oxidation in Methylotrophy

TMADH was first purified from a species of bacteria isolated from river water, Bacterium 4B6 (Colby & Zatman, 1974). All subsequent studies of the native enzyme have used TMADH purified from *Methylophilus methylotrophus*, sometimes referred to as bacterium W_3A_1, a strain isolated from soil (Colby & Zatman, 1975b). *M. methylotrophus* was once the subject of considerable research, being used as the source organism for an attempt by Imperial Chemicals Industries to provide a cheap source of nutrition in the form of single cell protein, under the commercial name of 'Pruteen' (Large, 1983; Anthony, 1982; Windass *et al.*, 1980).

M. methylotrophus belongs to the family of bacteria known as methylotrophs, which are a family of bacteria that can grow non-autotrophically at the expense of compounds which contain one or more carbon atoms but have no carbon-carbon bonds (so-called C-1 compounds) (Colby & Zatman, 1975a; Large, 1983). Substrates for methylotrophic organisms include formaldehyde, methanol and the methylated amines dimethylamine, methylamine and TMA (Colby & Zatman, 1973). Methylotrophy is only a specialised kind of heterotrophy, but methylotrophs are marked out as an individual biological group by virtue of occupying an intermediate position in nature between autotrophs and heterotrophs, and possessing special pathways of energy generation and carbon assimilation (Large, 1983).

Possession of TMADH is one way by which certain species of facultative methylotrophic bacteria, such as *M. methylotrophus* begin TMA metabolism (Colby & Zatman, 1973). For these species TMA can be used as the sole source of carbon and nitrogen. Because TMADH is located within the cytoplasm of host cells (Kasprzak & Steenkamp, 1983), possibly associated with invaginations of the cell membrane (Meiberg & Harder, 1979), TMA probably enters the cell using a uniport

mechanism (Burton *et al.*, 1983). The metabolism of TMA proceeds with the sequential removal of TMA methyl groups producing TMA, DMA and methylamine at each step (Large, 1983; Anthony, 1982). In addition, each step also produces formaldehyde and releases two electrons. Although formaldehyde is toxic to many organisms, it is used by methylotrophs either as an immediate source of energy, i.e. oxidised to CO_2, or is incorporated into the organism through a hexulose phosphate cycle. Ammonia, which remains after TMA has been stripped of its methyl groups, is assimilated by the glutamine synthetase/glutamate synthase system (Anthony, 1982).

As intimated earlier, methylotrophs possess alternative routes for the metabolism of TMA. Although TMADH is found in obligate methylotrophs and some restricted facultative methylotrophs, such as *M. methylotrophus*, the majority of methylotrophs use a trimethylamine monooxygenase to breakdown TMA (Colby & Zatman, 1973; Colby & Zatman, 1975a); this enzyme generates trimethylamine-N-oxide, which is subsequently converted to dimethylamine and formaldehyde by trimethylamine-N-oxide demethylase (or aldolase). A nicotinamide-dependent TMADH has also been identified (Loginova & Trotsenko, 1978).

1.1.4 Identification of the Prosthetic Groups of TMADH

TMADH has two active redox centres at its' active site, FMN and a 4Fe-4S centre (Figure 1.3), and an enzymatically inert ADP bound per enzyme dimer. TMADH was the first flavoenzyme in which covalent attachment of flavin to the protein was demonstrated to be through C-6 of the isoalloxazine ring (Mewies et al., 1998). Identification of the 6-*S*-cysteinyl linkage was a protracted process. Initially, the covalent nature of the attachment of the then-unknown chromophore to TMADH was revealed when it was demonstrated that the chromophore could not be released by denaturation, but was solubilised by proteolytic digestion (Steenkamp & Singer, 1976). While it was suspected that the chromophore was flavin, neither the spectrum or the fluorescent properties of the solubilised cofactor agreed with those of any known flavin derivative (Steenkamp & Mallinson, 1976).

The TMADH chromophore was isolated as a chymotryptic-tryptic aminoacyl twelve amino acid peptide and, although it was conjectured that the cofactor could be a pteridine derivative (Steenkamp & Singer, 1976), UV-visible spectral evidence and NMR studies supported the argument for the presence of flavin (Steenkamp *et al.*, 1978a). Additionally, ^{1}H-NMR evidence demonstrated that the coenzyme was

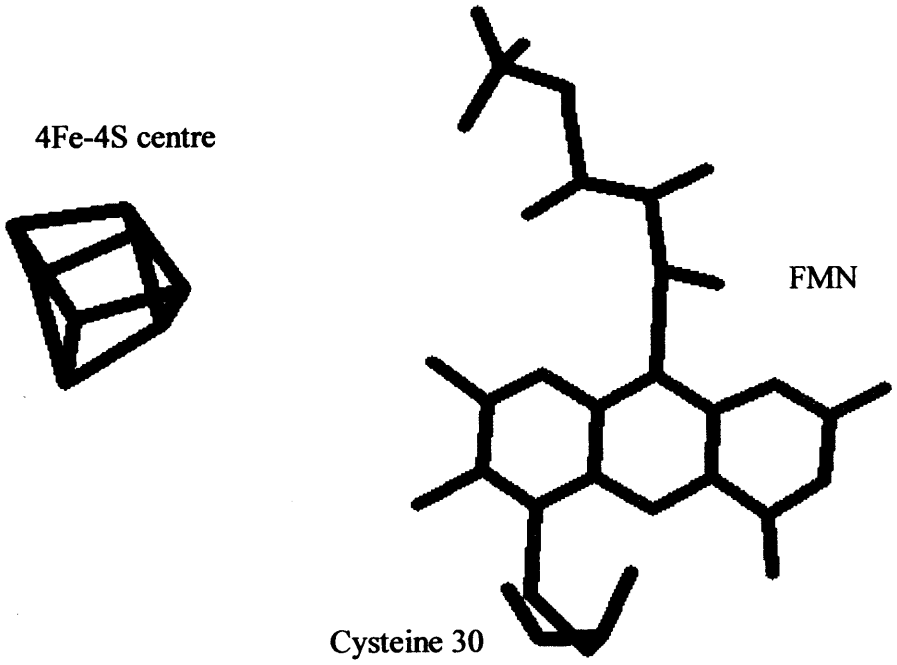

Figure 1.3: Type and relative positions of the redox active prosthetic groups of TMADH.

markedly different from all known 8α-substituted flavins and the presence of unchanged methyl groups at positions 7α and 8α, suggested substitution at either the C-6 or C-9 position (Steenkamp *et al.*, 1978b). The dephosphorylated aminoacyl flavin was isolated from the enzyme and reacted with the sulfhydryl agent *N*-ethylmaleimide (MalNEt), demonstrating that the FMN was attached through a thiol (Steenkamp *et al.*, 1978b). Final confirmation of attachment through C-6 of the isoalloxazine ring followed the chemical synthesis of 6-*S*-cysteinylriboflavin, which was identical to the dephosphorylated aminoacyl coenzyme isolated from TMADH (Steenkamp *et al.*, 1978b) and the development of methods for the chemical synthesis of 6-substituted flavins (Ghisla, 1980).

The presence of an iron-sulphur centre in TMADH was much less problematic. The iron-sulphur clusters were removed from TMADH using a core extrusion method, and the EPR spectra of the extruded clusters was compared with those of control extrusion reactions on oxidised ferredoxins from *Clostridia pasteurianum* and spinach (Hill et al., 1977). The structure of the iron-sulphur centre was therefore shown to be of the conventional ferredoxin-like 4Fe-4S type, although initially it was deduced that only one cluster was present per enzyme dimer. However, spectral evidence and SDS-PAGE gave strong evidence that TMADH was made up of two identical subunits (it had been thought previously that the subunits were different) and that there were therefore one iron-sulphur centre per subunit (Kasprzak *et al.*, 1983). This was later confirmed by analysis of structural data (Lim *et al.*, 1984).

TMADH binds one molecule of ADP per subunit, but its presence went unnoticed until structural data from X-ray crystallography appeared to show that an ADP molecule was present (Lim *et al.*, 1988). This was confirmed by thin layer and high pressure liquid chromotagraphic analysis of the supernatant from a perchloric acid precipitation of the enzyme. TMADH binds ADP tightly, so that it is unable to exchange with [^{14}C] ADP in the solvent (Lim *et al.*, 1988).

1.1.5 Structure of TMADH

TMADH has proved to be amenable to crystallisation (Lim *et al.*, 1982) and detailed structural information was made available when the 2.4 Å structure was solved (Lim et al., 1986) (Brookhaven code 2tmd; Figures 1.4 and 1.5). The cloning and sequencing of the gene that encodes TMADH (the *tmd* gene, see Section 1.1.7)

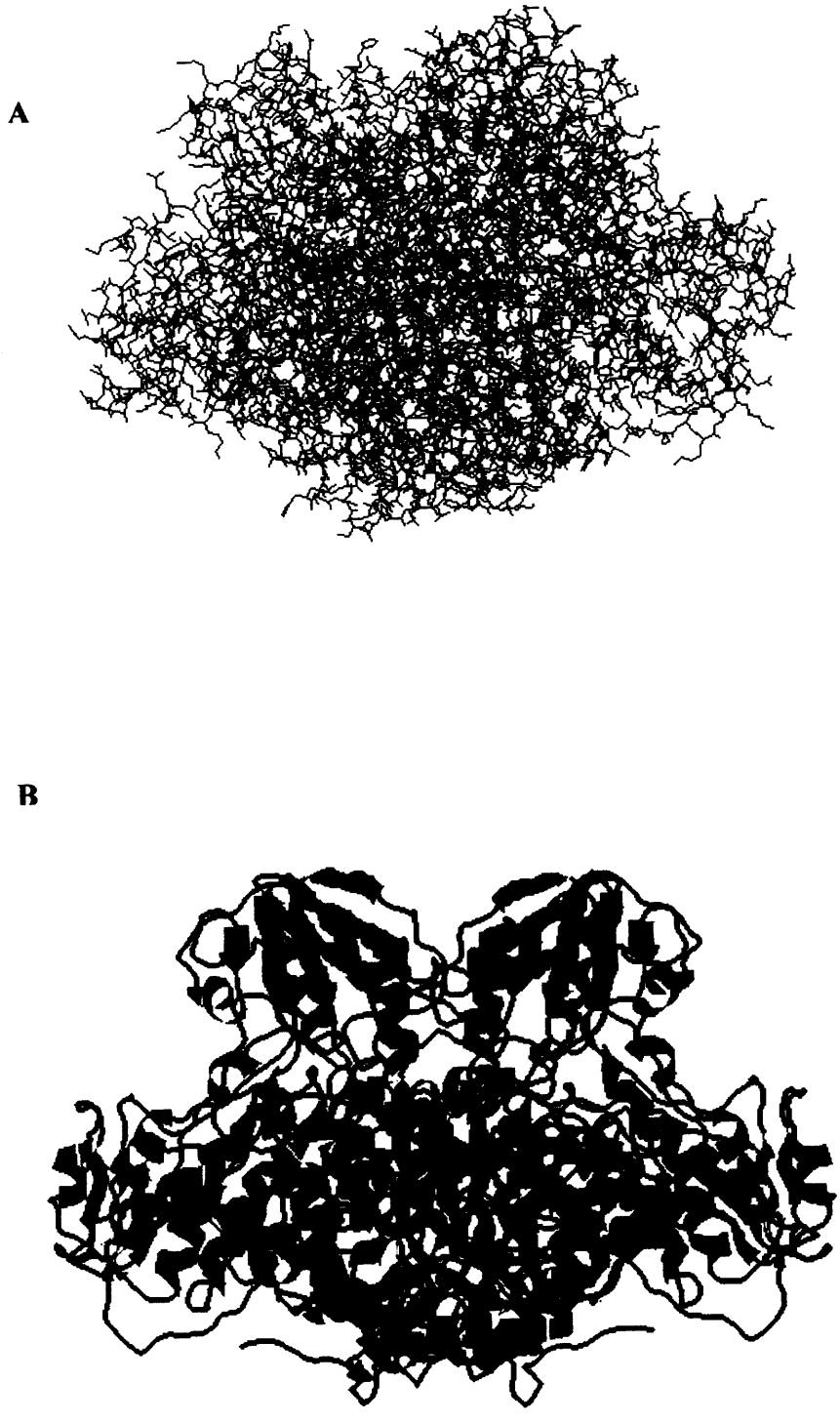

Figure 1.4: Structure of TMADH. A. Wireframe representation of structure. The different subunits of TMADH are coloured red and green. B. Same structure as a ribbon diagram, viewed from the same direction.

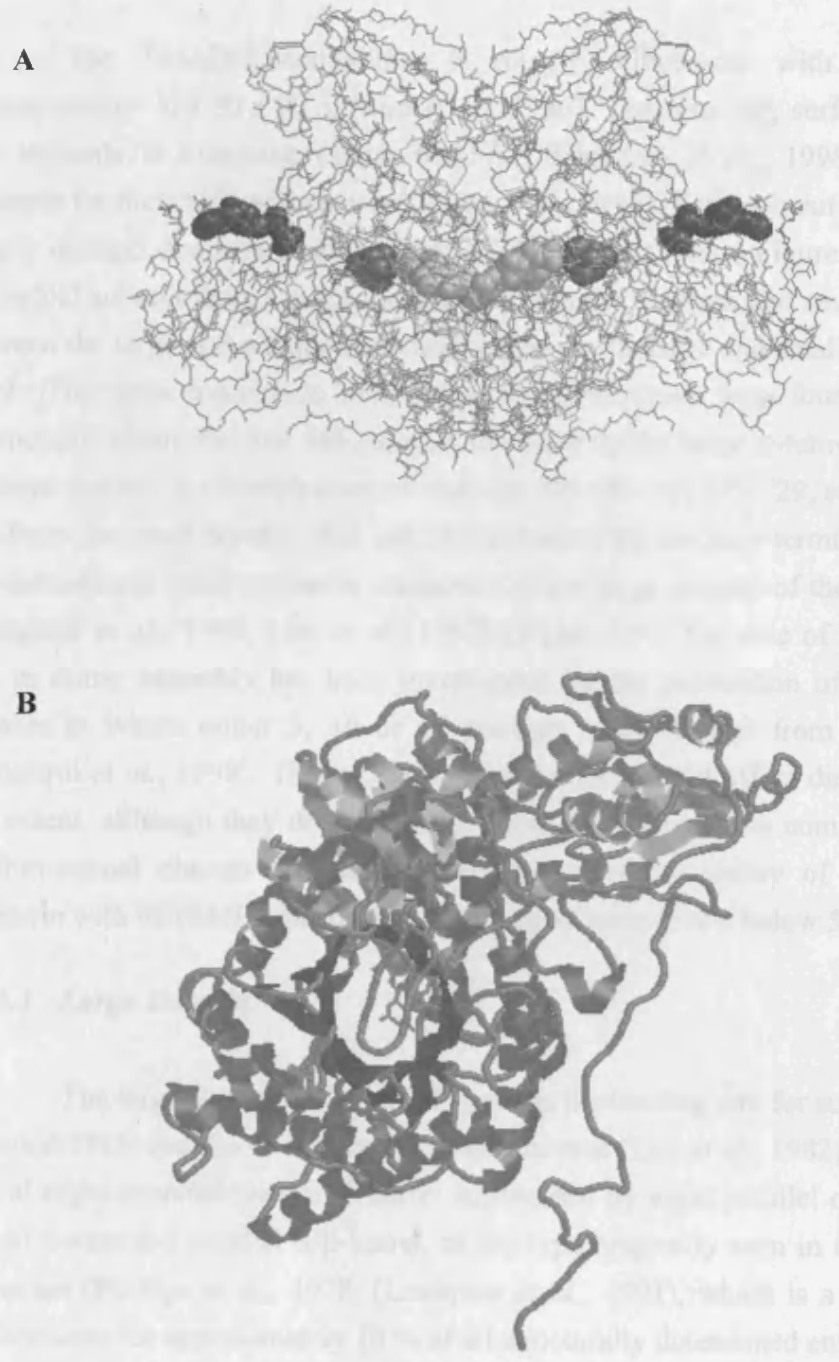

Figure 1.5: α/β Barrel of TMADH and Position of Prosthetic Groups. A. Prosthetic groups of TMADH: FMN, yellow, 4Fe-4S centre, red, and ADP, purple. B. View looking down the α/β-barrel of the large domain of TMADH. The 6-*S*-cysteinyl FMN of TMADH lies within the centre of this barrel. The 30 amino acid C-terminus 'arm', with which TMADH subunits interact with each other is seen extending from right to left beneath the protein.

has allowed further refinement of the crystal structure to 1.7 Å (Mathews *et al.*, unpublished).

The TMADH homodimer is roughly ellipsoidal with dimensions of approximately 70 x 80 x 90 Å (Lim et al., 1986). The touching surface between the two subunits is extensive (about 6100 $Å^2$; Ertughrul *et al.*, 1998) and probably accounts for their tight association (Colfen *et al.*, 1996). Each subunit consists of three clearly defined domains of about 40 kD, 24 kD and 19 kD (Figure 1.6). Within an individual subunit there are connections between the medium and small domains, and between the large and medium domains; however, the large and small domains do not touch. The three domains in each subunit are comprised from four sections of the polypeptide chain; the first 383 amino acids make up the large N-terminal domain, the medium domain is a combination of residues 384-494 and 649-729, and residues 495-648 form the small domain. The last 30 residues of the carboxy-terminus extend from one subunit and make extensive contacts with the large domain of the second subunit (Ertughrul *et al.*, 1998; Lim *et al.*, 1982) (Figure 1.5). The role of this polypeptide arm in dimer assembly has been investigated by the production of three TMADH mutants in which either 5, 10 or 17 residues were deleted from the C-terminus (Ertughrul *et al.*, 1998). These C-terminal deletions do not affect dimer assembly to any extent, although they do cause each dimer to adopt a more compact structure, a conformational change that severely compromises the ability of the enzyme to assemble with its FMN cofactor, reducing flavinylation levels below 5 %.

1.1.5.1 Large Domain

The large domain of TMADH contains the binding site for substrate, the 6-*S*-cysteinyl FMN and the 4Fe-4S centre of the enzyme (Lim *et al.*, 1982). It consists of a central eight-stranded parallel β-barrel surrounded by eight parallel α-helices: it is a typical 8-stranded parallel α/β-barrel, of the type originally seen in triose phosphate isomerase (Phillips *et al.*, 1978; (Lindqvist *et al.*, 1991), which is a recurring motif that accounts for approximately 10 % of all structurally determined enzyme molecules (Scrutton, 1993). There are also four smaller α-helices external to the main β-barrel. The first of these is found in an N-terminal loop, covering the bottom of the barrel; the three remaining helices are located towards the C-terminal end of the barrel and act to cover the top of the α/β-barrel.

The 6-*S*-cysteinyl FMN is attached to cysteine 30, which is found on strand 1 of the α/β-barrel, and is completely buried in the centre of the domain (Lim *et al.*, 1982) (Figure 1.5). Access to the FMN is postulated to be through a channel about

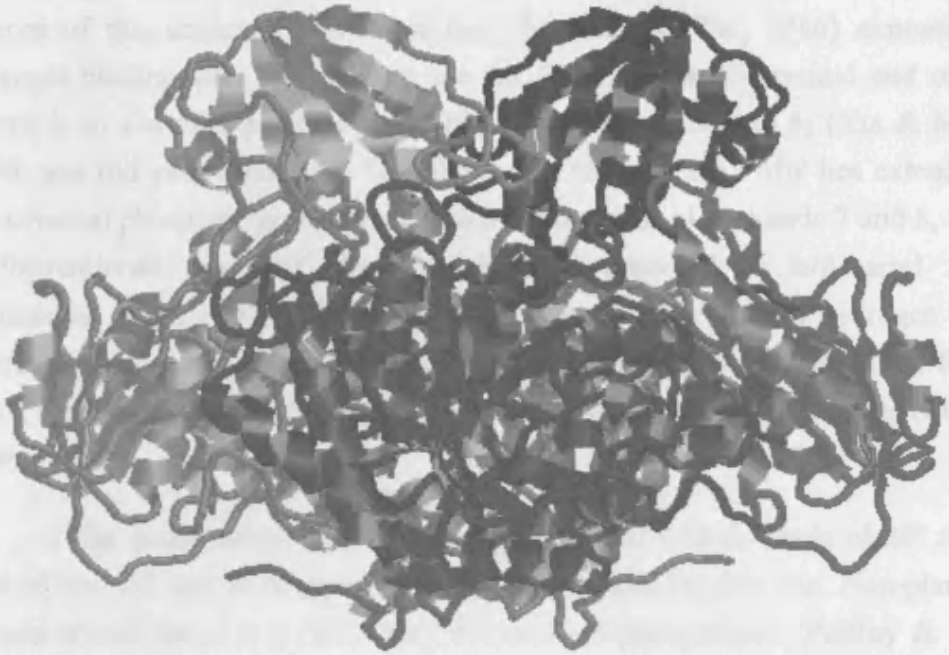

Figure 1.6: Domains of TMADH. Large domain, red, medium domain, green, and small domain, purple.

14 Å deep which opens into the centre of the enzyme dimer and intersects with a second channel formed by the axis of the two small domains. The flavin lies at the bottom of this channel, with its *si* face (Manstein & Pai, 1986) exposed to the substrate-binding site. The binding site for FMN, at the C-terminal end of a α/β-barrel, is in a similar position to the FMN in flavocytochrome b_2 (Xia & Mathews, 1990) and old yellow enzyme. The ribityl side chain of the FMN lies extended with the terminal phosphate group located between the ends of β-strands 7 and 8, which is a conventional mode of phosphate binding observed in α/β-barrel domains (Wilmanns *et al.*, 1991; Bork *et al.*, 1995). Numerous ionic and hydrogen bonding interactions, in addition to an induced dipole at the N-terminal end of the fourth α-helix, are thought to account for the strong binding of the phosphate group (Lim *et al.*, 1986).

The isoalloxazine ring of the FMN is folded with an angle of 20° along the axis of the N-5 and N-10 atoms towards the substrate binding site. Non-planarity of protein-bound flavin is a fairly well documented phenomenon (Palfrey & Massey, 1998), and it has been speculated that it contributes to modulation of flavin redox potential (Hasford *et al.*, 1997). Recent structural and computational studies on TMADH (Mathews *et al.*, 1999) indicate that inducing a bend into the isoalloxazine ring does indeed raise the two-electron reduction potential of the FMN. These studies also reveal that the 'butterfly' bend in TMADH is induced by the local protein environment, and is not caused by its covalent attachment to Cys-30.

Within each subunit, the 4Fe-4S cluster is buried in a pocket formed by the large and medium domains within the structure of the enzyme, 15 Å from the protein surface. The structure of the iron-sulphur centre is related to bacterial ferredoxins, although it has it's own distinguishing features, such as containing a significant amount of helix within the cluster binding loop and in the use of a simple α/β motif to bind the cluster (Lim *et al.*, 1982). The 4Fe-4S centre and FMN are separated by a centre-to-centre distance of 12 Å. However, the 8α methyl of the FMN comes to within 6 Å of the closest iron atom of the cluster and is almost in van der Waals contact with a sulphur atom (on Cys-351) that forms part of the cluster. Hence, electron transfer is speculated to occur from the 8α methyl of the FMN to the iron-sulphur centre via Cys-351 (Lim *et al.*, 1986).

1.1.5.2 Medium and Small Domains

The medium and small domains of TMADH are of similar structure, comprising a core of five β-sheets flanked by combinations of α-helices and anti-parallel β-sheets (Lim *et al.*, 1986). They play no direct role in substrate breakdown, but are involved in the interaction of TMADH with ETF and the subsequent transfer of substrate-derived electrons.

The medium domain has a folding pattern similar to that seen in flavodoxin, glutathione reductase and other NAD-linked dehydrogenases (Lim *et al.*, 1986) (Scrutton, 1993). The ADP molecule bound by TMADH is located in this domain at a site that corresponds to the ADP moiety of the FAD which is bound by the FAD-binding domain of glutathione reductase. Because this ADP appears to have no physiological function, it is thought to be a vestigial dinucleotide binding domain recruited during the evolution of TMADH (Lim et al., 1986). The topology of the small domain is very similar to the NADPH-binding domain of the flavoprotein glutathione reductase.

1.1.6 Substrate Binding in TMADH

Investigations into the mode of substrate binding in TMADH have been carried out by studying enzyme crystals in three oxidation states: oxidised, 2-electron reduced and 3-electron reduced (Bellamy *et al.*, 1989). As purified, TMADH is in the oxdised state, and the binding of substrate to oxidised enzyme was mimicked by soaking crystals of the enzyme with a solution containing tetramethylammonium chloride (TMAC), a potent inhibitor of TMADH which binds at the active site, but does not reduce the enzyme. 2-electron reduced enzyme is produced in two ways, either by soaking crystals with TMA, or by soaking dithionite-reduced TMADH in a TMAC solution. 3-electron reduced enzyme was generated by soaking TMADH crystals with the reducing agent dithionite in the absence of substrate or TMAC.

TMA binds to TMADH as the protonated cation trimethylammonium (Scrutton & Raine, 1996). The substrate-binding site of TMADH consists of the phenolic and indole rings of three aromatic residues: Tyr-60, Trp-264 and Trp-355, and the binding site has therefore been described as an 'aromatic bowl' (Raine *et al.*, 1995) (Figure 1.7). The substrate TMA and the inhibitor TMAC are bound by cation-π interactions within this bowl. Briefly, a cation-π bond is formed between the delocalised electrons on the face of an aromatic side chain and a protonated or

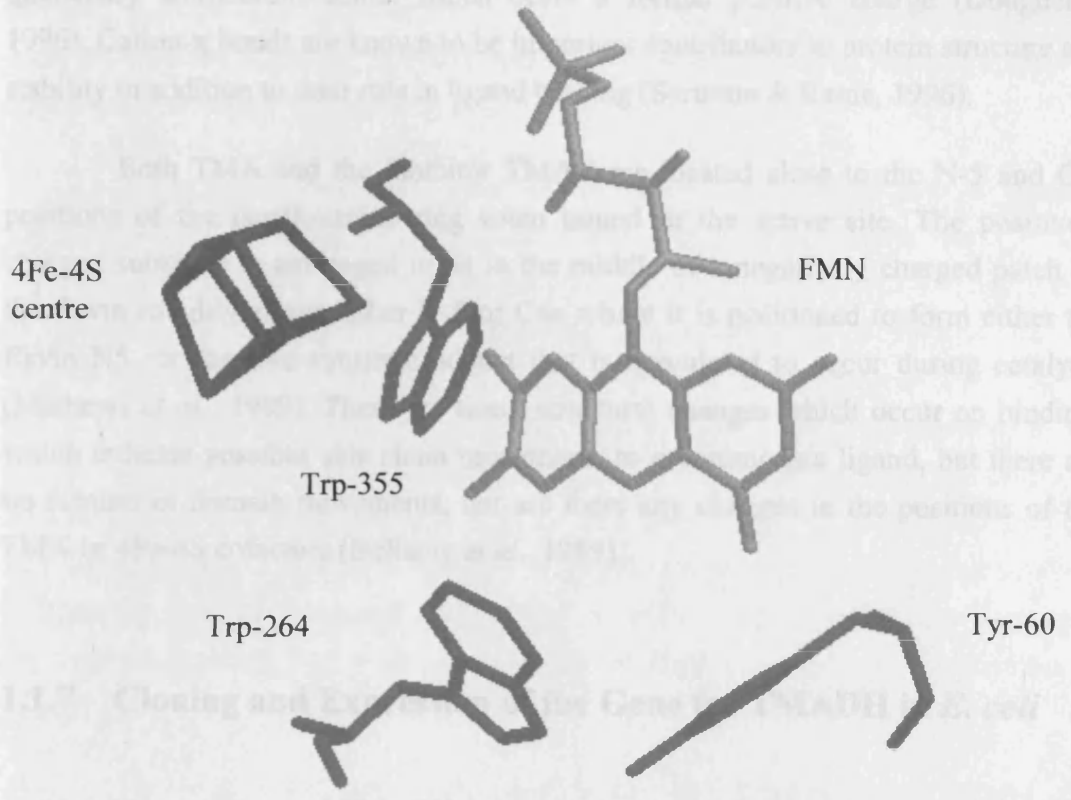

Figure 1.7: Substrate binding site of TMADH. TMA is bound within a so-called 'aromatic bowl' consisting of three aromatic amino acid residues, Tyrosine-60, Tryptophan-264 and Tryptophan-355.

quaternary ammonium amine which bears a formal positive charge (Dougherty, 1996); Cation-π bonds are known to be important contributors to protein structure and stability in addition to their role in ligand binding (Scrutton & Raine, 1996).

Both TMA and the inhibitor TMAC are located close to the N-5 and O-4 positions of the isoalloxazine ring when bound in the active site. The positively charged substrate is envisaged to sit in the middle of a negatively charged patch on the flavin roughly above either N-5 or C4a where it is positioned to form either the flavin N5- or the C4a-substrate adduct that is speculated to occur during catalysis (Mathews *et al.*, 1999). There are small structural changes which occur on binding, which indicate possible side chain movements to accommodate ligand, but there are no subunit or domain movements, nor are there any changes in the positions of the FMN or 4Fe-4S cofactors (Bellamy *et al.*, 1989).

1.1.7 Cloning and Expression of the Gene for TMADH in *E. coli*

Many aspects of TMADH have been revealed following the cloning of the *tmd* gene from *M. methylotrophus* (Boyd *et al.*, 1992). The cloning of the *tmd* gene provides an abundant source of recombinant enzyme, but more importantly, in concert with high resolution structural data, it allows mutagenic investigation of the structure and function relationships that occur in the enzyme.

The gene for TMADH was sequenced as follows (Boyd *et al.*, 1992): a 530 bp *tmd* gene sequence, coding for nucleotides 1470-2000, was isolated from *M. methylotrophus* by PCR. This gene fragment was used to probe a genomic library from *M. methylotrophus* and led to the isolation of a *tmd* gene fragment coding for amino acid residues 34 to 729. Further PCR amplification from genomic DNA recovered the missing N-terminal fragment and the full length *tmd* gene was assembled in the phage vector M13mp18. DNA sequencing showed that the *tmd* gene is composed of 2190 bp, encoding a protein of 730 amino acids.

When the *tmd* gene was first sequenced, numbering of the amino acids was adopted from an earlier study, in which the X-ray structure of TMADH was compared with data from N-terminal protein sequencing of the enzyme (Barber *et al.*, 1992). In this study, the alanine which occurs as the second residue in the sequence of TMADH had been designated as position 1, even though the initiating methionine residue determined from sequencing the *tmd* gene was found in about 25 % of the samples

studied by N-terminal sequencing (Boyd *et al.*, 1992). This initiating methionine is referred to as position 0. Therefore, in the scientific literature and in this thesis, the number assigned to each TMADH residue has a value that is one less than its appearance in the amino acid sequence.

After DNA sequencing, the *tmd* gene was subcloned into a plasmid expression vector, creating a plasmid termed pKTM, and placed under IPTG-inducible control by the *tac* promoter (Scrutton *et al.*, 1994). However, the expression of TMADH in this system was unstable, so a system was developed for the constitutive expression of the enzyme. The *tmd* gene was reconstructed by PCR, the N-terminus was modified to incorporate an upstream *Nco* I site at the position of the methionine initiation codon, and a low abundance Arg codon was replaced with one of high abundance at nucleotides 4 to 6. The gene was then subcloned into the *Bacillus subtilis/E. coli* shuttle vector pSV together with a synthetic vegetative (*veg*) promoter in front of the gene, creating the expression vector which has been used since for the expression of wild-type recombinant TMADH: pSV2tmdveg (Scrutton *et al.*, 1994).

The high expression obtained with the pSV2tmdveg vector means that TMADH accounts for about 15 % of the total cell protein in the *E. coli* host, compared with about 3 % in *M. methylotrophus* (Colby & Zatman, 1974). The recombinant form of TMADH assembles stoichiometrically with the 4Fe-4S centre and ADP (Scrutton *et al.*, 1994). However, recombinant wild-type TMADH has much lower levels of flavin than enzyme isolated from the native source, with typical flavinylation levels between 25 and 35 %. This leads to slightly altered kinetic and physical properties between the native and recombinant wild-type enzymes, e.g. hydrodynamic studies have revealed that the deflavo form of the enzyme is less compact than the fully flavinylated TMADH obtained from the native source (Ertughrul *et al.*, 1998).

1.1.8 Flavinylation in TMADH

A fortunate consequence of under-flavinylation in recombinant TMADH was to stimulate studies into the mechanism by which the enzyme binds to its FMN cofactor and to reveal a mechanism for flavinyation which provides a rationale for the existence of covalently bound flavin in some flavoproteins.

The pSV2tmdveg vector gives a typical yield of about 25 mg recombinant wild-type TMADH per litre of cell culture. However, as already stated, the amount of FMN associated with the protein is variable, and the level of flavinylation depends on the particular form of TMADH, i.e. whether wild-type or mutant. Flavinylation levels therefore vary between 0 % in certain mutant forms of TMADH to 60 % in others (Scrutton *et al.*, 1994; Packman *et al.*, 1995; Ertughrul *et al.*, 1998). A small amount (~ 2 %) of deflavo enzyme is also found in preparations from *M. methylotrophus* (Packman *et al.*, 1995). The incorporation of FMN into TMADH occurs during the folding of the enzyme (Packman *et al.*, 1995; Mathews *et al.*, 1999) and, in the case of both recombinant and native proteins, production of deflavo enzyme is thought to reflect the inability of host cells to maintain FMN synthesis at a sufficient level for incorporation into the nascent TMADH polypeptide. Introducing riboflavin into the growth medium does not improve flavinylation (Scrutton *et al.*, 1994). Enzyme lacking FMN (deflavo enzyme) could not be reconstituted in the presence of excess FMN, even with the use of a mild chaotropic agent such as KBr.

As a start to investigating the role of the covalent link in TMADH, the 6-*S*-cysteinyl bond to the isoalloxazine ring was disrupted by the production of a Cys-30→Ala (C30A) mutant (Scrutton *et al.*, 1994). In the absence of a covalent link, spectral analysis revealed that about 30 % of the enzyme possessed flavin. The C30A mutant exhibited variable properties with regard to its ability to be reconstituted with FMN. For example, FMN could be removed and reconstituted with that fraction of the C30A mutant enzyme that had been originally purified in the flavinylated form. However, the fraction that had originally been purified as deflavo enzyme was unable to incorporate FMN, even with the use of chaotropic agents (Scrutton *et al.*, 1994). This was a very strong indication that once enzyme has folded as the deflavo form, it remains in a 'locked' conformation and is permanently unable to bind FMN.

The nature of the locked conformation of deflavo TMADH has recently been solved (Mathews *et al.*, 1999). ^{31}P NMR studies of the recombinant wild-type enzyme have shown that in deflavo enzyme, the site which would be occupied by the FMN ribityl phosphate is occupied by an inorganic phosphate ion derived from solvent (Mathews *et al.*, 1999). This inorganic phosphate cannot be removed from the enzyme despite the use of aggressive procedures involving urea and guanidine-HCl and is clearly bound with high affinity, which might mirror the strong binding of the FMN ribityl phosphate in flavinylated enzyme. There are subtle structural differences between the flavinylated and deflavo forms of recombinant enzyme, because flavinylated C30A TMADH does not bind inorganic phosphate after FMN has been removed, whereas deflavo enzyme appears unable to expel the inorganic phosphate

molecule from its binding site (Mewies et al., 1998). Hence, it seems that once folded, TMADH is permanently locked into one of two forms, depending on whether FMN is available to the developing protein during the folding process.

1.1.9 A Rationale for the Existence of Covalent Attachment of Flavin to Enzymes

About 25 flavoproteins have been so far discovered to have covalently bound flavin at their active sites (Mewies *et al.*, 1998). In the majority of cases, flavin attachment is at the 8α-methyl of the isoalloxazine ring, with the two exceptions being TMADH and DMADH, where attachment is to the C-6 (Palfrey & Massey, 1998) (Mewies *et al.*, 1998). There has been some debate about the presence of covalent attachment of flavin to some flavoproteins. For example, because all flavoproteins bind to flavin with a high affinity, covalent attachment is not a strategy for attaining active site saturation (Mewies *et al.*, 1998). In addition, several covalent flavoenzyemes have homologous flavin-dissociable counterparts that display similar enzyme activities (Fraaije *et al.*, 1999). In some cases it has been hypothesised that covalent attachment might be responsible for modulating the redox potential of flavin (Edmondson & De Francisco, 1992), and while this is the case for some enzymes (Fraaije *et al.*, 1999), it does not appear to be so for TMADH (Mathews *et al.*, 1999). Recent studies on vanillyl-alchohol oxidase, have found that covalent attachment is required for efficient redox catalysis, but removal of the link does not destroy catalytic activity (Fraaije et al., 1999). Hence, there are a probably a number of reasons for the presence of covalently attached flavin at the active site of some flavoenzymes. Mutagenic studies on the flavin binding site of TMADH provide evidence that the nature of the covalent link is to stop chemical inactivation of flavin (Scrutton *et al.*, 1994; Packman *et al.*, 1995; Mewies *et al.*, 1995; Mewies *et al.*, 1996).

The production of the C30A TMADH mutant demonstrated that the 6-S-cysteinyl bond to FMN in TMADH is not essential for catalysis, because the C30A TMADH mutant is able to turn over substrate. However this mutant is inactivated after about 9 turnovers (Huang *et al.*, 1996), and this inactivation occurs due to hydroxylation of the flavin at C-6, the position at which the FMN would normally be linked to native TMADH. The formation of 6-hydroxy FMN was initially thought to be due to a 'substrate assisted' mechanism, in which nucleophilic attack by solvent-derived OH^- upon the C-6 atom was facilitated by the electron withdrawing property

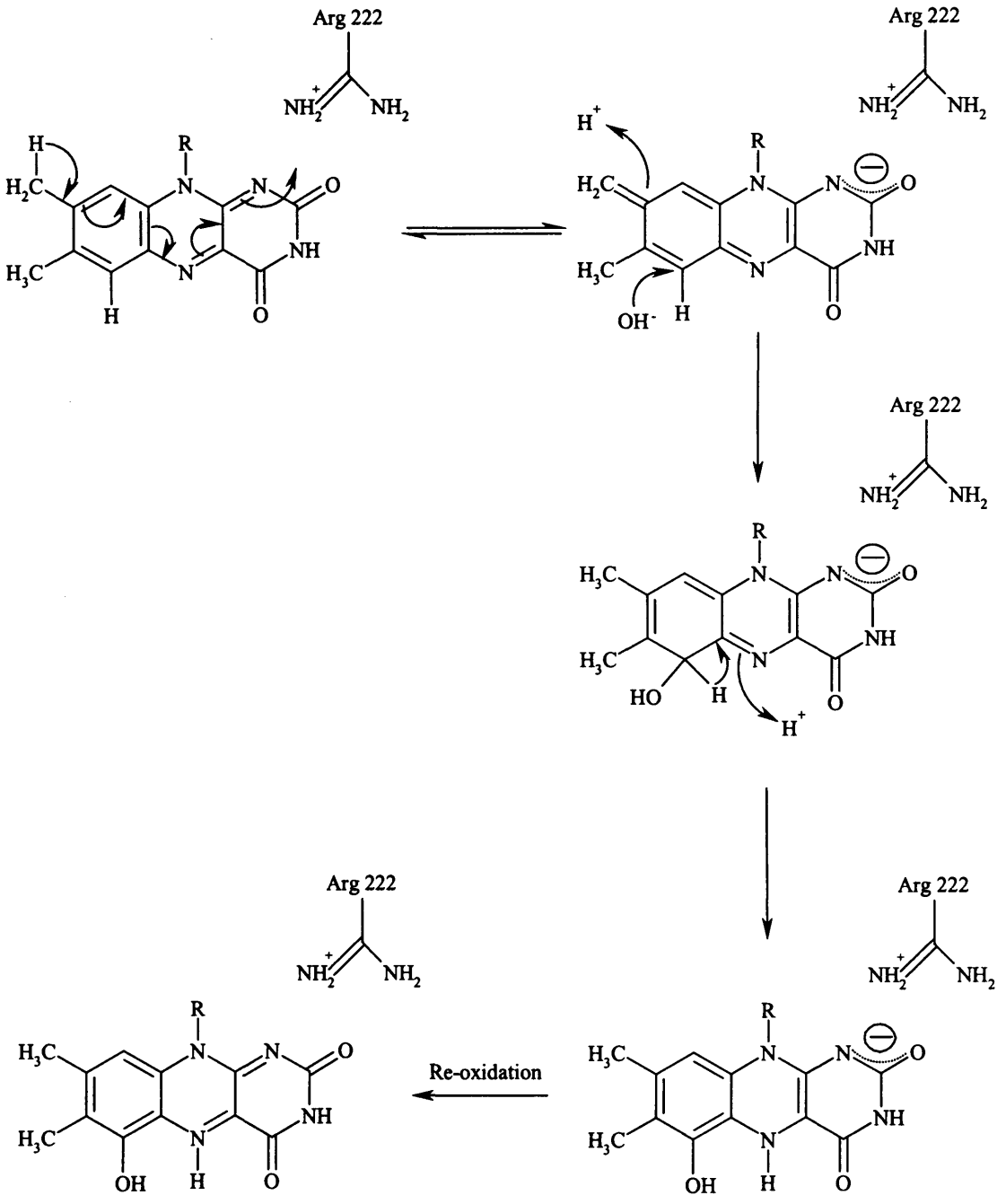

Figure 1.8: Proposed mechanism for the formation of 6-hydroxy-FMN from a flavin iminoquinone methide. Formation of a negative charge at the N-10/O-2 positions of the flavin is stabilised by the amide cation of Arg-222. Electrophilic attack by hydroxide at the C-6 atom is accompanied by the release of a proton from the 8α-methyl group and the transfer of a proton to the C-5 atom. Subsequent re-oxidation of the flavin yields the 6-hydroxy-FMN. Reproduced from Mewies *et al.*, 1997).

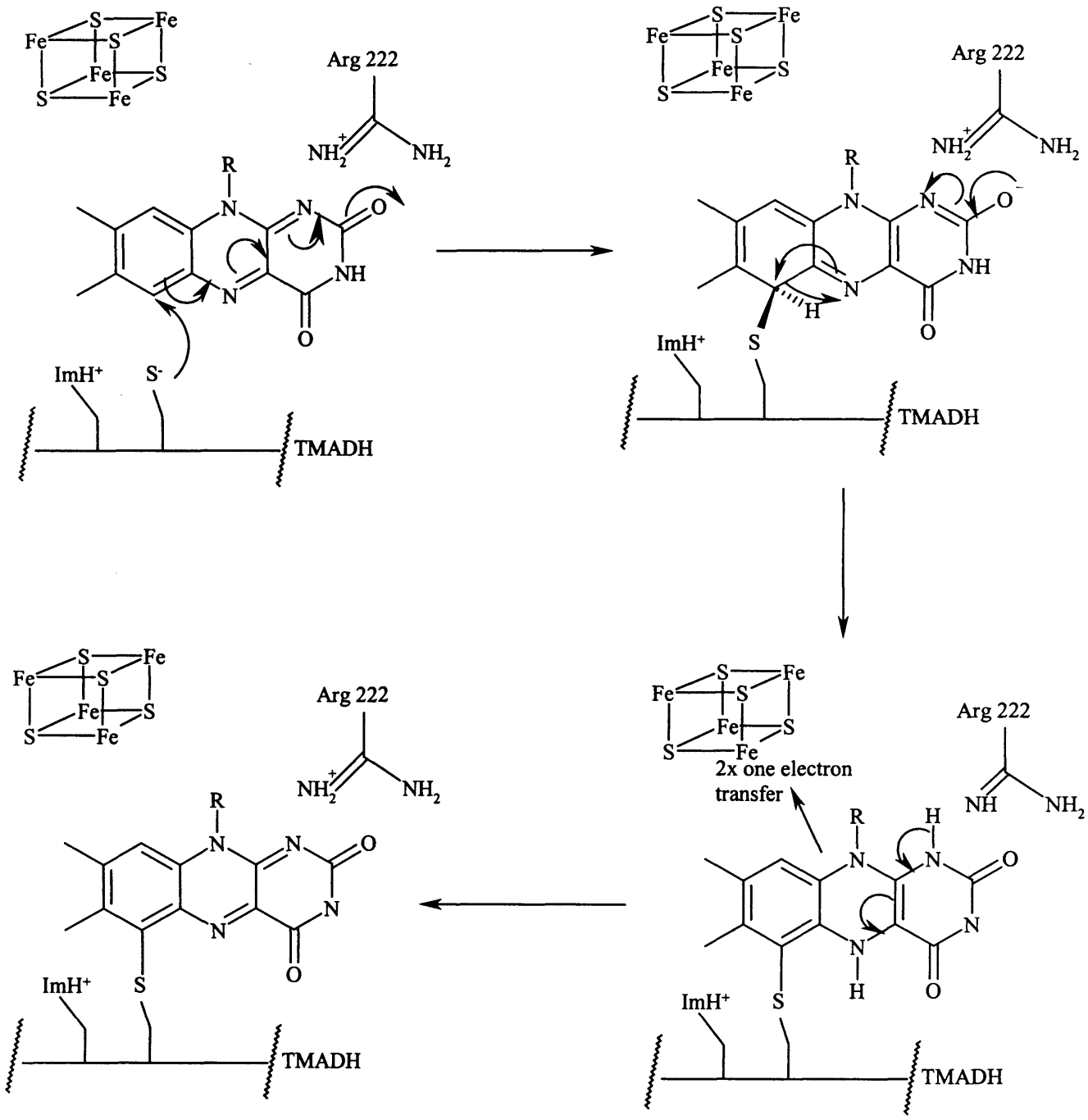

Figure 1.9: The proposed flavinylation mechanism of TMADH. ImH^+ represents the protonated imidazole side chain of His-29 that is thought to aid the nucleophilic attack of Cys-30 at the C-6 atom of the isoalloxazine ring by the formation of an imidazolium/thiolate ion-pair. The role of Arg-222 in stabilising the negative charge that develops at the N-1/O-2 positions of the flavin is indicated. Re-oxidation of the flavin occurs through electron transfer to the 4Fe-4S centre (reproduced from Scrutton *et al.*, 1994).

of a substrate-flavin adduct at the N-5 position of the isoalloxazine ring (Rohlfs & Hille, 1994) (Huang *et al.*, 1996). However, the production of a Trp-355→Leu (W355L) TMADH mutant demonstrated that 6-hydroxy FMN could be formed in the absence of any contact with substrate (Mewies *et al.*, 1997). Hence, an alternative proposal was developed that simultaneously accounted for the 6-hydroxylation of FMN in TMADH and for the mechanism of covalent binding of flavin to the enzyme (Figures 1.8 and 1.9). This new mechanism proposes that during flavinylation an iminoquinone tautomeric state of non-covalently bound FMN forms in the active site of TMADH. This iminoquinone state enhances the electrophilicity of the flavin C-6 atom, enabling it to interact with Cys-30, the reactive nucleophile. In the absence of covalent linkage, for example in the C30A mutant, or in the W355L mutant where active site misfolding slightly perturbs binding, the electrophilicity of the C-6 atom makes it susceptible to attack by hydroxide derived from solvent.

It therefore appears likely that covalent linkage at the C-6 atom of the FMN isoalloxazine ring prevents 6-hydroxylation by linking directly to the C-6 position. Analogously, the involvement of an iminoquinone methide has been proposed for the flavinylation reactions of 6-hydroxy-D-nicotine oxidase (Brandsch & Bischler, 1991) and *p*-cresol methylhydroxylase (Kim *et al.*, 1995). In these cases too, linkage at the 8α methyl group of the flavin could prevent the subsequent formation of a 6-hydroxy FMN derivative. Thus, the role of covalent linkage of flavin in some flavoproteins appears to prevent hydroxylation at the flavin C-6 atom and therefore enzyme inactivation, in cases where the structure of the isoalloxazine ring, as determined by its protein environment, renders the C-6 susceptible to nucleophilic attack (Mewies *et al.*, 1997; Mewies *et al.*, 1998).

1.1.10 TMADH Reaction Kinetics

1.1.10.1 Introduction

The oxidative demethylation of TMA proceeds by a ping-pong (double displacement) mechanism, in which the enzyme is first reduced by substrate, followed by re-oxidation by an electron acceptor (Figure 1.10). In steady-state analyses the enzyme is inhibited at high concentrations of TMA. This substrate inhibition starts to manifest itself at about 100 μM TMA, depending on the conditions, and continues until a non-zero limiting rate of reaction is reached at high concentrations. The steady-

state inhibition of TMADH forms the basis of the study presented in Chapter 3, where the subject is discussed in greater detail.

1.1.10.2 The Spectral Properties of TMADH

As with all flavoproteins (Macheroux, 1999; Murataliev, 1999), TMADH has proved particularly amenable to study by various spectroscopies. Full reduction of TMADH requires three electrons per subunit: two for the 6-*S*-cysteinyl FMN and one for the 4Fe-4S centre. However, the oxidative demethylation of TMA produces only two electrons; three-electron reduced TMADH can only be generated by titration with dithionite. The informative region of the TMADH absorption spectrum lies between 350 nm and 600 nm (Figure 1.10). Reduction by two electrons initially produces the hydroquinone form of the enzyme, but this is a transient species whose formation and disappearance is too rapid to be observed except by stopped-flow spectroscopy. Subsequent to stoichiometric titration with TMA the spectrum produced is that of the enzyme species in which internal electron transfer from flavin hydroquinone to 4Fe-4S centre has already taken place, producing TMADH containing anionic flavin semiquinone and reduced iron-sulphur centre. This distribution of electrons produces a characteristic spectrum with three peaks: a major peak at 365 nm and two smaller peaks at 440 nm and 520 nm (Figure 1.10). The peak at 365 nm indicates the presence of anionic flavin semiquinone, while the spectral collapse between 380 nm and 550 nm represents the reduction of both FMN and the 4Fe-4S centre. The three-electron reduced spectrum of TMADH that is produced following titration with dithionite, shows a complete spectral collapse between 400 nm and 550 nm, obviously with no semiquinone signal at 365 nm.

The distribution of two electrons in substrate reduced TMADH is affected by pH and the concentration of TMA (Rohlfs & Hille, 1994). At pH 7.5 and below, and at low substrate concentrations, the TMADH species favoured is that containing hydroquinone and oxidised 4Fe-4S centre. At pH's above 7.5, or at high substrate concentrations, the electrons are split between the redox centres to produce anionic flavin semiquinone and reduced 4Fe-4S centre.

EPR spectroscopy is often used to study electron distribution in flavoproteins with multiple redox centres (Palfrey & Massey, 1998), and has been a useful technique in studies of TMADH (Steenkamp & Beinert, 1982b) (Stevenson *et al.*, 1986). EPR is the only technique by which the electron distribution between FMN and 4Fe-4S centre can be accurately determined in 2-electron reduced forms of TMADH. The EPR spectrum of 2-electron reduced TMADH has been described as

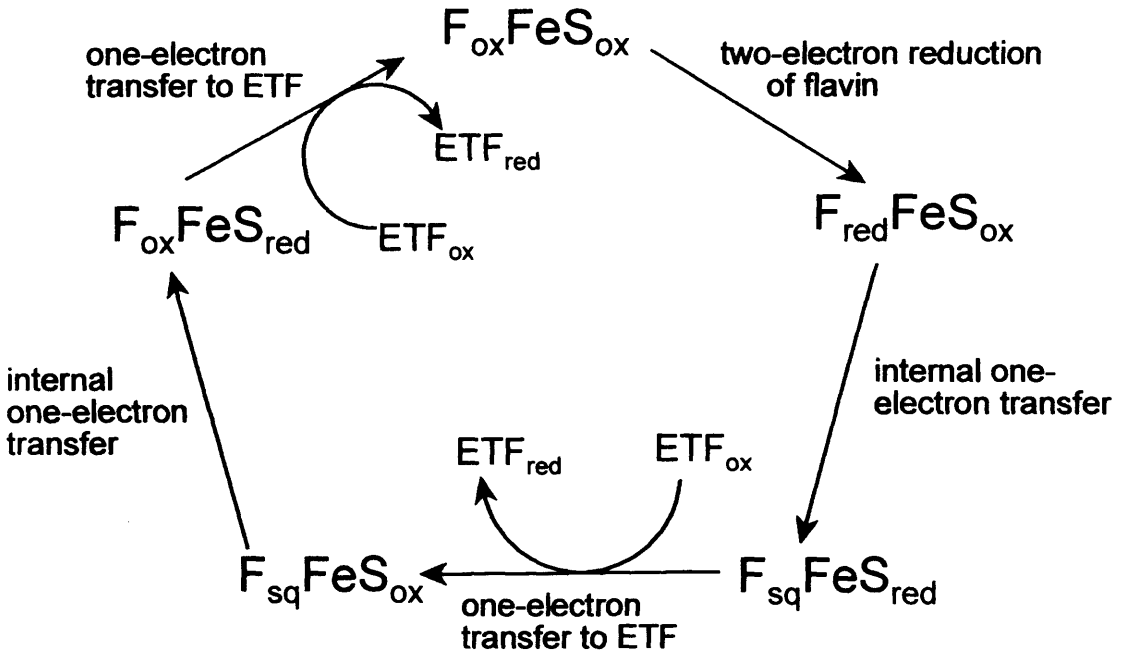

B

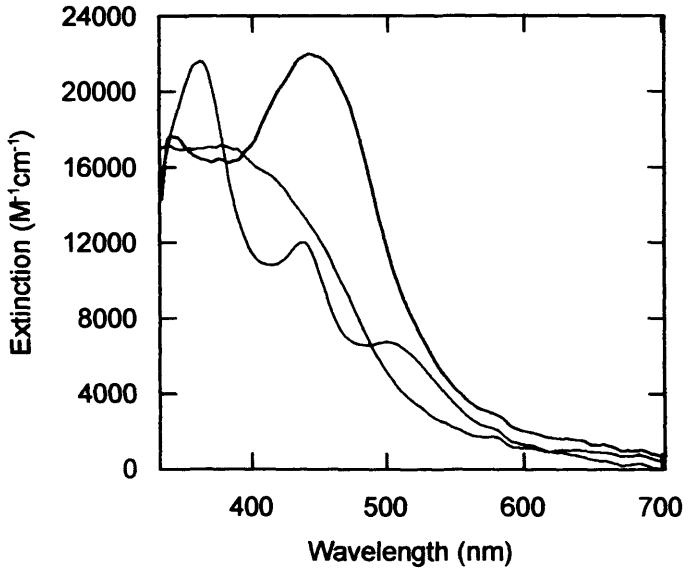

Figure 1.10: Reaction cycle of TMADH and spectral properties of enzyme intermediates. A. TMADH reaction cycle. F = 6-*S*-cysteinyl FMN, FeS = iron-sulphur centre, ETF = electron transferring flavoprotein. Ox = oxidised, red = reduced, sq = semiquinone. B. Spectral intermediates of TMADH. Black line = oxidised spectrum. Red line = 2-electron reduced TMADH with hydroquinone FMN and oxidised 4Fe-4S centre. Blue line = 2-electron reduced TMADH with semiquinone FMN and reduced 4Fe-4S centre.

1000 s^{-1} pH 8.5 at 10 °C (Jang *et al.*, 1999a), which presents difficulties even when monitored by stopped-flow spectroscopy.

The intermediate and slow phases of the TMADH reductive half-reaction are both monitored within the biphasic increase in absorbance at 365 nm associated with formation of anionic flavin semiquinone (Falzon & Davidson, 1996a). The faster of the two phases provides the value for k_{int}, while the slower of the two phases provides the value of k_{slow}.

The second phase of the reductive half-reaction, k_{int}, reflects internal electron transfer in TMADH (Rohlfs & Hille, 1994). In the presence of substrate, the rate of this electron transfer is unusually slow (Steenkamp *et al.*, 1978c), considering that the two redox centres of TMADH are separated by only 4 Å and that electron transfer can occur over much larger distances than this (Wilson *et al.*, 1995). In the overall kinetic scheme of TMADH, this internal electron transfer is the rate-limiting step. However, pH-jump studies in the absence of substrate have shown that the rate of internal electron transfer is intrinsically very rapid (Rohlfs & Hille, 1991). It is clear that the presence of substrate in the active site affects internal electron transfer. This has led to the proposal that the decay to product of a substrate-flavin adduct, formed during k_{fast}, is responsible for gating intramolecular electron transfer to the 4Fe-4S centre (Rohlfs & Hille, 1994). The initial decay of the substrate-flavin adduct is proposed to lead to the formation of a dimethylimminium which remains bound non-covalently within the active site of TMADH at the end of k_{fast}.

The extent to which k_{int} and k_{slow} contribute to the kinetic trace obtained at 365 nm is dependent on substrate concentration (Falzon & Davidson, 1996a). The amplitude of the phase by which k_{int} is determined decreases as substrate concentration increases, while that by which k_{slow} is measured increases until, at high TMA concentrations, the 365 nm trace is dominated by k_{slow}. Freeze-quench EPR studies have demonstrated that processes occurring in the slow kinetic phase are responsible for full development of the spin-interacting state (Steenkamp & Mallinson, 1976). Because the development of the spin-interacting state requires the presence of substrate at the active site of the enzyme, k_{slow} is thought to represent the dissociation and/or hydrolysis of the dimethylimminium ion within the substrate binding site of TMADH, followed by the binding of a second TMA molecule (Rohlfs & Hille, 1994).

1.1.10.4 Investigations of the Fast Phase of the Reductive Half-Reaction

At high substrate concentrations the majority of the spectral change associated with FMN reduction is lost in the dead-time of stopped-flow apparatus. Therefore, in order to observe flavin reduction at a rate that is more informative, the reductive half-reaction of TMADH has been studied with diethylmethylamine (DEMA), a substrate with which limiting rate constants were found to be 540 s^{-1} at pH 8.5, 25 °C (Rohlfs & Hille, 1994). The use of slower substrates as alternatives to TMA, or the production of active site mutants of the enzyme has revealed much information about the fast phase of the TMADH reductive half-reaction.

pH dependence studies of k_{fast} have been conducted over the pH range 6-11 with both DEMA and TMA (Rohlfs & Hille, 1994; Jang *et al.*, 1999a). The pH dependence of k_{lim}/K_d[1], is bell-shaped, with pK_a's of around 9.3 and 10, attributed to a basic residue in the active site and the ionisation of substrate respectively. The pK_a value of 9.3 is thought to represent the ionisation of Tyr-60, one of the residues involved in the binding of substrate. The k_{lim} versus pH plot produced from studies of the native enzyme with TMA is approximately sigmoidal, and suggests a single ionisation of pK_a value of 7.1, which is thought to show the ionisation of an active site base. This pK_a value is difficult to assign because of the very fast flavin reduction rates using TMA at this pH. However, what is clear from pH dependence studies of TMADH is that substrate must be protonated in order to bind to the enzyme, consistent with the role of cation-π bonding, and that an ionisable group on the enzyme is involved in substrate binding. In addition, the low pH asymptote drawn from the k_{lim} versus pH plot is non-zero, indicating that the basic residue with a pK_a value of 7.1 is involved, but not strictly required, for catalysis (Jang *et al.*, 1999a).

Recently, the pH dependence studies above have been combined with mutagenic studies to identify the 'critical' active site base in TMADH (Basran *et al.*, 1999c; Basran *et al.*, 1999a). Although Tyr-60 has been thought to be the most likely candidate, there are a total of four candidate residues that could fulfil this role: three tyrosine residues (numbers 60, 169 and 174) and one histidine residue (172), which are all either near to, or accessible to the substrate via rotation of a side chain (Jang *et al.*, 1999a). Tyr-169 and His-172 are part of a Tyr-His-Asp triad in the active site of TMADH, with the asparagine residue of this triad located at position 267. The proximity of this triad close to the pyrimidine ring of the flavin isoalloxazine ring is

[1]The ratio k_{lim}/K_d reports on the reaction between free enzyme and substrate, while the pH dependence of k_{lim} tracks the formation of the Michaelis complex.

thought to influence the mechanism of electron transfer from substrate to flavin, as described in the following section (1.1.10.5).

In order to better characterise the pH dependence of the fast phase of the reductive half-reaction, pH dependency studies have been repeated with perdeuterated TMA and active site mutants of TMADH (Basran *et al.*, 1999c; Basran et al., 1999a). The studies with perdeuterated TMA have revealed the presence of ionisations with pK_a values of 6.5 and 8.4 in the k_{lim} versus pH plot. The pK_a value of 8.4 has been assigned to the ionisation of His-172 in the Michaelis complex, because this ionisation is absent in a His-172→Gln mutant (H172Q) (Basran *et al.*, 1999c). The two ionisations in the k_{lim} versus pH plot are also clearly resolved in another mutant form of TMADH, in which Tyr-169 has been replaced by phenylalanine (Y169F) (Basran *et al.*, 1999a). The origin of the pK_a value of 6.5 is at present unclear. However, it is apparent that Tyr-169 and His-172 are not the 'critical' active site base, and preliminary studies of the Y60F mutant indicate that Tyr-60 does not provide the ionisation seen at pK_a 9.3 in the k_{lim}/K_d versus pH plot.

1.1.10.5 Investigations of the Intermediate and Slow Phases of the Reductive Half-Reaction

The rate constant of the intermediate phase is controlled by an ionisable group with a pK_a of 7.3 (Rohlfs & Hille, 1994), which is thought to represent one of the four active site bases identified from the crystal structure of TMADH. The equilibrium distribution of electrons between the FMN and 4Fe-4S centre, at the end of the intermediate phase, is controlled by an ionisable group with a pK_a of approximately 6, which is thought to be due to ionisation at the N-1 position of the flavin ring (Rohlfs & Hille, 1994). At the conclusion of the intermediate phase it is envisaged that TMADH contains non-covalently bound product with an equilibrium distribution of reducing equivalents between FMN and 4Fe-4S that is influenced by the ionisation of the flavin hydroquinone N-1.

The slow kinetic phase represents additional processes that result in full formation of the spin-interacting state subsequent to intramolecular electron transfer. At pH ~ 7.5, the kinetic difference spectrum for the slow kinetic phase is identical to that observed for the intermediate kinetic phase, implying that electron transfer is also taking place during this phase. Therefore, not all of the 4Fe-4S centres are reduced at the conclusion of the intermediate phase and during the slow kinetic phase there is a shift in the distribution of reducing equivalents between the FMN and 4Fe-4S centre towards the further reduction of the iron-sulphur centre (Rohlfs & Hille, 1994).

pH-jump stopped-flow experiments have been used to demonstrate that intramolecular electron transfer in TMADH is not intrinsically rate-limiting in catalysis and is under prototropic control (Rohlfs *et al.*, 1995). The prototropic control of electron transfer is exerted at the level of the flavin. In electron transfer reactions under prototropic control, nuclear motion (i.e. protonation) must occur prior to electron transfer because electron transfer is much more rapid than any nuclear motion of the reactants, and the deprotonation/protonation reactions are not lost in the dead-time of the stopped-flow apparatus. The observed rate constants fall into the range 230 s^{-1} to 1200 s^{-1}, depending on the pH-jump conditions used; in all cases these values are significantly faster than the rates of internal electron transfer measured by stopped-flow studies with TMA. These results support the conclusion that internal electron transfer is controlled by the decay of a covalent flavin-substrate adduct.

The factors that influence the formation of the spin-interacting state have also been investigated (Rohlfs *et al.*, 1995). pH-jump studies were employed to study the interconversion of three states of TMADH in H_2O and D_2O; the three states were hydroquinone-oxidised 4Fe-4S (formed at pH 6), flavin semiquinone-reduced 4Fe-4S (formed at pH 8), and spin-interacting state (formed at pH 8). These forms of TMADH were formed in the absence of substrate. The kinetics were found to be consistent with a reaction mechanism that involves sequential protonation/deprotonation and electron events. At least three protonation/deprotonation events are associated with internal electron transfer, with pK_a values of 6, 8 and 9.5. The pK_a's at 6 and 8 represent deprotonation of hydroquinone and flavin semiquinone respectively, while the pK_a at 9.5, which controls the formation of the spin-interacting state was originally assigned to an unknown active site base. Following the production of a Y169F mutant of TMADH (Basran *et al.*, 1999a), the unknown active site base was identified as Tyr-169, one of the residues in the triad of TMADH that consists of Tyr-169, His-172 and Asp-267 (Section 1.1.8.3).

EPR studies of the Y169F mutant demonstrated that its ability to form the spin-interacting state is substantially compromised when reacted with excess substrate at pH 7.0 and pH 10 (Basran *et al.*, 1999a). Unlike native enzyme, this mutant can also be reduced to the level of three electrons by dithionite titration in the presence of the substrate analog TMAC. It has been inferred from the absorption spectrum that this is due to perturbation of the redox potential of the enzyme. From these results, the role of Tyr-169 has been rationalised in terms of the structure of the enzyme. The phenolic ring of Tyr-169 is positioned close to the C-2 carbonyl group of the flavin ring where it is in van der Waals contact with the flavin. On binding of substrate or

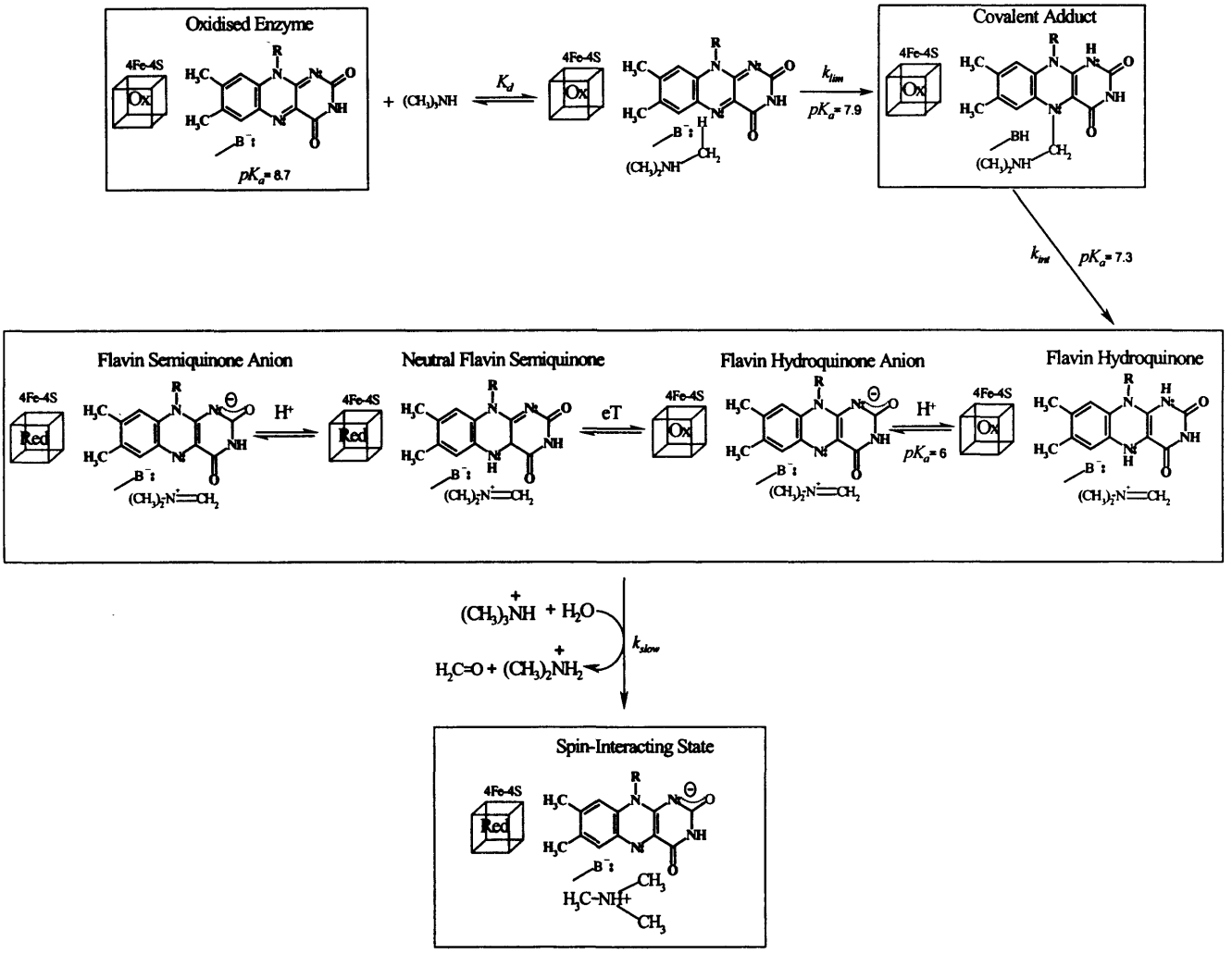

Figure 1.11: Proposed mechanism for the reductive half-reaction of TMADH. Spectroscopically identifiable enzyme species are indicated in boxes. Ox = oxidised, Red = reduced, eT = electron transfer, B= active site base. Reproduced from Rohlfs and Hille, 1994.

TMAC to 2-electron reduced TMADH, the hydroxy group of Tyr-169 is deprotonated and the negative charge redistributes the electron density in the flavin by electrostatic repulsion, in effect 'pushing' electrons towards the 4Fe-4S centre. This redistribution of electron density reduces the spin-spin distance and favours formation of spin-interacting state.

1.1.10.6 The Oxidative Half-Reaction

The oxidative half-reaction of TMADH involves the interaction with, and electron transfer to, its physiological redox partner, ETF (Chen & Swenson, 1994). Electron transfer from the reduced 4Fe-4S centre of TMADH to the FAD of ETF can be conveniently studied by stopped-flow spectroscopy (Huang *et al.*, 1995). However, the reaction of ETF with two-electron dithionite-reduced enzyme is complicated by multiphasic kinetics. Studies can be simplified by inactivating the 6-*S*-cysteinyl FMN by treatment with phenylhydrazine, which places a phenyl group on the C-4a atom of the flavin, rendering it inert and unable to accept electrons (Nagy *et al.*, 1979). Therefore, treatment of phenylhydrazine-inactivated TMADH with dithionite produces enzyme that is reduced by one electron solely at the 4Fe-4S centre. Rapid mixing of this form of TMADH with ETF gives rise to a biphasic transient. The fast phase of this reaction reports on interprotein electron transfer, and is dependent on ETF concentration. The origin of the slow phase is as yet uncertain (Huang *et al.*, 1995). A limiting rate of 172 s^{-1} and K_d for the complex of 10 μM has been calculated for the TMADH:ETF complex, which is similar to that measured by sedimentation equilibrium methods for oxidised TMADH and ETF (Wilson *et al.*, 1997b). The value of the limiting rate constant shows that external electron transfer is not rate-limiting in overall catalysis.

The approximate site of interaction between TMADH and ETF has been determined from the crystal structure of the enzyme and site-directed mutagenesis studies of the proposed pathway of electron transfer (Wilson *et al.*, 1996). The target residues for mutagenesis were Tyr-442 and Val-344. Tyr-442 is located at the centre of a large concave region at the surface of TMADH,with an area of 1200 ^{2} which is probably the docking site for ETF. The phenyl hydroxyl of Tyr-442 is 11.6 from the closest iron of the 4Fe-4S centre. The residue is located along one side of a small surface indentation, the bottom of which is occupied by residue Val-344. Val-344 is the closest of the surface residues to the 4Fe-4S centre of TMADH, being in Van der Waals contact with Cys-345 (a cysteinyl ligand of the 4Fe-4S centre). These two

residues have therefore proved to be attractive targets for mutagenic investigation of the TMADH:ETF interaction.

Mutation of Tyr-442 of TMADH illustrates that this residue is implicated in assembly of the TMADH:ETF complex, although its precise role has to be determined. Mutating Tyr 442 to Phe Leu, Cys or Gly, causes major reductions in the rate of electron transfer to ETF, but not to ferricenium hexafluorophosphate, Fc^+ (Wilson *et al.*, 1997a; Basran *et al.*, 2000). Val–344 has also been the subject of multiple mutations, to Ala, Cys, Gly, Ile and Tyr. The introduction of smaller side chains at position 344 leads to enhanced rates of electron transfer to Fc^+, while the introduction of large side chains (isoleucine and tyrosine) substantially reduces the rate of electron transfer to Fc^+. Conversely, mutation of Val-344 does not affect electron transfer to ETF, suggesting that electrons transfer either via, or close to Tyr-442 and Val-344, and that the size of the electron acceptor can influence whether transfer is favoured by the tyrosine or the valine residues (Basran *et al.*, 1999b). Fc^+, which is small, appears to receive electrons via Val-344, while ETF cannot access Val-344, so receives electrons via Tyr-442. The effect of mutating Tyr-442 on electron transfer to ETF might be due to direct disruption of the electron transfer pathway, or a perturbation of the interaction between ETF and TMADH in the productive electron transfer complex leading to less efficient coupling between the redox centres.

No structure for ETF is available, although crystals have been isolated (White *et al.*, 1994). In the absence of a crystal structure, a homology model for ETF has been constructed, based on the crystallographic co-ordinates for human ETF, with which *M. methylotrophus* ETF shares 31 % homology (Chohan *et al.*, 1998). In this model, ETF is seen to consist of three domains, which comprise two subunits. The possible interaction of ETF with TMADH has also been modelled. The structural model of ETF suggests that it possesses domain flexibility and is able to adopt two conformations relative to its main function: an eT-inactive (non-complexed) and eT-active (complexed) form. An accumulation of kinetic evidence appears to support an argument for a conformational change in ETF. Stopped-flow reoxidation studies of ETF have demonstrated that flavin reoxidation is slow, suggesting that conformational gating occurs for electron transfer in this instance. More recent studies (Jang *et al.*, 1999b) have shown that when reduced TMADH and ETF form a complex it is possible to reduce ETF to the hydroquinone form, which has previously been only achieved by dithionite titration. Formation of the hydroquinone ETF is sluggish, and probably does not occur *in vivo*, but this work again supports the suggestion that

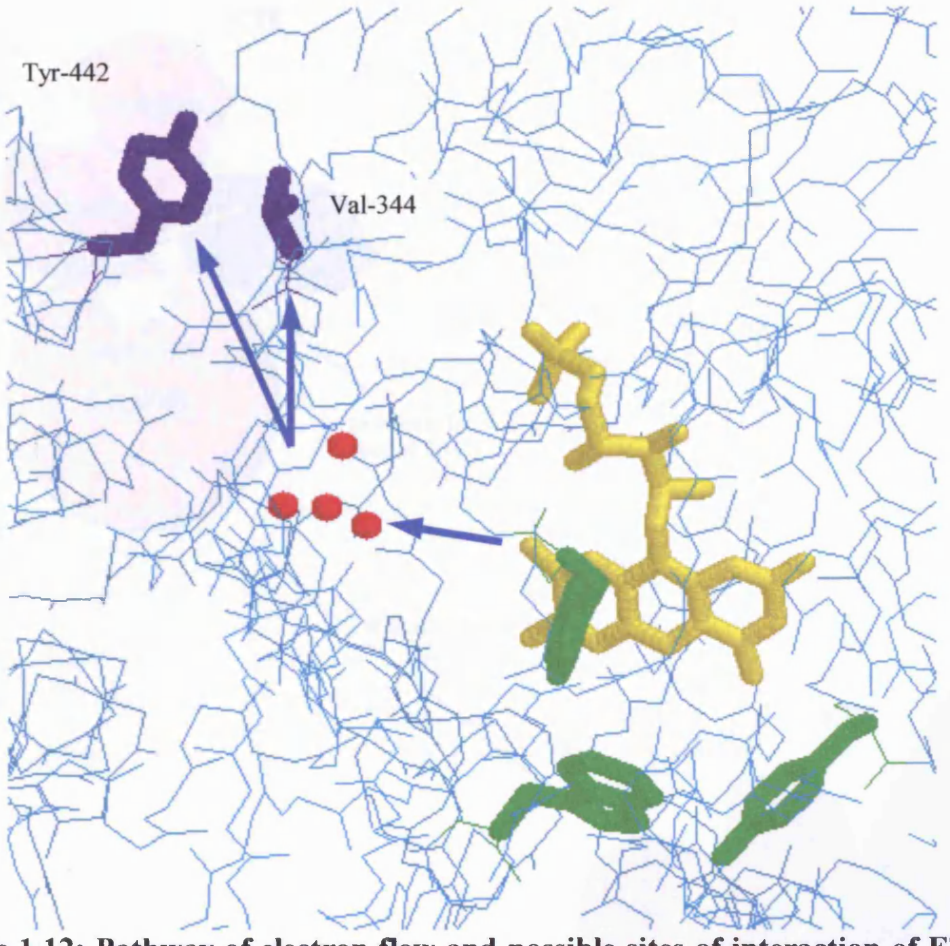

Figure 1.12: Pathway of electron flow and possible sites of interaction of ETF in TMADH. Movement of electrons from 6-*S*-cysteinyl FMN to the 4Fe-4S centre is most likely to be via the 8α methyl of flavin. External electron transfer from TMADH is through either tyrosine-442 or valine-344, depending on the electron acceptor. ETF has been shown to couple via Val-344, while the artificial electron acceptor Fc^{+} favours coupling through Tyr-442.

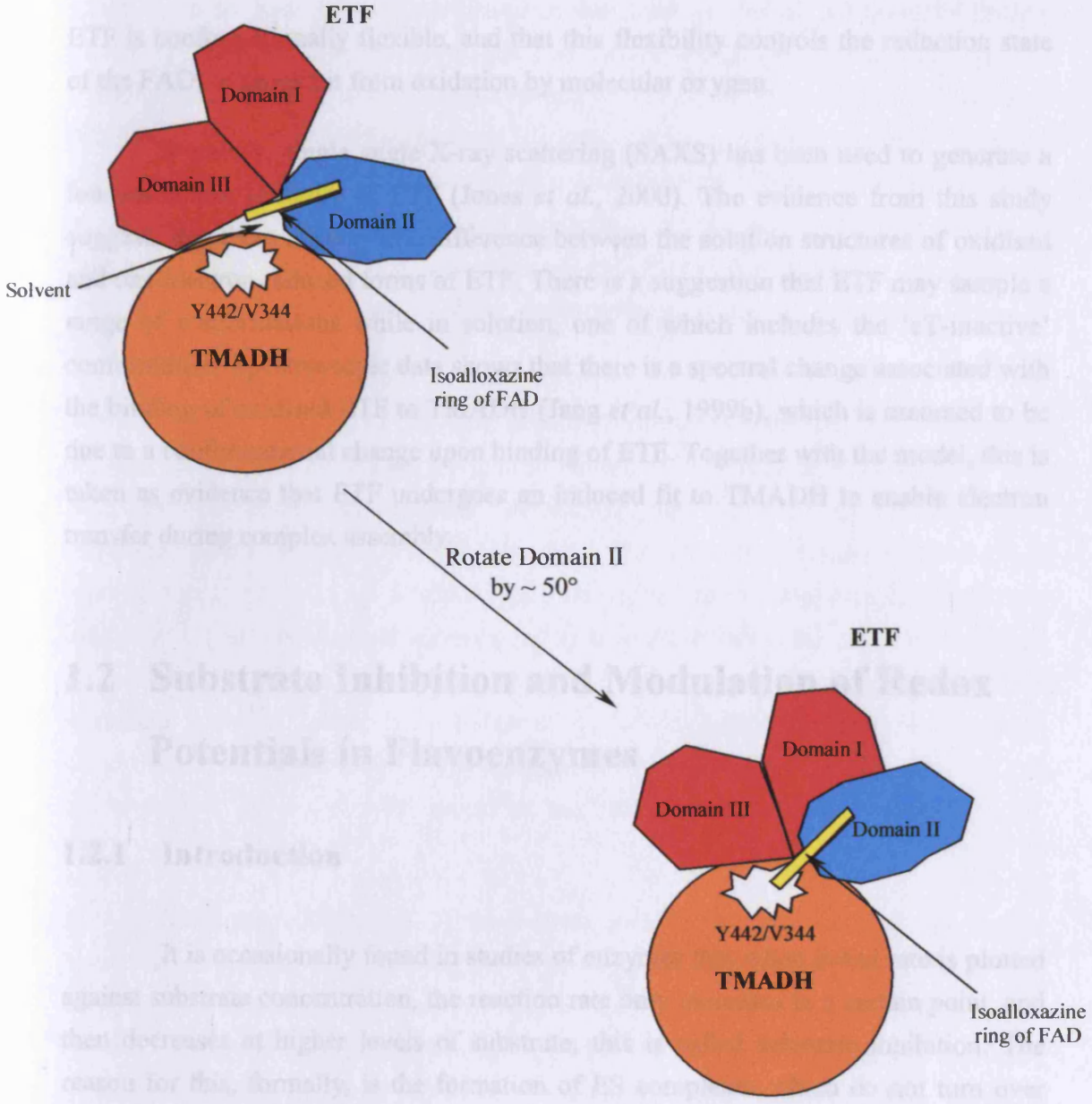

Figure 1.13: Schematic representation of TMADH-ETF interaction in the oxidative half-reaction of TMADH. A. 'Inactive' complex, with electron transfer to ETF-bound FAD impeded. B. 'Active' complex, with electron transfer to FAD accomplished. Adapted from (Chohan *et al.*, 1998).

ETF is conformationally flexible, and that this flexibility controls the reduction state of the FAD, or protect it from oxidation by molecular oxygen.

Recently, single angle X-ray scattering (SAXS) has been used to generate a low resolution structure of ETF (Jones *et al.*, 2000). The evidence from this study suggests that there is very little difference between the solution structures of oxidised and one-electron reduced forms of ETF. There is a suggestion that ETF may sample a range of conformations while in solution, one of which includes the 'eT-inactive' conformation. Spectroscopic data shows that there is a spectral change associated with the binding of oxidised ETF to TMADH (Jang *et al.*, 1999b), which is assumed to be due to a conformational change upon binding of ETF. Together with the model, this is taken as evidence that ETF undergoes an induced fit to TMADH to enable electron transfer during complex assembly.

1.2 Substrate Inhibition and Modulation of Redox Potentials in Flavoenzymes

1.2.1 Introduction

It is occasionally found in studies of enzymes that when initial rate is plotted against substrate concentration, the reaction rate only increases to a certain point, and then decreases at higher levels of substrate; this is called substrate inhibition. The reason for this, formally, is the formation of ES complexes which do not turn over (Sinnot *et al.*, 1998). The substrate inhibition of TMADH by TMA forms the basis of the investigation in Chapter 3 of this thesis and presents an opportunity to discuss what is a fairly neglected aspect of enzyme catalysis, despite being one of the most commonly observed deviations from Michaelis-Menten kinetics (Gutfreund, 1965; Fersht, 1985; Kuhl, 1994).

Substrate inhibition can arise for a number of reasons. Substrate can combine as a dead-end inhibitor with an enzyme form with which it is not supposed to react, causing total substrate inhibition in which the rate goes to zero at infinite inhibitory substrate concentration (Boyer, 1970). If high levels of substrate cause an altered addition of reactants or in any other way generate an altered reaction pathway, partial substrate inhibition is observed (Cleland, 1979). In addition, the substrate may

combine at an allosteric site and cause either total or partial substrate inhibition. Levels of substrate above the middle millimolar range may cause non-specific inhibition as a result of increased ionic strength, or a higher level of toxic counterions (Cleland, 1979). If one of the reactants is water, a very high concentration of substrate effectively leads to a reduction in water concentration. This is seen with certain enzymes in the presence of large concentrations of sucrose or alcohol (Dixon & Webb, 1979). Finally, the presence of inhibitory contaminants in substrate preparations will lead to errors in the determination of kinetic constants (Dixon & Webb, 1979; Tipton, 1996).

A particular case of substrate inhibition can arise if the true substrate for the enzyme is a substrate-activator complex (Tipton, 1996). This is frequently the case with metal-ion dependent enzymes. For example, the Mg-ATP complex is the true substrate for many kinases (MacRae & Segel, 1999). If the uncomplexed substrate can bind to the enzyme as an inhibitor, this will give rise to apparent high-substrate inhibition unless experiments are designed to ensure that the metal ion concentrations are adequate to allow the substrate to remain complexed as its concentration is increased. A similar balance of substrate ratios for a two-substrate enzyme appears to be applicable for soybean lipoxygenase-1, which is inhibited by linoleic acid, but can be restored to full activity by increasing the concentration of oxygen (Berry *et al.*, 1997).

Substrate inhibition is in most cases considered to be a non-physiological phenomenon (Boyer, 1970; Cleland, 1979; Kuhl, 1994), and is thus seen in the normal physiological direction of a reaction only at levels of substrate considerably above those found in the cell (Cornish-Bowden, 1995). In the non-physiological direction, substrate inhibition is thought to be more relevant. A well known example, although arguments exist as to its physiological significance (Ureta, 1978), is the formation of enzyme-pyruvate:NAD^+ abortive complexes in heart (H_4) lactate dehydrogenase (Boyer, 1970; Eszes *et al.*, 1996). This is thought to be a strategy that favours production of lactate to pyruvate in the heart. In this way, the heart can aerobically channel pyruvate into metabolism (Mathews & van Holde, 1990). Kuhl argues that substrate inhibition is more physiologically relevant than is otherwise appreciated and proposes the concept of 'allochrony' as an explanation of substrate inhibition in enzymology and high-dose inhibition in pharmacology (Kuhl, 1987; Kuhl, 1994). This theory rests upon the importance of a recovery period between product dissociating from the active site of an enzyme and the binding of fresh substrate. Under conditions of high substrate the minimum period of non-occupancy of the

active site is not satisfied and substrate molecules combine with the 'wrong' isomeric form (inactive or less active) of the enzyme.

1.2.2 Substrate Inhibition: Theory

Substrate inhibition gives rise to a range of behaviour, depending on the mechanism of the enzyme system affected. Although substrate inhibition can be a nuisance to kineticists trying to determine kinetic patterns, it is considered to be one of the best diagnostic tools for studying mechanisms (Boyer, 1970; Cleland, 1979). Hence, a range of characteristic kinetic plots and equations for analysis are produced for single-substrate enzymes, and those which utilise sequential or ping-pong mechanisms (Dixon & Webb, 1979; Cleland, 1979; Tipton, 1996).

1.2.2.1 Total Substrate Inhibition

Substrate inhibition is found most commonly in enzymes with two or more substrates. This allows study of the phenomenon by varying a non-inhibitory substrate at differing high levels of the inhibitory one and see whether the slopes, intercepts, or both, of the reciprocal plots show the inhibitory effect. These are called competitive, uncompetitive and non-competitive substrate inhibition, respectively. In general, the likelihood of recognising whether substrate inhibition is occurring is determined more by the range of data plotted than the type of plot (Cornish-Bowden, 1995).

Competitive substrate inhibition is characteristic of classic ping-pong mechanisms (Boyer, 1970). Substrate inhibitions other than competitive will be rare in ping-pong mechanisms (Cleland, 1979). In a ping-pong mechanism, the enzyme oscillates between two stable enzyme forms, E and F for example, which react with substrates A and B respectively (Figure 1.14). In aminotransferases, E and F would be pyridoxal-enzyme and pyridoxamine-enzyme respectively (Cleland, 1979). As represented, substrate A is shown reacting only with E, and B only with F. If substrate B is also able to combine with enzyme form E, a competitive effect is seen and gives characteristic reciprocal plots with increasing concentration of B, the inhibitory substrate (Figure 1.14) (Boyer, 1970; Tipton, 1996). As can be seen, the lines, instead of being parallel as expected for the ping-pong mechanism (Fersht, 1985), show slopes that increase in a linear fashion with B.

If substrate A can sometimes combine with enzyme form F in dead-end fashion, double competitive substrate inhibition arises, although this is thought to be

more applicable for the non-physiological direction of a reaction. On a Lineweaver-Burk plot this is manifested in a 'wild but very characteristic pattern' (Boyer, 1970) (Figure 1.14). Analysis of such data to extract the values of all kinetic constants apparently presents no special problems (Boyer, 1970; Cleland, 1979).

Uncompetitive substrate inhibition is the expected pattern for ordered sequential mechanisms of the type illustrated in Figure 1.14 and occurs when the second substrate B can combine in dead end fashion with the EQ as well as the EA complex. In this case the EBQ complex can only break down to give EQ and B, i.e., the release of Q is prevented. In the resulting initial velocity pattern, the slopes decrease with B as expected, but go through a minimum and then increase again at high B levels. Plotting the intercepts versus B concentration thus produces a hyperbola. This type of inhibition is seen in several pyridine nucleotide linked dehydrogenases. For example, with pig heart isocitrate dehydrogenase, inhibition is non-competitive versus α-ketoglutarate, showing that CO_2 (or bicarbonate) combines as a dead end inhibitor at the nucleotide site (Boyer, 1970; Cleland, 1979).

In single-substrate enzymes, substrate inhibition is manifested in Lineweaver-Burk plots as an upward curvature at low values of 1/[S]. This is seen for example with hydrolysis of D-fructose, 1,6 bisphosphate (FBP) catalysed by fructose bisphosphatase; upward curvature of the plots takes place at FBP concentrations of >0.1 mM (Price & Steven, 1982). A 'classical' explanation for this is a combination of two substrate molecules each getting part of themselves stuck in part of the active site, leading to formation of a dead-end ES_2 complex (Boyer, 1970; Dixon & Webb, 1979; Cleland, 1979). However, it can also occur if product release is ordered, as is common for some hydrolytic enzymes, where the reaction is ping-pong with water as the second substrate. These mechanisms can be told apart by running a product inhibition experiment in which A is varied over a wide concentration range at several fixed levels of product, P (Boyer, 1970; Cleland, 1979).

1.2.2.2 Partial Substrate Inhibition

Partial substrate inhibition, i.e., producing finite rate at infinite substrate concentration, can result from allosteric combination of the substrate. An example of this is the inhibition of 2,3-dihydroxybiphenyl 1,2 dioxygenase by binding of substrate, 2,3-dihydroxybiphenyl, at an auxiliary substrate binding site (Vaillancourt *et al.*, 1998). However, partial substrate inhibition more commonly represents some randomness in the mechanism. For example in the glutamate dehydrogenase reaction, α-ketoglutarate shows partial uncompetitive inhibition versus ammonia which is due

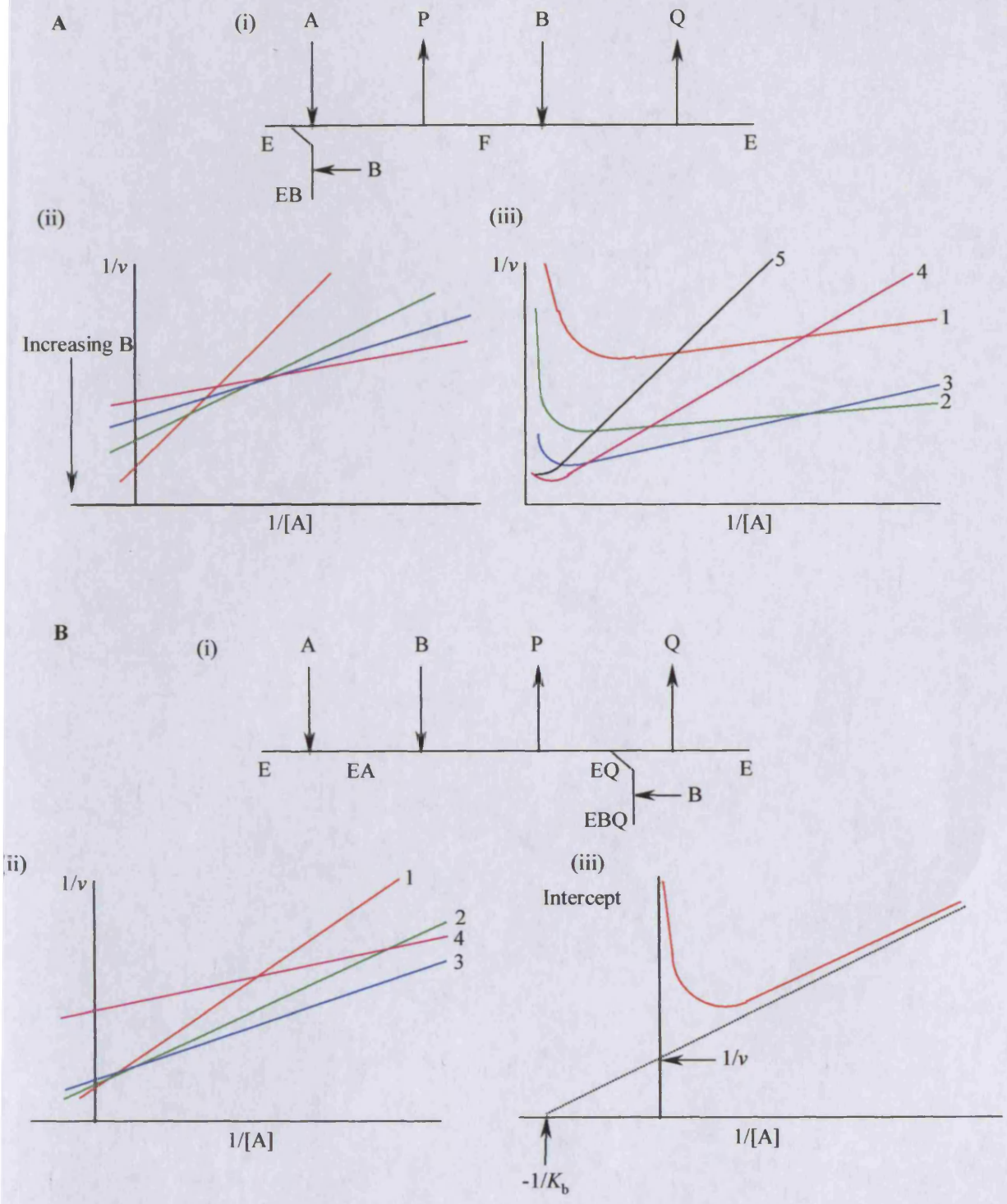

Figure 1.14: Manifestation of substrate inhibition in different types of enzyme-catalysed reactions: A. Ping-pong mechanism; (i) representation of mechanism; (ii) with competitive inhibition and (iii) with double-competitive inhibition. B. Ordered sequential mechanism; (i) representation of mechanism; (ii) with uncompetitive substrate inhibition and (iii) plot of the intercepts from B(ii).

to a four-fold reduction in the release of NAD when α-ketoglutarate is present (Cleland, 1979).

1.2.2 Control of Flavoproteins by Modification of Flavin Redox Potentials

It has frequently been pointed out that flavoenzymes have an important role in metabolism, operating at the interface between obligate two-electron donors and one-electron acceptors (Singer & Edmondson, 1978). They therefore present potential points for metabolic control and there is some evidence to suggest that substrate and product binding acts on certain flavoenzymes so as to stabilise a certain redox state of the flavin, modulating electron flow through respiratory or oxidative chains (Tegoni *et al.*, 1986).

An early model suggesting modulation of redox equilibria as a means of regulation was proposed by Sligar and Gunsalus (Sligar & Gunsalus, 1976) for the reaction of flavocytochrome P-450 with camphor. Flavocytochrome P-450 from *Bacillus megaterium* is a 119 kD protein whose haem and diflavin domains are fused to produce a fatty acid monooxygenase. Electron flow to the haem iron in P-450cam is known to be controlled by a camphor-dependent increase in the redox potential of the haem iron, measured as -303 mV (substrate free) to -173 mV (camphor bound). Recently (Daff *et al.*, 1997), it has been demonstrated that the increase in redox potential caused by the binding of fatty acids to the active site of the enzyme prevents the futile cycling of electrons from the electron donor NADPH.

There are a number of examples of substrate product binding modulating or altering the redox potentials of flavin cofactors in enzymes. Mitochondrial succinate dehydrogenase is an important metabolic enzyme that is subject to rigorous regulation, mostly positive, by way of substrates, anions, reduced quinone, ATP and reduction. The single negative modulator is oxaloacetate. This inhibition has been investigated and it has been shown that flavin redox potential in free enzyme is -3 mV, high enough to allow reduction by succinate, whereas with oxaloacetate bound it is -196 mV, too low to be reduced by substrate (Gutman, 1977). Oxaloacetate binding takes place preferentially to the oxidised form of the enzyme and appears to depress turnover activity in this enzyme. In the flavoenzyme NADH:cytochrome b_5 reductase in the presence of NAD^+, binding of the 'product' stabilises the fully

reduced form of the enzyme and depresses turnover. The value of the redox potential of the E-FAD/E-FADH—NAD^+, shifts from 195 mV to 115 mV in the presence of excess NAD^+. Hence the semiquinone state is stabilised by NAD^+ (Iyanagi *et al.*, 1984). Pyruvate binds preferentially to the semiquinone from of yeast cytochrome b_5 with a concomitant shift in the midpoint potentials corresponding to the one-electron flavin couples (Tegoni *et al.*, 1986). The K_m for pyruvate in oxidised enzyme is 8 mM, which drops to 0.4 mM for the semiquinone form.

Tegoni (Tegoni *et al.*, 1986) suggests that redox potential modulation could be a type of regulation effective for the whole class of enzymes in which a semiquinone intermediate is an obligatory enzyme species. Similarly, for those flavoenzymes in which the one-electron reduced form of flavin has no functional activity, it is suggested that a similar type of control is exerted by substrate that favours two-electron transfer via changes for midpoint potentials of flavin couples.

How could ligand binding affect the redox properties of flavin? It is well documented that flavoenzymes control the reactivity of the isoalloxazine ring by providing specific interactions with the protein, giving rise to a wide range of redox potentials (Singer & Edmondson, 1978; Palfrey & Massey, 1998). One means by which this could be achieved is by the imposition of bent geometries on flavin by the protein-binding environment (Hasford *et al.*, 1997; Massey & Hemmerich, 1980). Another means is by fine-tuning the flavin chemistry. In free solution, the sites of highest charge density of oxidised flavin and the radical anion are N(1)/O(2α) and N(5) respectively. These are the sites which are susceptible to the effects of any kind of electrophile which decreases the net charge density at a given site, whether by an ionic, or sigma-covalent bond, or a H-bond. These electrophilic effects are referred to as 'blocking' effects. Hemmerich *et al.* (Hemmerich & Massey, 1982) have characterised the general requirements for thermodynamic stabilisation of redox states in protein bound flavin by blocking. If a lone pair in the flavin radical anion is blocked at position 1/2α, the corresponding neutral radical is destabilised in favour of the oxidised or 2-electron reduced states. On the other hand, if a lone pair at position 5 is blocked, the corresponding neutral radical is stabilised at the expense of the oxidised and fully reduced state.

The preferential binding of oxaloacetate to oxidised succinate dehydrogenase was earlier presented as an example of ligand binding stabilising a particular redox state of a flavoenzyme. The precise mechanism by which the shift in redox potential of 200 mV is brought about has been treated by (Gutman, 1977). In active protein, the high reduction potential and two electron reduction of succinate to fumarate is

accounted for by a positive charge between the flavin and apo-protein at position 1/2α. The non-active enzyme is in a configuration where the positive charge interacting with position 1/2α is lost and this configuration is stabilised by forming a very tight complex (K_d approximately 0.2 μM) with oxaloacetate. Displacement of oxaloacetate by binding of activators to a separate regulatory site of succinate dehydrogenase leads to restoration of enzyme activity, as the affinity of the enzyme for oxaloacetate falls (K_d approximately 400 μM). However, this is a slow transition characterised by a high energy of transition.

The effect of substrate binding on D-amino acid oxidase (Van den Berghe-Snorek & Stankovich, 1985) can also be accounted for if the effects of 'blocking' (Hemmerich & Massey, 1982) are invoked. This enzyme catalyses the oxidation of α-amino acids to the corresponding α-keto acid (Palfrey & Massey, 1998), accepting two electrons from substrate and transferring two electrons to molecular oxygen. In common with other flavoprotein oxidases (Palfrey & Massey, 1998), D-amino acid oxidase is able to stabilise the anionic semiquinone when reduced with an artificial electron donor in the absence of substrate, even though formation of this species is not part of the catalytic mechanism (Van den Berghe-Snorek & Stankovich, 1985). However, when benzoate, a substrate analog, is bound, the potential for the transfer of the first electron shifts (from -99 mV to -260 mV) so that it is more negative than the value for transfer of the second electron. Thus, the first electron is thermodynamically more difficult to transfer than the second electron, creating the conditions for two-electron transfer observed in the catalytic mechanism. At the time of this study, it was thought that an active site arginine residue near the 1/2α position of the flavin was responsible for the stabilisation of the anionic semiquinone; this was later shown to be the positive end of a helix dipole by Mattevi (1996). However, this does not alter the interpretation of results. Benzoate binding may neutralise the positive charge thus destabilising the ability of the enzyme to form semiquinone. Hence the mode of electron transfer (one electron versus two electron transfer) is regulated by substrate binding.

Hence, there is a body of fragmentary, but growing evidence of the effect that ligand binding has on redox potentials of enzyme-bound flavins. If the data can be shown to be related to the physiological concentrations of substrate or product, then it may be that a further level for the metabolic control of enzyme activity, particular to flavoenzymes, can be added to the standard textbook examples (Fersht, 1985) of allosteric effectors and covalent modification.

1.3 The Role of Hydrogen Tunnelling and Protein Dynamics During C-H Bond Cleavage in Enzymes

1.3.1 Introduction

Proteins are dynamic structures (Karplus & McCammon, 1986; Karpen & Brooks, 1996) and it is well documented that numerous enzymes undergo a range of conformational changes during ligand binding, allosteric regulation, or covalent modification (Stryer, 1988; Mathews & van Holde, 1990; Lehninger *et al.*, 1993). However, while the role of these fairly large-scale structural changes is understood, it has been argued that the role of intrinsic, small-scale, low frequency vibrations of proteins ('breathing') in enzyme catalysis have been somewhat less well appreciated (Karplus & McCammon, 1986; Gavish, 1986; Gutfreund, 1995). A hydrated protein has been described as resembling a highly associated viscous liquid (Gavish, 1986); over pico- to milli-second timescales (Brunori *et al.*, 1999; Gutfreund, 1995), the range of motions includes the movement of individual amino acid side chains, twisting of the polypeptide chain (Karplus & McCammon, 1986), and can lead to areas of localised viscoelasticity within the structural scaffold of the protein (Gavish, 1986). However, despite studies demonstrating a link between protein motion and enzyme function (Rasmussen *et al.*, 1992; Rudd *et al.*, 1994), a full qualitative and quantitative framework for catalysis that incorporates these observations has yet to be produced (Kohen & Klinman, 1999).

Recently, it has been shown that the dynamic properties of proteins are utilised by enzymes that catalyse the cleavage of carbon-hydrogen (C-H) bonds (Basran *et al.*, 1999d; Kohen *et al.*, 1999; Harris *et al.*, 2000). The critical aspect of these studies is that the transfer of hydrogen from reactant to product states does not proceed via a transition state at the top of a potential energy barrier to a reaction; instead hydrogen is transferred *through* the barrier, in a process termed 'tunnelling', a phenomenon arising from a quantum mechanical consideration of the movement of particles. Hydrogen-tunnelling (H-tunnelling) is a function of the transfer distance between donor and acceptor groups; protein dynamics facilitate tunnelling by (i) reducing the distance between these groups effectively reducing the width of a potential energy barrier, and (ii) equalising the energy states between reactants and products. Since, enzyme-catalysed hydrogen transfer is one of the most common of

biological reactions (Scrutton *et al.*, 1999), the utilisation of protein 'breathing' motions to facilitate tunnelling of hydrogen from the ground state of reactants ('extreme tunnelling'; (Basran et al., 1999d)) is an attractive mechanism for overcoming the inherent energetic difficulties of cleaving stable C-H bonds.

The purpose of this section is to provide an introduction to the way in which H-tunnelling in enzyme-catalysed reactions has been investigated since its discovery (Cha *et al.*, 1989), and explain how recent studies provide direct evidence for modern concepts of the role of protein dynamics in this process (Sutcliffe & Scrutton, 2000). This explanation has to include such subjects as transition state theory, quantum mechanics, and the origin and interpretation of kinetic isotope effects. However, despite the potential complexities of these subjects, there are good qualitative accounts of how the thermally enhanced motions of proteins promote C-H bond cleavage by H-tunnelling (e.g. see Kohen & Klinman, 1999; Scrutton *et al.*, 1999 and Sutcliffe & Scrutton, 2000)). This work is intended as a background to the work presented in Chapter 4, which forms part of ongoing investigations into the mechanism of C-H bond cleavage in TMADH.

1.3.2 Theories of Reaction Rates

1.3.2.1 Transition State Theory

Enzymes often catalyse rate enhancements in the range 10^7-10^{14} times faster than the equivalent uncatalysed reactions (Lehninger *et al.*, 1993). A widely-accepted explanation for this rate-enhancement is provided by transition state theory (TST) (Glasstone *et al.*, 1941; Kraut, 1988). TST is the 'textbook' version of how enzymes work and is probably popular because of the apparent simplicity in the presentation of the theory in a useful diagrammatic representation (Gutfreund, 1995).

In TST, the reaction coordinate is described by free energy minima for reactants and products, separated by a static potential energy barrier for activation (Figure 1.15). The basic assumption of TST is that the unidirectional rate k of a reaction $S \rightarrow P$ is a two-step process which can be written as follows:

$$S \rightleftharpoons X^{\ddagger} \rightarrow P$$

where $X^{\ddagger}$ is the so-called 'transition state' or 'activated complex', corresponding to the highest-energy intermediate structure that occurs microscopically during the

transition between S and P (Gavish, 1986). The substrate and product molecules have a number of independent capacities for holding energy: translational, rotational and vibrational, collectively referred to as 'degrees of freedom'; $X^{\ddagger}$ is assumed to be a molecular structure that differs from a normal one by the loss of one vibrational degree of freedom because all of the vibrational energy is converted into translational energy along the reaction coordinate (Gavish, 1986; Kyte, 1995). Central to TST is the *quasi-thermodynamic assumption* that the concentration of $X^{\ddagger}$ is in thermal equilibrium with the reactant (More O'Ferral, 1975; Gavish, 1986), leading to the quasi-equilibrium constant

$$K^{\ddagger} = \exp(-\Delta G^{\ddagger}/RT) \qquad \textbf{Equation 1.1}$$

where $\Delta G^{\ddagger}$ is the (Gibbs) free energy difference between the reactant and transition states. In its simplest version the first order rate constant for the decomposition of the ground state is given by

$$k = (kT/h) \exp(-\Delta G^{\ddagger}/RT) \qquad \textbf{Equation 1.2}$$

The Gibbs energy of activation may be separated into enthalpic and entropic terms by using another relationship from equilibrium thermodynamics,

$$\Delta G^{\ddagger} = \Delta H^{\ddagger} - T\Delta S^{\ddagger} \qquad \textbf{Equation 1.3}$$

where $\Delta H^{\ddagger}$is the enthalpy, and $\Delta S^{\ddagger}$ the entropy, of activation. The rate constant thus becomes

$$k = (kT/h) \exp(S^{\ddagger}/R) \exp(-\Delta H^{\ddagger}/RT) \qquad \textbf{Equation 1.4}$$

(A more rigorous approach includes a factor known as the transmission coefficient, but this is generally close to 1 so it may be ignored (Fersht, 1985; Gavish, 1986))

The importance of Equation 1.4 is that the rate of reaction is related only to the height of a static reaction barrier. TST explains much about reaction rates and enzyme catalysis; it has led to the widely accepted notion that enzymes are flexible molecular templates, designed by evolution to be complementary to the reactants in their activated transition-state geometry (Kraut, 1988; Kohen & Klinman, 1999). By stabilising the transition state relative to the ground state the concentration of species that occupy the transition state is increased and, in effect $\Delta G^{\ddagger}$ is decreased, greatly enhancing reaction rates (Kraut, 1988).

TST is backed up with some quite convincing evidence. For example the substrate binding site of lysozyme is complementary to the transition-state geometry

of the reaction (Stryer, 1988; Kraut, 1988) while serine proteases are inhibited by molecules that resemble the expected tetrahedral transition state for substrate hydrolysis (Kraut, 1988). In addition, transition state analogs are found to bind to enzymes with stronger affinities than the natural substrate; and antibodies with limited catalytic properties have been developed from transition state analog haptens (Kraut, 1988) (Kohen & Klinman, 1999). This has stimulated a great deal of research in predictions of transition state structures and enzyme inhibitors (Cleland, 1982; O'Leary, 1988; Schramm *et al.*, 1994; Berti, 1999). However, TST is probably an oversimplification when applied to enzyme catalysis (Sutcliffe & Scrutton, 2000); it was originally developed to account for gas phase reactions. Questions have been raised to the general applicability of TST, particularly to enzyme-catalysed reactions (Gavish, 1986; Gutfreund, 1995; Scrutton et al., 1999; Sutcliffe & Scrutton, 2000). These authors advocate an approach which takes solvent dynamics and the natural breathing of the protein molecules into account, and favour Kramers approach to the theory of reaction rates (Kramers, 1940).

1.3.2.2 Kramers Theory: An Alternative to TST

TST is the most widely accepted explanation for reaction rate enhancement by enzymes (Kraut, 1988). However, at the same time that TST was being developed by Eyring and co-workers (Glasstone et al., 1941), Kramers (Kramers, 1940) developed an alternative theory that recognises solvent dynamics.

In Kramers' theory, reactions can still be viewed in terms of a traditional reaction coordinate diagram (Figure 1.15) (Gavish & Werber, 1979; Gavish, 1986). In this case however, the act of the chemical reaction S $\rightarrow$ P is described by the process of diffusion over a potential energy barrier. The driving forces for the reaction process are thermally generated structural fluctuations (e.g. in solvent molecules, or protein), whose shuttling actions are transferred to the substrate; their random nature enables them to induce any degree of strain in the substrate, enabling progression along the reaction coordinate and over the energy barrier to the reaction. Thus the particle is acted upon by a highly fluctuating random force that *'energises'* its motion and by a Stokes-like (i.e., viscous) friction force that *dissipates* its kinetic energy (Gavish, 1986). In the context of enzyme-catalysed reactions, the driving force

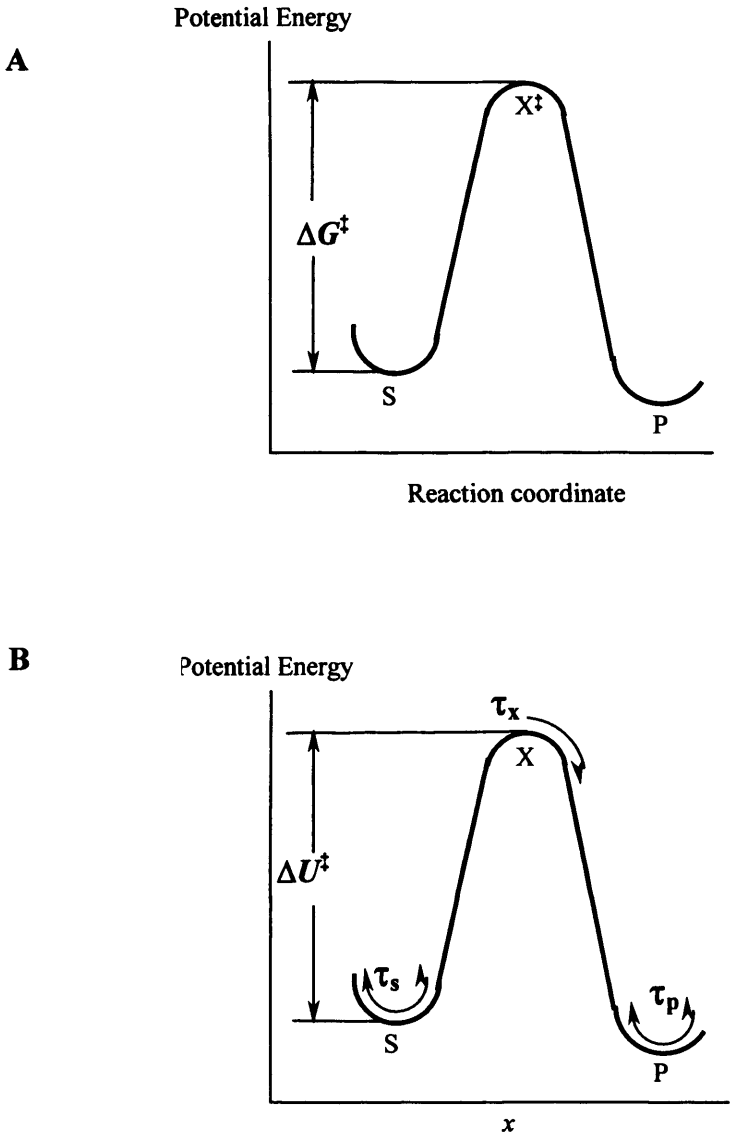

Figure 1.15. Potential energy diagrams for transition state theory and Kramers' theory. A.The transition state theory of reaction rate. The conversion of substrates S into product P at initial rate k is assumed to involve an 'activated complex' $X^{\ddagger}$. $X^{\ddagger}$ is assumed to be a structure in equilibrium with S that moves unidirectionally to the P state. The predicted k involves the free energy difference between $X^{\ddagger}$ and S. **B. Kramer' theory of reaction rate.** The conversion of S to P is modelled by the diffusion of a particle in the presence of a field of force, which is derived from a potential that possesses barrier characteristics. The spatial coordinate x is identified with the reaction coordinate over which the potential is uniquely defined., for example the length of a sissile bond. τ_s τ_p and τ_x are respectively, the periods of free oscillations in the S and P states and the decay time from the top of the barrier.

for the reaction is derived from random structural fluctuations in the protein that energise the substrate (Gavish, 1986; Scrutton *et al.*, 1999).

Kramers relationship between the rate constant, k, and the height of the potential energy barrier, ΔU, is written as follows:

$$k = \tau^{-1} \exp(-\Delta U/RT) \qquad \textbf{Equation 1.5}$$

where τ, the time constant of structural fluctuations, is proportional to the viscosity of the medium. This equation is the same form as the Arrhenius equation (Equation 1.13), but with ΔU replacing ΔE. The dynamic nature of molecules is incorporated into ΔU but not ΔE (Sutcliffe & Scrutton, 2000). It is important to note that the dependence of k on local viscosity is related to effects on structural fluctuations and not the diffusion of substrate into the active site of the enzyme (Scrutton *et al.*, 1999).

If energy barriers are no longer considered static as in TST, but are treated in terms of dynamic, fluctuating amplitudes, then the effect of solvent viscosity on enzyme reactions can be accounted for (Gavish & Werber, 1979; Gutfreund, 1995). Kramers' theory however, includes viscosity as one of its parameters and is therefore seen to provide a conceptual framework from which to develop new theories for enzymatic H-tunnelling (Scrutton *et al.*, 1999).

1.3.3 The Use of Kinetic Isotope Effects as a Probe of Hydrogen Tunnelling

There are many examples of H-transfer in biology including that between substrate cofactors, proton transport across cell membranes, and the functional isomerisation of intermediary metabolites (Kohen & Klinman, 1999). Although H-transfer often involves transfer from oxygen or nitrogen, in the vast majority of cases, cleavage of a substrate or cofactor carbon-hydrogen (C-H) bond is required. One of the most useful tools available to the enzymologist for studying C-H bond cleavage is the isotopic replacement of hydrogen with its' heavier isotopes deuterium (^{2}H, D) and tritium (^{3}H, T).

Isotopic replacement has an important role in mechanistic enzymology (Northrop, 1981; Northrop, 1982; Klinman, 1978; Cleland & Northrop, 1999). This is due to the kinetic isotope effect (KIE). The incorporation of heavier isotopes into the

substrates, cofactors or solvent of chemical systems causes measurable differences in rates of reactions when compared to reactions with the lighter, abundant isotopes. The KIE is a value obtained when the rate of reaction with one isotope is divided by the rate of reaction using a heavier isotope. KIEs can be classified as primary, secondary and tertiary (solvent) effects, depending on whether they involve isotopic substitution in a bond that is broken/made, in some other part of the reacting species, or in the solvent respectively (Bell, 1980; More O'Ferral, 1975; Schowen & Schowen, 1982).

Data derived from isotope studies can be used to evaluate the kinetic importance of the chemical conversion step(s) in a complex enzyme reaction, or distinguish stepwise from concerted mechanisms and determine the nature of intermediates in chemical transformations involving multiple bond cleavages (Klinman, 1978). A major goal of using isotopic replacement is to deduce the changes in bonding and structure that accompany the formation of transition states (Schramm, 1999; Berti, 1999). 'Heavy isotope replacement', i.e. use of isotopes of carbon, oxygen, nitrogen and sulphur are used as mechanistic probes in enzymology (Klinman, 1978), but form no part of the work presented in this thesis; the emphasis will be on the effect of replacing hydrogen with its isotopes D and T.

1.3.3.1 The Origin and Magnitude of Hydrogen Kinetic Isotope Effects

The hydrogen KIE is particularly useful because the mass ratio of its isotopes is much larger than for any other element, resulting in relatively large KIEs (Kohen & Klinman, 1999). An explanation of the origin of KIEs invokes both classical and quantum physics and is thus a 'semi-classical' derivation, which has been explained in detail by a number of authors (Van Hook, 1971; More O'Ferral, 1975; Bell, 1980). The usual starting point for discussing isotope effects arises from the Born-Oppenheimer approximation, namely, that because the mass of an electron is 1836-fold smaller than the lightest atomic nucleus (the proton), the motions of electrons and nuclei can be treated separately. Following the substitution of one nuclei by its isotope, the potential energy curves and surfaces in which the nucleus moves remains the same; this is because interatomic and intermolecular forces depend on attractions or repulsions between the charges on electrons and nuclei, and not upon the masses of nuclei (Bell, 1980). Isotope effects are therefore unique mechanistic probes of chemical reactions, in that isotopic substitution in principle is 'non-perturbing' (Klinman, 1978) and does not alter the structure of transition states.

So where does the KIE arise? Isotopic substitution affects mass and moments of inertia; these changes affect the translational, rotational and vibrational modes of a

substrate (the degrees of freedom of the molecule). However, changes in translational and rotational modes have only a small effect on isotopic discrimination and can be considered to be negligible; by far the most important factor determining the size of a KIE is the effect of isotopic substitution on vibrational energy levels. Specifically, the effects of isotopic substitution on rates of reaction are due to the differences in zero point energies between isotopically different bonds.

The simplest case to illustrate the effect that differences in zero point energies will have on reaction rates is demonstrated by considering the dissociation of a C-H bond, compared to that of a carbon-deuterium (C-D) bond (Figure 1.16). It follows from the Born-Oppenheimer approximation that a potential energy curve, plotted as a function of the distance of the nuclei, is the same whether a C-H or C-D bond is considered. Furthermore, at physiological temperatures the only vibrational state that is substantially occupied is that of the zero point energy. However, the zero point energy occupied by a particle is not at the bottom of the potential energy curve, because then the position and momentum of the H or D atom with respect to the C atom would be known, in violation of the Heisenberg uncertainty principle. Therefore, the zero point energy is always above the electronic potential minimum; its energy is estimated by its de Broglie wavelength:

$$\varepsilon = \tfrac{1}{2} h\nu \qquad \textbf{Equation 1.6}$$

where h is Plancks constant and ν is the vibration frequency of the bond, given by the expression for a harmonic oscillator:

$$\nu = \tfrac{1}{2} \pi\sqrt{k/m} \qquad \textbf{Equation 1.7}$$

where k is the force constant ('stiffness') of the bond, and m is the reduced mass $(mM)/(M + m)$, with m and M being the mass of the proton/deuteron and the carbon nucleus respectively.

The vibrational frequencies normally observed by infrared spectroscopy for the C-H and C-D bonds are 2900 cm^{-1} and 2100 cm^{-1} respectively. Therefore, the zero point energy for a C-H bond is about 17.4 $kJ \cdot mol^{-1}$, and that for a C-D bond is about 12.6 $kJ \cdot mol^{-1}$. According to TST, in the transition state all of this vibrational energy is converted into translational energy along the reaction coordinate and, if the transition state is symmetrical and linear, a C-H bond requires 4.8 $kJ \cdot mol^{-1}$ *less* free energy of

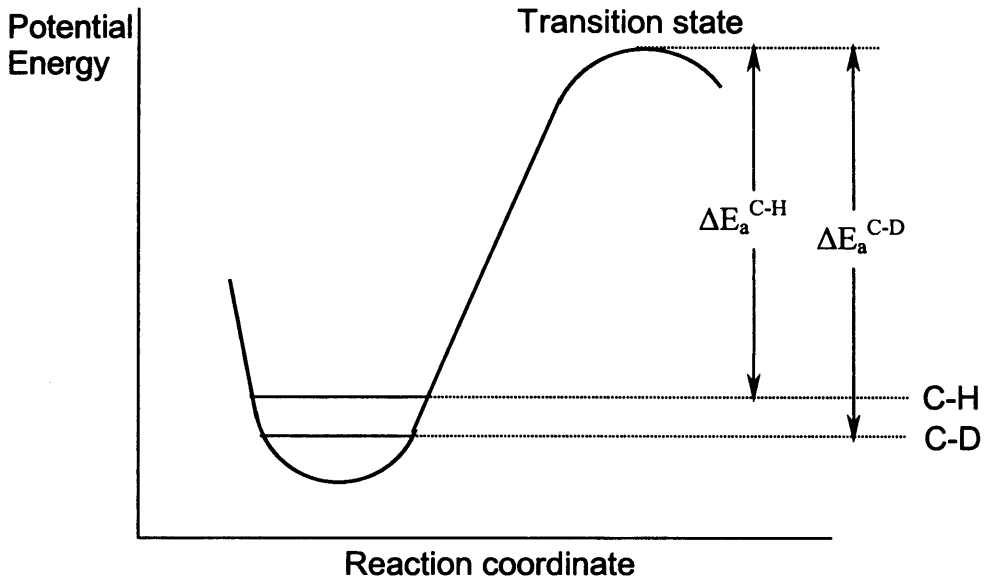

Figure 1.16: The effect of zero point energies on the activation energies for cleavage of C-H and C-D bonds.

activation than the equivalent C-D bond to reach that transition state (Gutfreund, 1995; Fersht, 1985).

The rate enhancement, i.e. the KIE, for cleavage of a C-H bond compared to a C-D bond can be predicted by TST because

$$k_H/k_D = \exp(-\Delta\Delta G^{\ddagger}/RT) = 7 \qquad \textbf{Equation 1.8}$$

Therefore TST places an upper limit of 7 for the KIE of parallel reactions in which the cleavage of C-H or C-D bonds is catalysed.

It can be shown that, in the absence of tunnelling, k_H, k_D and k_H/k_T are related by the Swain-Schaad relation (Swain *et al.*, 1958)

$$(k_H/k_D)^{1.44} = k_H/k_T \qquad \textbf{Equation 1.9}$$

so that TST places an upper limit of about 16.5 for the tritium isotope effect.

This is a simplified presentation for the origin of KIEs; no mention has been made about the effects that isotopic substitution may have on the chemical equilibria of reactions. More sophisticated and thorough treatments of the origin of KIEs have been made with the application of statistical mechanics to the effects of isotopic replacement (Van Hook, 1971; More O'Ferral, 1975; Bell, 1980). Thorough treatments of equilibrium isotope effects use rotational, translational and vibrational partition functions, which take into account the masses and moments of inertia of the reactants and transition state, and the effects of low frequency vibrations. Equations are then derived containing factors for all the vibrations of the reactant and transition states. In many cases these factors will cancel out to a good approximation and, for discussion of hydrogen isotope effects, the contribution of zero point energies are much greater than any other effects which might arise (Bell, 1980).

1.3.3.2 Deviations from Predicted KIEs

In practice, the values of observed KIEs often show deviations from the maxima predicted by their semi-classical derivation (Westheimer, 1961). It is these effects which give the use of isotopic replacement such experimental value: variations in isotope effects are used as empirical guide to changes in transition state structure, or to demonstrate that quantum mechanical tunnelling of hydrogen is occurring.

Changes in the primary hydrogen isotope effect are caused by a number of reasonably well established phenomena. H-tunnelling leads to higher than expected KIEs, and will discussed in Section 1.3.5. There are two common causes for lower than expected KIEs:

1. Asymmetric Transition State. The association between the symmetry of the transition state structure and KIEs has been made by Westheimer (Westheimer, 1961). The 'Westheimer effect' can be visualised with a three-centre model for the transition state:

$$AH + B \rightleftharpoons A\text{----}H\text{----}B \rightleftharpoons A + HB$$

where A and B are atoms or molecules which are donating and accepting a proton respectively, and A----H----B is a linear transition state. Cleavage of a C-H bond rarely involves a simple dissociation: in most cases hydrogen is transferred between one atom and another.

The transition state has two stretching vibrations, symmetric and asymmetric:

←A----H----B→	←A----H→ ←B
Symmetric stretch	Asymmetric stretch

If the transition state is truly symmetrical, i.e., the stretching vibrations of A and B are opposite, the transferred H-nucleus remains motionless and the vibration frequency is independent of isotope, so zero point energy differences are dominant and the full KIE effect is expressed. However, a reduction in KIE is predicted to occur as the transition state for H-transfer becomes 'asymmetric', and the proton is more associated with one atom or the other during transfer. In this case, the symmetric stretching component of the transition state now shows some sensitivity to isotopic substitution (More O'Ferral, 1975) leading to considerable cancellation of ground state frequencies by transition state vibrational frequencies. This causes small isotope effects (Klinman, 1978). Therefore, the Westheimer model predicts a large variation in the observed isotope effect and a dependence of KIEs on the position of hydrogen in the transition state. To support this rationalisation, isotope effects are at a maximum when acid and base have similar pK_a values (Cox & Jencks, 1981).

The Westheimer effect can be understood conceptually in terms of the Hammond postulate, which relates the structure of the transition state to the thermodynamic driving force of the reaction. For example, when the transition state resembles the structure of reactant or product, ($\Delta G > 0$ or $\Delta G < 0$ respectively) there

is a reduction in KIE. However, in isoenergetic reactions ($\Delta G = 0$) the transition state is predicted to be symmetrical and the maximum KIE is expressed (Klinman, 1978).

(2) Non-linear Hydrogen Transfer. The Westheimer model is based on the assumption that hydrogen is transferred in a linear fashion. However, if transfer occurs in a non-linear fashion, the KIE is predicted to be lowered (Bell, 1980). Some H-transfer reactions proceed with the origin, terminus and transferred hydrogen non-collinear. An example from enzymology is the intramolecular C-2 to C-1 hydride transfer catalysed by enzymes of the glucose/xylose isomerase family. These are predicted and observed to have low isotope effects because of rearrangements in substrate that accompany proton transfer (van Bastelaere *et al.*, 1995).

1.3.4 Kinetic Complexity in Enzymatic Reactions

The framework within which KIEs can be understood in biology is complicated by the nature of enzyme catalysis. Although non-enzymatic reactions tend to provide full expression of the isotope effect on measured rates of reaction, this is not the case for enzymes (Klinman, 1978). Enzyme-catalysed reactions take place within multiple steps in the reaction coordinate, often of comparable energetic barriers, so that the chemical step which gives the intrinsic KIE could be buried between enzymatic steps that include forward and reverse commitment, rate-limiting product release, or rate-limiting enzymatic conformational changes (Albery & Knowles, 1976; Cleland & Northrop, 1999; Schramm, 1999). The composite rate constant for the overall reaction usually includes the rate constants for these steps (Kyte, 1995).

A consequence of the kinetic complexity of enzymatic reactions, relevant to the use of KIEs as probes of reactions, is that the *observed* KIE might not have the same value as the KIE on the isotopically sensitive step of a reaction, known as the *intrinsic* KIE (Bahnson & Klinman, 1995). In using KIEs to study C-H bond cleavage for example, it is therefore vital to be able to relate the intrinsic KIE to the observed KIE of a reaction, or to ensure that the KIE being measured directly reflects C-H bond cleavage (Cha et al., 1989; Grant & Klinman, 1989).

The deconvolution of intrinsic KIEs from observed effects is a major challenge. Approaches to solving this problem have been dealt with in the literature, particularly by those workers who are interested in using the effects of isotopic replacement to determine the transition-state structure of enzyme-catalysed reactions

(Cleland, 1982; Northrop, 1981; Schramm et al., 1994). These authors have been mainly concerned with the effect of isotopic replacement steady-state reactions. Here, KIEs are expressed in the Michaelis-Menten parameters k_{cat} and k_{cat}/K_m, which in the 'Wisconsin' (Northrop-Cleland) nomenclature are termed V and V/K respectively (Northrop, 1981). However, these terms are still complex aggregates of rate constants for individual molecular processes, only some of which are isotopically sensitive. Hence, the idea of 'commitments to catalysis', or simply 'commitments' is presented as a key conceptual aid to determining intrinsic KIEs.

The concept of commitments to catalysis can be illustrated by a reaction coordinate diagram for an enzyme-catalysed reaction consisting of a number of energetic barriers (Figure 1.17). The rate-limiting step for the reaction corresponds to the step with the highest activation barrier in the energy profile. If the isotopically sensitive chemical step is essentially rate-limiting, by being several kcal·mol^{-1} above all others, the isotope effect will be fully expressed (in the V/K term, above, Kyte, 1995; Schramm, 1999; Northrop, 1981). However, if the chemical step does not have the highest barrier, isotope effects are suppressed by commitments to catalysis. A commitment is defined as the ratio of the rate constant for the isotopically-sensitive step to the net rate constant for the first irreversible effect in the other direction away from this step, for example, the release of substrate or product or a chemically irreversible step (Schramm, 1999). Hence, there are both 'forward' or 'reverse' commitments to catalysis. Forward commitments precede the isotopically-sensitive step, reverse commitments follow it.

The presence of a forward commitment in a reaction represents a tendency for the ES species to go on to react to form product, rather than dissociate to precursors. As the forward commitment to a reaction increases from negligible to dominant, observed KIEs will vary between intrinsic and unity, i.e., for a reaction that *always* proceeds to product formation following substrate binding, no KIE will be observed (Sinnot *et al.*, 1998). Reactions that are energetically reversible often exhibit reverse commitments, in which enzyme-bound products 'revert' to form enzyme-bound substrate before product release occurs. Observed KIEs in the presence of reverse commitments can vary in value between the intrinsic KIE and the equilibrium effect that the heavier isotope has on the reaction (usually close to unity) (Kyte, 1995). The full isotope effect will only be seen if both commitments are small. Unfortunately, this almost never happens and commitments have to be determined experimentally (Kyte, 1995; Klinman, 1978; Northrop, 1981)

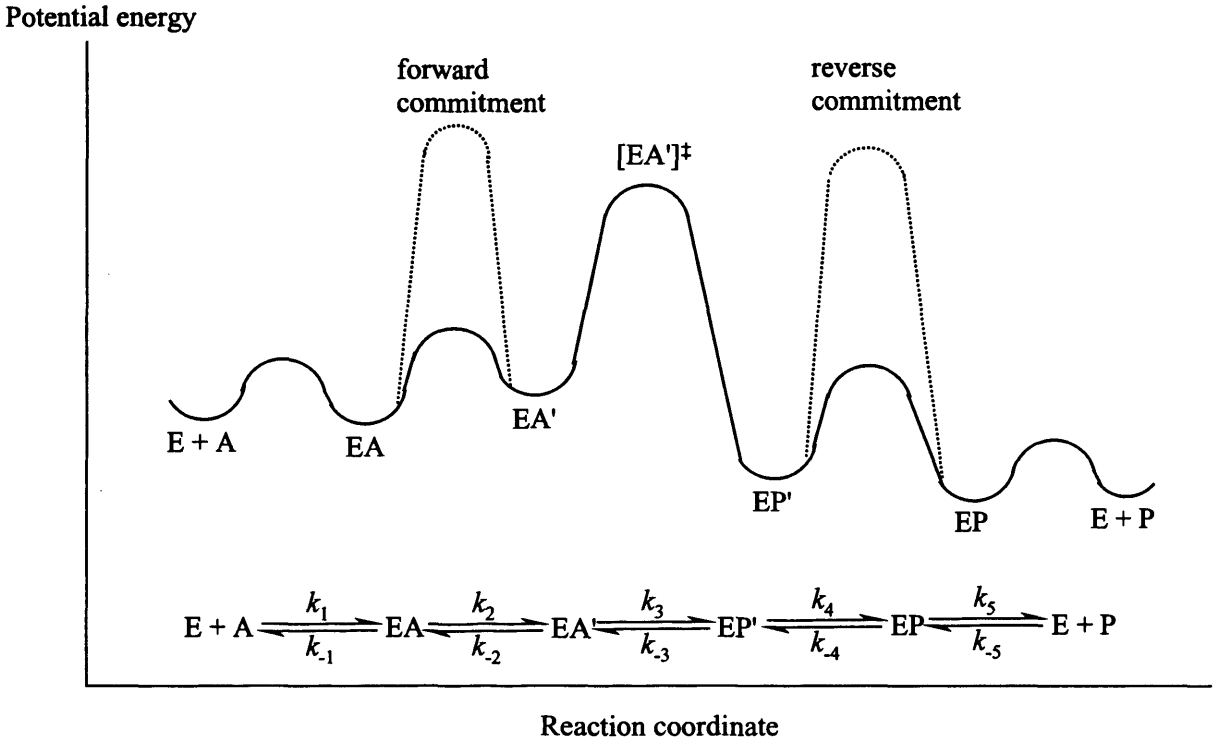

Figure 1.17: Commitments to Catalysis.

(Palcic & Klinman, 1983) or removed by changing experimental conditions (Bahnson *et al.*, 1993; Sinnot *et al.*, 1998). However, it should be noted that techniques used to determine intrinsic KIEs may not be applicable in the presence of quantum mechanical tunnelling of hydrogen (Sinnot *et al.*, 1998).

1.3.5 Quantum Mechanical Tunnelling of Hydrogen

The major phenomenon that increases predicted values for KIEs is the so-called tunnel effect (Bell, 1980; Atkins, 1982). Tunnelling arises from a consideration of quantum mechanics, in which particles possess wave-like properties. This allows particles to penetrate into areas that are forbidden by classical physics by 'tunnelling' through a potential energy barrier. Every particle possesses a finite probability that it can appear on the other side of a potential energy barrier without possessing the required energy to surmount the barrier from a consideration of classical physic.

The probability that a particle will be able to tunnel is greatly influenced by its size. Using a rectangular potential energy barrier model, the tunnelling probability is related to the mass of the tunnelling particle by the following relationship:

$$P_{\text{tunnel}} \propto \exp(-2S/h) \qquad \textbf{Equation 1.10}$$

where S is the Wentzel-Kramers-Brillouin (WKB) action (Miller, 1986), and can be understood in terms of the 'resistance' to barrier penetration; it is related to the mass of the transferred atom and the potential energy barrier between reactant and product states in such a manner that the transmission probability decreases exponentially with the thickness of the barrier and with increasing particle mass. Hence, particles with low mass are more able to tunnel through barriers than heavier particles; and particles in general tunnel more readily through thin barriers. For the electron, tunnelling is already a well-established phenomenon and occurs over large distances- up to 25 Å. On the other hand, it is a good approximation to apply classical mechanics to the motion of carbon or heavier atoms.

In terms of particle size, hydrogen is the next best candidate particle after the electron for tunnelling in chemical reactions. The mass of the H nucleus is 1840 times larger than an electron. This means that the probability that an electron will tunnel up to 25 Å is matched by the probability that protium will tunnel up to 0.58 Å, which is similar to the length of a reaction coordinate (Sutcliffe & Scrutton, 2000). The larger

masses of deuterium and tritium lead to transfer distances of 0.41 Å and 0.34 Å respectively.

1.3.6 Detection of H-Tunnelling from Kinetic Isotope Effects and Temperature Dependencies of Reactions

1.3.6.1 Kinetic Isotope Effects as a Probe of Tunnelling

The semi-classical (zero point energy) derivation for the origin of KIEs has been used in the past as an experimental probe for tunnelling in chemical reactions, because a k_H/k_D effect greater than the theoretical upper limit of 7 (Equation 1.8) provides evidence that tunnelling is occurring (Bell, 1980). In addition, Saunders (Saunders, 1985) has demonstrated an important deviation from the Schwaan-Schaid relation (Equation 1.9). Formulating the semi-classical relation between the two isotope effects k_H/k_T and k_D/k_T in terms of reduced-mass considerations leads to the following equation (Klinman, 1989):

$$(k_D/k_T)^{3.26} = k_H/k_T \qquad \textbf{Equation 1.11}$$

which differs from the Schaad-Schwain relation in that tritium, not protium, is the common atom connecting both sides of the equation. Equation 1.11 has led to the development of so-called 'competitive labelling' experiments to detect tunnelling (Bahnson & Klinman, 1995), in which the H/T and D/T isotope effects on a reaction are measured in parallel (Cha et al., 1989). In a protium versus tritium experiment, the experimentally measured value for H/T $[(k_H/k_T)_{obs}]$ is determined. In a parallel experiment, the D/T effects for the reaction are measured and used to *calculate* a value for the H/T effects $[(k_H/k_T)_{calc}]$ If H-tunnelling is occurring in a reaction, $(k_H/k_T)_{obs}$ will be inflated above semi-classical limits, and a comparison of $(k_H/k_T)_{obs}$ to $(k_H/k_T)_{calc}$ yields the following inequality:

$$(k_D/k_T)^{3.26} = (k_H/k_T)_{calc} < (k_H/k_T)_{obs} \qquad \textbf{Equation 1.12}$$

This relationship has been regularly exploited to reveal H-tunnelling in enzyme-catalysed H-transfers (Cha *et al.*, 1989; Klinman, 1989; Bahnson & Klinman, 1995).

1.3.6.2 Temperature Dependence Studies as a Probe of Tunnelling

Another common probe of tunnelling can be derived from studies of the temperature dependencies of rates of reaction (Bell, 1980). Traditionally, the temperature dependence of reaction velocity is examined in terms of the Arrhenius equation, which is found to hold empirically over at least a limited range of temperature:

$$k = A \exp(-\Delta E_a/RT) \qquad \textbf{Equation 1.13}$$

Where A is the 'Arrhenius pre-exponential factor' or 'prefactor'. The other terms have their usual meaning. Typically, reaction rates are measured over a range of temperatures and plotted on a graph of ln(*rate*) versus 1/T. The relationship presented in the Arrhenius equation allows calculation of the activation energy of reactions, which is obtained from the slope of a plot, $\Delta E_a/R$; A is the value of the intercept on the x-axis.

Tunnelling is investigated by carrying out temperature dependence studies with substrates that have undergone isotopic substitution. Factors indicative of tunnelling include:

(i) Curvature of Arrhenius plots (Bell, 1980; Stern & Weston, 1974a). Although curvature in Arrhenius plots has been observed for some chemical systems (Brunton *et al.*, 1976; Wang & Williams, 1972), the denaturation of proteins at elevated temperatures makes it impractical to study enzyme-catalysed reactions over a sufficient temperature range to detect curvature. It should also be noted that other reasons for non-linearity in Arrhenius plots can occur; for example, temperature-induced interconversion of two forms of an enzyme (Dixon & Webb, 1979; Gutfreund, 1995).

(ii) Ratios for the Arrhenius pre-exponential factors $A_H:A_D < 1$ (Bell, 1980; Schneider & Stern, 1972; Stern & Weston, 1974b). The link between tunnelling and its effects on the ratios of Arrhenius pre-exponential factors is illustrated in Figure 1.18.

(iii) Large differences in the activation energies between protium and deuterium transfer (Bell, 1980). The calculated maximum difference between ΔE_a^D and ΔE_a^D for classical transfer based on differences in zero-point energies is about 5.4 kJ·mol^{-1}. Values for $\Delta E_a^H - \Delta E_a^D > 5.4$ kJ·mol^{-1} would indicate that protium was being transferred by H-tunnelling.

To summarise, the evidence for tunnelling from Arrhenius plots is restricted to non-classical values for the ratio of Arrhenius pre-exponential factors and a difference in ΔE_a^{H-D}>5.4 kJ·mol^{-1}; these factors, in addition to inflated KIEs, have been the prime means of detecting tunnelling in enzyme-catalysed reactions (Scrutton *et al.*, 1999).

1.3.7 Hydrogen Tunnelling in Enzyme Systems

H-tunnelling was not revealed in enzyme-catalysed H-transfer reaction until 1989, which seems relatively late considering the use of isotopic replacement as probes of reaction mechanism before this date. Unusually high hydrogen isotope effects observed in some enzyme systems were not interpreted in terms of tunnelling (Klinman, 1978; Reinsch *et al.*, 1980; Palcic & Klinman, 1983). It is likely that this was due to interpretation of kinetic isotopes and Arrhenius plots within the restrictions of semiclassical theory and a misconception that the large mass of hydrogen precluded tunnelling (Scrutton *et al.*, 1999). In addition, tunnelling was only thought to contribute substantially to barrier crossing at very low temperatures at which enzymes are not normally studied (Ringe & Petsko, 1999). The following section illustrates some examples of enzyme systems in which tunnelling was detected by deviations from semi-classical behaviour.

1.3.7.1 Yeast Alcohol Dehydrogenase

The first demonstration of an enzyme-catalysed H-transfer by tunnelling was in the yeast alcohol dehydrogenase (YADH) reaction (Cha *et al.*, 1989). In the YADH-catalysed conversion of benzyl alcohol and NAD^+ to benzaldehyde and NADH respectively is rate limiting. In addition, a theoretical study had earlier modelled experimental data for NAD^+/NADH-dependent dehydrogenases and attributed 80 % of the H-transfer process in YADH to a tunnelling event (Huskey & Schowen, 1983).

Tunnelling was investigated in YADH using a competitive, double-labelling protocol (Klinman, 1989; Bahnson & Klinman, 1995). Interestingly, given the subsequent discovery of H-tunnelling in this reaction, the Arrhenius plots were not indicative tunnelling. To investigate tunnelling, it was decided to exploit the relationship in Equation 1.12 (Saunders, 1985). This approach compared rates of hydrogen-isotope transfer to NAD^+, from a reaction mixture containing two forms of

substrate: tritiated benzyl alcohol and [^{14}C]-labelled benzyl alcohol (ring-labelled). The 'competitive' aspect of the investigation was caused by changing the nature of the hydrogen isotope on the [^{14}C]-labelled substrate, using either protium or deuterium. Scintillation counting was used to determine the ratio between the amount of ^{3}H incorporated into NAD to the amount of [^{14}C]-labelled benzaldehyde. Data were then analysed in light of the relation proposed in Equation 1.12. The relationship between calculated and observed isotope effects were consistent with H-tunnelling. Values of $(k_H/k_T)_{calc}$ were about 5.91, compared to values for $(k_H/k_T)_{obs}$ of about 7.13. Secondary KIEs showed a relationship of $(k_H/k_T)_{calc} = 1.11$ versus $(k_H/k_T)_{obs}$ of 1.35. The values of the exponent required to 'match' the measured D/T and H/T isotope effects were 3.58 and 10.2 for primary and secondary KIEs respectively, both of which are well outside the theoretical upper limit of 3.34 for isotope effects deriving purely from a semi-classical consideration (Klinman, 1989). It was therefore proven for the first time that tunnelling occurred during an enzyme-catalysed H-transfer reaction.

1.3.7.2 Bovine Serum Oxidase

Demonstration of H-tunnelling in YADH was rapidly followed by unveiling of tunnelling in the reaction catalysed by the TPQ- and copper-containing enzyme bovine serum oxidase (BSAO) (Grant & Klinman, 1989). This enzyme catalyses the conversion of amines to aldehydes. A previous study had indicated that there were large primary isotopes for this reaction (Palcic & Klinman, 1983) and there were no problems of commitments to consider.

For BSAO, k_D/k_T and k_H/k_T isotope effects and the temperature dependence for the oxidation of benzylamine were measured using substrates labelled in a manner analogous to the YADH reaction, i.e., [^{14}C]-labelled benzylamine, either protiated or deuterated, was used in a competitive reaction against tritiated benzylamine. Primary H/T and D/T isotope effects determined by stopped-flow spectroscopy were 35.8 and 3.07 respectively. The Arrhenius plot of the primary isotope effects yielded an Arrhenius pre-exponential factor ratio, A_H/A_T of 0.12, well below the semi-classical limit of 0.6 (Bell, 1980; Schneider & Stern, 1972). In addition, the A_D/A_T value of 0.51 showed that deuterium was also tunnelling (semi-classical lower limit = 0.9).

1.3.7.3 Horse Liver Alcohol Dehydrogenase

Tunnelling was revealed in horse liver alcohol dehydrogenase (LADH), using the same approach as for YADH (Bahnson *et al.*, 1993). However, in LADH the

oxidation of benzyl alcohol is limited by dissociation of the product benzaldehyde: an internal commitment which masks the intrinsic KIE. This presented an opportunity to see whether tunnelling could be revealed by the introduction of mutations which increased the rate of product dissociation. The approach involved either increasing or decreasing the size of the alcohol binding pocket by substitution of hydrophobic amino acids that contact the bound alcohol. Increasing the size of the binding pocket of LADH only slightly decreased kinetic complexity and produced no significant change in isotope effects or the exponential relationship between k_D/k_T and k_H/k_T. k_D/k_T By contrast, the mutations Leu-57 → Phe and Phe-93 → Trp, introduced in separate instances to decrease the size of the binding pocket, provided a clear demonstration of protium tunnelling; secondary KIEs became significantly elevated from 4.1 in wild-type enzyme to 8.5 and 6.3 in the L57F and F93W mutants respectively. A temperature dependence study of the F93W mutant provided Arrhenius pre-exponential ratios, $A_H/A_T = 0.49$, strongly suggesting protium tunnelling.

1.3.7.4 Monoamine Oxidase B

Strong evidence of H-tunnelling has found in monoamine oxidase B (MAO-B) (Jonsson *et al.*, 1994), a flavoprotein containing covalently linked (8α-S-cysteinyl) FAD, that catalyses the oxidation of a large number of amines (Fersht, 1985). Again, a competitive labelling protocol was applied, using *p*-methoxybenzylamine as substrate.

The reaction catalysed by MAO-B contains internal commitments, which affected measurement of primary KIEs, reducing the exponents relating k_D/k_T and k_H/k_T below semi-classical values. Despite this, the data indicated that the effect of commitments were found to be constant over the temperature range used and were considered to exert only a small influence on the interpretation of data from Arrhenius plots. As with BSAO, the ratio of Arrhenius pre-exponential factors, A_H/A_T and A_D/A_T, provided evidence of tunnelling, having values of 0.13 and 0.52 respectively. Although Arrhenius pre-exponential factors are affected by internal commitments (Koch & Dahlberg, 1980), the consistent expression of these commitments over the temperature range used was considered to only marginally alter the determination of intrinsic values (Jonsson *et al.*, 1994). Therefore, as with BSAO, it was shown that protium and deuterium undergo tunnelling in the MAO-B-catalysed reaction.

1.3.7.5 Other Systems

Unusually large isotope effects have been seen in the triosephosphate isomerase (Alston *et al.*, 1996), methane monooxygenase (Nesheim & Lipscomb, 1996) and glucose oxidase (Kohen *et al.*, 1997) systems. In each case, they have been interpreted as being indicative of tunnelling and have shown that H-tunnelling is a phenomenon that occurs in different classes of enzymes.

1.3.7.6 Soybean Lipoxygenase and the Development of Criteria for Interpreting Tunnelling from Arrhenius Plots

The unveiling of tunnelling in the systems described so far were based on fairly small deviations from classical behaviour, in which Arrhenius plots showed non-classical behaviour, with pre-exponential factors deviating from unity. However, Jonsson *et al.* (1996) have additionally characterised H-transfer in the reaction catalysed by soybean lipoxygenase (SBL). Investigation of steady-state KIEs in the SBL reaction indicated the largest deuterium isotope effects reported for a biological system ($k_H/k_D = 48$ at 25 °C, Glickman & Klinman, 1995). Temperature dependence studies of k_{cat} for the steady-state oxidation of linoleic acid (LA) revealed a maximum isotope effect of about 56 at 32 °C. Arrhenius plots were almost horizontal, parallel lines, with enthalpies of activation of 5.0 and 6.7 kJ·mol^{-1} for H-LA and D-LA respectively. The ratio of Arrhenius prefactors showed very large deviations from classical behaviour: $A_H/A_T = 27$ from steady-state and 50 from stopped-flow analysis, respectively.

Jonsson *et al.* (1996) developed criteria for understanding the behaviour of SBL and other enzymes in the context of the Arrhenius equation. As a phenomenological description of a classical, thermally activated process, deviations from Arrhenius behaviour will arise under conditions of activationless quantum mechanical behaviour. However, as mentioned in Section 1.3.6.2, experimental observation of such behaviour is rare, and is unlikely to be seen over the limited temperature range useable for studying enzyme reactions. Following the description of the SBL data, Jonsson *et al.* proposed a classification of Arrhenius plots for a light and heavy isotope into four regions (Figure 1.18). Region I corresponds to classical behaviour, with large enthalpies of reaction and extrapolated values for $A_H/A_T \approx 1$. Region II represents a pattern commonly seen, in which isotope effects may be inflated and extrapolated Arrhenius prefactor ratios become less than unity; this reflects greater tunnelling, and hence curvature in the Arrhenius plot for the lighter isotope, and is the effect observed in the BSAO and MAO-B reactions. Extension of

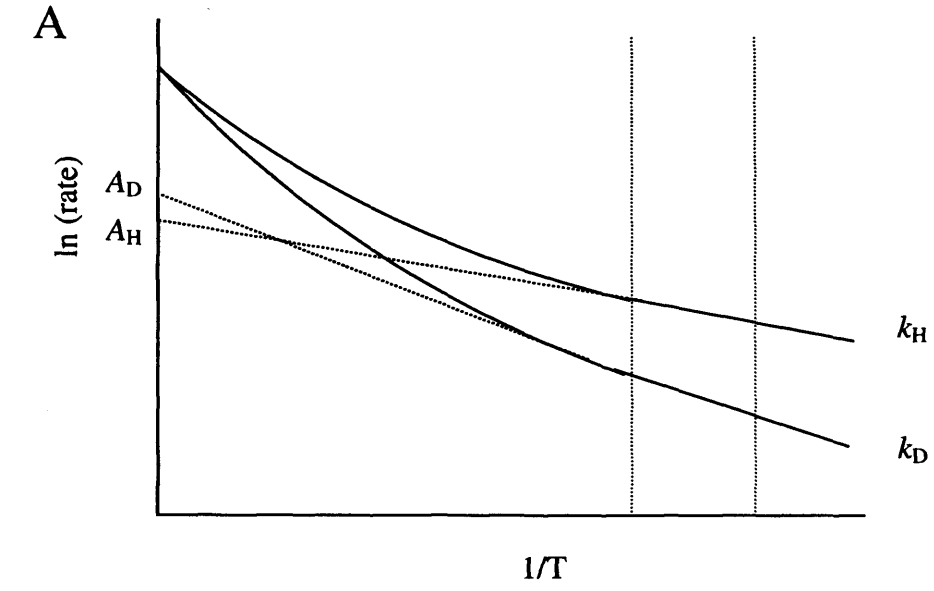

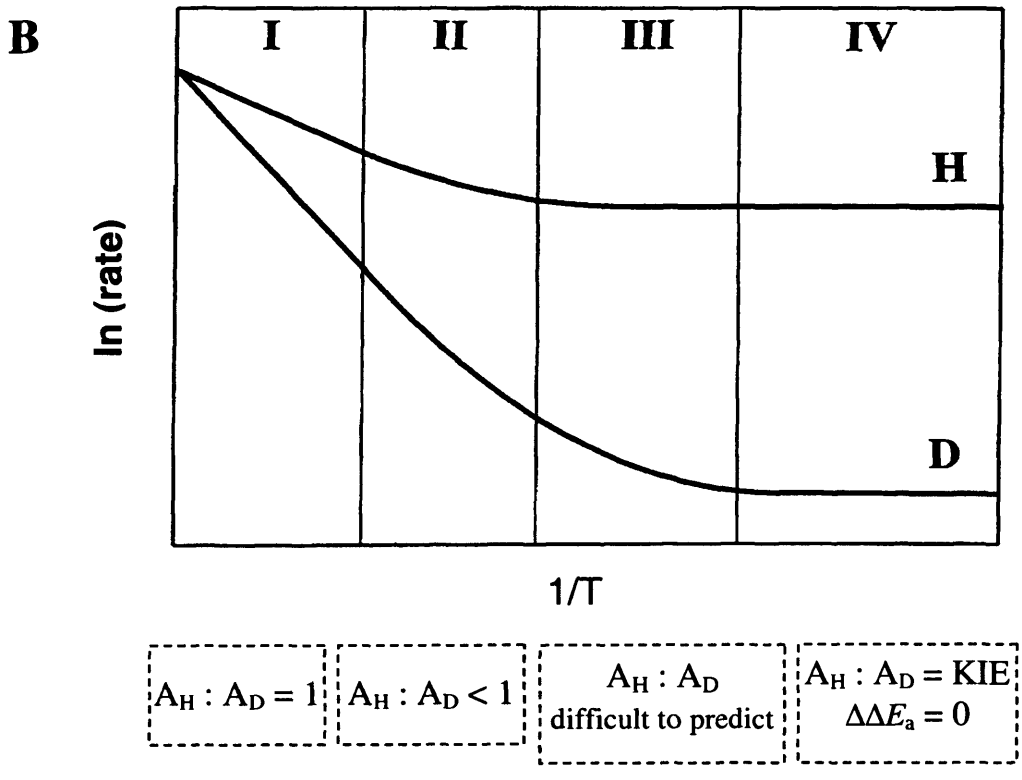

Figure 1.18: A. Effect of curvature on the value for ratios of Arrhenius prefactors. Dotted lines indicate the accessible temperature range. **B. Static Barrier Model for Tunnelling.** Based on evidence from a series of reactions modelled on static barriers, this sets the criteria by which Arrhenius plots will be used to detect the extent of tunnelling in a reaction. H = hydrogen, D = deuterium (Jonsson *et al.*, 1996). Later versions of this model are split into only three regions (Kohen & Klinman, 1998, Kohen & Klinman, 1999).

Arrhenius plots to a temperature range where significant tunnelling of all isotopes of hydrogen leads to a process that is nearly activationless for both H and D transfer (Region IV). The horizontal nature of these Arrhenius plots predicts enthalpies of activation close to zero, may lead to extremely large isotope effects, and predicts Arrhenius prefactor ratios close to the KIEs themselves.

Thus, the reaction properties of the SBL reaction indicated that the reaction was operating in, or close to Region IV. Two predictions are made from the Arrhenius plots as presented in Figure 1.18: (1) that systems will be found that operate between regions II (BSAO, MAO-B) and IV (SBL) and (2) that a trend of decreasing enthalpy of activation will emerge as tunnelling becomes more prominent. Region III, which presents the intermediate tunnelling behaviour, has properties that are hard to predict, since small changes in rate may lead to values of A_H/A_T which are either normal or inverse. Earlier studies of glucose oxidase suggested that it perhaps operated in Region III, as small changes in k_{cat} for this enzyme correspond to a marked shift in the value of A_H/A_T from inverse to well above unity (Kohen *et al.*, 1997) . Supporting evidence for prediction (2) is seen among the enzyme systems studied in the group of Klinman (BSAO, MAO-B, GO and SBL), where a change in Arrhenius prefactor ratios from inverse values to large values corresponds to decreasing $\Delta H^{\ddagger}$.

1.3.8 Evidence for Hydrogen Tunnelling Driven by Protein Dynamics

1.3.8.1 Methylamine Dehydrogenase

The relationship between Arrhenius plots and the extent of tunnelling illustrated in Figure 1.18 set a framework within which to interpret temperature dependence data. One of the predictions from the plot, that ΔE_a decreases to zero as tunnelling becomes more prominent, appeared to hold for the enzyme systems described so far. Recently however, this relationship has been found to break down for the reaction catalysed by methylamine dehydrogenase (MADH) from *Methylophilus methylotrophus* (Basran *et al.*, 1999d). MADH catalyses the oxidative demethylation of methylamine to formaldehyde and ammonia, in a reaction similar to that of TMADH. However, in MADH the cofactor reduced by two electrons is TTQ; measurement of TTQ reduction by stopped-flow provides a direct measurement of C-H bond cleavage.

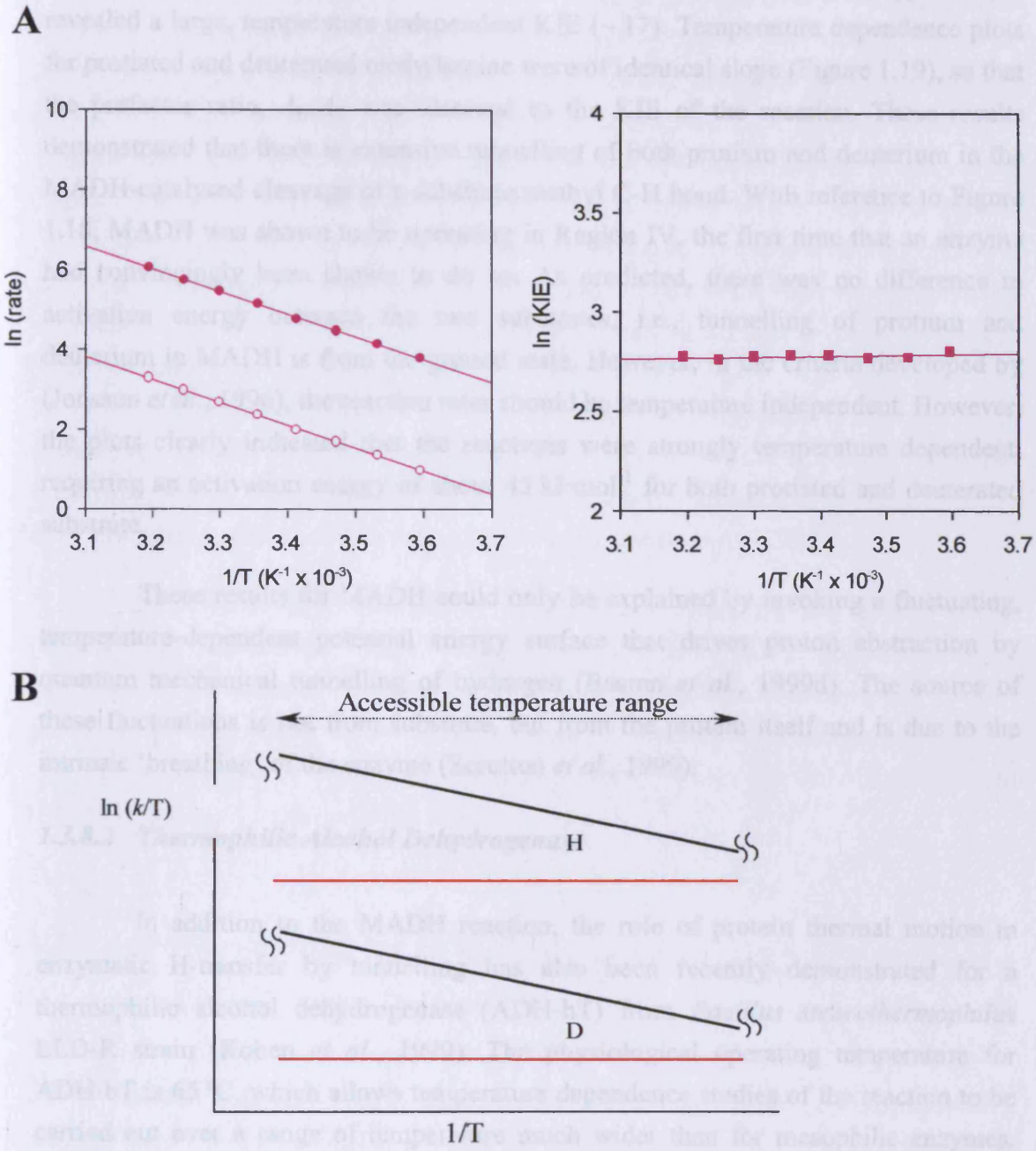

Figure 1.19: A. Temperature dependence and KIE data for MADH. (i) Temperature dependence plots for MADH with methylamine (closed circles) and perdeuterated methylamine (open circles). (ii) Plot of ln KIE vs 1/*T*. **B. General relationship describing how the rate of H-transfer depends on temperature.** Comparison of temperature dependence in region IV of Figure 1.18 for a static (red line) and a fluctuating (black line) barrier in the accessible temperature range.

Temperature dependence studies of the reaction catalysed by MADH revealed a large, temperature independent KIE (~ 17). Temperature dependence plots for protiated and deuterated methylamine were of identical slope (Figure 1.19), so that the prefactor ratio, A_H/A_T was identical to the KIE of the reaction. These results demonstrated that there is extensive tunnelling of both protium and deuterium in the MADH-catalysed cleavage of a substrate methyl C-H bond. With reference to Figure 1.18, MADH was shown to be operating in Region IV, the first time that an enzyme had convincingly been shown to do so. As predicted, there was no difference in activation energy between the two substrates, i.e., tunnelling of protium and deuterium in MADH is from the ground state. However, in the criteria developed by (Jonsson *et al.*, 1996), the reaction rates should be temperature independent. However, the plots clearly indicated that the reactions were strongly temperature dependent, requiring an activation energy of about 45 $kJ \cdot mol^{-1}$ for both protiated and deuterated substrate.

These results for MADH could only be explained by invoking a fluctuating, temperature-dependent potential energy surface that drives proton abstraction by quantum mechanical tunnelling of hydrogen (Basran *et al.*, 1999d). The source of these fluctuations is not from substrate, but from the protein itself and is due to the intrinsic 'breathing' of the enzyme (Scrutton *et al.*, 1999).

1.3.8.2 Thermophilic Alcohol Dehydrogenase

In addition to the MADH reaction, the role of protein thermal motion in enzymatic H-transfer by tunnelling has also been recently demonstrated for a thermophilic alcohol dehydrogenase (ADH-hT) from *Bacillus stearothermophilus* LLD-R strain (Kohen *et al.*, 1999). The physiological operating temperature for ADH-hT is 65 °C, which allows temperature dependence studies of the reaction to be carried out over a range of temperature much wider than for mesophilic enzymes. Kohen *et al.*(1999) set out to study hydrogen tunnelling as a function of temperature in ADH-hT with emphasis on how protein mobility affected the contribution of hydrogen tunnelling to the reaction rate. If protein mobility is important, a decreased contribution of tunnelling to the reaction rate would be expected due to increased protein rigidity at lower temperatures. This would contrast to models of H-tunnelling through a rigid barrier, which predict an increased contribution of tunnelling to rate with decreased temperature (Goldanskii, 1979).

The temperature dependence of the ADH-hT-catalysed reaction was studied using the methodology as previously described for YADH (Cha *et al.*, 1989) (Section

1.3.7.1). The contribution of tunnelling to the reaction, as indicated by the value of the exponent relating k_H/k_T and k_D/k_T, was found to decrease as temperature fell below 30 °C. Also, while KIEs were essentially temperature independent between 65 and 30 °C, their value was found to rise steeply as the temperature fell below 30 °C. A physical change in the behaviour of ADH-hT at temperatures below 30 °C was clearly indicated by Arrhenius plots of hydrogen and deuterium effects. Between 65 and 30 °C, the plots have slopes at elevated temperatures that are essentially identical for protonated and deuterated substrates, with $A_H/A_T > 1$. Below the transition temperature of about 30 °C, the slope for protonated and deuterated substrates begin to diverge, with increased values for enthalpy of activation and $A_H/A_T < 1$. The source of decreased tunnelling in ADH-hT at 30 °C and below was attributed to a temperature-dependent transition in the behaviour of the protein which impairs hydrogen tunnelling, with the decreased extent of tunnelling being ascribed to increased rigidity of thermophilic proteins at reduced temperatures (Kohen *et al.*, 1999).

As with MADH (Basran *et al.*, 1999d Scrutton *et al.*, 1999), in the physiological temperature range of ADH-hT, the $\Delta H^{\ddagger}$ for deuterated substrate compared to protonated substrate is close to zero, while the individual values for $\Delta H^{\ddagger}$ are quite sizeable (about 15 kcal·mol^{-1}). Hence, tunnelling from the ground state of reactants was shown to require an 'activation energy' which can only be ascribed to thermally activated motions of the protein.

1.3.9 Interpretation of the MADH and ADH-hT Data Through Dynamic Theories for Catalysis

In TST (Section 1.3.2), progress from the reactant to the product states of a reaction must overcome a static potential energy barrier. Enzymes speed up the rate of reactions by stabilising the transition state and effectively lowering the height of the barrier. However, tunnelling is not influenced by the height of a potential energy barrier: the most important factor in determining the contribution of tunnelling to reaction rates is barrier *width* (Bruno & Bialek, 1992).

For a number enzyme-catalysed H-transfer reactions it has been demonstrated that tunnelling of hydrogen occurs (Cha *et al.*, 1989 Bahnson *et al.*, 1993; Jonsson *et al.*, 1994; Jonsson *et al.*, 1996; Kohen *et al.*, 1997). However, investigations of these early systems were interpreted within the semi-classical view of KIEs; in the case of larger than expected values for KIEs, deviations from semi-

classical limits were interpreted as being indicative of tunnelling. Within these systems, tunnelling could be visualised as occurring once there was sufficient energy in the system for reactants to progress up a potential energy barrier to a point where the barrier was narrow enough for tunnelling to occur. For MADH and ADH-hT however, and as recently shown for sarcosine oxidase (Harris *et al.*, 2000), H-tunnelling occurs from the ground state of reactants; yet these systems require an input of energy and their reactions are therefore temperature-dependent. This paradox can be accounted for by considering the motions of the protein itself.

Like all molecules, proteins are subject to thermal excitation, which is reflected in an increased frequency of vibrations. Taking these vibrations into consideration provides an answer to (i) how barrier width is reduced in enzyme reactions, and (ii) the requirement of activation energy for a process, which occurring from the ground state, is essentially 'activationless'. Proteins movements reduce barrier width, by reducing the distances between donor and acceptor atoms, while the enthalpy of activation is a reflection on the energy required to produce a configuration in the protein structural scaffold that is conducive for H-transfer to occur by quantum mechanical tunnelling (Scrutton *et al.*, 1999).

A role for protein breathing motions in the C-H bond cleavage event was hypothesised from the earliest discovery of H-tunnelling in an enzyme (Cha *et al.*, 1989). The importance of thermally activated vibrations in non-enzymatic reactions has been appreciated for some time (Suarez & Silbey, 1990; Borgis & Hynes, 1991; Antoniou & Schwartz, 1997). One of these studies has been applied in analysis of the BSAO data (Grant & Klinman, 1989), but only the role of substrate oscillations is treated; the protein molecule is treated statically. Molecular dynamics studies have suggested a dynamic role for the protein molecule in enzymatic H-tunnelling (Bala *et al.*, 1996; Hwang *et al.*, 1991; Hwang & Warshel, 1996). Some theoretical studies have recognised the role of thermal motion in H-tunnelling (Sumi & Ulstrop, 1988; Dognadze *et al.*, 1977). Generally though, these models are unable to adequately describe the observations of experiments where KIEs have been used to detect H-tunnelling. Some authors have questioned the applicability of TST to enzyme catalysis at all, given the dynamic properties of proteins (Gavish, 1986; Gutfreund, 1995; Scrutton *et al.*, 1999). These authors favour an approach similar to Kramers view of catalysis in which a diffusive Brownian motion 'energises' the reactants to proceed over a potential energy barrier. This is a view favoured by Scrutton (Scrutton *et al.*, 1999), as a basis from which to develop models for enzyme catalysis.

The first and only theoretical treatment to explicitly recognise the role of protein dynamics and relate this to the observed KIE was described by Bruno and Bialek (Bruno & Bialek, 1992; Scrutton *et al.*, 1999). As outlined in Scrutton *et al.*, (1999), the data for MADH-catalysed reaction can be fitted to the model of 'vibrationally enhanced tunnelling', developed by Bruno and Bialek (Bruno & Bialek, 1992). This theory has been termed vibrationally enhanced ground state tunnelling theory (VEGST) (Scrutton *et al.*, 1999). A key prediction of this theory is that H-tunnelling can occur even when the value of the H/D KIE falls within semi-classical limits, thus suggesting that KIEs might be poor indicators of quantum tunnelling in enzymes.

Bruno and Bialek analysed data for the BSAO reaction (Grant & Klinman, 1989) using VEGST (Bruno & Bialek, 1992). This experiment, the first to demonstrate H-tunnelling in an enzyme reaction, had originally been analysed in terms of a static potential energy surface (Cha *et al.*, 1989). The BSAO data were found to be consistent with VEGST theory, but importantly do not verify it. In VEGST theory, thermal fluctuations of the protein scaffold are responsible for shortening the distance the hydrogen must tunnel, and the average tunnelling probability is decreased when heavier isotopes are transferred, thus giving rise to a KIE > 1. Tunnelling is assumed to occur from the vibrational ground states- as vibrational quanta are comparable to barrier height- and the relationship between the KIE and temperature is described by an expression that predicts a parabolic dependence on temperature.

Although VEGST can be used to adequately describe the MADH reaction, it does not adequately describe those reactions where tunnelling occurs just below the saddlepoint of a potential energy barrier to a reaction. However, it does provide a framework from which at least qualitative descriptions for the role of protein dynamics in H-tunnelling. Such descriptions have been provided by (Scrutton *et al.*, 1999; Sutcliffe & Scrutton, 2000; Kohen & Klinman, 1999). In this discussion, H-transfer from reactant to product states is treated as a double-well system across the reaction coordinate with a potential energy barrier in between (Figure 1.20). Tunnelling occurs when the probability distribution for a particle in the reactant well overlaps with the probability distribution of finding a particle in the product well. The extent of tunnelling between the two bound states is a function of the shape of both reactant and product wells and of the barrier. The thermally induced breathing of the protein molecule may pass the nuclear geometry through the reactant and product intersection many times before H-tunnelling occurs. If the potential surface is rigid, and tunnelling takes place between two vibrational ground states of equal energy, the

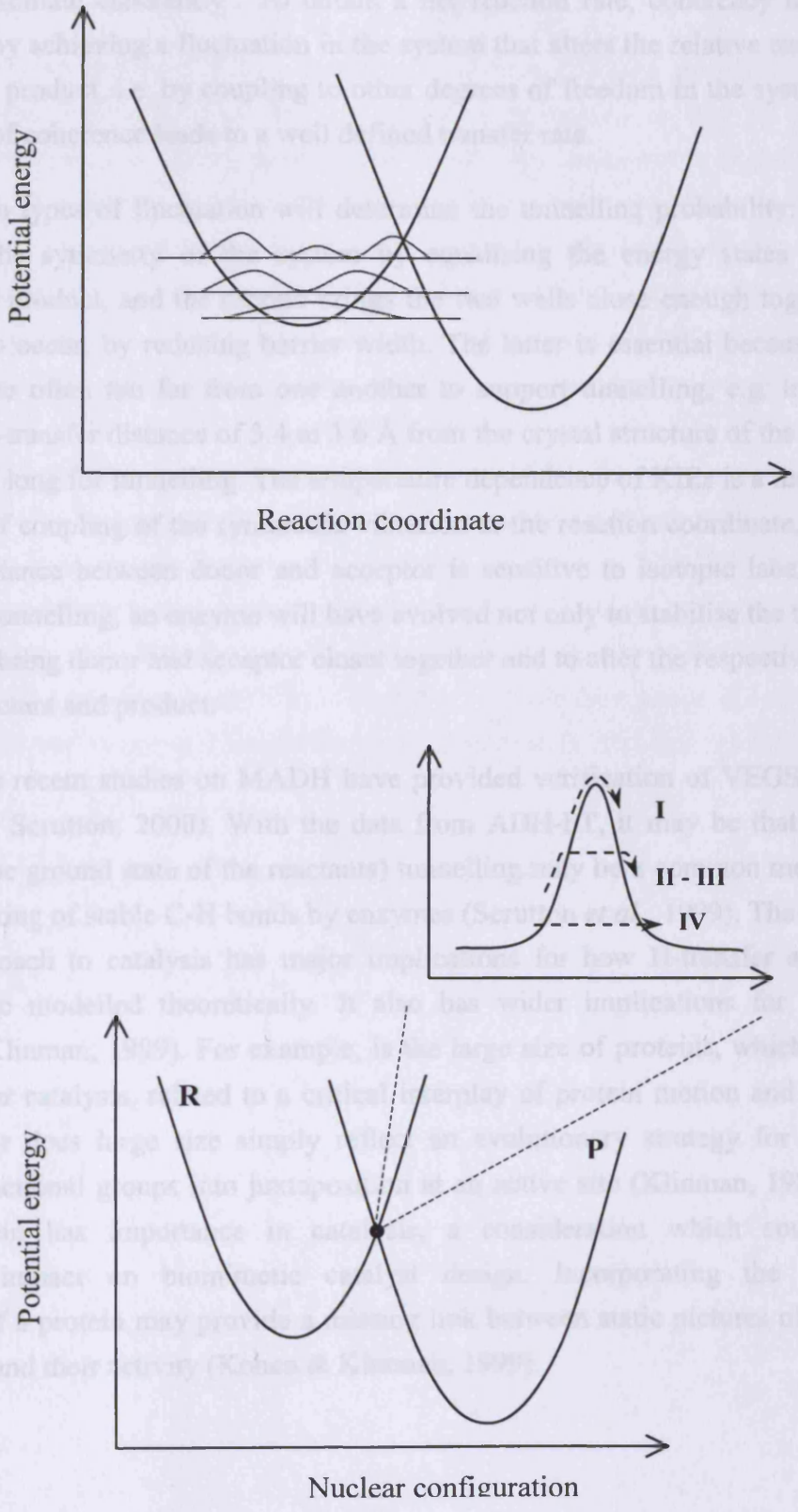

Figure 1.20:The dynamic barrier model of H-tunnelling.

particle will simply tunnel back and forth between the reactant and product wells- they will 'oscillate coherently'. To obtain a net reaction rate, coherency has to be destroyed , by achieving a fluctuation in the system that alters the relative energies of reactant and product, i.e. by coupling to other degrees of freedom in the system. Fast destruction of coherence leads to a well defined transfer rate.

Two types of fluctuation will determine the tunnelling probability: the first influences the symmetry of the system by equalising the energy states between reactant and product, and the second brings the two wells close enough together for tunnelling to occur, by reducing barrier width. The latter is essential because bound substrates are often too far from one another to support tunnelling, e.g. in YADH indicate a H-transfer distance of 3.4 to 3.6 Å from the crystal structure of the enzyme, which is too long for tunnelling. The temperature dependence of KIEs is a function of the degree of coupling of the symmetric vibration to the reaction coordinate, because only the distance between donor and acceptor is sensitive to isotopic labelling. To promote H-tunnelling, an enzyme will have evolved not only to stabilise the transition state, but to bring donor and acceptor closer together and to alter the respective energy levels of reactant and product.

The recent studies on MADH have provided verification of VEGST theory (Sutcliffe & Scrutton, 2000). With the data from ADH-hT, it may be that extreme (i.e., from the ground state of the reactants) tunnelling may be a common mechanism for the breaking of stable C-H bonds by enzymes (Scrutton *et al.*, 1999). The dynamic barrier approach to catalysis has major implications for how H-transfer and other reactions are modelled theoretically. It also has wider implications for catalysis (Kohen & Klinman, 1999). For example, is the large size of proteins, which appears necessary for catalysis, related to a critical interplay of protein motion and catalytic efficiency or does large size simply reflect an evolutionary strategy for bringing multiple functional groups into juxtaposition at an active site (Klinman, 1989)? The entire protein has importance in catalysis, a consideration which could have significant impact on biomimetic catalyst design. Incorporating the dynamic behaviour of a protein may provide a missing link between static pictures of enzyme active sites and their activity (Kohen & Klinman, 1999).

1.4 Aims

The work presented in this thesis looks at three different aspects of catalysis in the enzyme TMADH. The first investigation presented is that of substrate inhibition in the enzyme. The long-standing debate into the causes and nature of the excess substrate inhibition is presented and a model for substrate inhibition is tested. Is there anything in the redox properties of the enzyme during steady-state turnover to indicate what is happening when TMADH is inhibited, and what are the effects of mutations that seem to abolish inhibition? Secondly, there are recent findings that quantum tunnelling of hydrogen occurs from the ground state of reactants in the enzyme MADH. Given the similarity of the MADH reaction with that of TMADH, is there any evidence that tunnelling occurs in this enzyme? Does the reaction require interpretation in dynamic terms? The work is presented against a background of investigations into the mechanism of C-H bond cleavage in TMADH. In the last results chapter, an attempt at rational protein design in TMADH is presented, asking the question: can fairly straightforward changes to the active site of TMADH induce a modest change in substrate specificity? Given the possible therapeutic use of enzymes as biosensors, the successful engineering of enzymes is a major goal of protein engineering.

Chapter 2

Materials and Methods

2.1 Materials

2.1.1 Chemicals and Reagents

Trimethylamine hydrochloride (TMA), dimethylamine (DMA) 2,6-dichlorophenolindophenol (DCPIP), phenazine methosulphate (PMS) and methamphetamine (δ-N, α-dimethylphenethylamine; δ-desoxyephedrine) were from Sigma Chemical Company. N, N-diethylmethylamine (DEMA), N, N-dimethylethylamine (EDMA), N, N-dimethylbutylamine (DMButA), N, N-dimethylbenzylamine (DMBenA) and triethylamine (TEA) were from Aldrich. Perdeuterated TMA was from CK Gas Products Ltd. Sodium dodecyl sulphate (SDS) was from BDH chemicals and ethidium bromide was from Bachem. 'Protogel' (37.5:1 w/v acrylamide:bisacrylamide) was from National Diagnostics. [^{35}S]dATP-αS triethylammonium salt for DNA sequencing (1000 Ci·mmol^{-1}) was supplied by Amersham Life Science. All other chemicals described in the text were supplied by Sigma-Aldrich, Fisher or BDH and were of analytical grade wherever possible.

Ferricenium hexafluorophosphate had been previously prepared in the laboratory, using the method of (Lehman & Thorpe, 1990).

Complex bacteriological media were from Difco Laboratories, ultra pure agarose was purchased from Life Technologies Inc. and 'Timentin' (15:1 w/w ticarcillin sodium:potassium clavulanate) was from Beecham Research Laboratories.

Water used was glass-distilled and deionised.

2.1.2 Bacterial Strains and Media

Methylophilus methylotrophus (species W_3A_1, NCIMB11348) was a gift from Professor F. Scott Mathews (Department of Biochemistry Washington University School of Medicine, St Louis, Missouri, USA). *E. coli* strain TG1 [K12,(r_k^-, m_k^-, r_b^- m_b^-), Δ (*lac-pro*), *sup* E, *thi, hsd* D5/F' *tra* D36, *pro* A^+ B^+, *lac* I^q, *lac* Z ΔM15] was purchased from Stratagene. *E. coli* XL1-Blue strain *recA1 endA1 gyr!96 thi-1 hsdR17 supE44 relA1 lac* [F′ *pro AB lacI*^{q} *ZΔM15* Tn*10* (Tet^r)] was purchased from Stratagene. *E. coli* NM522 *mut*S strain *thi, sup*E, Δ(*hsd*MS-*mcr*B)*5*,

Δ(*lac-pro*AB) [*mut*S::Tn 10] F' [*proAB*$^+$ *lac*I^q *lac* ZΔM15] was supplied with the Unique Site Elimination (U.S.E.) mutagenesis kit from Pharmacia.

E. coli strains were grown in 2x YT media, which contains, per litre: 10 g tryptone, 10 g yeast extract and 5 g NaCl. Solid growth media used was LB (Luria-Bertani) medium which contains, per litre: 10 g tryptone, 5 g yeast extract, 5 g NaCl and 15 g bacteriological agar.

M. methylotrophus (sp. W_3A_1) was grown in the mineral media of Colby and Zatman (Colby & Zatman, 1973), which contains, per litre: 1.2 g K_2HPO_4, 0.62 g KH_2PO_4, 0.05 g $CaCl_2 \cdot 6H_2O$, 0.2 g $MgSO_4 \cdot 7H_2O$, 0.1 g NaCl, 1.0 mg $FeCl_3 \cdot 6H_2O$, 0.5 g $(NH_4)_2SO_4$, 5.0 μg $CuSO_4 \cdot 5H_2O$, 10 μg $MnSO_4 \cdot 5H_2O$, 10 μg Na_2MoO_4, 10 μg H_3BO_3, 70 μg $ZnSO_4 \cdot 7H_2O$, 5 μg $CoCl_2 \cdot 6H_2O$. The pH of the solution was adjusted to 7.0 with HCl. After autoclaving and cooling to room temperature, a freshly made solution of filtered substrate (0.2 μm filter) was added to the medium to give a final concentration of 0.3 % (w/v). Solid Colby and Zatman medium was produced by the addition of purified agar to 1.5 %.

2.1.3 DNA Modifying Enzymes

Restriction endonucleases *Eco* RI, *Hin* dIII, *Kpn* I, *Bam* HI and *Dpn* I were supplied by MBI Fermentas Molecular Biology. T4 DNA ligase was obtained from Promega. Calf-intestinal alkaline phosphatase was supplied by Boehringer Mannheim. T4 polynucleotide kinase was from USB.

2.1.4 Chromatographic Media and Membranes

Pre-swollen diethylaminoethyl cellulose (DE-52) anion exchange media was from Whatman Biosystems Ltd. Phenyl Sepharose high performance hydrophobic interaction media was obtained from Pharmacia.

PM30 Diaflo ultrafiltration membranes were supplied by Amicon.

2.2 Molecular Biology Methods

2.2.1 DNA Purification

For small-scale plasmid DNA isolation (miniprep), a single *E. coli* colony was picked from an agar plate and used to inoculate 5 ml or 10 ml of 2x YT medium, containing 50 μg/ml 'Timentin'. For large-scale plasmid isolation (maxiprep), 5 ml of an overnight *E. coli* culture was used to inoculate 500 ml of 2x YT medium containing 50 mg/litre 'Timentin'. Cultures were grown overnight at 37 °C in a shaking incubator at 200 rpm.

Minipreps were carried out using either the Wizard *Plus* DNA Purification kits supplied by Promega or the Recovery System supplied by Hybaid. Maxipreps were carried out using the Wizard *Plus* DNA Purification kits supplied by Promega. For the purification of DNA from low melting point agarose gels, the PCR Purification Kit supplied by Promega was used.

2.2.2 Transformation of *E. coli* Cells with DNA

Competent cells were prepared using a modified version of the calcium chloride/rubidium chloride method described by Sambrook *et al.* (1989) and kindly supplied by Dr J. Basran, University of Leicester.

Competent cells were removed from -70 °C storage, and allowed to thaw. Plasmid DNA (approximately 1 μg-5 μg of DNA in 5 μl-10 μl of solution) was introduced into the cell suspension, gently mixed, and the cells left on ice for 30 min. The cells were then heat-shocked at 42 °C for 90 s before being returned to ice for 2 min. 1 ml of 2x YT media was added to the cells, which were then incubated at 37 °C with shaking for 1 h. Aliquots of between 10 μl to 200 μl from this incubation were plated on to LB agar plates containing 'Timentin' at a concentration of 50 $\mu g \cdot ml^{-1}$. The plates were allowed to stand on the bench for 15 min to ensure adequate absorption of the liquid and were then inverted and incubated at 37 °C overnight.

2.2.3 Enzymic DNA Modifications

DNA restriction digests, or any other reactions involving DNA were carried out using commercial enzyme preparations (Section 2.1.3). Reactions were therefore carried out using the appropriate buffers and instructions supplied by the enzyme manufacturers.

Phosphorylation of the 5' end of DNA fragments was achieved using T4 polynucleotide kinase. After incubation for 30 min at 37 °C the reaction was terminated by heat inactivation (65 °C for 10 min).

The terminal 5' phosphate of DNA fragments was removed by treatment with calf intestinal alkaline phosphatase. The reaction was terminated after 1 h by extracting the protein using phenol/chloroform (1:1 v/v).

For DNA ligation, the reaction mixture contained alkaline phosphatase-treated vector DNA, the fragment DNA to be cloned into the vector and T4 DNA ligase. The reaction was incubated at 16 °C overnight in a water bath.

DNA restriction digests were carried out using approximately 1 μg of DNA. The reaction was incubated at 37 °C for 3 to 4 h, then terminated by heat inactivation if necessary.

2.2.4 Agarose Gel Electrophoresis

Agarose gels (0.8% w/v, 11 cm x 12 cm) containing 0.6 μg·ml ethidium bromide were cast, and electrophoresis was performed in TAE buffer (50x TAE buffer is 242 g Tris base, 18.6 g EDTA and 57.1 ml glacial acetic acid in 1 l final volume), typically at 150 V for 40 min. Samples (20 μl) were loaded into the gel in 1x loading buffer (6x loading buffer is composed of 0.25 % bromophenol blue, 0.25 % xylene cyanol and 30 % v/v glycerol in water). Nucleic acid was visualised by exposure to long wavelength UV light on a UVP transilluminator.

DNA markers (1 kb ladder) were from MBI Fermentas. Band sizes were, in base pairs: 10000, 8000, 6000, 5000, 4000, 3500, 3000, 2500, 2000, 1500, 1000, and 500.

2.2.5 DNA Sequencing

Dideoxynucleotide DNA sequencing (Sanger *et al.*, 1977), for verification of successful mutagenesis and gene re-sequencing purposes, was carried out using the T7 system, supplied by Pharmacia.

During the sequencing of plasmid DNA, template denaturation was accomplished by the addition of 8 µl of freshly made 2 M NaOH to about 2 µg of DNA contained in 32 µl water or TE buffer. Primer (4 µl of a 3.0 OD_{260} $nm \cdot ml^{-1}$ stock) was added and the mixture incubated at 37 °C for 30 min. Neutralisation was carried out with 7 µl of 3 M potassium acetate, pH 4.8. The template DNA was precipitated by addition of 150 µl ethanol and then placed on dry ice for 15 min. Following microcentrifugation at 13000 rpm for 15 min, the pelleted, annealed template-primer material was air-dried and resuspended in appropriately diluted manufacturer's annealing buffer. The manufacturer's instructions were observed from the labelling stage of the procedure onwards.

Completed sequencing reactions were subjected to PAGE through a 40 cm wedge gel composed of 13.3 ml 'Protogel' acrylamide mix, 25 ml 46.7 % (w/v) urea, 5 ml 10x TBE buffer (108 g Tris-HCl, 55 g boric acid and 10 g disodium EDTA per litre pH 8.2) made up to 50 ml with water. After filtering and degassing, polymerisation was initiated by the addition of 150 µl 10 % ammonium persulphate (APS) and 70 µl N, N, N' N'-tetramethylethylenediamine (TEMED).

The acrylamide gel mixture was injected between taped and clamped sequencing plates using a 50 ml syringe. The flat end of a shark tooth comb was placed at the top of the gel and it was left to polymerise for at least 1 h. Before the samples were loaded onto the gel, the tape was removed from the bottom of the sequencing plates, and the gel was pre-run for about 1 h in 1x TBE buffer, at 45 W/40 mA/1500 V. The shark tooth comb was inverted and the sequencing samples loaded. Gels were typically run for between 1 h to 3 h at 45 W/A/1200 V. The gel was transferred to 3 M paper (Whatman), fixed by washing with 10 % methanol 10 % acetic acid and dried under vacuum on a gel dryer at 80 °C for 2 h. X-ray film was exposed to the gel and the film was developed after 16-24 h.

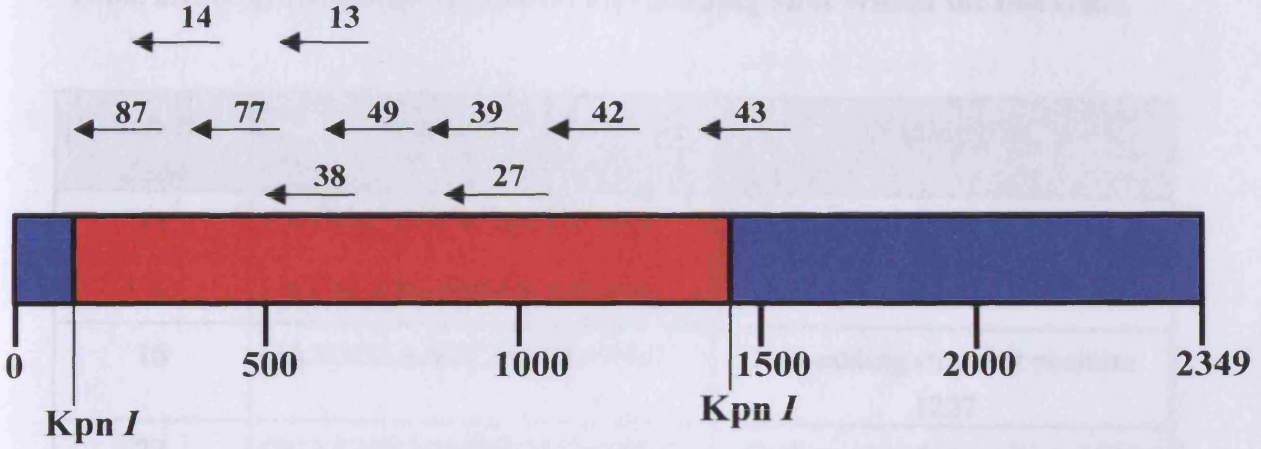

Figure 2.1. Sequencing Strategy Used for the *tmd* Gene. Sequencing was carried out within a region flanked by two *Kpn* I sites used in the subcloning procedure described in Chapter 5, Section 5.2.3. Oligonucleotides are given their laboratory code number. Their DNA sequences and precise binding sites within the *tmd* are given in Table 2.1.

Table 2.1. Oligonucleotide Sequences and Binding Sites Within the *tmd* Gene.

Laboratory Code	Sequence 5' - 3'	Binding Site
13	CATTTCTTTACAGTAGGA	Coding strand at position 733
14	CATACTTCTGACCATCCA	Coding strand at position 420
16	GATGGAAAGCGGTTATAC	Non-coding strand at position 1227
27	GGATATCGTCTTAGCGACC CTGC	Coding strand at position 1030
38	ATCCACGCCGAATTTTGTCG CAATCGC	Coding strand at position 681
39	TGCTGTCGCATCCCGGGTAC AAAT	Coding strand at position 1013
42	CCACTCACCCAAGCCAG	Coding strand at position 1323
43	GGTGTGAGTTGATCTGG	Coding strand at position 1553
49	CCAATTTAAACGAGGGATG GT	Coding strand at position 859
77	CAGCGGATAAGATTGCGCA CCGTATACGTA	Coding strand at position 525
87	CCAGATACGTGCGGTCAAA CGATG	Coding strand at position 237

2.2.6 Site-Directed Mutagenesis

The TMADH Quad-, Penta- and Hexa-mutants (see Abbreviations and Chapter 5 for the positions and types of mutations referred to by these titles), were generated using the Unique Site Elimination (U.S.E.) mutagenesis kit from Pharmacia. The design of the oligonucleotides used in the mutagenesis procedure are shown in Table 2.2. TMADH expression plasmids incorporating mutations of the *tmd* gene to produce TMADH mutants Y60L, Y60A, W264L, Y169F and H172Q were prepared and donated by Dr J. Basran and Dr M. Mewies.

The design of the mutagenic oligonucleotides took into consideration factors such as codon usage in the *tmd* gene (Boyd *et al.*, 1992), sufficient flanking regions either side of the mutation site to ensure tight binding, and the absence of stem-loop structures generated by the sequence, checked using the GCG package (Genetics Computer Group).

Oligonucleotides were synthesised by the Protein and Nucleic Acid Laboratory (PNACL), University of Leicester.

Table 2.2. DNA Sequence of Oligonucleotides Used for Site-Directed Mutagenesis

Type and Position of Mutation	DNA Sequence of Mutagenic Oligonucleotide[1]
Threonine 257→ Arginine (T257N)	5'-GCAATATCACCAAT**GTT**GATATCCCACAT-3'
Glutamine 131→ Alanine (E131A)	5'-GTAGGACAGCGT**AGC**AAACTCTGACGC ATA-3'
Histidine 71→ Leucine and Leucine 73→ Isoleucine (H71L.L73I)[2]	5'-CACCTTCGTCCCAGATACGTGC**GGTAAT** ACG**CAA**TGTATCATCTGACTC-3'
Eco RI 'knockout'[3]	5'-CGGATCTCGTGCCATGAAC**TCC**ACCTC ACTAC-3'

[1]Mutagenic regions are shown in **bold.**

[2]This mutagenic oligonucleotide was used to introduce the H71L.L73I mutations into the Quad mutant of TMADH; it therefore incorporates the mutation Serine 74→ Threonine (S74T) that was already present in that particular mutant.

[3]Used to eliminate *Eco* RI site at -8 position of *tmd* gene, necessary for U.S.E. mutagenesis protocol (See Section 5.2).

2.2.7 Isolation of New TMADH Mutants

The template plasmid for production of TMADH mutants was the expression plasmid pSV2tmdveg (Scrutton *et al.*, 1994; Basran *et al.*, 1997; Figure 2.1). Mutant plasmids were identified by restriction analysis, and incorporation of mutagenic sequence was confirmed by dideoxy DNA sequencing (Sanger *et al.*, 1977).

To minimise the amount of re-sequencing (performed to ensure no spurious changes arose during the mutagenesis procedure) and to restore the upstream *Eco* RI site for further rounds of mutagenesis, a 1.4 kbp *Kpn* I DNA fragment containing about 50 % of the *tmd* gene was excised from the mutagenised plasmid and used to replace the equivalent fragment in the plasmid pSV2tmdY60A, provided by Dr J. Basran, University of Leicester. The successfully mutated plasmid was then used in further rounds of mutagenesis.

Table 2.3. DNA Fragment Sizes Obtained by Restriction Analysis of Plasmid pSV2tmdveg.

Restriction Enzyme	Expected Fragment Sizes (kb)
Eco RI	4.97
Hin dIII	4.25, 0.72
Kpn I	3.6, 1.4
Bam HI	4.97
Eco RI/*Hin* dIII	2.6, 1.65, 0.72
Eco RI/*Hin* dIII	4.25, 0.72
Hin dIII/*Bam* HI	2.78, 1.47, 0.72

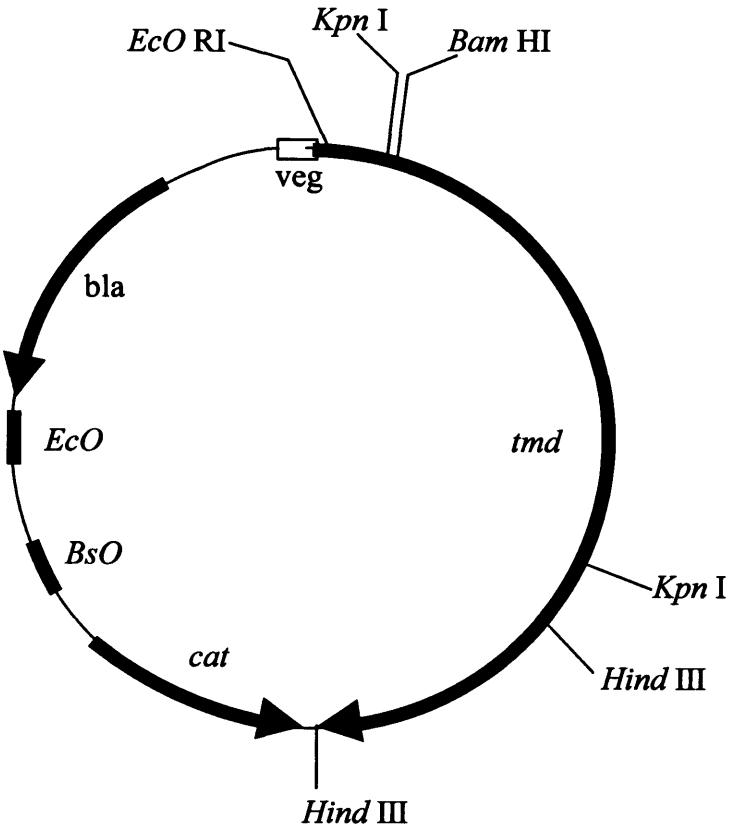

Figure 2.2. Construction of plasmid pSV2tmdveg. *EcO*: *E. coli ori*, *BsO*: *B. subtilis ori*, *tmd*: trimethylamine dehydrogenase gene, bla: ß-lactamase gene, *cat:* chloramphenicol acetyltransferase gene, veg: *B. subtilis* vegetative promoter. The restriction sites illustrated are those relevant to the mutagenesis and subcloning procedures as described in the text. Expected sizes of DNA fragments from restriction digests are listed in Table 2.3.

2.3 Protein Methods

2.3.1 SDS Polyacrylamide Gel Electrophoresis

SDS polyacrylamide gel electrophoresis (SDS PAGE) was carried out according to the method described by (Laemmli, 1970), using either 12 % acrylamide gels in a slab gel system or by using Pharmacia precast 12.5 % 'Phastgels', which were run using a Pharmacia LKB Phast System. The slab gel compositions were as follows: 4 % stacking gel was 1.33 ml 'Protogel', 1.25 ml 1 M Tris-HCl (pH 6.9), 7.26 ml water, 100 µl 10 % SDS, 50 µl 10 % APS and 10 µl TEMED. All the resolving gels contained 3.0 ml 1.5 M Tris-HCl (pH 8.8), 100 µl 10 % SDS, 50 µl 10 % APS and 10 µl TEMED. The acrylamide mixes were as follows: the 12 % resolving gel was 4.8 ml 'Protogel', and 4.04 ml.

Crude cell extracts were prepared as follows: 3 ml to 5 ml of cell cultures were pelleted by microcentrifugation. Pellets were initially solubilised in 20 µl 8 M urea and then 20 µl of 10 % SDS was added. If necessary, cells were manually disrupted by repeatedly passing through a 0.5 mm gauge needle attached to a 1 ml syringe. The extracts were then treated exactly as other protein samples: protein samples were added to an equal volume of 2x 'loading buffer' (20 mM DTT, 2 % SDS, 250 mM Tris-HCl, pH 6.8, 10 % glycerol, 0.01 % bromophenol blue) and placed in a boiling water bath for 5 min before being loaded on to the gel.

Gels were run at a constant current of 35 mA until the dye front reached the base of the gel (about 2 h). Running buffer is 2.9 g glycine, 6.0 g Tris and 1.0 g SDS in 1 litre. Gels were stained using Coomassie Brilliant Blue R250 (0.25 % in 5:1:5 v/v solution of methanol: acetic acid: water) for 20 min to 30 min and then destained in 5:1:5 v/v methanol: acetic acid: water.

Pre-stained protein molecular weight standards were supplied by Gibco-BRL Life Technologies Inc., (Gaithersburg, MD, USA); apparent sizes were 11, 29, 45, 63, and 83 kD.

2.4 Methods for the Analysis of TMADH

2.4.1 TMADH Purification

Purification of native and recombinant TMADH was carried out using the scheme devised by Steenkamp & Mallinson (1976) and McIntire (1990) with the modifications described in (Scrutton *et al.*, 1994).

For preparations of native TMADH, cells of *M. methylotrophus* were cultured in carbuoys containing 20 l of Colby-Zatman media (Section 2.1.2), aerated at ambient temperature for 48 h. For preparations of recombinant mutant TMADH, transformed *E. coli* strain TG1 containing the mutant plasmid construct was cultured in 2x YT medium containing 'Timentin' at 50 $mg \cdot l^{-1}$, supplemented with 100 $mg \cdot l^{-1}$ riboflavin and 200 $mg \cdot l^{-1}$ $FeSO_4 \cdot 7H_2O$. Cells were grown at 20 °C with vigorous shaking for 40 h. Recombinant TMADH enzymes are expressed constitutively under the control of the synthetic *veg* promoter (Scrutton *et al.*, 1994). After about 40 h growth, cells were harvested by centrifugation (5,000 rpm for 10 min at 4 °C).

All cells were grown in batch culture and between "grow-ups", cell pellets were stored at -20 °C. Typically, 50 litres cell culture were required to obtain sufficient enzyme for kinetic analysis of native TMADH preparations and some TMADH mutants (see Chapter 5). However, most recombinant forms of TMADH require 10 l culture. After the last batch of cells had been harvested, the cell pellets were thawed and resuspended in 50 mM potassium phosphate buffer, pH 7.5, 4 °C. Cells were disrupted by passing through a French pressure cell at 4 °C using a cell pressure of about 20,000 psi. The resulting extract was subject to DNase I treatment for 1 h at room temperature before being centrifuged (15,000 rpm for 30 min at 4 °C). The cleared supernatant was brought to 50 % saturated $(NH_4)_2SO_4$ by the addition of the solid salt. The mixture was centrifuged at 10,000 rpm for 30 min, using a GSA rotor. The supernatant was brought to 80 % saturated $(NH_4)_2SO_4$ and centrifuged at 10,000 rpm for 30 min. The resultant pellet was dissolved in 100 ml 20 mM potassium phosphate buffer, pH 7.5 and dialysed against 16 litres of the same buffer, with at least three changes of buffer. The dialysed sample was applied to a column (3 cm x 40 cm) of diethylaminoethyl cellulose (DE52), previously equilibrated with 20 mM potassium phosphate buffer, pH 7.5. After washing (1 litre of buffer), the column was eluted using a linear gradient of 0-0.5 M NaCl contained in 20 mM potassium phosphate buffer, pH 7.5.

Fractions containing TMADH (eluted at about 0.2 M NaCl; (Scrutton et al., 1994)) were identified by absorption spectra and SDS-PAGE then pooled and reduced in volume to about 60 ml in an ultrafiltration cell fitted with an Amicon PM30 Diaflo membrane. The concentrated sample was brought to 50 % saturated $(NH_4)_2SO_4$ by the addition of the solid salt and then applied to a Phenyl-sepharose HP hydrophobic interaction column (1 cm width x 15 cm length) pre-equilibrated with 20 mM potassium phosphate buffer, pH 7.5, saturated to 50 % with $(NH_4)_2SO_4$. The column was eluted using a linear gradient (600 ml) of 50-0 % $(NH_4)_2SO_4$ contained in 20 mM potassium phosphate buffer, pH 7.5. The fractions containing TMADH, eluted at approximately 20 % $(NH_4)_2SO_4$, were pooled and either equilibrated (by dialysis) with 20 mM potassium phosphate buffer, pH 7.5 for use in steady state assays or with 100 mM potassium phosphate buffer, pH 7.5 for use in stopped-flow experiments. The dialysed sample was concentrated by ultrafiltration through an Amicon PM30 Diaflo membrane.

For long-term storage, ethylene glycol was added to the concentrated enzyme to a final concentration of 20% v/v. The enzyme was then stored at -20 °C. For some experiments (see Chapter 4) the enzyme was not stored by freezing. In these cases, TMADH was filter-sterilised by passing through a 0.2 μm syringe filter (Acrodisc), and then stored at 4 °C. Samples stored in this manner were stable and free of bacterial growth for up to 2 weeks.

2.4.2 Protein estimation

Protein concentration of enzyme samples was determined using UV-visible spectroscopy. The extinction coefficient of native TMADH at 280 nm is 201,610 $M^{-1}cm^{-1}$ (Wilson *et al.*, 1996). The extinction coefficient at 443 nm depends on the flavin content (see below and the Results section).

2.4.3 Flavin determination

All recombinant forms of TMADH so far studied are under-flavinylated (Scrutton *et al.*, 1994; Packman *et al.*, 1995; Mewies *et al.*, 1995). The flavin content of mutant enzymes was determined using the spectrophotometric method described by (Scrutton *et al.*, 1994). The flavin content of native and recombinant TMADH enzymes is routinely assessed using Equation 2.1. Deduction of the ratio of

absorbance of the purified enzymes at 382 nm and 442 nm allows a calculation of flavin content using the following relationship, based on the observations described in (Scrutton et al., 1994):

$$\text{Proportion of flavinylated enzyme } (flvn) = \frac{x - 0.82}{0.48} \qquad \textbf{Equation 2.1}$$

where x is the A_{442}/A_{382} ratio.

0.82 and 0.48 are the A_{442}/A_{382} values obtained for fully flavinylated (native) and totally deflavo (a recombinant form) TMADH respectively. It is assumed that a linear relationship exists between these two extremes, dependent purely on the FMN content of the enzyme.

Theoretical extinction coefficients at 442 nm for mutant TMADH enzymes are calculated using the expression:

$$E_{442} = (flvn \times 27300) + [(1 - flvn) \times 15000] \qquad \textbf{Equation 2.2}$$

Where necessary, covalently bound flavin content was also assessed by precipitation with perchloric acid. Samples of purified enzyme were treated with 0.5 M perchloric acid and the resulting protein precipitate collected by microcentrifugation for 5 min at 13,000 rpm. The protein pellet was washed briefly in acetone and resuspended in 6 M guanidine hydrochloride contained in 100 mM potassium phosphate buffer, pH 7.5, and the flavin content estimated by examining the absorbance at 442 nm.

2.5 Kinetic Analysis of TMADH

2.5.1 Steady-state Analysis using PMS and DCPIP

TMADH activity was measured by the method described by Colby and Zatman (1973). Assays were performed at 30 °C. Each assay mix contained 10 µl of 20 mM PMS, 10 µl of 9 mM DCPIP and 20-300 µl of the protein sample to be assayed, made up in 0.1 M sodium pyrophosphate buffer pH 8.5. Reactions were initiated by microlitre additions of 2 M substrate, prepared in 0.1 M sodium pyrophosphate buffer pH 8.5, to a final assay volume of 1 ml. The decrease in absorbance at 600 nm was monitored using a Hewlett Packard 8452A diode array

spectrophotometer. Initial rates for reaction velocity were monitored as a decrease in DCPIP absorbance at 600 nm, and quantified as μM DCPIP reduced per second using an extinction coefficient of 21,900 $M^{-1} \cdot cm^{-1}$. Initial rates of reaction were corrected for the slow non-enzymatic reaction of PMS. Duplicate assays were carried out for each substrate concentration used.

2.5.2 Steady-state Analysis using Ferricenium Hexafluorophosphate

TMADH activity was measured according to the method of Lehman *et al.*, (1990). Stock solutions of ferricenium were prepared by dissolving the salt in 10 mM HCl, spinning the solution in a microcentrifuge and filtering through a 2 μm syringe filter (Acrodisc). The concentration of this stock solution was determined by measuring the absorbance at 300 nm using an extinction coefficient of 4300 $M^{-1} \cdot cm^{-1}$ (Lehman & Thorpe, 1990). Each assay mix contained variable volumes of the protein sample to be assayed and microlitre additions of substrate, prepared in 20 mM potassium phosphate buffer, pH 7.0. Reactions were initiated by the addition of ferricenium hexafluorophosphate to the desired concentration (between 100-400 μM), to a final volume of 1 ml.

Kinetic parameters from assays were calculated by performing least squares fits of the observed rates to appropriate rate equations, using Grafit (Leatherbarrow, 1992).

2.5.3 Fitting of Steady-State Data

Data for TMADH is fitted to the equation of Falzon and Davidson (Falzon & Davidson, 1996a). This equation takes into account the observed substrate inhibition when a second molecule of TMA binds to the enzyme, causing gated electron transfer from the flavin to the 4Fe-4S centre of TMADH, (the rate-limiting step in catalysis):

$$v = \frac{\left(1 + \frac{b[S]}{K_i}\right) V_{max}}{1 + \frac{K_s}{[S]} + \frac{K_s}{K_i} + \frac{[S]}{K_i}}$$

Equation 2.3

where K_m is the Michaelis constant, and K_i is the inhibition for the 'modulatory site'; [S] is the substrate concentration. In this equation, V_{max} is the final limiting velocity observed at high concentrations of substrate; it is modulated by the factor b that reflects the extent of inhibition.

If no substrate inhibition was observed within the range of substrate concentration used, which can occur with some TMADH mutants, steady-state data was fitted to the Michaelis-Menten equation.

2.5.4 Stopped-flow kinetic analyses

An Applied Photophysics SF.17MV stopped-flow spectrophotometer was used to carry out pre-steady-state kinetic assays. Rapid-scanning, time-dependent stopped-flow reactions were carried out using a photodiode array detector and X-SCAN software (Applied Photophysics). Global analysis and numerical integration were performed using PROKIN software (Applied Photophysics) and single wavelength studies were analysed using Spectrakinetic software (Applied Photophysics), on an Archimedes 410-1 microcomputer.

Experiments were performed under aerobic conditions, since the half-life for the reoxidation of substrate-reduced TMADH is greater than 15 min (Wilson *et al.*, 1996), making anaerobic conditions unnecessary. Reactions were carried out by mixing an equal volume of enzyme contained in 100 mM potassium phosphate buffer, pH 7.5, and various concentrations of substrate, contained in the same buffer at 30 °C. The concentration of substrate employed was at least ten-fold greater than that of the enzyme, thus ensuring pseudo-first order conditions. At least three replicate measurements, each containing 800 points, were made at each substrate concentration and the traces averaged prior to analysis.

As previously reported (Rohlfs & Hille, 1994; Falzon & Davidson, 1996a), under these pseudo-first order conditions, the kinetic transients recorded at 443 nm were monophasic, and fitted to Equation 2.4

$$Abs = Ce^{-k_{obs}t} + b \qquad \textbf{Equation 2.4}$$

where C is the amplitude of the phase and b is the final absorbance. The rate constants derived (k_{obs}) were found to be dependent on substrate concentration and were modelled on the general reaction scheme given in Equation 2.5:

$$A + B \underset{k_2}{\overset{k_1}{\rightleftharpoons}} C \underset{k_4}{\overset{k_3}{\rightleftharpoons}} D$$ **Equation 2.5**

Where A is oxidised TMADH, B is substrate, C is the Michaelis complex and D is two electron reduced TMADH. The data were then fitted to Equation 2.6 (Strickland *et al.*, 1975) using the Kaleidograph software package.

$$k_{obs} = \frac{k_3[S]}{K_d + [S]} + k_4$$ **Equation 2.6**

For the fitting of this Equation 2.6, k_4 is given a value of zero, i.e. the reverse reaction is considered to be negligible or not occurring.

2.5.5 Recording of Spectral Forms of TMADH Under Steady-State Conditions

The recording of spectral changes in TMADH under steady-state conditions was performed on an Applied Photophysics SF.17MV stopped-flow spectrophotometer. Rapid-scanning, time-dependent stopped flow reactions were carried out using a photodiode array detector and X-SCAN software (Applied Photophysics). Global analysis and numerical integration were performed using PROKIN software (Applied Photophysics). TMADH at a mixing chamber concentration of 4 μM was rapidly mixed with substrate and ferricenium hexafluorophosphate at the concentrations desired.

Chapter 3

Substrate Inhibition in TMADH

3.1 Introduction

3.1.1 Overview

The catalytic cycle of TMADH can be divided into four steps that encompass the reductive and oxidative half-reactions: reduction of 6-*S*-cysteinyl FMN, internal electron transfer from FMN to the 4Fe-4S centre, formation of the spin-interacting state and oxidation by ETF. Single-turnover stopped-flow studies and EPR freeze-quench studies have revealed important kinetic information concerning these individual steps in the catalytic cycle of TMADH (Jang *et al.*, 1999a; Rohlfs & Hille, 1992; Rohlfs & Hille, 1994; Rohlfs *et al.*, 1995; Steenkamp & Beinert, 1982a; Steenkamp & Beinert, 1982b; Steenkamp *et al.*, 1978c), and steps towards determining the mode of C-H bond breakage in the enzyme are being made (Basran *et al.*, 1999a; Basran *et al.*, 1999c). However, there has been some debate concerning a synthesis of this information so as to satisfactorily explain the steady-state behaviour of TMADH, which is manifest as substrate inhibition at infinite concentrations of TMA (Falzon & Davidson, 1996b; Jang *et al.*, 1999a).

During steady-state analyses of native TMADH, substrate inhibition becomes obvious at about 100 μM TMA and the reaction rate declines sharply as TMA concentrations reach low millimolar levels. The substrate inhibition is partial: a non-zero limiting rate is reached, and by fitting to the equation of Falzon and Davidson (Falzon & Davidson, 1996b; Equation 2.3) the rate at infinite substrate concentration is usually predicted to reach a value that is about 2 % of the theoretical V_{max}. This substrate inhibition is not an artefact of using artificial electron acceptrs in steady-state assays of TMADH: it is also observed with the physiological electron acceptor, ETF (Steenkamp & Beinert, 1982b).

The rate-limiting step in TMADH catalysis where substrate inhibition is exerted is internal electron transfer from FMN to the 4Fe-4S centre, which is found to become slower in the presence of excess substrate (Steenkamp & Beinert, 1982a; Steenkamp & Beinert, 1982b). Debate on the substrate inhibition of TMADH has centred on the exact way in which excess TMA causes inhibition, either through a second regulatory allosteric site for substrate (Falzon & Davidson, 1996b), or through some other mechanism. The experimental work presented in this chapter was devised to address questions about substrate inhibition in TMADH and provide evidence that catalysis proceeds via a mechanism in which the redox state of the enzyme, and therefore its ability to be reduced by substrate, is influenced by the relative

concentrations of substrate and electron acceptor, which introduce potential branch points into the catalytic cycle of the enzyme through which it can follow either an inhibitory or uninhibitory route (Huang *et al.*, 1995; Jang *et al.*, 1999a).

3.1.2 Studies of Substrate Inhibition in TMADH

During the earliest kinetic characterisation of TMADH (Steenkamp & Mallinson, 1976), the steady-state behaviour of the enzyme was attributed to product inhibition by DMA. It was initially concluded that TMADH underwent conformational isomerisation between two stable forms; with inhibition occurring if product or PMS interacted with the 'wrong' form of the enzyme which, with TMA as substrate, would be a one-carbon product-enzyme complex (Steenkamp & Mallinson, 1976).

Later studies of TMADH moved onto the kinetics of internal electron flow in the enzyme (Steenkamp *et al.*, 1978c) and identified internal electron transfer from 6-*S*-cysteinyl FMN to the 4Fe-4S centre is the rate-limiting step in catalysis. This is considered unusual, because intramolecular electron transfer is rarely the rate-limiting step in enzymatic reactions, and with no structural information available for the enzyme, substrate inhibition was attributed to a conformational change on binding of TMA that promoted the formation of the spin-interacting state after initial reduction, possibly through a shift in the relative positions of the FMN and 4Fe-4S centre, or cooperativity between the subunits of the enzyme dimer (Kasprzak *et al.*, 1983; Steenkamp & Beinert, 1982a; Steenkamp & Beinert, 1982b). The argument for a conformational changes was strengthened by the observation that, in the presence of TMAC, TMADH can only be titrated with dithionite to the level of two electrons, while in its absence could be reduced to three electrons. Therefore, substrate binding was shown to profoundly effect the number of electrons that the enzyme was able to take up and to influence the formation of the spin-interacting state, which is not formed in the absence of substrate at the active site. The view that substrate produced a conformational change in TMADH was essentially held until the results of substrate binding studies were published (Bellamy *et al.*, 1989), which revealed that substrate binding did not change the enzyme conformation.

Despite the preference for a conformational solution for the manifestation of substrate inhibition in TMADH, there was an early suggestion that the oxidation-reduction potentials of the redox centres of the enzyme could be influenced by

substrate binding (Steenkamp & Beinert, 1982a). Midpoint potentials of +44 mV and +36 mV were indicated for the FMN/FMN_{sq} and $FMN_{sq}/FMNH_2$ couples respectively, and +102 mV for reduction of the 4Fe-4S centre(Pollock *et al.*, 1988). The separation of the two redox potentials indicates greater stabilisation of the flavin semiquinone. This stability of the semiquinone in TMADH became more significant when the redox potentials of the enzyme were determined by means of UV-visible spectroelectrochemistry in the presence of the inhibitor TMAC (Pace & Stankovich, 1991). When TMAC is bound at the active site of the enzyme there is a very large (+0.2 V) shift in the redox potential for conversion of oxidised TMADH to flavin radical and a -0.1 V shift in the redox potential for conversion of flavin radical to two-electron reduced flavin. Essentially, an isopotential transfer of electrons from the FMN of TMADH to the 4Fe-4S centre is changed upon TMAC binding into a state of marked semiquinone stabilisation over a 0.3 V range. With TMAC bound at the active site of the enzyme, the change in FMN redox potential combines with a smaller negative shift (-0.04 V) in the redox potential of the 4Fe-4S centre to create a state of the enzyme in which electron transfer from the semiquinone of TMADH to the 4Fe-4S centre has a very negative driving force (-0.17 V at pH 7.0) and requires a positive change in Gibbs free energy (+3.9 kcal). From the TMAC studies, it can be inferred that there are similar changes in the redox potentials of FMN and the 4Fe-4S centre when TMA binds to the enzyme following reduction, stabilising the FMN in the semiquinone form, causing substrate inhibition.

Following the cloning of the *tmd* gene and the production of mutant forms of TMADH, it was found that some TMADH mutants have lost the ability to be inhibited by TMA (Basran *et al.*, 1997). This is attributed to a slowing in the rate of flavin reduction, so that this is now the rate-limiting step in catalysis, leading to kinetic mixing with the phase in which internal electron transfer occurs, as monitored at 365 nm or by EPR spectroscopy. With an apparent loss in the attenuation of internal electron transfer there is therefore a concomitant loss in substrate inhibition.

3.1.3 Recent Debate About Substrate Inhibition in TMADH

With the large body of information available about the kinetics, structural data and redox potentials of TMADH, the mechanism by which substrate inhibits the enzyme has been the subject of recent debate, and has led to two main proposals to explain the steady-state behaviour of TMADH.

3.1.3.1 The Model of Falzon and Davidson

As outlined in the Introduction (Section 1.1.10), the rates corresponding to k_{int} and k_{slow} of the reductive half-reaction are obtained from kinetic transients monitored at 365 nm, which report on internal electron transfer from 6-*S*-cysteinyl FMN to the 4Fe-4S centre of TMADH. By carrying out a detailed analysis of these transients, Falzon and Davidson produced a kinetic model for intramolecular electron transfer in TMADH, that also attempted to explain the steady-state kinetic behaviour of the enzyme (Falzon & Davidson, 1996b; Falzon & Davidson, 1996a). During single turnover of TMA by TMADH, the transients observed by stopped-flow spectroscopy at 365 nm are biphasic, and the extent of the reaction which corresponds to the faster and slower parts of this kinetic phase is dependent on substrate concentration. The faster rate is dominant at low substrate concentrations, while the slower rate becomes dominant at high substrate concentrations. This observation was used to develop a model for the reductive half-reaction of TMADH in which two molecules of TMA simultaneously bind to TMADH.

In the model of Falzon and Davidson, one molecule of TMA binds at the active site of oxidised enzyme and is converted to product (Falzon & Davidson, 1996b). At high substrate concentrations, a second molecule of TMA also binds, but is not converted to products. Instead, this second TMA molecule attenuates the rate of intramolecular transfer and is responsible for the slower rate of the reductive half-reaction by binding at a modulatory site and presumably causing some conformational change. Analysing the faster and slower phases of internal electron transfer separately yielded apparent dissociation constants for TMA of 148 μM, for binding to the second, non-catalytic site, while the faster phase was analysed to yield a K_d of 36 μM for the catalytic site of TMADH.

Falzon and Davidson also attempted to address the question of whether there is a physiological reason for the occurrence of substrate inhibition in TMADH, suggesting that the inhibition of TMADH by TMA is a mechanism by which intracellular levels of formaldehyde are controlled in *Methylophilus methylotrophus*. Even though methylotrophs are capable of assimilating formaldehyde, it is a toxic compound that might be harmful in large amounts even to those organisms that are capable of using it as a carbon source. As such, it is unsuitable to use as a regulatory signal, so there is a requirement for control to be exerted at the level of substrate.

3.1.1.2 A Branching Mechanism for Substrate Inhibition (Jang et al., 1999a)

Some aspects of the study of Falzon and Davidson were contentious. Firstly, crystallographic studies of TMADH provide no evidence for the existence of a second binding site for substrate (Bellamy *et al.*, 1989; Lim *et al.*, 1982). Secondly, the rates of flavin reduction obtained by these authors (230 s^{-1} at pH 7.5, 30 °C) were significantly slower than previous (and subsequent) rates reported for flavin reduction, which are at least four-fold faster than this rate (Jang *et al.*, 1999a; Steenkamp & Beinert, 1982a; Steenkamp & Beinert, 1982b).

In order to try and clarify the disagreement concerning the kinetic behaviour of TMADH, a comprehensive pH dependence study of the enzyme reaction with TMA was performed (Jang *et al.*, 1999a), the details of which have been discussed in the main Introduction. However, this study also provided an alternative model to account for substrate in TMADH that does not involve a second binding site for TMA. Instead, it takes into account the potential for TMADH to form 1-, 2- and 3-electron reduced states under conditions where there is continual turnover of substrate by the enzyme and continual removal of electrons by an electron acceptor.

Reduction of TMADH by substrate generates 2-electron reduced enzyme. However, it is acknowledged by the basic catalytic scheme of TMADH that there is the possibility for a 1-electron reduced species to exist during turnover, due to the requirement for two oxidative half-reactions (Figure 1.20, page 27). Therefore, a one-electron reduced species of TMADH could transiently exist during steady-state turnover, to which TMA would be able to bind following product release. TMA will not be able to reduce the FMN as long as it is reduced by one electron to the anionic semiquinone form. However, following internal electron transfer from FMN to the 4Fe-4S centre, substrate turnover would occur, which would generate 3-electron reduced enzyme.

During conditions of continual reduction by substrate and continual oxidation by electron acceptor, the redox state of TMADH has the potential to fluctuate between 0-, 1-, 2-, and 3-electron reduced states (Jang *et al.*, 1999a). Extension of this idea has led to the development of a scheme consisting of two linked catalytic cycles, one uninhibitory, the other inhibitory (Scheme I), within which TMADH passes through different extents of oxidation and reduction. The uninhibitory cycle occurs at low substrate concentrations, while the inhibitory cycle at high substrate concentrations. In addition, Scheme I predicts that the concentration of electron acceptor has an effect on substrate inhibition, with the uninhibitory cycle operating at high concentrations of

electron acceptor and the inhibitory cycle operating at low concentrations of electron acceptor. The two cycles are termed the 0/2 (uninhibitory) and 1/3 (inhibitory) cycles; the numbers denote the minimum/maximum number of reducing equivalents taken up per enzyme subunit respectively within each cycle. Essentially, the 0/2 cycle comprises the reductive half-reaction of the enzyme, followed by two consecutive oxidative half-reactions with ETF or an artificial electron acceptor (similar to Figure 1.20). The 1/3 cycle derives from three potential branch points in the 0/2 cycle, when a second molecule of TMA binds at the active site of TMADH while the enzyme is in a partially (1- or 2- electron) reduced state.

Binding of a TMA molecule at the active site of reduced TMADH does not affect the rate of internal electron transfer from hydroquinone, nor the rate of external electron transfer from the 4Fe-4S centre of the enzyme to an external electron acceptor. Instead, inhibition is manifest when TMADH is in the one-electron reduced, anionic semiquinone form, and TMA is bound at the active site. It has been shown that binding of TMAC (and by inference, TMA) to reduced enzyme stabilises the semiquinone form of the FMN by increasing the redox potential of the FMN/4Fe-4S redox couple (Pace & Stankovich, 1991). When this occurs, internal electron transfer from anionic flavin semiquinone to the 4Fe-4S centre is perturbed and because the one-electron reduced 6-*S*-cysteinyl FMN of TMADH is unable to take up two electrons from TMA, substrate inhibition results. Only after internal electron transfer has occurred from the anionic flavin semiquinone to the 4Fe-4S centre can the TMA molecule bound at the active site be turned over and the catalytic cycle continue.

This model of substrate inhibition has the advantage over that presented by Falzon and Davidson in that it does not invoke the presence of an inhibitory binding site in TMADH, for which there is no structural evidence. Furthermore, TMADH has shown itself to be amenable to reduction to the level of three electrons, albeit by titration with dithionite, and there appear to be no reasons that would preclude it from passing through a 3-electron reduced state in a cyclic process such as that presented in Scheme I. Finally, as discussed in Section 1.2, the stabilisation of redox states by the binding of excess substrate or product is a shared property of other flavoenzymes and could represent a regulatory mechanism for these enzymes (Gutfreund, 1965; Gutman, 1977; Gutman *et al.*, 1980).

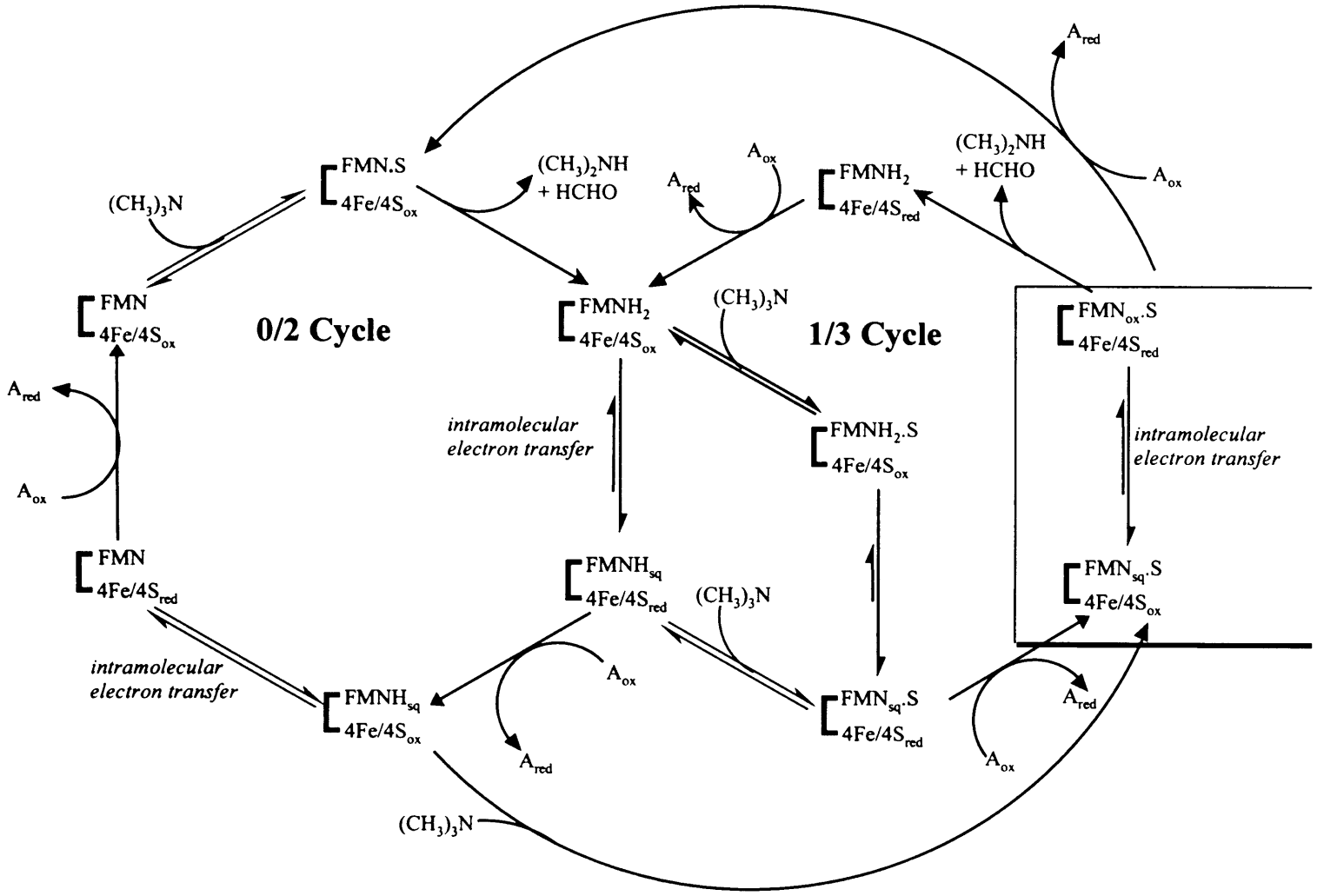

Scheme I: Proposed branching mechanism for steady-state turnover of TMADH. The 0/2 cycle represents the non-inhibitory state in which enzyme turns over between oxidised and two-electron reduced states. Population of the 1/3 cycle leads to substrate inhibition of TMADH when a molecule of TMA binds to *reduced* enzyme. The electron acceptor, which can be ETF, or an artificial electron acceptor (Fc^+ or PMS), is represented by the letter A. Inhibition occurs when substrate binds to 1-electron reduced enzyme, where FMN is in the anionic flavin semiquinone form, perturbing internal electron transfer (boxed).

The work in this chapter was designed to investigate substrate inhibition in TMADH, with reference to the catalytic mechanism shown in Scheme I. An experimental scheme was devised so that the spectral changes that occur during steady-state turnover of TMADH could be monitored; by collecting steady-state data with a range of tertiary amine substrates and with active site mutants of TMADH, evidence is presented that supports the branching model of Scheme I and illustrates the effect of substrate binding on inhibition in TMADH.

3.2 Results

3.2.1 Artificial Electron Acceptors and the Direction of Electron Flow in TMADH

The different redox states of TMADH have characteristic spectra (Figure 1.20). As a basis for studying steady-state turnover in TMADH it was proposed to directly monitor spectral changes that occur in the enzyme during steady-state turnover, using a photodiode array to measure whole spectrum changes in a stopped flow spectrophotometer. In steady state assays of TMADH, artificial electron acceptors are routinely used in place of the physiological electron acceptor ETF. Although ETF can be used as the electron acceptor in steady-state analysis of TMADH there are constraints in using a protein molecule as a substrate in steady-state reactions: the concentrations of oxidising substrate required for routine analysis make the use of ETF impracticable. PMS and dichlorophenolindophenol (DCPIP) have been used widely in previous studies of TMADH (Steenkamp & Mallinson, 1976; Steenkamp & Beinert, 1982a). However, because these electron acceptors have intense absorption in the visible region they are unsuitable for studies in which spectral changes associated with the redox centres of TMADH are monitored in the course of an enzyme-monitored turnover experiment. However, ferricenium hexafluorophosphate (Fc^+), that has been used as an electron acceptor in more recent studies on TMADH (Rohlfs & Hille, 1994) produces much less interference in those regions of the visible spectrum of TMADH that are informative (Figure 3.1), so the use of Fc^+ therefore enables spectroscopic characterisation of the enzyme during steady-state turnover. Fc^+ was therefore used as the electron acceptor during the studies of native TMADH presented in this Chapter.

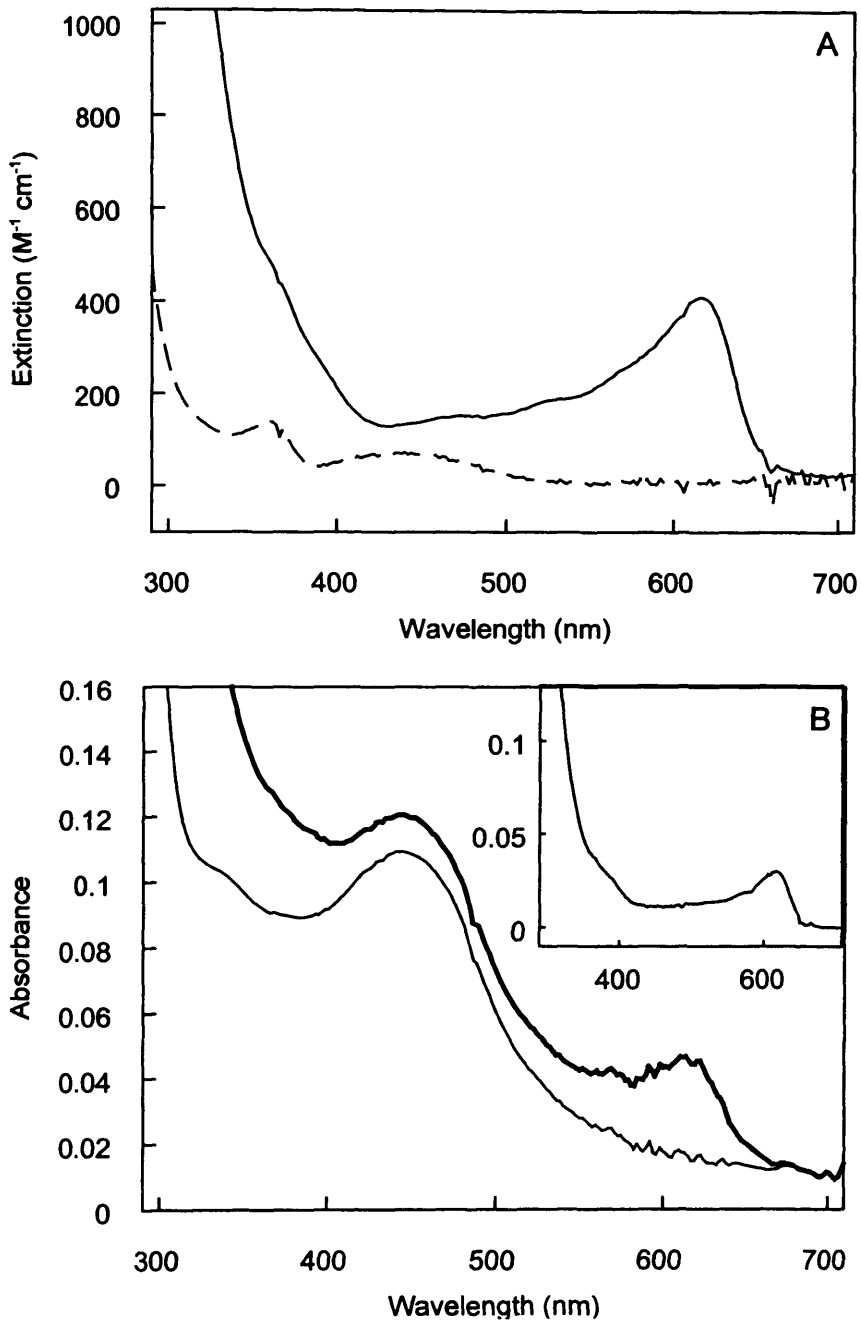

Figure 3.1: Spectra of oxidised and reduced Fc^+ and effects on the spectrum of oxidised TMADH. A. Oxidised (solid line) and reduced (dashed line) Fc^+ in 20 mM potassium phosphate buffer, pH 7.0. Reduction of Fc^+ was achieved in the presence of 0.1 nM TMADH and 100 μM TMA. B Spectrum of oxidised TMADH (4 μM, thin line) and oxidised TMADH (4 μM) plus Fc^+ (100 μM, thick line). Inset: difference spectrum showing contribution made by Fc^+.

It should be noted that in parallel studies conducted to complement this work by Dr J. Basran, it was confirmed that electron transfer from TMADH to Fc^+ occurs via the 4Fe-4S centre of TMADH (see attached paper, Roberts *et al.*, 1999)). This study demonstrated that electron transfer only occurs from the 4Fe-4S centre to Fc^+, and in this regard the flow of electrons during catalysis is comparable to that with the physiological electron acceptor, ETF (Huang *et al.*, 1995).

3.2.2 Steady-State Assays with Fc^+ as Electron Acceptor

Because prolonged incubation (over several hours) of TMADH with Fc^+ at pH 10 leads to inactivation of the enzyme (Huang *et al.*, 1995), potential inactivation is a major concern in any kinetic analysis that makes use of Fc^+ as electron acceptor. The success of any assay procedure depends on whether inactivation by Fc^+ can be prevented or suppressed on the timescale of the assay. At pH 7.0, preincubation of TMADH and Fc^+ for about 30 s prior to the addition of TMA reduces the observed initial velocity compared with reactions initiated by addition of Fc^+ (Wilson *et al.*, 1996). Loss of activity increases with incubation time, indicating that pre-incubation with Fc^+ effects an irreversible inactivation of TMADH, through effects on the 4Fe-4S centre of the enzyme (Huang *et al.*, 1995). However, when assays are initiated by adding Fc^+ or enzyme, the measured rates are linear over the time course of the experiment (typically between 30 s and 60 s), unlike the curvilinear traces expected for progressive inactivation of TMADH. Moreover, linear traces were obtained irrespective of the Fc^+ concentration, indicating that enzyme inactivation is negligible under the assay conditions employed. Therefore, to avoid inactivation of TMADH during the steady-state analyses described below, all reactions were initiated by the addition of Fc^+.

As reported by Steenkamp and Beinert (Steenkamp & Beinert, 1982a), TMADH is inhibited by high concentrations of the physiological substrate TMA using PMS and DCPIP as electron acceptors. The same is true when Fc^+ is used as oxidant (Table 3.1; Figure 3.2). As with PMS and DCPIP, the degree of substrate inhibition is also affected by the Fc^+ concentration: at low Fc^+ concentrations, inhibition is more pronounced, whereas at high Fc^+ concentrations the degree of inhibition is less so. This observation is consistent with a mechanism in which substrate inhibits enzyme by formation of a catalytically non-productive complex with partially reduced enzyme (Scheme I). In this mechanism, high concentrations of Fc^+

will favour partitioning into the 0/2 redox cycle from the enzyme species containing flavin semiquinone and reduced 4Fe-4S centre, rather than the catalytically compromised 1/3 cycle.

Table 3.1. Steady-State Parameters for the Reaction of TMADH: Effect of Increasing the Concentration of the Electron Acceptor, Fc^+

$[Fc^+PF_6^-]$ (μM)	K_m (μM)	K_i (μM)	b	k_{cat} (s^{-1})	k_{cat}/K_m (x10^3) ($M^{-1}s^{-1}$)
50	49.4 ± 6.2	65.8 ± 9.8	0.082 ± 0.001	32.2 ± 3.5	651.8 ± 152.7
100	127.6 ± 16.3	120.4 ± 15.6	0.014 ± 0.008	42.5 ± 5.1	333.1 ± 82.5
200	197.0 ± 19.0	223.7 ± 25.0	0.021 ± 0.008	50.6 ± 4.5	256.9 ± 47.6
300	215.2 ± 17.8	252.2 ± 24.2	0.021 ± 0.008	48.3 ± 3.7	224.4 ± 35.8
400	291.3 ± 35.0	372.3 ± 54.6	0.017 ± 0.014	58.77 ± 6.4	201.8 ± 46.2

Reactions were performed in 20 mM potassium phosphate buffer, pH 7.0 at 30 °C, and were initiated by the addition of Fc^+.

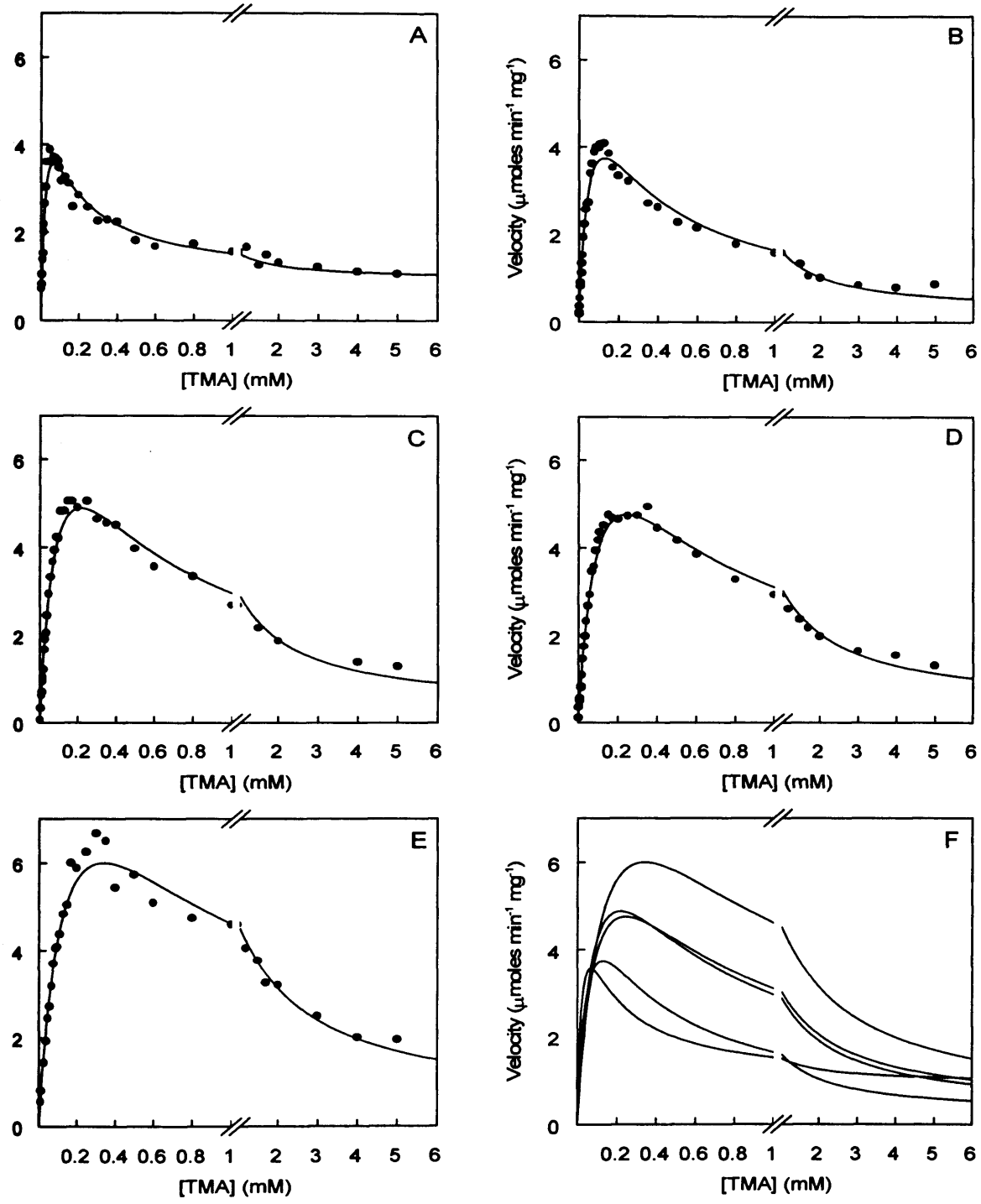

Figure 3.2: Plots of Initial Velocity Against Substrate Concentration for Reactions of TMADH with TMA and Fc^+. Reaction components were contained in 20 mM potassium phosphate buffer, pH 7.0, 30 °C, and the reactions were initiated by the addition of Fc^+. Fc^+ concentrations are (A) 50 μM, (B) 100 μM, (C) 200 μM, (D) 300 μM and (E) 400 μM. (F) Overlay of the fits for each data set shown in panels A-E. Data are fitted to Equation 3.2.

Other, non-physiological substrates for TMADH were also examined for excess substrate inhibition. Of the substrates investigated, ethyldimethylamine (EDMA), diethylmethylamine (DEMA), and triethylamine (TEA) were all found to inhibit TMADH at high concentrations (Table 3.2; Figure 3.3); only *n*-butyldimethylamine (DMButA) did not display marked substrate inhibition. DMButA was therefore chosen for direct spectral analysis in comparison with the physiological reductant TMA. Curiously, in both steady-state and stopped-flow studies, EDMA is a more effective substrate for TMADH than the physiological substrate TMA. However, it does not provide a suitable growth substrate for *M. methylophilus*.

Table 3.2. Steady-State Parameters for the Reaction of TMADH with Various Amine Substrates

Substrate	K_m (μM)	K_i (μM)	b	k_{cat} (s^{-1})	k_{cat}/K_m (x10^3) ($M^{-1}s^{-1}$)
TMA	128 ± 16	120 ± 16	0.14 ± 0.01	40.5 ± 5	317 ± 79
EDMA	23.5 ± 3.8	25.3 ± 3.8	0.10 ± 0.02	23.7 ± 4	1009 ± 312
DEMA	111 ± 17	1009 ± 277	0.10 ± 0.03	3.8 ± 0.4	34.2 ± 8.4
TEA	2614 ± 325	25820 ± 6820	0.05 ± 0.09	0.6 ± 0.02	0.23 ± 0.04
DMButA	382 ± 20	($2 \times 10^{11} \pm 8 \times 10^{12}$)	($7 \times 10^4 \pm 3 \times 10^6$)	0.11 ± 0.01	0.29 ± 0.005

Reactions were performed in 20 mM potassium phosphate buffer, pH 7.0, 30 °C and were initiated by the addition of Fc^+. Fc^+ concentration was 100 μM. The poor ability of DMButA to inhibit TMADH at high concentrations prevents meaningful evaluation of K_i and b for this substrate (figures are shown in parentheses).

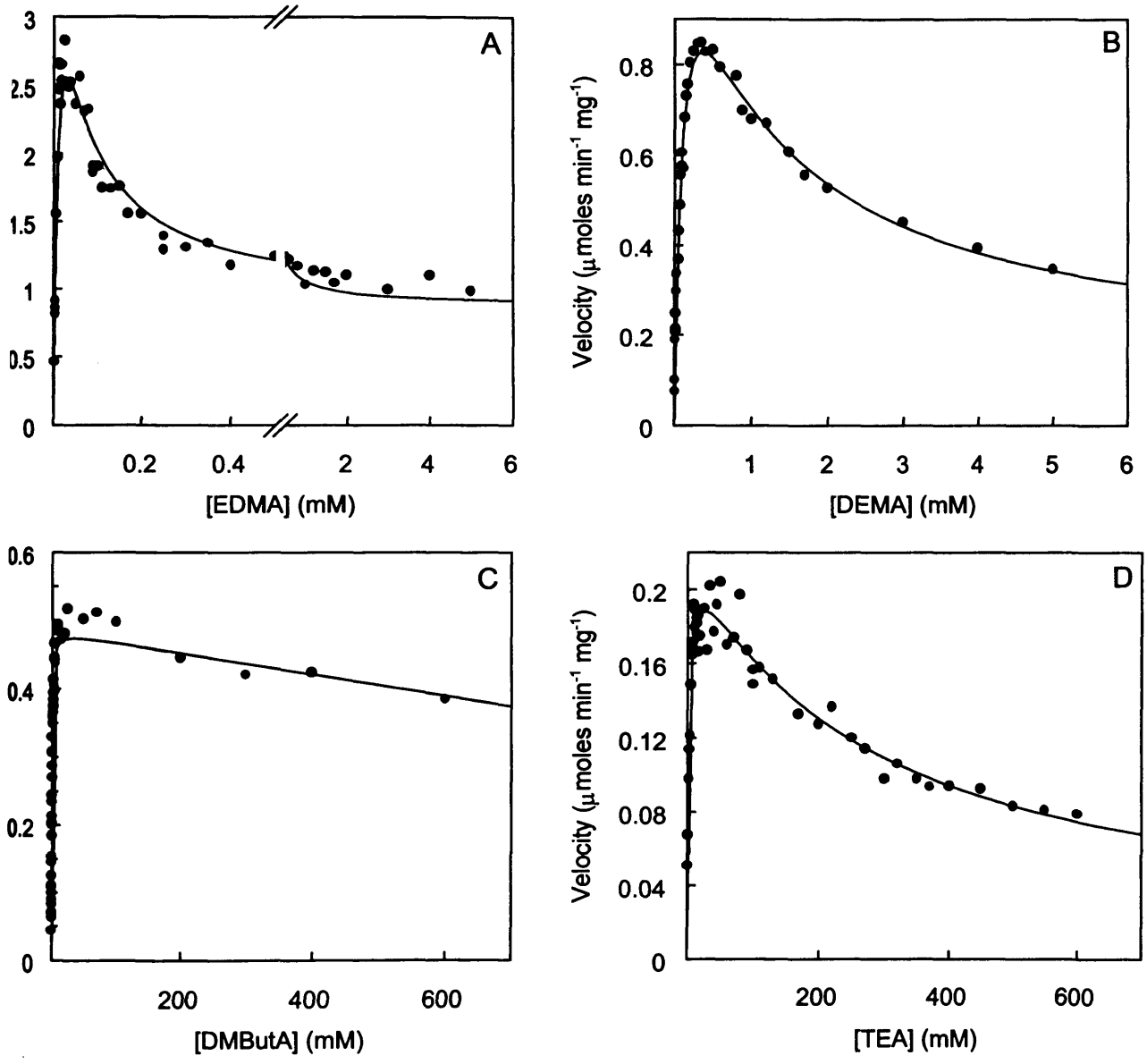

Figure 3.3: Plots of initial velocity against substrate concentration for reactions of TMADH with non-physiological amines and Fc^+. Reaction components were contained in 20 mM potassium phosphate buffer, pH 7.0, 30 °C, and the reactions were initiated by the addition of Fc^+. Fc^+ concentration was 100 μM. (A) EDMA, (B) DEMA, (C) DMButA and (D) TEA. Data are fitted with Equation 2.3.

3.2.3 Stopped-Flow Studies

The rate of flavin reduction in TMADH was studied with TMA and the amine substrates EDMA, DEMA, DMButA and TEA (Figure 3.4, Table 3.3). When viewing this data with regard to substrate inhibition in TMADH, it must be remembered that the rate of flavin reduction does not reflect ability of substrate inhibition caused by that substrate. Rather, it is binding of the substrate to reduced forms of TMADH. Therefore, for the substrates EDMA, DEMA and TMA, there appears to be correlation between inhibition and fast rates of flavin reduction and tight binding of substrate, reflected in K_d values. However, this correlation breaks down for the substrates DMButA and TEA. DMButA has the tightest binding of any of the substrates tested, but clearly does not show any inhibition, whereas TEA has the lowest K_d, but clearly inhibits TMADH. It would appear that the binding of DMButA to reduced forms of TMADH is either less tight than other amines, or does not perturb internal electron flow in the enzyme.

Table 3.3. Kinetic Parameters for Flavin Reduction Determined by Stopped-Flow Analysis of the Reaction of TMADH with Various Amine Substrates

Substrate	K_d (mM)	k_{lim} (s^{-1})	k_{lim}/K_d ($M^{-1} s^{-1}$)
TMA	3.4 ± 0.2	643 ± 12	190 ± 12
EDMA	1.0 ± 0.1	1021 ± 35	1031 ± 98
DEMA	35 ± 2	193 ± 4	5.6 ± 0.4
TEA	70 ± 2	4.4 ± 0.1	0.06 ± 0.003
DMButA	0.36 ± 0.02	0.53 ± 0.01	1.5 ± 0.1

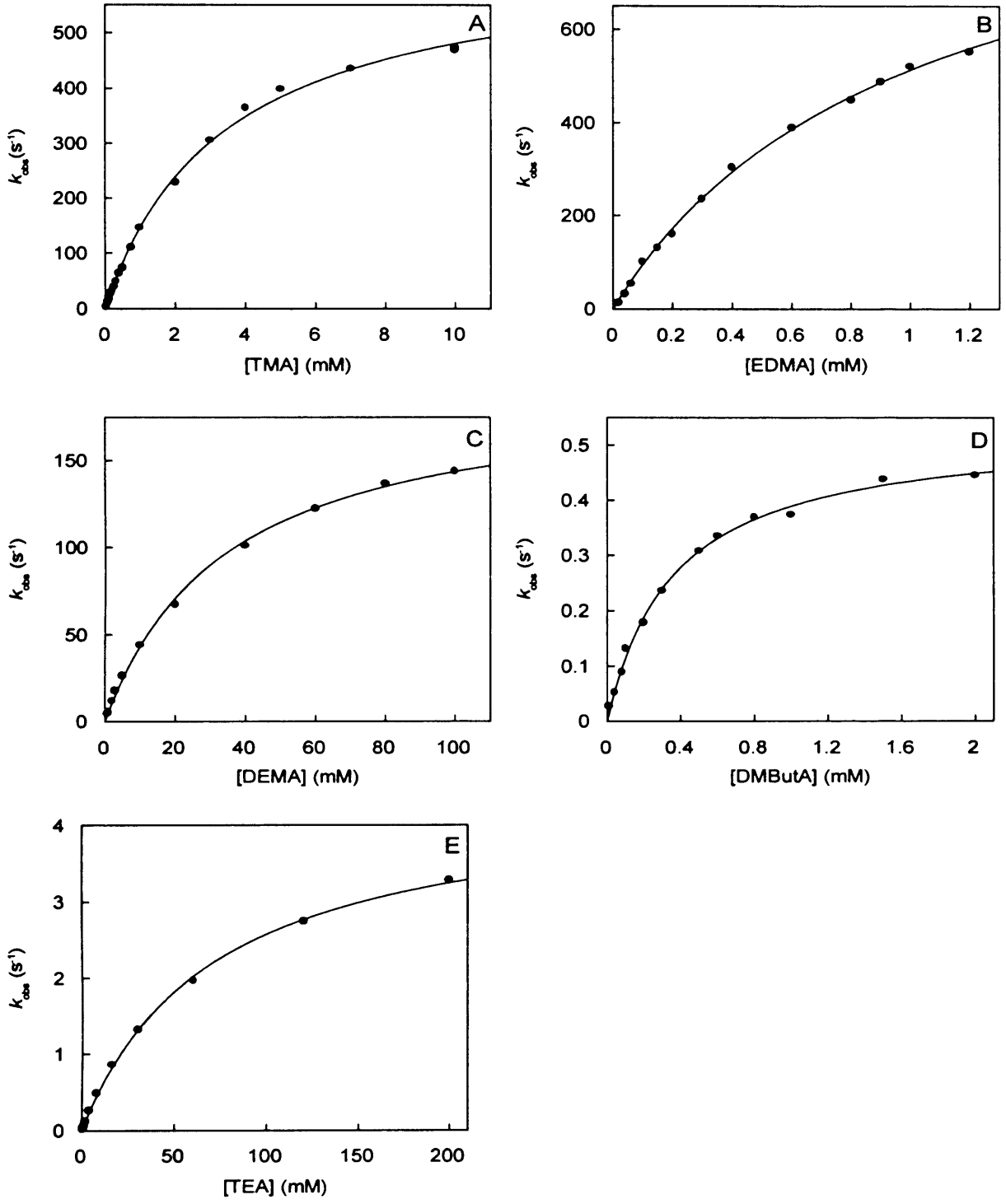

Figure 3.4: Plots of observed rate constants for flavin reduction against substrate concentration for reactions of TMADH with various amine substrates. Reactions were performed in 20 mM potassium phosphate buffer, pH 7.0 at 25 °C. Flavin reduction was monitored at 443 nm and data were fitted to Equation 2.4.

3.2.4 Spectroscopic Analysis of TMADH During Steady-State Reactions

3.2.4.1 TMA as Substrate

Previous stopped-flow studies of the reaction of TMADH with TMA have enabled deconvolution of the spectral forms of intermediates encountered in the reductive half-reaction (Basran *et al.*, 1997; Figure 3.5). During single turnover, four characteristic spectra are produced: that of the oxidised enzyme, two-electron reduced (dihydroquinone), two-electron reduced (flavin semiquinone and reduced iron-sulphur centre) and the so-called spin-interacting state (Steenkamp & Beinert, 1982a; Steenkamp *et al.*, 1978c). These spectra are therefore available as a guide to the redox state of TMADH observed during steady-state turnover.

Direct analysis of the redox state of TMADH during steady-state reactions was obtained by performing enzyme-monitored turnover experiments in which TMADH was rapidly mixed in the stopped-flow with a mixture of TMA and Fc^+. In these turnover experiments, the concentration of TMADH was maintained at 4 μM, and Fc^+ was present at 100 μM. The reaction was monitored between 350 nm and 550 nm, the most informative region of the enzyme spectrum, where Fc^+ contributes little to the observed spectral change. In addition, the exhaustion of Fc^+ can be montored independently in the course of this experiment by observing the disappearance of the Fc^+ peak at 617 nm.

Enzyme monitored turnover experiments were performed over a range of TMA concentrations (20 μM, 100 μM, 500 μM and 2 mM) at 100 μM Fc^+ (Figure 3.6). Depending on the TMA concentration, the minimum steady-state period observed lasted about 5 s, extending to about 10 s at the highest TMA concentrations. The concentration of TMA profoundly affects the spectrum obtained during steady-state turnover. At high TMA concentrations (e.g. 500 μM and 2 mM), the spectrum exhibits a high absorption at 365 nm that is characteristic of the anionic flavin semiquinone. However, the relatively large absorption at 440 nm also indicates the 4Fe-4S centre of TMADH is substantially oxidised (compare with the spectrum of two-electron reduced TMADH with one electron in the flavin and one in the 4Fe-4S centre; Figure 3.5). The data therefore indicate that one-electron reduced TMADH (flavin semiquinone/oxidised 4Fe-4S centre) is the predominant species present during steady-state turnover at high concentrations of TMA. It is this form of TMADH that is predicted to accumulate during steady-state turnover in the 1/3 cycle

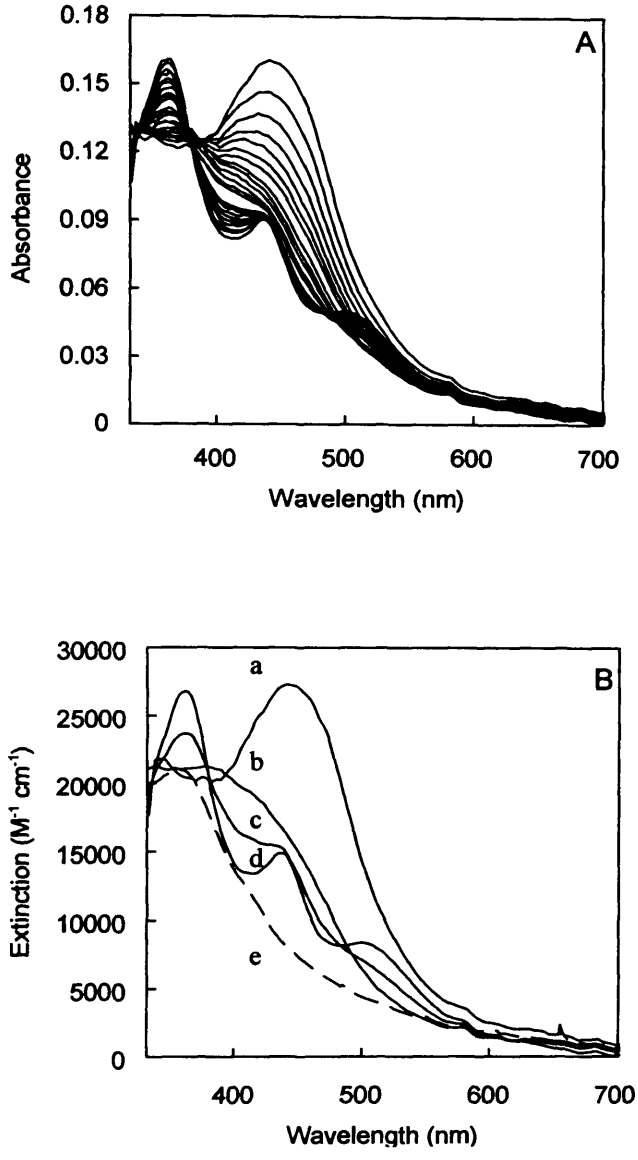

Figure 3.5: Time-dependent spectral changes for TMADH in single turnover reactions with TMA. TMADH (7.5 μM) was rapidly mixed with TMA (125 μM) at pH 7.5. A.Time-dependent spectral changes; the first spectrum is recorded 1.28 ms after mixing (for clarity, only selected subsequent spectra are shown). B Spectra of the intermediate forms during the course of the reductive half-reaction generated by global analysis and numerical integration methods with ProKin software (Applied Photophysics Ltd). Spectrum a, oxidised enzyme; spectrum b, two-electron reduced enzyme (hydroquinone); spectrum c, two-electron reduced enzyme (flavin semiquinone and reduced iron-sulphur centre); spectrum d, spin interacting state of TMADH. The spectrum of three-electron reduced TMADH (generated under anaerobic conditions by titration with sodium dithionite) is also illustrated (dashed spectrum, e). Data for this figure was donated by Dr J. Basran.

of Scheme I. In reactions performed at low concentrations of TMA (20 μM), on the other hand, the steady-state spectrum reflects only a small quantity of anionic flavin semiquinone. Under these conditions the enhanced absorption at 365 nm seen at high TMA concentrations is lost. The steady-state spectrum at low TMA concentrations is similar to that of oxidised TMADH (increased absorption at 443 nm and loss of signature at 365 nm) indicating that oxidised enzyme is the predominant species at low substrate concentrations. Clearly in the this regime the 1/3 cycle does not predominate, and the majority of the catalytic throughput is through the 0/2 cycle. At intermediate TMA concentrations (55 μM and 100 μM) a situation is observed in which the 365 nm absorption indicative of the 1/3 cycle is present, but is much less intense than that seen at high TMA concentrations. Additionally, the 443 nm absorbance is higher than that seen with reactions performed at higher concentrations of TMA. In this intermediate regime, therefore, both the 0/2 and 1/3 cycles appear to operate, and as might be expected a hybrid spectrum is observed.

Scheme I predicts that the concentration of electron acceptor will effect the partitioning of TMADH between the 0/2 and 1/3 cycles. The effect of reducing the Fc^+ concentration to 50 μM is seen in Figure 3.6, where even at 20 μM TMA, the lowest concentration studied, the spectrum indicates that anionic flavin semiquinone/oxidised 4Fe-4S centre is the predominant redox species. Therefore, the switch from the 1/3 cycle to the 0/2 cycle (Scheme I) that is seen with 100 μM Fc^+ does not occur when the Fc^+ concentration is reduced to 50 μM. The data thus indicate that partitioning between the two redox cycles is critically dependent on both TMA and Fc^+ concentration as predicted by Scheme I, and demonstrate that as the ratio of reducing to oxidising substrate increases, the level of enzyme reduction in the steady-state also increases.

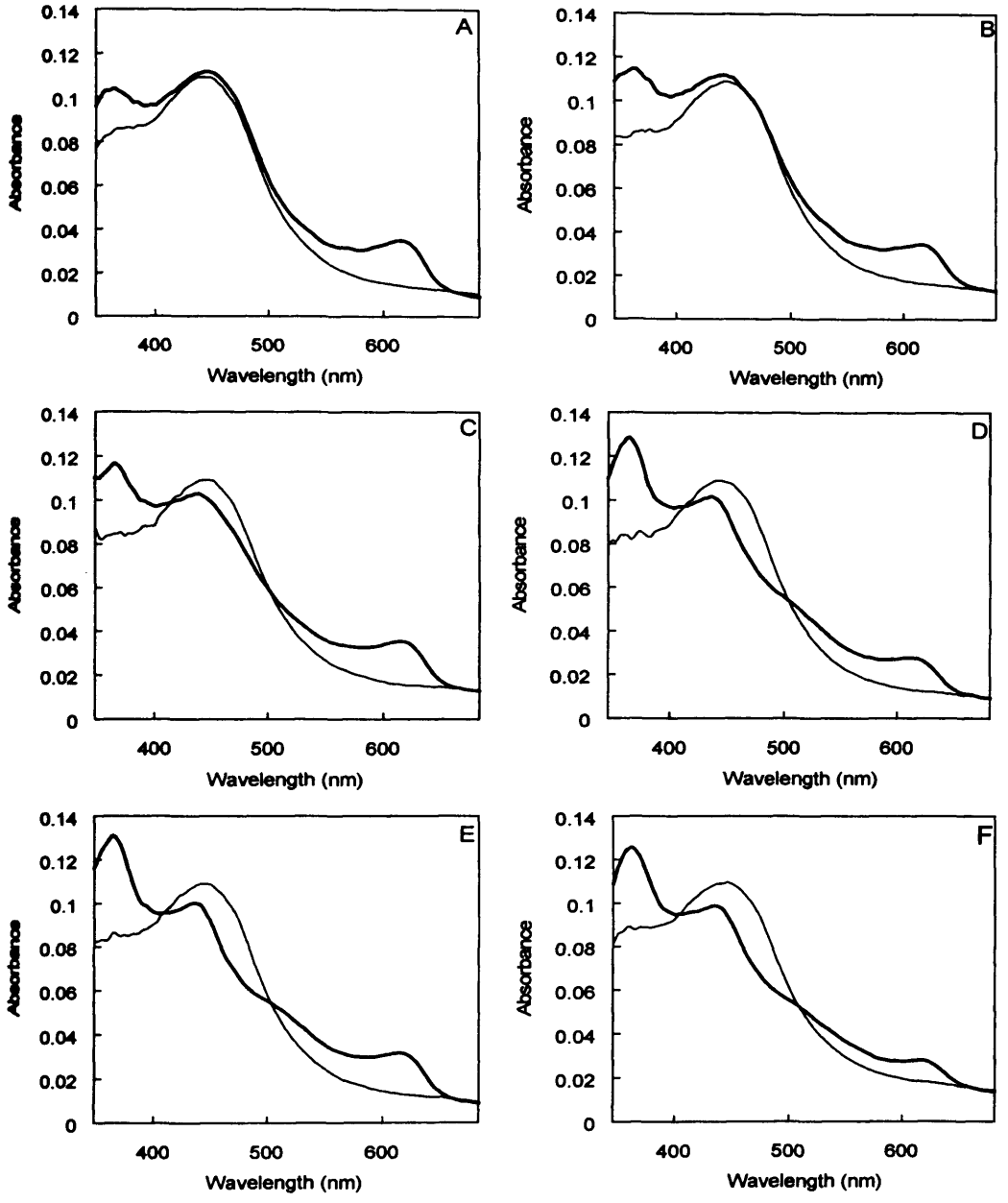

Figure 3.6. Spectral changes of TMADH observed during steady-state turnover with TMA and Fc^+. For reference, in all panels the spectrum of oxidised enzyme is indicated by the thinner line. (A) Steady-state spectrum (thick line) observed in the presence of 20 μM TMA and 100 μM Fc^+; (B) Steady-state spectrum (thick line) observed in the presence of 55 μM TMA and 100 μM Fc^+; (C) Steady-state spectrum (thick line) observed in the presence of 100 μM TMA and 100 μM Fc^+; (D) Steady-state spectrum (thick line) observed in the presence of 500 μM TMA and 100 μM Fc^+; (E) Steady-state spectrum (thick line) observed in the presence of 2 mM TMA and 100 μM Fc^+; (F) Steady-state spectrum (thick line) observed in the presence of 20 μM TMA and 50 μM Fc^+. All reactions were performed in 20 mM potassium phosphate buffer, pH 7.0 at 25 °C.

3.2.4.2 DMButA as Substrate

It was of interest to see whether the enzyme-monitored turnover experiments that were obtained with TMA as substrate could be related to the steady-state kinetic data obtained with alternative amine substrates for the enzyme. The steady-state assays had demonstrated that the inhibition seen with DMButA is much less marked than that with other substrates (Figure 3.7). Enzyme-monitored turnover experiments were therefore of interest, to ascertain whether the 0/2 cycle predominated to a greater extent than is seen with TMA. Reactions were performed with 100 μM Fc^+, and over a range of DMButA concentrations (100 μM, 20 mM and 200 mM). In all cases, the spectra obtained during steady-state turnover show only incomplete development of the 365 nm absorption of the anionic semiquinone and a 440 nm absorbance similar to that of oxidised TMADH. Therefore, with DMButA as substrate the 1/3 cycle is populated only to a small extent during steady-state turnover and the majority of substrate oxidation occurs exclusively via the 0/2 cycle. This analysis thus provides an explanation for the lack of marked substrate inhibition seen with this non-physiological substrate at high concentrations.

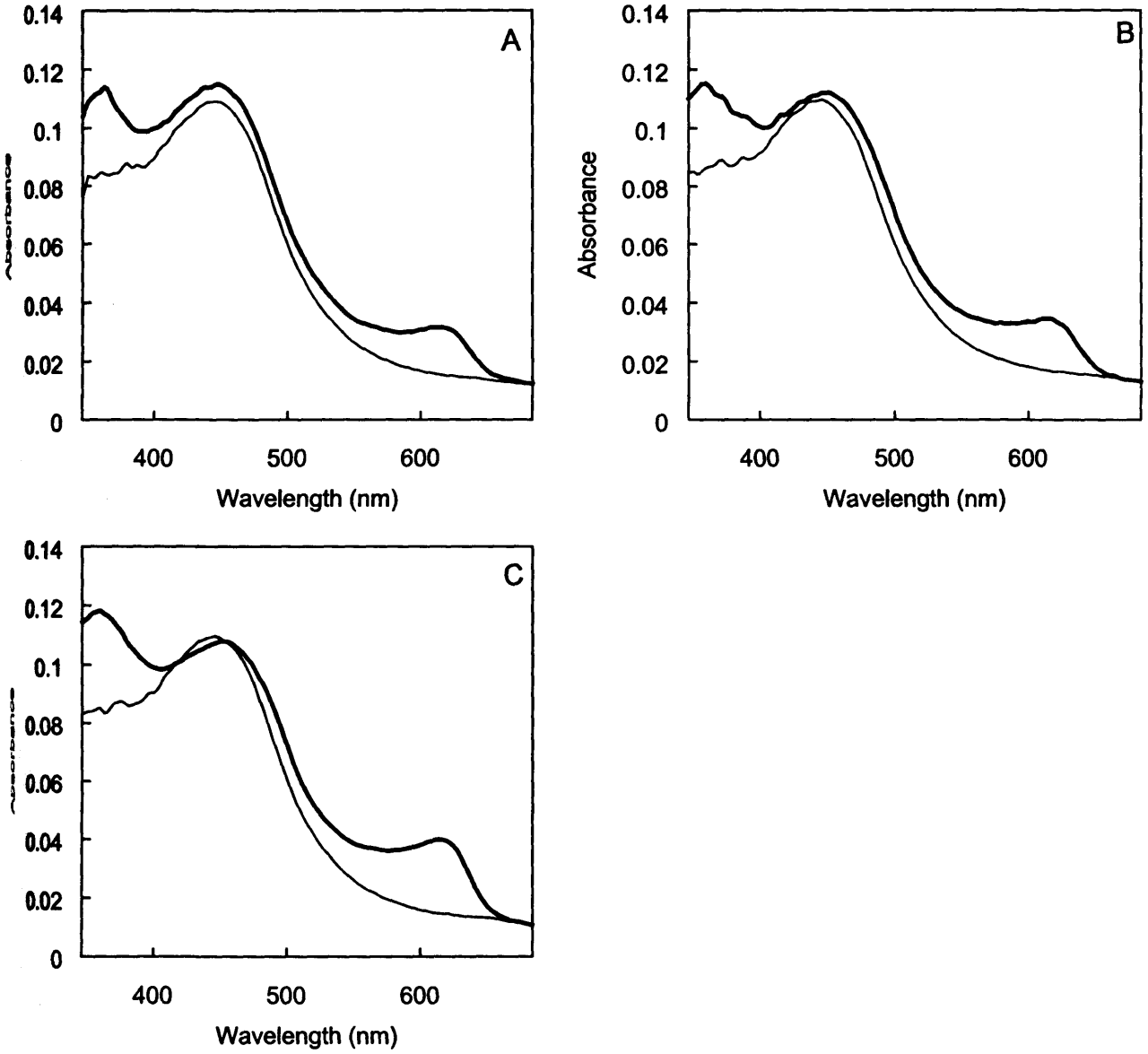

Figure 3.7. Spectral changes of TMADH observed during steady-state turnover with DMButA and Fc^+. For reference, in all panels the spectrum of oxidised enzyme is indicated by the thinner line. (A) Steady-state spectrum (thick line) observed in the presence of 100 μM TMA and 100 μM Fc^+; (B) Steady-state spectrum (thick line) observed in the presence of 2 mM TMA and 100 μM Fc^+; (C) Steady-state spectrum (thick line) observed in the presence of 200 mM TMA and 100 μM Fc^+. All reactions were performed in 20 mM potassium phosphate buffer, pH 7.0 at 25 °C.

3.2.5 Single Wavelength Enzyme-Monitored Studies of the Steady-State Reaction

To more effectively correlate the properties of TMADH in the steady-state, enzyme-monitored experiments were performed in which 4 μM enzyme was reacted with 100 μM Fc^+, varying the of TMA concentration over the range 250 μM - 2 mM (all concentrations after mixing). At each TMA concentration the reaction was monitored at three wavelengths: 443 nm, monitoring the net level of enzyme reduction; 365 nm, monitoring the accumulation of the anionic flavin semiquinone in the course of the steady-state; and 617 nm, monitoring the enzyme-catalysed reduction of Fc^+ in the course of the reaction. Several qualitative trends are evident (Figure 3.8). First, excess substrate inhibition is seen as a decrease in the slope of the 617 nm transients and because the reaction is inhibited, the time taken for the reduction to reach endpoint takes longer as the TMA concentration increases. Secondly, an increased accumulation in anionic flavin semiquinone in the steady-state as TMA concentration increases is evident as a loss of the pronounced bowing in the 365 nm transients in going from 250 μM TMA to 2 mM TMA. This loss of bowing is seen more readily when the transients at 365 nm are compared directly (Figure 3.9). These spectral changes are made against a background loss in absorbance due to reduction of Fc^+. The principal observation is that, as predicted by the model in Scheme I, there is a substantial increase in the amount of semiquinone accumulating and persisting while the enzyme is undergoing steady-state turnover. By comparing the areas under the curves of the transients at 365 nm, the amount of semiquinone is calculated to more than double in going from 250 μM TMA to 2 mM TMA (Table 3.4).

An analysis of the transients at 443 nm at short time intervals can be used to determine how long the enzyme takes to reach steady-state (Figure 3.9). The approach to the steady-state is increasingly rapid as the TMA concentration increases, as expected given the known behaviour of the fast phase of the reaction of enzyme with both DEMA and TMA. A transient over-reduction of the enzyme is observed at all concentrations of TMA, due to the initial reduction of FMN in the fast phase of the first turnover by substrate. This overshoot of the steady-state level of enzyme reduction increases with TMA concentration, as the reaction of enzyme with substrate in the first turnover goes increasingly to completion prior to entering the steady-state, yielding the full absorbance change associated with reduction of the enzyme flavin. The rate constants obtained from this pre-steady-state portion of the

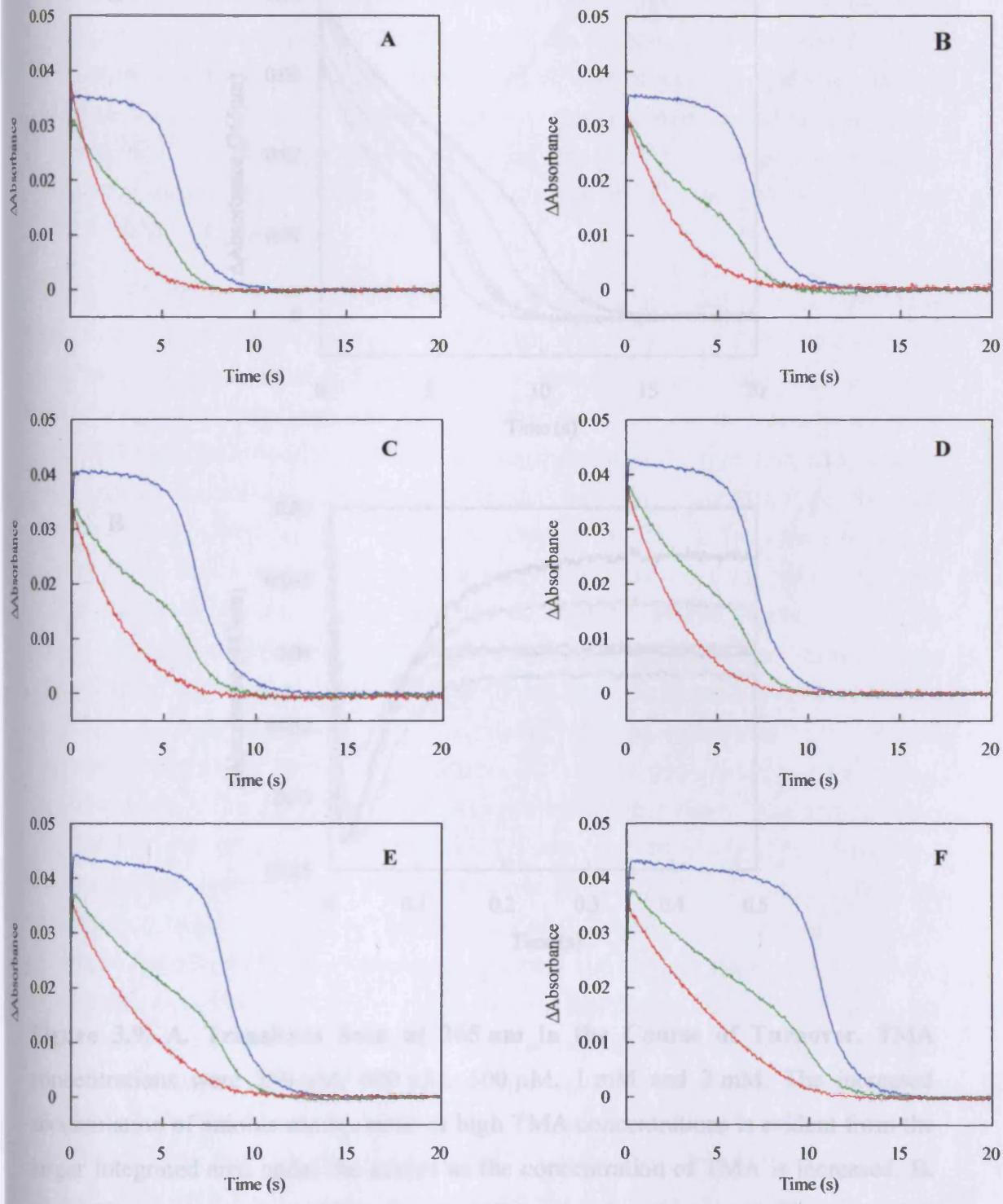

Figure 3.8: Transients Obtained From Enzyme-Monitored Turnover Experiments. All reactions were performed in 20 mM potassium phosphate buffer, pH 7.0 at 25 °C. TMA concentrations were (A) 250 μM, (B) 300 μM, (C) 400 μM, (D) 500 μM, (E) 1 mM and (F) 2 mM. In all panels: blue transient, 443 nm; green transient 365 nm; red transient, 617 nm.

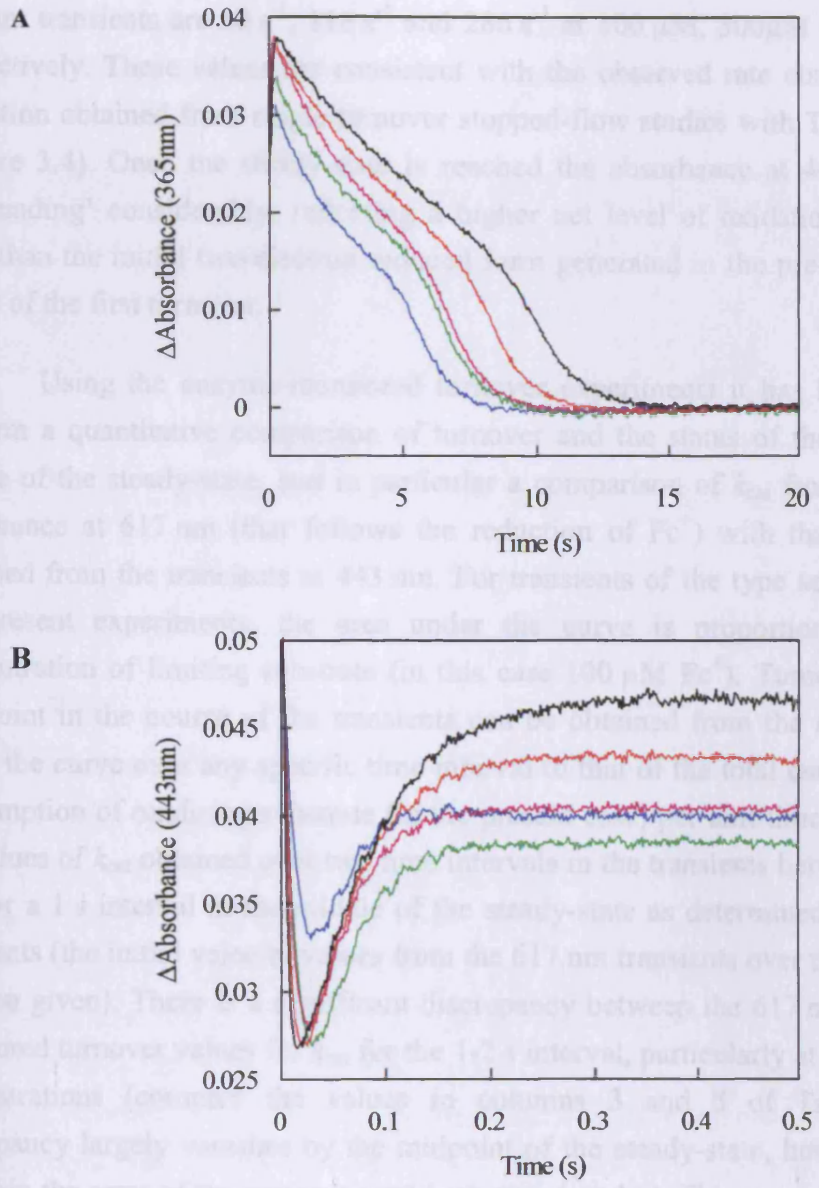

Figure 3.9. A. Transients Seen at 365 nm in the Course of Turnover. TMA concentrations were 250 μM, 400 μM, 500 μM, 1 mM and 2 mM. The increased accumulation of anionic semiquinone at high TMA concentrations is evident from the larger integrated area under the curves as the concentration of TMA is increased. **B. Short-Time Absorbance Changes at 443 nm in the Course of Turnover.** All reactions were performed in 20 mM potassium phosphate buffer, pH 7.0 at 25 °C. TMA concentrations were 250 μM, 400 μM, 500 μM, 1 mM and 2 mM. The increased absorbance at 0.5 s in going from 400 μM to 2 mM reflects the increasingly oxidised state of the enzyme as the reductive half-reaction slows down when excess substrate inhibition is observed.

443 nm transients are 50 s^{-1}, 116 s^{-1} and 286 s^{-1} at 100 μM, 500μM and 2 mM TMA respectively. These values are consistent with the observed rate constants for flavin reduction obtained from single turnover stopped-flow studies with TMA as substrate (Figure 3.4). Once the steady-state is reached the absorbance at 443 nm increases, 'rebounding' considerably, reflecting a higher net level of oxidation in the steady-state than the initial two-electron reduced form generated in the pre-steady-state fast phase of the first turnover.

Using the enzyme-monitored turnover experiments it has been possible to perform a quantitative comparison of turnover and the status of the enzyme in the course of the steady-state, and in particular a comparison of k_{cat} from the change in absorbance at 617 nm (that follows the reduction of Fc^+) with that which can be obtained from the transients at 443 nm. For transients of the type seen at 443 nm in the present experiments, the area under the curve is proportional to the total concentration of limiting substrate (in this case 100 μM Fc^+). Turnover numbers at any point in the course of the transients can be obtained from the ratio of the area under the curve over any specific time interval to that of the total curve, yielding the consumption of oxidising substrate (in the present case) per unit time. Table 3 shows the values of k_{cat} obtained over two time intervals in the transients between 1 s and 2 s and for a 1 s interval in the middle of the steady-state as determined by the 443 nm transients (the initial velocity values from the 617 nm transients over the 0-1 s interval are also given). There is a significant discrepancy between the 617 nm and enzyme-monitored turnover values for k_{cat} for the 1-2 s interval, particularly at the lower TMA concentrations (compare the values in columns 3 and 5 of Table 3.5). This discrepancy largely vanishes by the midpoint of the steady-state, however, probably to within the error of the measurement (columns 4 and 6). This trend is evident in the transients themselves (Figure 3.8) as the 617 nm transient is distinctly bowed in the steady-state region (particularly at low TMA concentrations), whereas the absorbance at 443 nm changes relatively little in this region until the Fc^+ has been consumed at the end of the steady-state. Again, this bowing in the 617 nm transients becomes significantly less pronounced at higher TMA concentrations. The 617 nm absorbance change must reflect the actual enzyme turnover, but the 443 nm transients better define the duration of the steady-state. Over the course of the steady-state, catalytic throughput decreases significantly, particularly at higher TMA concentrations, precisely what the model predicts as the system switches from the more efficient 0/2 cycle to the less efficient 1/3 cycle.

Table 3.5. Steady-State Kinetic Parameters Determined from Quantitative Analysis of Enzyme-Monitored Turnover Experiments

	Turnover number (s^{-1})				
[TMA] (μM)	$k_{cat}^{617nm}{}_0$	$k_{cat}^{617nm}{}_1$	$k_{cat}^{617nm}{}_2$	$k_{cat}^{emt}{}_1$	$k_{cat}^{emt}{}_2$
250	9.9	5.8	4.0	4.3	4.2
300	7.9	4.9	3.6	4.3	4.0
400	6.3	4.0	3.0	3.5	3.5
500	4.6	3.8	2.5	2.7	2.6
1000	4.8	3.4	2.5	2.8	2.7
2000	2.9	2.9	2.0	2.3	2.2

Reactions were performed in 20 mM potassium phosphate buffer, pH 7.0 at 25 °C. TMADH was 4 μM and Fc^+ concentration was 100 μM. $k_{cat}^{617nm}{}_0$: turnover number calculated from the initial velocity of the 617 nm transient in the 0-1 s range; $k_{cat}^{617nm}{}_1$: turnover number calculated for the 617 nm transient in the 1-2 s range; $k_{cat}^{617nm}{}_2$: turnover range calculated for the 617 nm transient from a 1 s interval in the middle of the steady-state period as determined by the 443 nm; $k_{cat}^{emt}{}_1$: enzyme monitored turnover number calculated from the 443 nm transient in the 1-2 s range; $k_{cat}^{emt}{}_2$: enzyme monitored turnover number calculated from the 443 nm transient for a 1 s interval in the middle of the steady-state period. Calculations were performed in collaboration with Professor R. Hille, Ohio State University.

3.2.6 Investigation of Inhibition in Active Site Mutants of TMADH

To augment studies of native enzyme, an investigation into the effect that mutations have on the ability of TMA to inhibit TMADH was carried out. Previously (Basran et al., 1997), it has been observed that some mutants of TMADH retain the ability to be inhibited by substrate, while in others substrate appears to have lost this effect. It was decided to investigate three mutant forms of TMADH based around mutations introduced into the substrate binding aromatic bowl of TMADH, to see

whether the kinetic characteristics of these mutants would reveal anything about the nature of loss of inhibition.

3.2.6.1 Steady-State Studies of the Y60A, Y60L and Y60Q TMADH Mutants

The steady-state reaction of the TMADH active site mutants, which contain the mutations Y60A, Y60Q and W264L was carried out using PMS and DCPIP as electron acceptors (Table 3.5 and Figure 3.11). The Y60A and Y60L mutants were found to have retained their ability to be inhibited by TMA as substrate. However, this inhibition is manifest at much higher concentrations than seen for the native enzyme, and the final extent of inhibition is much less than that predicted for the native enzyme also. Conversely, the W264L mutant was not inhibited over the range of TMA used. To see whether the loss of inhibition in the W264L mutant was restricted to TMA, the ability of two alternative substrates for TMADH, EDMA and DEMA, to inhibit the W264L TMADH mutant was also investigated (Table 3.6, Figure 3.10).

Table 3.5. Steady-State Parameters for the Reaction of the Y60A, Y60L and W264L TMADH Mutants with TMA

TMADH Mutant	K_m (mM)	K_i (mM)	b	k_{cat} (s^{-1})	k_{cat}/K_m ($x10^3$) ($M^{-1}s^{-1}$)
Y60A	0.63 ± 0.10	7.67 ± 2.84	0.46 ± 0.03	1.64 ± 0.15	2.60 ± 0.65
Y60L	0.30 ± 0.10	1.74 ± 0.95	0.43 ± 0.09	9.21 ± 2.00	30.70 ± 16.9
W264L	1.95 ± 0.17	Not applicable	Not applicable	1.19± 0.01	0.61 ± 0.06

Reactions were performed in 100 mM sodium pyrophosphate buffer, pH 8.5 at 30 °C, with PMS and DCPIP as electron acceptors. Reactions were initiated by the addition of enzyme.

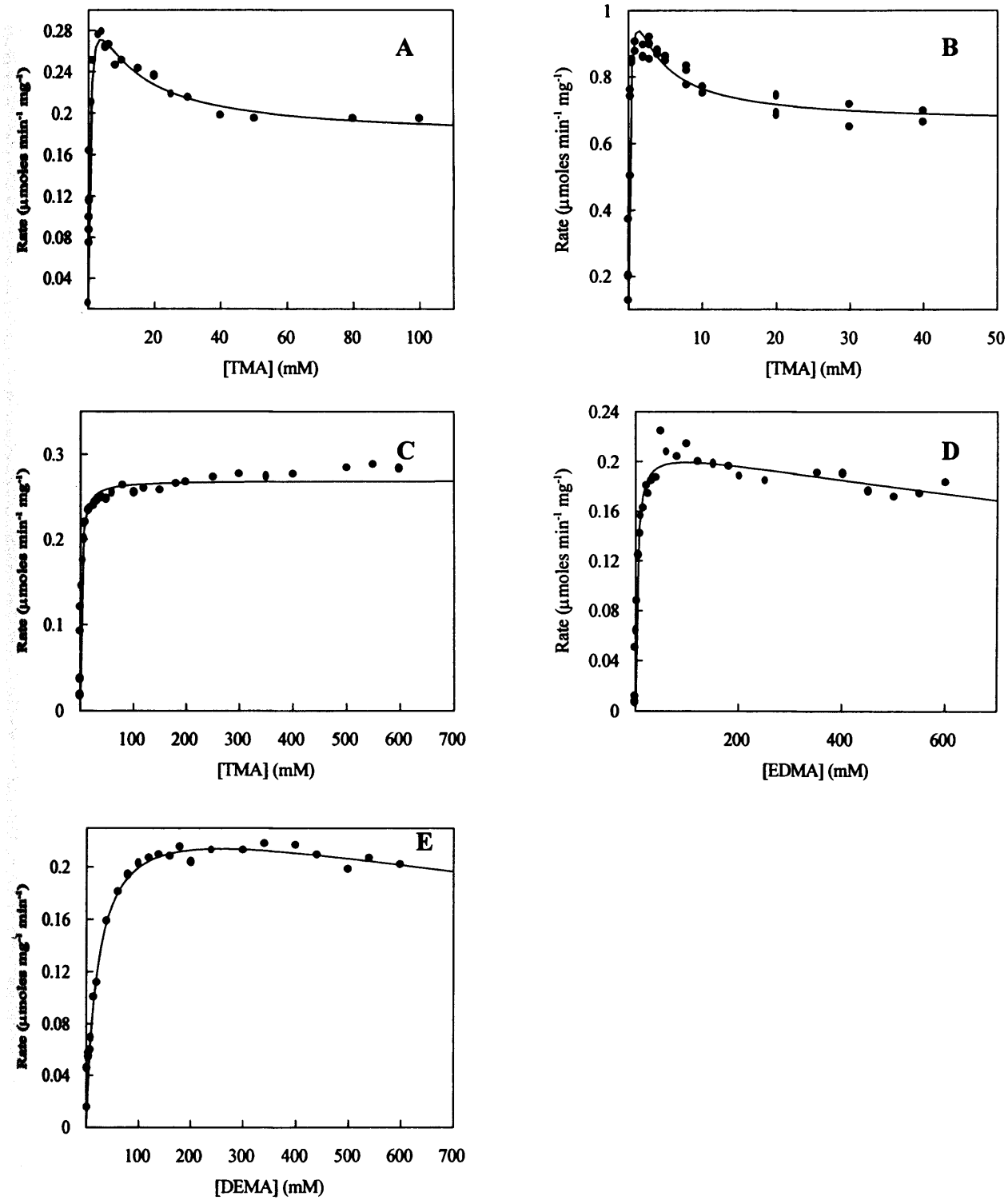

Figure 3.10: Plots of initial velocity against substrate concentration for reaction of the Y60A, Y60L and W264L TMADH mutants with TMA and other amine substrates. A. Reaction of the Y60A TMADH mutant with TMA. B. Reaction of the Y60L TMADH mutant with TMA. C. Reaction of the W264L TMADH mutant with TMA. D. Reaction of the W264L TMADH mutant with EDMA E. Reaction of the W264L TMADH mutant with DEMA.

Table 3.5. Steady-State Parameters for the Reaction of the W264L TMADH Mutant with EDMA and DEMA

Substrate	K_m (mM)	K_i (mM)	b	k_{cat} (s^{-1})	k_{cat}/K_m ($x10^3$) (M^{-1} s^{-1})
EDMA	2.20 ± 0.38	4.40 ± 2.41	0.99 ± 0.05	0.88 ± 0.05	0.4 ± 0.09
DEMA	23.13 ± 2.06	1120 ± 715	0.48 ± 0.20	1.14 ± 0.06	0.05 ± 0.01

Reactions were performed in 100 mM sodium pyrophosphate buffer, pH 8.5 at 30 °C, with PMS and DCPIP as electron acceptors. Reactions were initiated by the addition of enzyme.

Both EDMA and DEMA were found to be able to inhibit the W264L TMADH mutant. A study of the steady-state kinetic data for this mutant with the substrates TMA, EDMA and DEMA does not provide a strong rationale for the reintroduction of substrate inhibition into this mutant. It is possible that the loss of bulk in the active site of TMADH, caused by the mutation of Trp-264 could be compensated by these larger substrates, leading to improved binding to reduced enzyme, causing substrate inhibition.

To provide more information about substrate inhibition in the Y60A, Y60L and W264L TMADH mutants, stopped flow kinetic analyses were performed on these enzymes in order to determine the rates of flavin reduction and dissociation constants for substrate.

3.2.6.2 Stopped-Flow Studies of the Y60A, Y60L and W264L TMADH Mutants

Stopped-flow studies of the Y60A, Y60L and W264L TMADH mutants were performed at pH 8.5; to obtain kinetic transients that were slow enough to be measured accurately at this pH, reactions were performed at 5 °C The kinetic transients obtained for each of the mutants were fitted to monophasic rate equations (Figure 3.11). Limiting rate constants and apparent dissociation constants were calculated from the data (Figure 3.12) and are displayed in Table 3.6.

Table 3.6. Limiting Rate Constants and Apparent Dissociation Constants for the Monophasic Absorbance Changes Occurring at 443 nm for the Y60A, Y60Q and W264L TMADH Mutants

Mutant	K_d (mM)	k_{lim} (s^{-1})	k_{lim}/K_d (s^{-1} M^{-1})
Y60A	29.14 ± 3.28	19.15 ± 0.53	657
Y60L	33.00 ± 2.17	55.73 ± 1.14	1689
W264L	10.36 ± 2.03	17.20 ± 0.64	1660

Flavin reduction is severely compromised in all of these mutants, consistent with results for earlier TMADH mutants. The rates of flavin reduction in Table 3.6 are as slow as previous mutants of TMADH, in which flavin reduction is rate limiting and substrate inhibition is abolished (Basran *et al.*, 1997). However, while the lack of substrate inhibition observed in other mutants was attributed to flavin reduction becoming the rate-limiting step, this does not apply to the Y60 mutants, in which substrate inhibition is observed despite a very slow rate of flavin reduction. Here, it appears that the lower dissociation constants for the Y60 mutants, indicating tighter binding of substrate could account for the presence of inhibition in these mutants. Binding is the important factor for substrate inhibition; even though the W264L has the lowest k_d, it may be that the substrate is bound inappropriately to change redox potential.

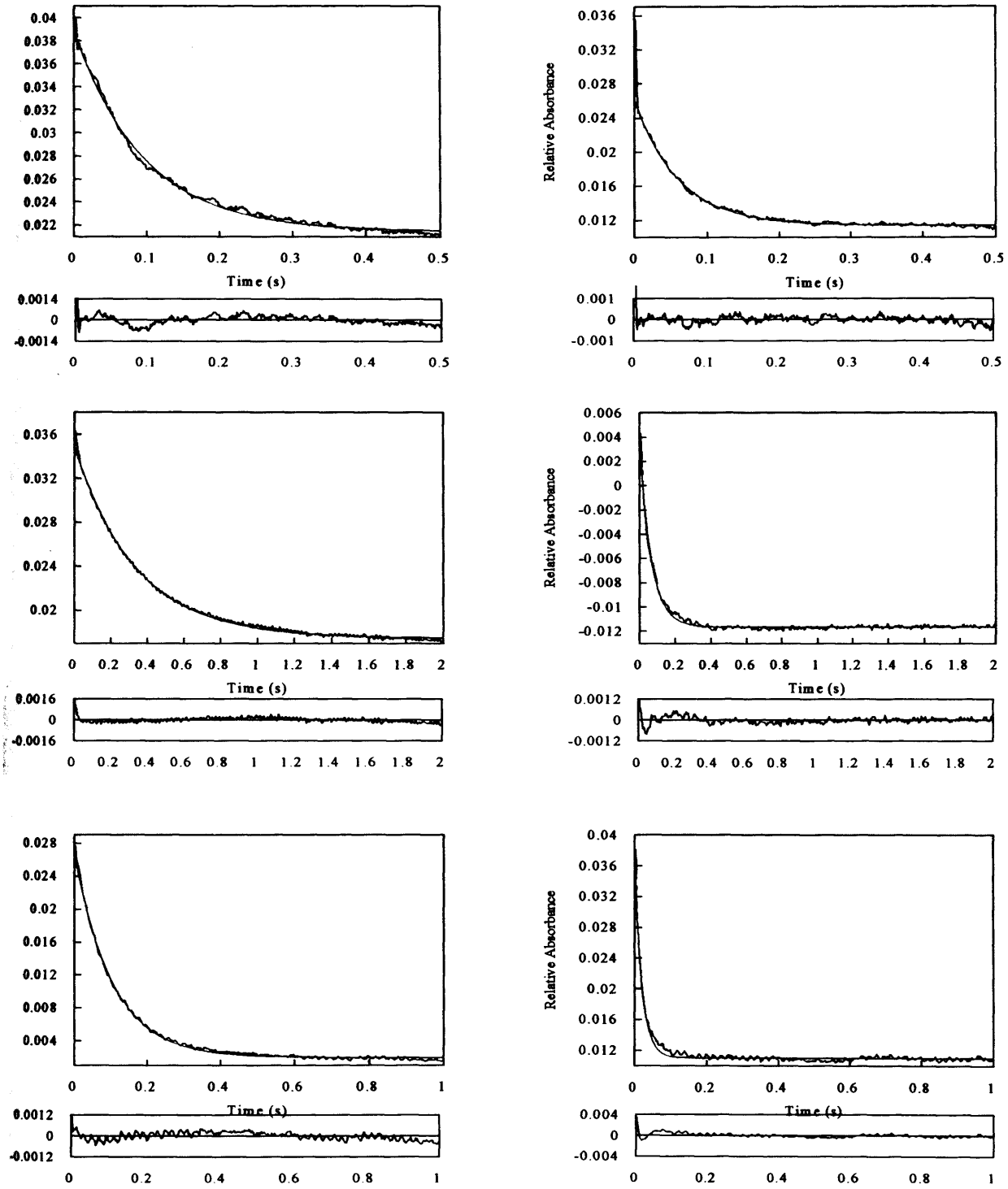

Figure 3.11: Kinetic transients illustrating the monophasic nature of the absorbance change measured at 443 nm for the Y60A, Y60L and W264L TMADH mutants. Two example traces are shown for each mutant, at (i) 10 mM TMA and (ii) 180 mM TMA. A. Y60A; B. Y60L and C. W264L. The lower panels show the plots of residuals for fits to a monophasic absorbance change.

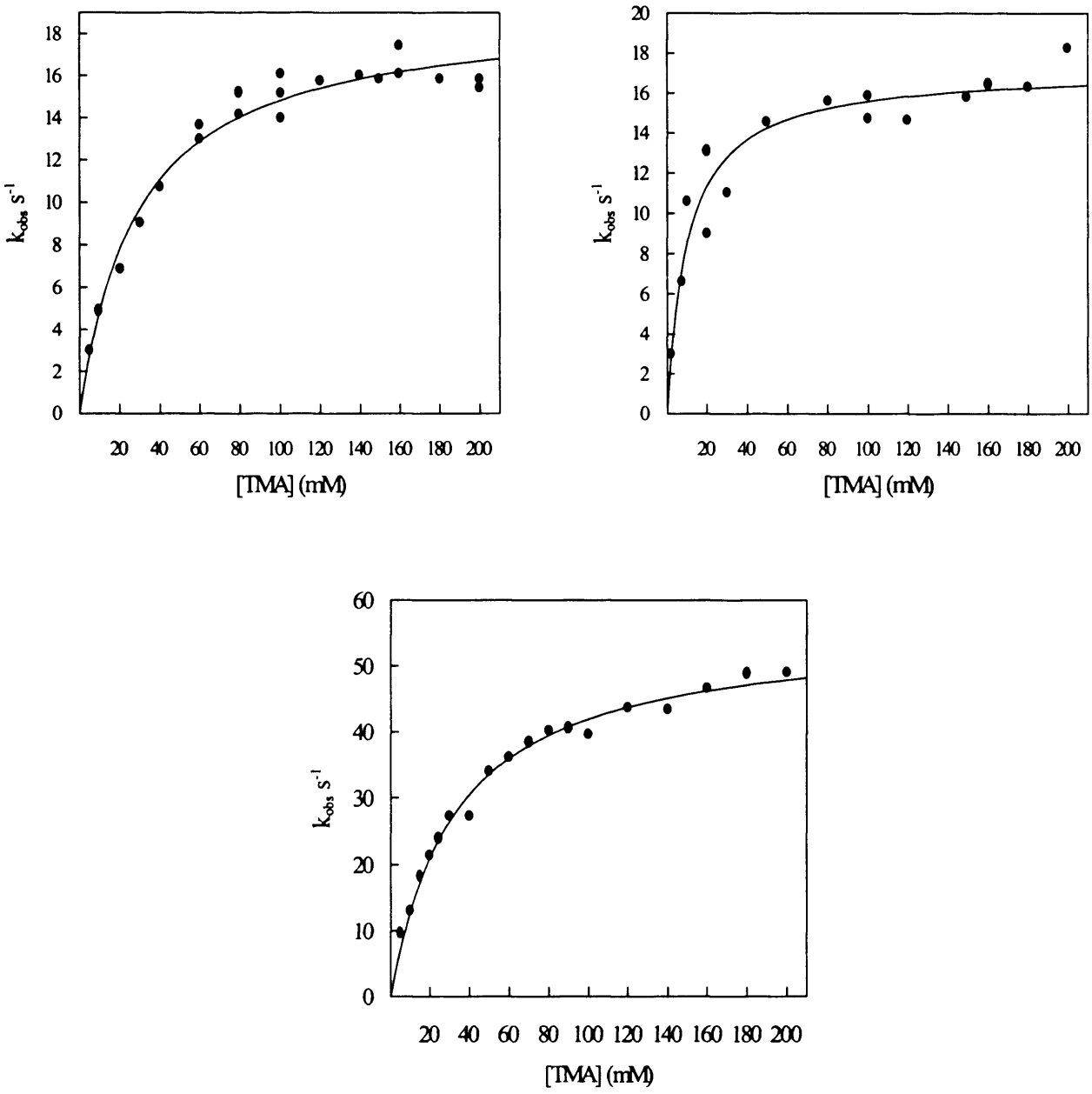

Figure 3.12. Plots of observed rate constants for flavin reduction for the Y60A, Y60L and W264L TMADH mutants with TMA. Reactions were performed in 20 mM potassium phosphate buffer, pH 7.0 at 25 °C. Flavin reduction was monitored at 443 nm and data were fitted to Equation 2.4.

3.3 Discussion

The work presented in this chapter provides evidence that TMADH undergoes different redox cycles during steady-state turnover (Jang *et al.*, 1999a). Previous studies have shown that the interaction between the FMN and 4Fe-4S centres in TMADH is profoundly affected by the binding of TMA or the substrate analogue TMAC (Steenkamp *et al.*, 1978c; Steenkamp & Beinert, 1982a). The distribution of reducing equivalents within two-electron reduced TMADH is known to be strongly influenced by substrate and pH: for dithionite-reduced TMADH at low pH, the distribution favours hydroquinone and oxidised 4Fe-4S centre (Rohlfs & Hille, 1991); at high pH, formation of flavin semiquinone and reduced 4Fe-4S centre is favoured, with the magnetic moments of the two paramagnetic centres interacting strongly to give a spin-interacting state (Rohlfs & Hille, 1991; Rohlfs *et al.*, 1995; Steenkamp & Beinert, 1982a; Steenkamp & Beinert, 1982b; Steenkamp & Singer, 1976). In addition, binding of the substrate analogue TMAC is known to perturb the reduction potentials of the flavin centre. On binding TMAC, the potential for the quinone/semiquinone couple increases from +44 mV to +240 mV at pH 7.0 (Pace & Stankovich, 1991) while that of the semiquinone/hydroquinone couple decreases from +36 mV to -50 mV. The effect is not simply to stabilise the semiquinone oxidation state of the flavin but to alter its value relative to the potential of the 4Fe-4S centre. At pH 7.0, this potential is 102 mV in the absence of TMAC, and +50 mV in its presence. Binding of TMAC (and by inference also TMA) is thus expected to significantly perturb the oxidation-reduction equilibrium between FMN and the 4Fe-4S centre by approximately 10:1 to favouring essentially quantitative formation of the flavin semiquinone. As the extent to which this occurs increases, the enzyme will not be able to oxidise the bound substrate as the flavin is in the wrong oxidation state. The substrate bound, one-electron reduced intermediate is unique to the proposed 1/3 cycle and this effect is expected to compromise catalysis by this cycle.

The spectroscopic and potentiometric data for native TMADH provide a framework for rationalising the observed steady-state behaviour of the enzyme. Falzon and Davidson have suggested that occupation by TMA of a second substrate binding site in the active site leads to substrate inhibition by attenuating internal electron transfer from the flavin to the 4Fe-4S centre (Falzon & Davidson, 1996a; Falzon & Davidson, 1996b). However, the X-ray structure of TMADH in complex with TMAC provides no evidence for a second binding site, and studies with ^{14}C-labelled TMA reveal that no more than one equivalent of substrate is bound to the

reduced enzyme (Steenkamp & Beinert, 1982a). However, this latter result can be interpreted in one of two ways: it either represents TMA bound to a now-vacant active site following substrate turnover and product release, or it represents TMA bound to the second binding site. Additionally, recent EPR studies have revealed that only one equivalent of TMAC is required to generate the spin-interacting state in two-electron reduced TMADH (Jang *et al.*, 1999a).

An alternative explanation for excess substrate inhibition has been proposed (Huang *et al.*, 1995) in which catalysis occurs via 0/2 and 1/3 catalytic cycles (Scheme I). Turnover via the 1/3 cycle is expected to predominate at high concentrations, and as discussed above is expected to be slower because of the unfavourable effect of substrate on flavin reduction potential. Fc^+, which has been demonstrated to react with TMADH at the 4Fe-4S centre has enabled a study of the reduction levels of the 6-*S*-cysteinyl FMN and 4Fe-4S centre in TMADH under steady-state conditions. These studies demonstrate that a one-electron reduced enzyme species containing the anionic flavin semiquinone form of the 6-*S*-cysteinyl FMN and an oxidised 4Fe-4S centre predominates under steady-state conditions in the presence of high concentrations of substrate, whereas at low substrate concentrations oxidised TMADH is the predominant form.

With alternative substrates, it has been demonstrated that other amines also exhibit excess substrate inhibition with TMADH. Stopped-flow studies reveal that the limiting rates for flavin reduction with some of these substrates (e.g. EDMA, DEMA and TEA) are substantially reduced compared with TMA. Consequently, and as predicted by Scheme I the rate of flavin reduction does not account for partitioning into the 1/3 cycle. Instead, predominance of the 1/3 cycle depends on the ability of substrate to bind to enzyme possessing the flavin semiquinone rather than the oxidised form (as reflected in the perturbation of flavin reduction potential upon binding of substrate). Binding of substrate to enzyme containing the flavin semiquinone perturbs the reduction potential of the oxidised/semiquinone flavin couple (thereby shifting the electron distribution within one-electron reduced enzyme in favour of semiquinone formation). Over the range of substrate concentrations used in this study, DEMA, EDMA and TEA are able to bind and perturb the flavin reduction potential of one-electron reduced enzyme. Interestingly, DMButA binds relatively tightly to oxidised TMADH and has the greatest affinity for oxidised TMADH of all the substrates used in this study. However, the lack of marked substrate inhibition seen in the steady-state with DMButA suggests that this substrate binds less well to reduced forms of the enzyme as compared to TMA. The expectation, therefore, that the anionic flavin semiquinone does not accumulate appreciably during steady-state turnover at all

DMButA concentrations studied, is consistent with the results of the enzyme-monitored turnover experiments.

The situation with DMButA as substrate might be similar to other mutants of TMADH that do not exhibit substrate inhibition. In particular, recent studies of a Y169F TMADH mutant have revealed that negative charge which develops on the side chain of Phe-109, has a strong influence on the formation of the spin-interacting state. Changing Tyr-169 in native enzyme to a phenylalanine means that the spin-interacting state does not form, and the enzyme is not inhibited, presumably as a result of the reduction potential of the semiquinone/oxidised flavin couple in this mutant not being perturbed in the same manner as for the native enzyme.

The Y60L and Y60A mutants of TMADH had retained their ability to be inhibited by TMA, and presumably TMA could still inhibit the redox potentials in these mutants. The W264L mutant has lost the ability to be inhibited by TMA. However, this particular mutant has retained the ability to be inhibited by the substrates EDMA and DEMA. It is tempting to suggest that the larger bulk of these substrates compensates for the loss of bulk in the active site caused by replacing Trp-264 with a leucine residue, and restores the ability of these substrates to influence the redox potential of the flavin. The limiting rate constant for flavin reduction was not determined for these enzymes, so it is not known whether the lack of substrate inhibition is due to a reduction in flavin reduction, making this the rate limiting step in catalytic turnover, or whether there is a genuine effect of introducing a mutation into the active site of the enzyme.

To summarise, the steady-state kinetic mechanism of native TMADH comprises two alternating redox cycles and the partitioning between these cycles is dependent on the concentration of substrate and electron acceptor. This kinetic scheme accounts for the observed inhibition of TMADH at high concentrations of substrate. The 1/3 cycle predominating at high TMA concentrations is catalytically compromised due to the unfavourable position of the equilibrium between the two redox active centres in the substrate-bound, 1-electron reduced enzyme (boxed in Scheme I). Binding of substrate to 1-electron reduced enzyme leads to the accumulation of a flavin semiquinone/oxidised 4Fe-4S intermediate in the so-called 1/3 cycle, leading to inhibition in the high substrate regime. Excess substrate inhibition is a necessary consequence of the shift in the reduction potential of the flavin and 4Fe-4S centres in one-electron reduced enzyme.

Chapter 4

Preliminary Investigations of H-Tunnelling in TMADH

4.1 Introduction

Recent studies have revealed that enzymatic H-transfer, as catalysed by at least three different enzyme systems (Basran *et al.*, 1999d; Harris *et al.*, 2000; Kohen *et al.*, 1999) occurs by H-tunnelling, mediated by the low frequency thermal motions of the protein scaffold. Although this is a fairly new area of investigation, there are good reasons for expecting that this phenomenon could be a ubiquitous mechanism for enzymatic H-transfer: invoking protein motions and tunnelling through a reaction barrier helps overcome the energetic difficulties associated with a 'static' view of enzymatic C-H bond cleavage, as invoked by TST (Scrutton *et al.*, 1999; Sutcliffe & Scrutton, 2000). It could also partly explain the large size of proteins in relation to their active sites (Klinman, 1989). The phenomenon of H-tunnelling driven by protein dynamics is being investigated at the University of Leicester in new enzyme systems (e.g. aromatic amine dehydrogenase, methanol dehydrogenase). As part of these studies, this chapter presents the initial results of an investigation into the role of H-tunnelling and protein dynamics in TMADH.

The oxidation of the amine TMA by TMADH involves the cleavage of a substrate C-H bond in a reaction similar to that catalysed by MADH and TSOX, both of which have temperature-dependent kinetic behaviour demonstrating H-tunnelling driven by protein dyamics (Basran *et al.*, 1999d; Harris *et al.*, 2000). In addition, many aspects of TMADH catalysis are fairly well characterised and the enzyme is amenable to study by stopped-flow and steady-state techniques. Hence, TMADH initially appears to be an attractive candidate for study of H-tunnelling through the interpretation of temperature dependence studies and KIEs, as occurred with MADH and TSOX. Both of these enzymes were studied by monitoring the absorbance change as protein-bound cofactor (TTQ or flavin) was reduced by the release of substrate-derived electrons. However, despite investigations that have tried to determine the exact mode of C-H bond cleavage in TMADH (Basran *et al.*, 1999a; Basran *et al.*, 1999c) there is still some uncertainty in whether measuring the rate of flavin reduction in a stopped-flow apparatus is a true reflection of the rate limiting step in TMADH, or if flavin reduction is subject to the effects of commitments to catalysis that 'mask' the bond breaking step. Therefore, the results in this chapter must be viewed in the light of the potential effects of kinetic complexity and the way in which these might change with pH and/or mutation (Bahnson *et al.*, 1993; Northrop, 1981).

A major implication of a dynamic view of catalysis is that the most important factor to influence H-tunnelling is barrier width rather than barrier height (Bruno &

Bialek, 1992; Scrutton *et al.*, 1999). Is there evidence that mutations in TMADH have an effect on barrier width? Starting with the assumption that H-tunnelling is likely to occur in native TMADH, two mutant forms of the enzyme were used: the Y169F and H172Q mutants. These two mutants have been subject to detailed pH-dependence analyses in an attempt to identify the role of a 'critical' active site base at the active site of TMADH (Basran *et al.*, 1999a; Basran *et al.*, 1999c), and were chosen for the temperature dependence study presented in this chapter with the intention of providing an overview of C-H bond cleavage in TMADH.

4.2 Results

4.2.1 Analysing Temperature Dependence KIE Data

Traditionally, temperature dependence studies of tunnelling in enzymes have been analysed in terms of the phenomenological Arrhenius plot (Equation 1.13)- i.e., a plot of ln (k) versus $1/T$. Although, the Arrhenius plot appears linear in the accessible temperature range, it is in fact curved and asymptotically approaches infinity at high temperatures (Schneider & Stern, 1972; Stern & Weston, 1974a; Stern & Weston, 1974b). Apparent linearity in the accessible temperature range does not compromise data analysis, but temperature dependence studies should be analysed in terms of the equation describing a unimolecular reaction (Basran *et al.*, 1999d; Harris *et al.*, 2000; Scrutton *et al.*, 1999). The temperature dependence for a unimolecular rate constant is given by

$$k = k_B/h\ [T\exp(-\Delta G^{\ddagger}/RT)] = k_B/h\ [T\exp(-\Delta H^{\ddagger}/RT)\exp(\Delta S^{\ddagger}/R]$$

Equation 4.1

where k_B and h are the Boltzmann and Planck constants respectively. A convenient way of plotting the temperature dependence of a unimolecular reaction is to use Equation 4.2:

$$\ln(k/T) = \ln(k_B/h) + \Delta H^{\ddagger}/R - \Delta H^{\ddagger}/RT \qquad \textbf{Equation 4.2}$$

The activation parameter $\Delta H^{\ddagger}$ is calculated from the slope of the plot. $\Delta S^{\ddagger}$ is calculated by extrapolation to the ordinate axis, and $\Delta G^{\ddagger}$ is calculated directly from Equation 4.1. The use of Equation 4.2 in plotting the temperature dependence of a unimolecular reaction is preferred over the use of the classical Arrhenius plot, and for

this reason was used in the studies of C-H bond cleavage in the MADH- and sarcosine oxidase-catalysed reactions (Basran *et al.*, 1999d; Harris *et al.*, 2000). A consequence of using Equation 4.2 is the need to define explicitly the meaning of values obtained from such plots. The use of the Arrhenius plot in the past has led to the development of criteria to indicate tunnelling based on the values for $\Delta\Delta E_a$ and the A_H/A_D ratio (calculated from the intercepts of the Arrhenius plot for protium and deuterium substrates). The corresponding parameters calculated from the slopes and intercepts of plots using Equation 4.2 are $\Delta\Delta H^{\ddagger}$ and A'_H/A'_D (the prime is used to distinguish this ratio from the A_H/A_D ratio calculated from the classical Arrhenius plot).

Ideally, in order to determine KIEs for native and mutant forms of TMADH, a full substrate dependence should be carried out at each temperature in order to determine the limiting rate constants for each enzyme in reaction with TMA and dTMA. However, there is a limit to the extent to which this can be done, both in terms of time available and the quantities of enzyme required to carry out a full substrate dependence at each temperature. Therefore, two approaches have been adopted here for determining KIEs in TMADH. When sufficient enzyme was available, a full substrate dependence for normal and deuterated substrate was carried out; this approach was used for native enzyme and the H172Q mutant. However, where the amount of enzyme was limiting, rate constants and KIEs were instead determined using substrate concentrations that were a minimum of 10 times the K_d value for the enzyme; this latter method was used with the Y169F mutant, having been previously used in the studies of MADH and TSOX that established the role of protein dynamics and H-tunnelling in these enzymes (Basran *et al.*, 1999d; Harris *et al.*, 2000).

4.2.2 Temperature Dependence Studies of Native TMADH

A temperature dependence study was carried out on native TMADH at pH 7.0 with TMA and dTMA as substrates. To obtain data points for the value of k, the rate of reaction for a plot of ln (k/T) versus 1/T, a full substrate dependence was carried out for both of these substrates at six temperature points: 3, 6, 9, 12, 15 and 18 °C. Flavin reduction was monitored at 443 nm in a stopped-flow device using TMA and dTMA as substrates. Data for native TMADH at pH 7.0 was fitted to a biphasic rate equation (Figures 4.1 and 4.2), with the fast phase of the reaction being used to indicate the rate of flavin reduction (Jang *et al.*, 1999a). Data were fitted to the Strickland equation (Equation 2.6) to obtain the dissociation constant for substrate and the limiting rate constant for reduction of 6-S-cysteinyl FMN (Figures 4.3 and 4.4).

For native TMADH at pH 7.0, the rates for flavin reduction obtained at even a fairly moderate temperature (e.g. 18 °C) extrapolate to k_{lim} values of over 1000 s^{-1} at the highest substrate concentrations. Where this occurs, the majority of the absorbance change associated with flavin reduction is lost within the dead-time of the stopped-flow apparatus (about 1 ms). Therefore, great care was taken to ensure that the kinetic transients obtained were of sufficient quality to allow confident determination of rate constants and every observed rate constant used for substrate dependence data was the average of at least four transients.

The results of a temperature dependence study on native TMADH at pH values of 6.5, 7.0 and 7.5 is presented in Table 4.1. Data at pH 6.5 and 7.5 was supplied by Dr Jaswir Basran and was collected using a TMA concentration of 10 times the K_d for TMA and dTMA at these pH's. The temperature dependence for the reaction of native TMADH at pH 7.0 is plotted in Figure 4.5.

There are three main indicators that H-tunnelling is occurring in the TMADH reaction:

(i) KIEs: the KIEs for the reactions of native TMADH with TMA and perdeuterated TMA generally fall just above the values associated with classical behaviour, varying between 8.9 and 10 at pH 7.0. From a classical consideration, this provides favourable evidence that tunnelling is occurring. However, even 'low' KIEs (i.e. 7 or less) can be incorporated into dynamic views of catalysis such as VEGST (Bruno & Bialek, 1992; Scrutton *et al.*, 1999). Unfortunately, the variability in the values obtained for the KIEs, which is mainly due to the fast rates of flavin reduction, makes it unclear as to whether they are completely temperature independent, as would be expected if ground state tunnelling is occurring, and this is one aspect of these results which might need further testing.

(ii) Arrhenius prefactor ratios: The ratio of Arrhenius preexponential factors at pH 6.5 are much smaller than 1, indicating that protium is tunnelling much more extensively than deuterium at this pH. At pH 7.0, the value of the prefactors has increased, being closer to 1.6. Taken alone, a prefactor ratio of 1.6 is close enough to the value of 1 expected for classical H-transfer (Bell, 1980). However, given the context of this value, lying between a prefactor ratio of 0.033 at pH 6.5 and a ratio of 4.31 at pH 7.5, it is more likely that this reflects greater tunnelling of deuterium as there is an increase in pH. This would be expected if there is movement towards a regime in which ground state tunnelling of both hydrogen isotopes occurs, in which case the Arrhenius prefactor ratio approaches the KIE for the reaction (Scrutton *et al.*, 1999).

(iii) The values of the activation parameters for the reaction: At pH 6.5, it has already been established that the Arrhenius prefactor ratio indicates that there is much greater tunnelling of protium compared to deuterium, and this is reflected in a fairly sizeable difference between, $\Delta H^{\ddagger}_{C\text{-}H}$ and $\Delta H^{\ddagger}_{C\text{-}D}$ of 13 kJ·mol^{-1}. As pH increase however, the differences in $\Delta H^{\ddagger}$ decrease, so that at pH 7.5 it is close to zero (albeit with a large error). Again, this would be expected if increasing the pH leads to a change in tunnelling regime such that ground state tunnelling becomes the dominant means of H-transfer. However, the individual activation energies for C-H and C-D bond cleavage are still fairly sizeable (33 kJ·mol^{-1}) and do not approach the zero values implied by a static model of ground state tunnelling (Jonsson *et al.*, 1996).

With reference to Figure 1.18 in the main Introduction, the data indicate that at pH 6.5 TMADH is operating somewhere between region II and III, because protium is tunnelling much more extensively than deuterium, as indicated by the A'_H/A'_D ratio <1. However, at pH 7.0, the A'_H/A'_D ratio has increased above 1 and is associated with a drop in the difference between activation parmeters, indicative of a move towards a regime where tunnelling of deuterium is more significant. The data at pH 7.0 indicates that the reaction is operating in a regime which more closely corresponds to region III of Figure 1.18, in which the A'_H/A'_D ratio approaches values close to the KIE, as ground state tunnelling of both protium and deuterium increasingly becomes the mode of H-transfer. At pH 7.5, the Arrhenius prefactor ratio and activation energy for the reaction indicate that TMADH is probably still operating within region III, but is now closer to region IV.

Taken together, these results are promising indicators as pH increases, the TMADH reaction is heading towards a regime where ground state tunnelling of both protium and deuterium is occurring. Despite the drop in activation energy for the reaction as pH is increased, the reactions are still clearly temperature dependent, and are very similar to temperature dependence plots for enzymes in which H-tunnelling is driven by low frequency thermal vibrations of the protein (Basran *et al.*, 1999d; Harris *et al.*, 2000; Kohen *et al.*, 1999). Due to the difficulties of determining reaction rates at pH 8.5 for TMADH, it can only be speculated that tunnelling of protium and deuterium from the ground state occurs at this, the pH optimum for the enzyme.

Table 4.1: Temperature Dependence Data for Native TMADH Using Normal and Perdeuterated TMA

pH	$\Delta H^{\ddagger}_{C\text{-}H}$ (kJ·mol^{-1})	$\Delta H^{\ddagger}_{C\text{-}D}$ (kJ·mol^{-1})	$\Delta\Delta H^{\ddagger}$ (kJ·mol^{-1})	A'_H/A'_D
6.5[1]	32.6 ± 1.1	45.6 ± 1.1	13.0 ± 2.2	0.033
7.0	20.2 ± 2.2	24.3 ± 1.3	4.1 ± 3.5	1.587
7.5[1]	33.0 ± 5.4	33.7 ± 8.8	0.7 ± 14.2	4.306

[1]Data supplied by Dr Jaswir Basran.

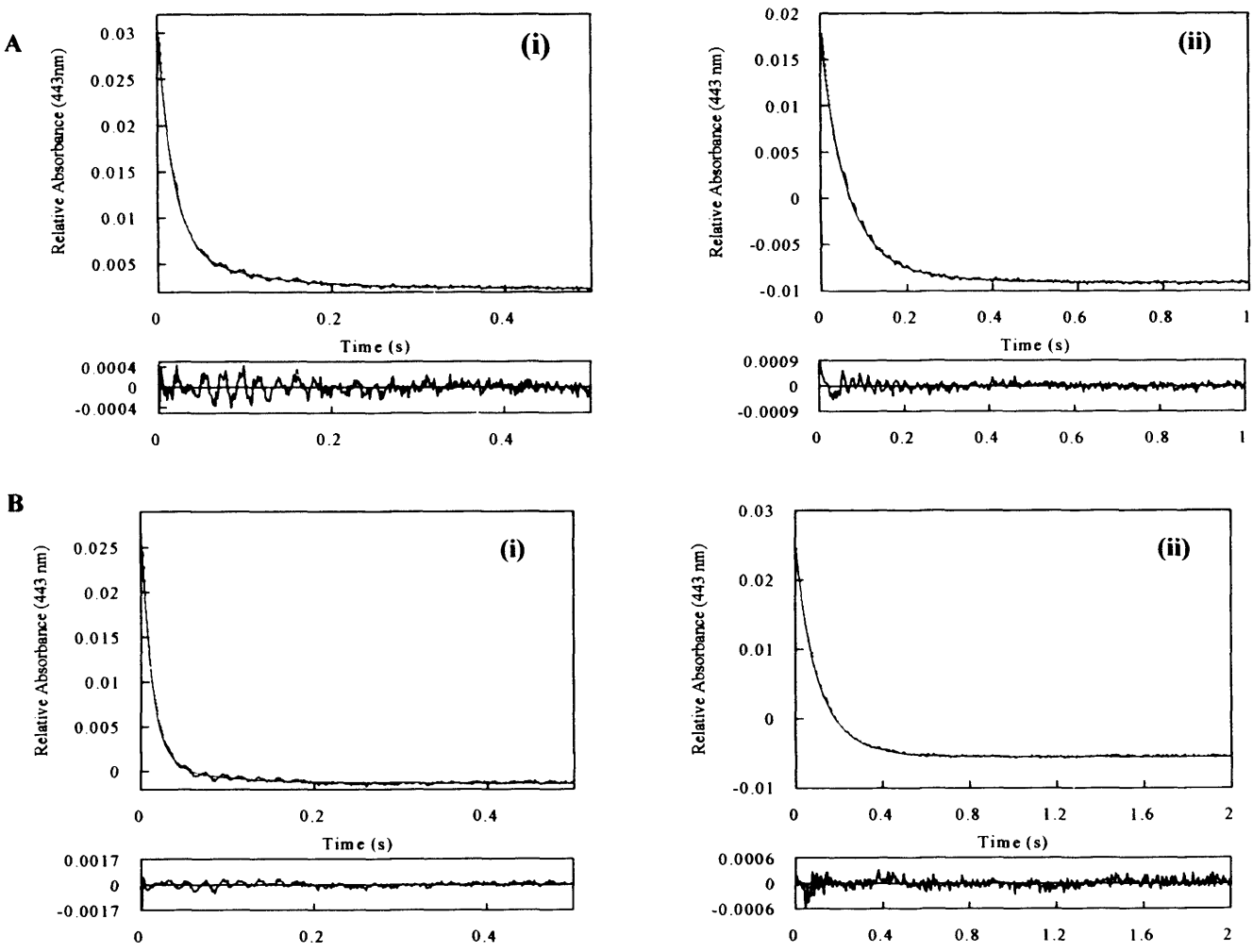

Figure 4.1: Kinetic transients for the reduction of flavin in native TMADH at pH 7.0, as monitored at 443 nm at low concentrations of TMA and dTMA (0.5 mM): A, 5 °C and B, 18 °C, with (i) TMA as substrate and (ii) dTMA as substrate. The lower panels show the plots of residuals for fits to a biphasic absorbance change.

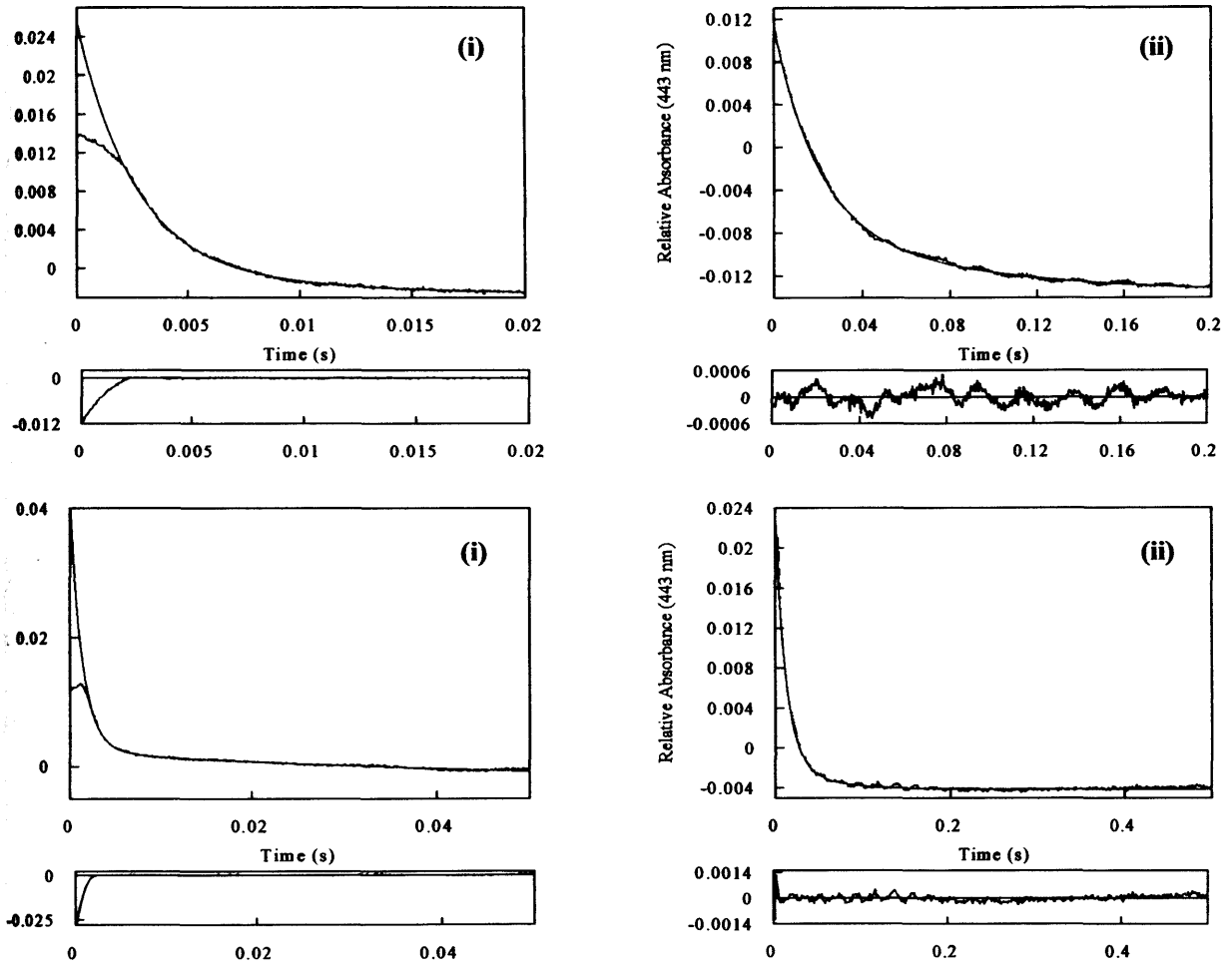

Figure 4.2: Kinetic transients for the reduction of flavin in native TMADH at pH 7.0, as monitored at 443 nm at high concentrations of TMA and dTMA (12 mM): A, 5 °C and B, 18 °C, with (i) TMA as substrate and (ii) dTMA as substrate. The lower panels show the plots of residuals for fits to a biphasic absorbance change.

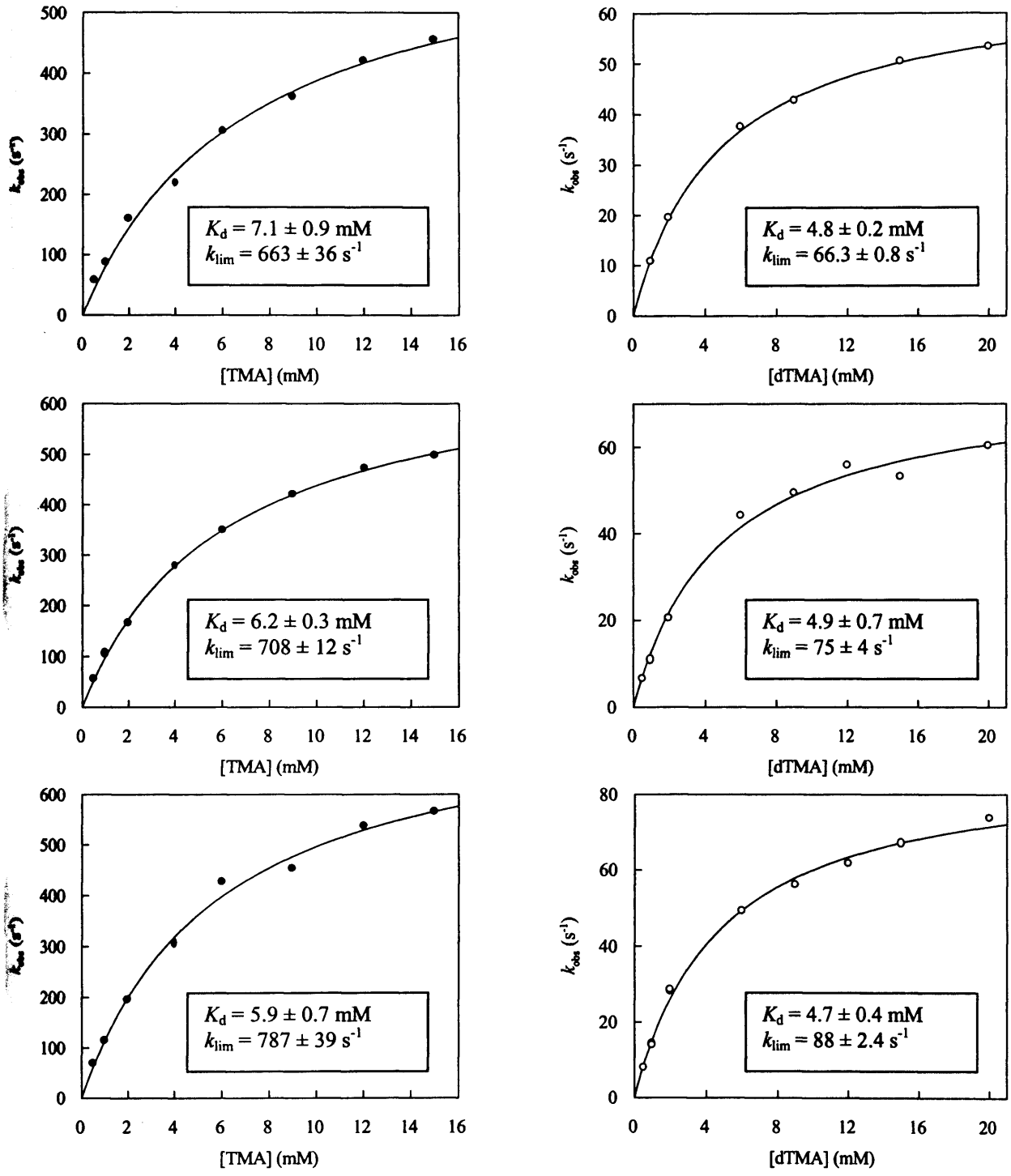

Figure 4.3: Plots of observed rate constants versus substrate concentration for native TMADH at pH 7.0, with TMA and dTMA as substrate. Reactions were performed in 20 mM potassium phosphate buffer at A: 3 °C, B: 6 °C and C: 9 °C. Flavin reduction was monitored at 443 nm and data were fitted to Equation 2.6.

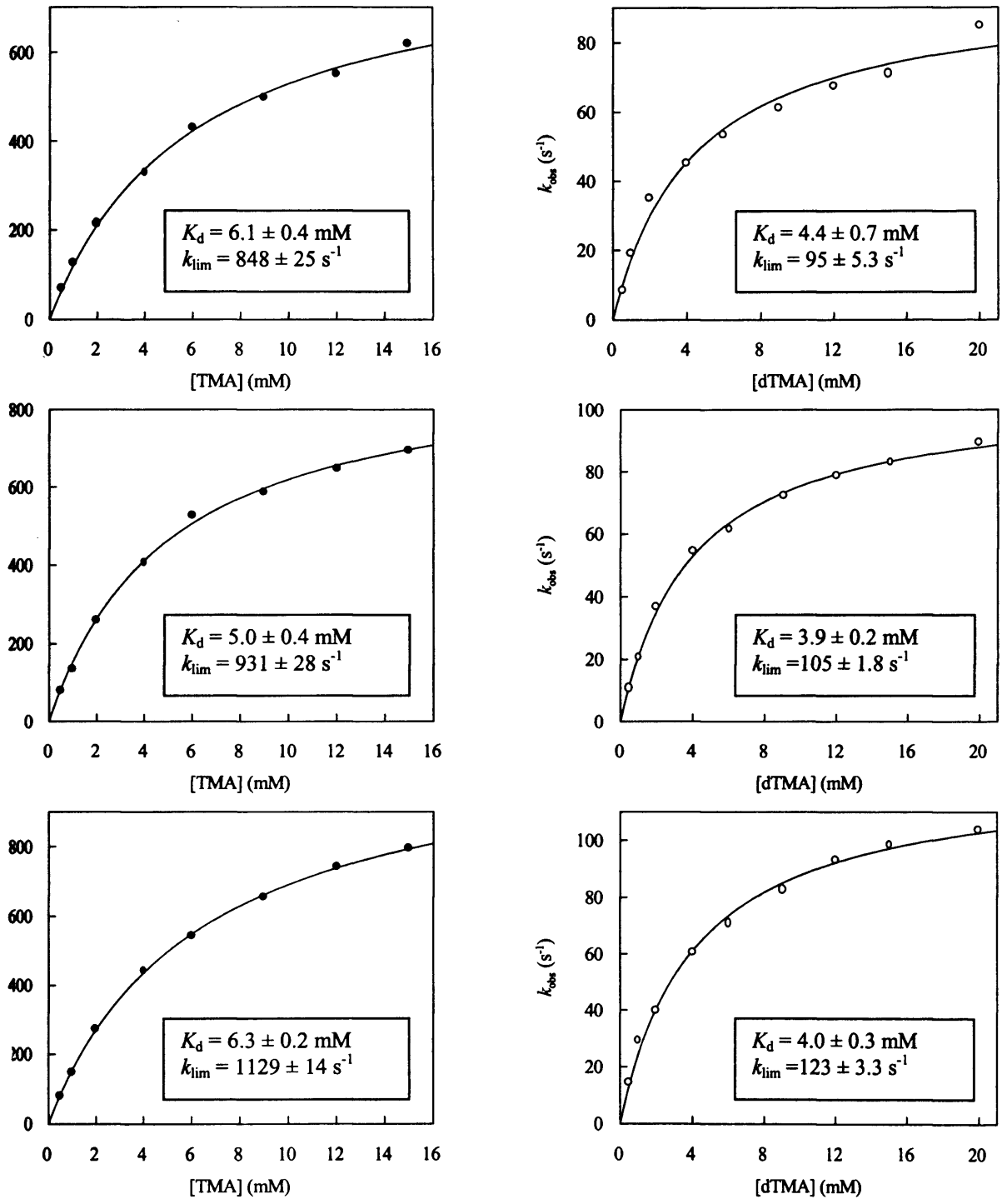

Figure 4.4: Plots of observed rate constants versus substrate concentration for native TMADH at pH 7.0, with TMA (closed circles) and dTMA (open circles) as substrate. Reactions were performed in 20 mM potassium phosphate buffer at A: 12 °C, B: 15 °C and C: 18 °C. Flavin reduction was monitored at 443 nm and data were fitted to Equation 2.6.

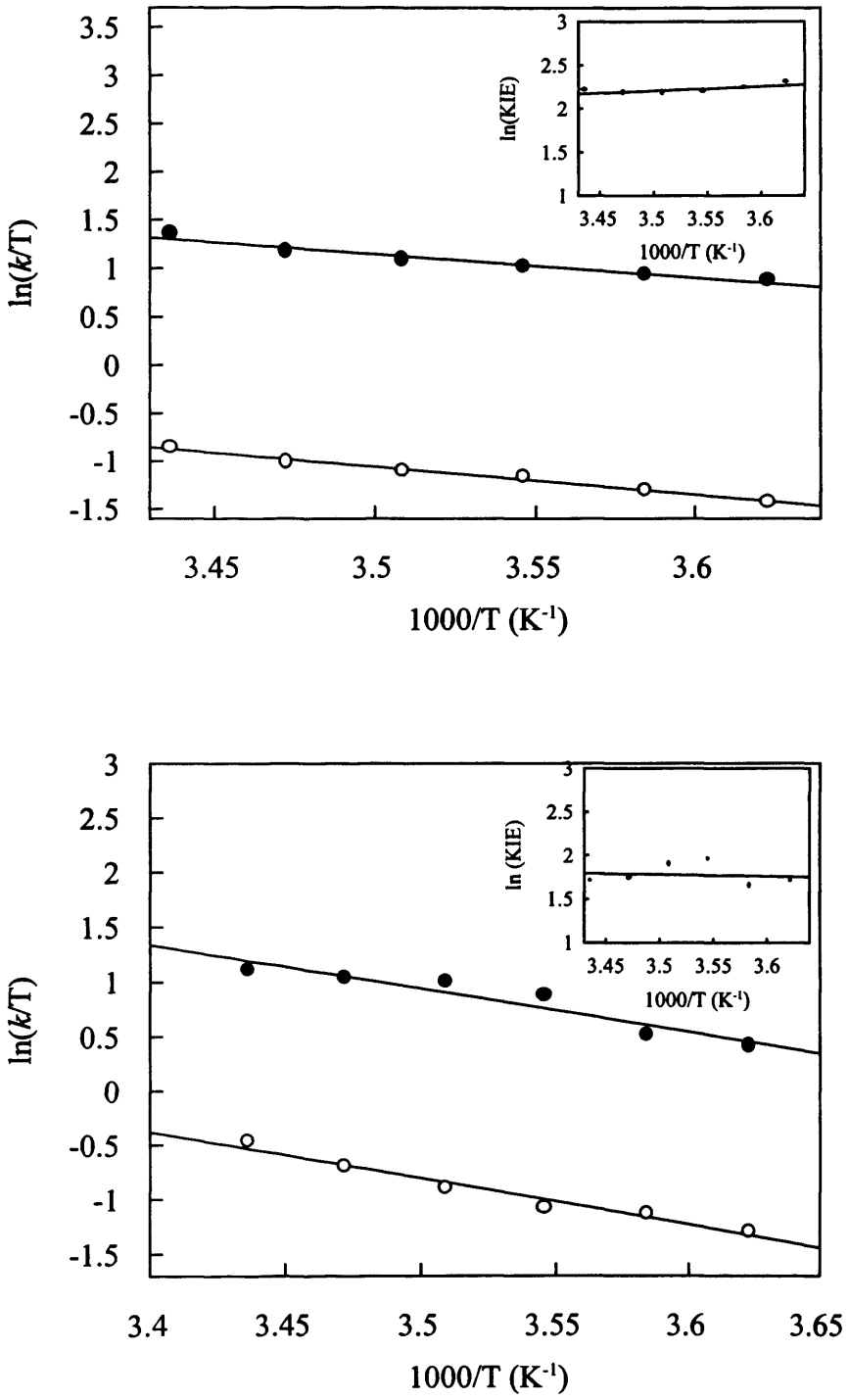

Figure 4.5: Temperature dependence and KIE data for native TMADH. (A) pH 7.0, (B) pH 7.5. Main panel: temperature dependence plots for native TMADH with TMA (closed circles) and dTMA (open circles) as substrates. Inset: plot of KIE versus 1000/T. Data obtained from these plots is presented in Table 4.1.

4.2.3 Y169F and H172Q TMADH Mutants

The Y169F and H172Q TMADH mutants were 48 % and 10 % flavinylated respectively, determined using Equation 2.1, similar to previously determined flavinylation levels for these mutants (Basran *et al.*, 1999a; Basran *et al.*, 1999c). The transients for both mutants were biphasic (Figures 4.4 and 4.5), with the fast phase of the reaction being used to determine the rate of flavin reduction as previously (Basran *et al.*, 1999a; Basran *et al.*, 1999c).

There was sufficient yield of the H172Q mutant enzyme to enable a full substrate dependence to be carried out using both TMA and dTMA. However, due to the relatively low yield of the Y169F mutant and the large amount of protein required to bring about a measurable absorption change at 443 nm, the data for this enzyme was always carried out at a concentration greater than 10 times the K_d (200 mM substrate). Substrate dependencies were carried out at pH 7.5 and pH 8.5 (Figure 4.6) to determine the K_d values for TMA and dTMA at these pH's. The substrate dependence of flavin reduction for the Y169F mutant at pH 7.0 has been determined previously (Basran *et al.*, 1999a).

4.2.3.1 Temperature Dependency Data for the Y169F TMADH Mutant

The results of a temperature dependence study on the Y169F TMADH mutant over the pH range 7.0 to 8.5 is presented in Table 4.2 and Figure 4.11. The considerably slower rate of flavin reduction for the Y169F TMADH mutant allows the temperature dependence of the reaction to be studied over a greater temperature range than for native enzyme, up to 35 °C.

The Y169F TMADH mutant has properties only slightly altered from the native enzyme. As with native enzyme, the KIEs obtained for the Y169F mutant are only slightly above those predicted from a semi-classical description of the reaction (average = 11), but, as has already been stated, low KIEs can be accounted for in dynamic models of catalysis (Bruno & Bialek, 1992). However, the trend of an increased tendency towards ground state tunnelling as pH increases, which is indicated in the study of native TMADH appears to be clearer in the Y169F mutant. At pH 7.0, the enzyme is operating between region II and III of Figure 1.18, as indicated by the inflated KIEs, combined with an $A'_H/A'_D < 1$ and a $\Delta\Delta H^{\ddagger}$ value (6.91 $kJ \cdot mol^{-1}$) that is close to the value expected from a semi-classical consideration of Arrhenius KIE data. At pH 7.5, the Y169F mutant appears to be operating

comfortably within regime III of Figure 1.18: the A'_H/A'_D ratio is just greater than 1 and with a convergence in the activation parameter, $\Delta H^{\ddagger}_{C-X}$ for the two isotopes that gives a value for $\Delta\Delta H^{\ddagger}$ of only 3.82 kJ·mol^{-1}. At pH 8.5 there is again a decrease in $\Delta\Delta H^{\ddagger}$, with a corresponding convergence in the values for the A'_H/A'_D and KIE. At this point, the Y169F mutant appears to be operating close to the interface between regimes III and IV, as the Arrhenius prefactor ratio at this pH has not yet approached the KIE. However, despite the apparent similarities exhibited in the tunnelling regime between native enzyme and the Y169F mutant at each pH, the reaction rates of the Y169F mutant are much slower. Within a dynamic view of enzyme catalysis, this can only be explained if the mutation has caused an increase in barrier width: the wavefunction that describes the movement of a proton through a potential energy barrier decays more extensively through a wide barrier than a narrow one, and this is expressed as a slower rate of reaction.

Table 4.2: Temperature Dependence Studies on the Y169F TMADH Mutant

pH	$\Delta H^{\ddagger}_{C-H}$ (kJ·mol^{-1})	$\Delta H^{\ddagger}_{C-D}$ (kJ·mol^{-1})	$\Delta\Delta H^{\ddagger}$ (kJ·mol^{-1})	A'_H/A'_D
7.0	38.56 ± 1.7	45.47 ± 2.0	6.91 ± 3.7	0.684
7.5	42.75 ± 1.1	46.57 ± 2.1	3.82 ± 3.2	1.391
8.5	54.53 ± 3.1	56.71 ± 3.6	2.18 ± 6.7	2.316

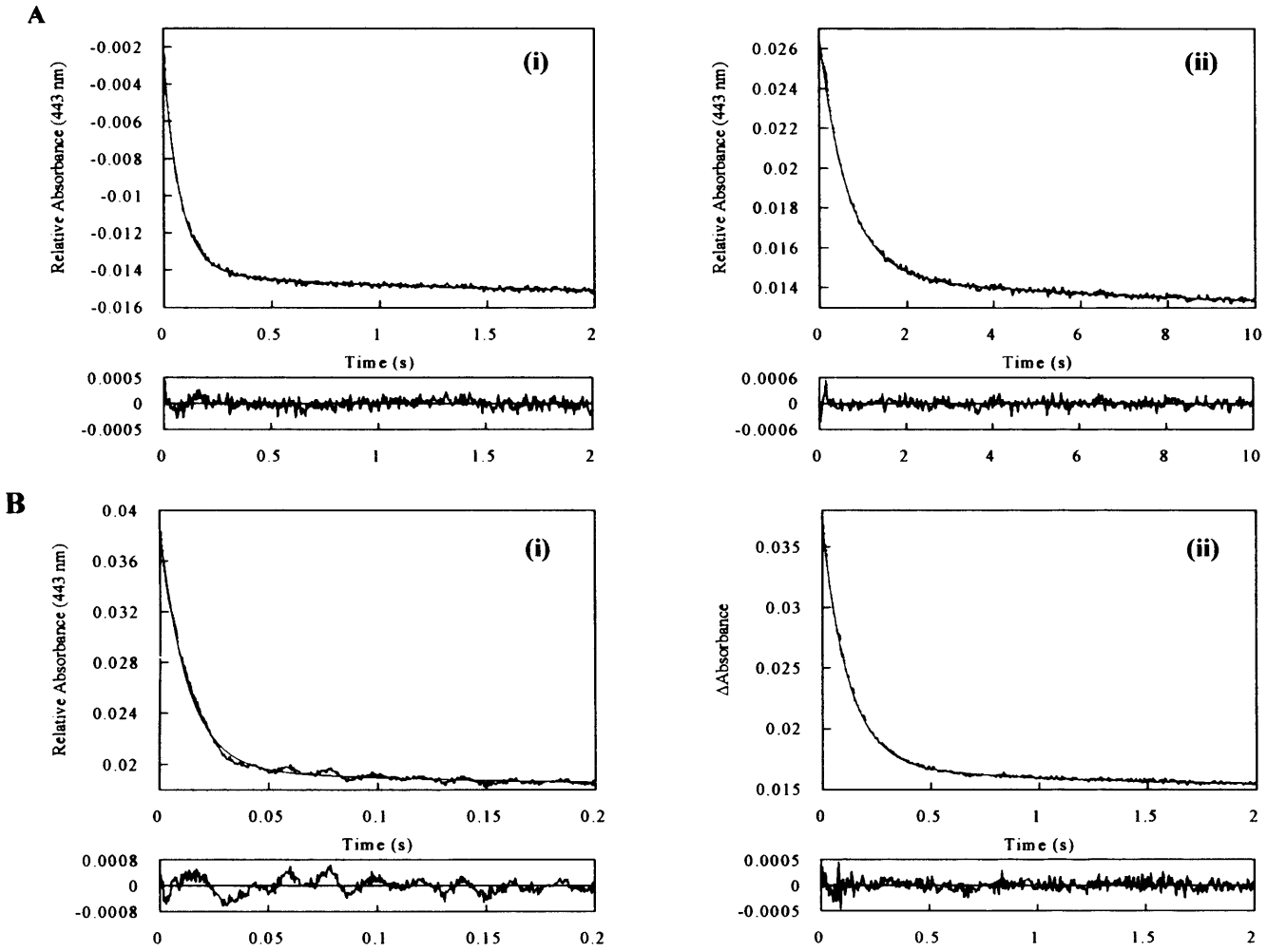

Figure 4.6: Kinetic transients for the reduction of flavin in the Y169F TMADH mutant at pH 7.0, as monitored at 443 nm. For illustrative purposes, the transients shown here were obtained at: A, 5 °C and B, 35 °C, with (i) TMA as substrate and (ii) dTMA as substrate. Substrate concentration was 200 mM in each case. The lower panels show the plots of residuals for fits to a biphasic absorbance change.

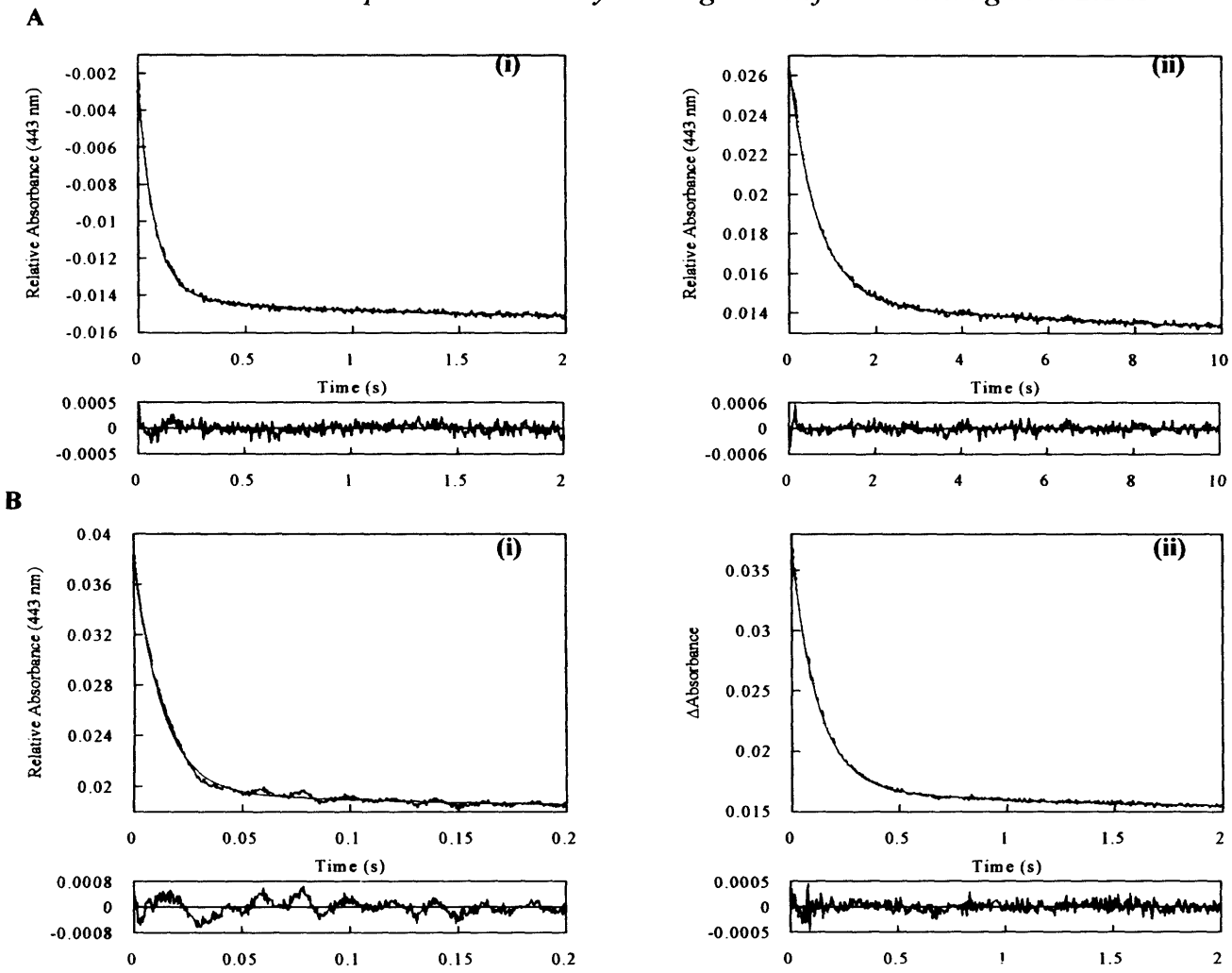

Figure 4.7: Kinetic transients for the reduction of flavin in the Y169F TMADH mutant at pH 7.5, as monitored at 443 nm. For illustrative purposes, the transients shown here were obtained at: A, 5 °C and B, 35 °C, with (i) TMA as substrate and (ii) dTMA as substrate. Substrate concentration was 200 mM in each case. The lower panels show the plots of residuals for fits to a biphasic absorbance change.

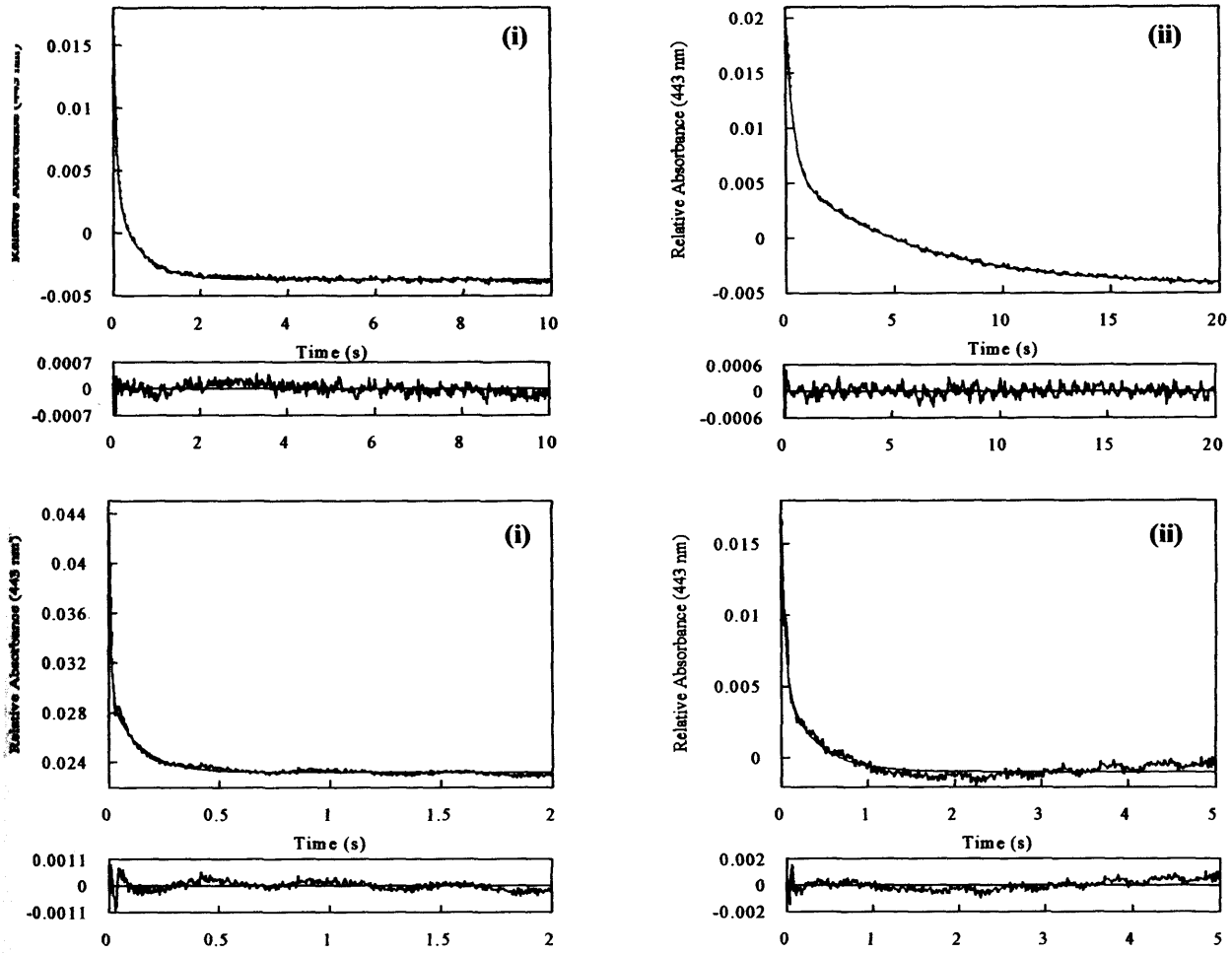

Figure 4.8: Kinetic transients for the reduction of flavin in the Y169F TMADH mutant at pH 8.5, as monitored at 443 nm. For illustrative purposes, the transients shown here were obtained at: A, 5 °C and B, 35 °C, with (i) TMA as substrate and (ii) dTMA as substrate. Substrate concentration was 200 mM in each case. The lower panels show the plots of residuals for fits to a biphasic absorbance change.

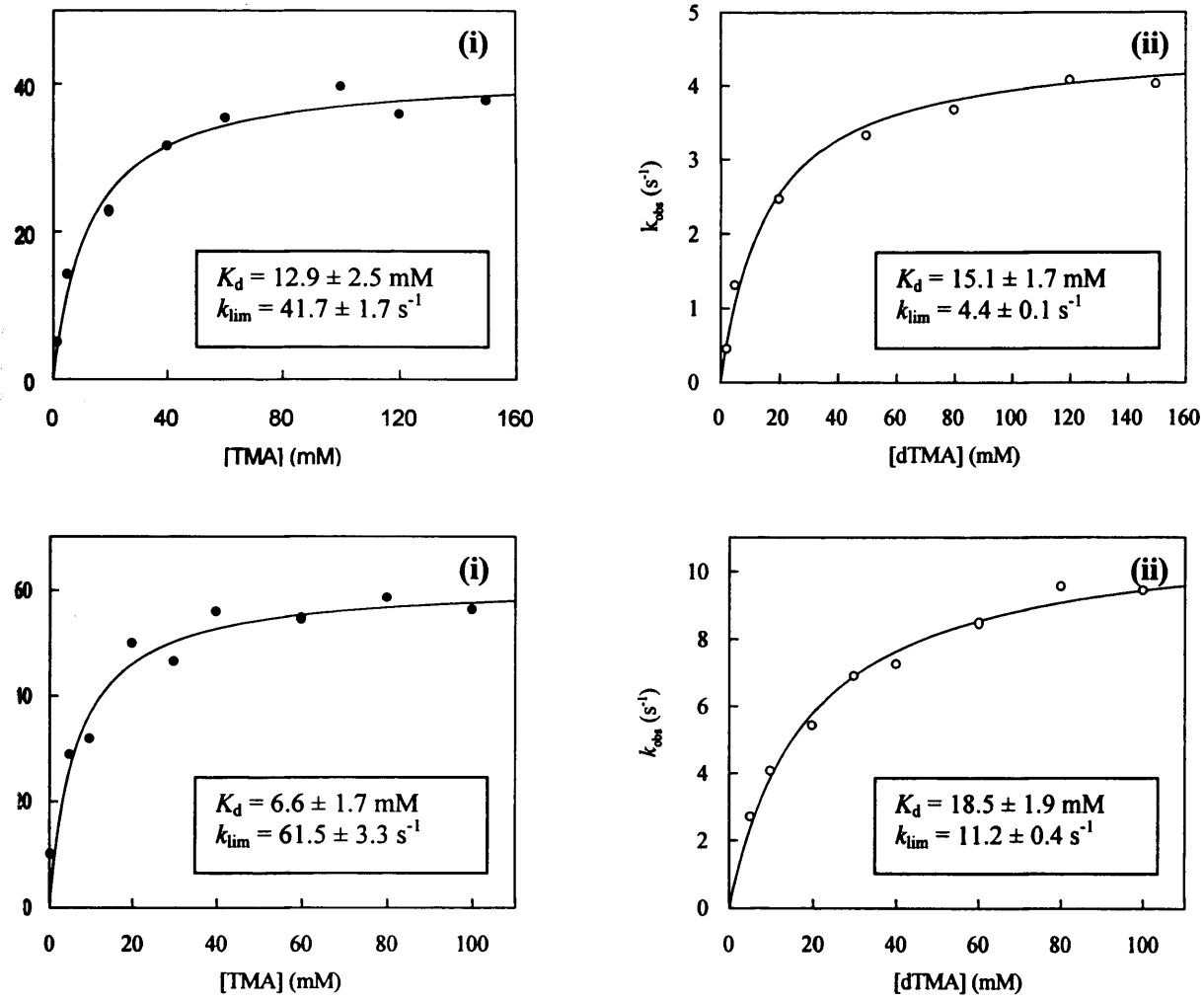

Figure 4.9: Plots of observed rate constants versus substrate concentration for the Y169F TMADH mutant. Reactions were performed in 20 mM potassium phosphate buffer, 25 °C at A, pH 7.5 and B, pH 8.5, using either (i) TMA or (ii) dTMA as substrate. Flavin reduction was monitored at 443 nm and data were fitted to Equation 2.6.

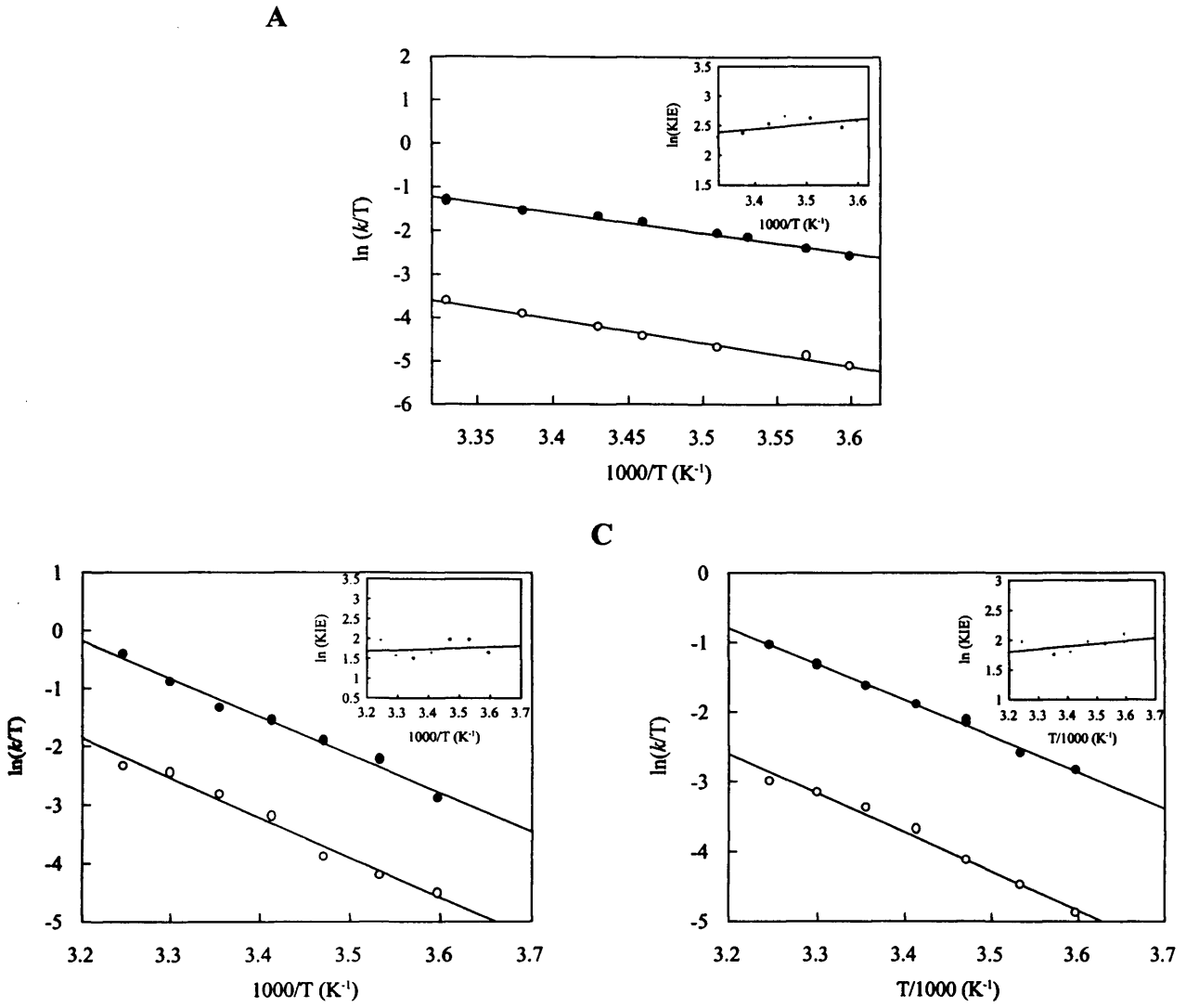

Figure 4.11: Temperature dependence and KIE data for the Y169F TMADH mutant. (A) pH 7.0, (B) pH 7.5 and (C) pH 8.5. Main panel: temperature dependence plots for the Y169F mutant with TMA (closed circles) and dTMA (open circles) as substrates. Inset: plot of KIE versus 1000/T. Data obtained from these plots is presented in Table 4.2.

4.2.3.2 Temperature Dependence of the H172Q TMADH Mutant

The results of a temperature dependence study on the H172Q TMADH mutant between pH 6.5 and 8.5 are displayed in Table 4.3 and Figure 4.3. Data obtained at pH 7.0 was obtained from substrate dependence studies on this enzyme with TMA and perdeuterated TMA at each temperature. Data at pH 8.5 was supplied by Dr J. Basran. As with native enzyme and the Y169F mutant, the trend appears to show that as pH increases the enzyme moves to a regime in which tunnelling occurs from the ground state of the reactants, i.e. there is a convergence of values in $\Delta H^{\ddagger}_{C\text{-}H}$, and an increase in the A'_H/A'_D ratio from values below 1 towards parity with the KIE. Again, as with the Y169F mutant, there is no strong difference between the tunnelling regime exhibited by the H172Q mutant, when compared with the native enzyme. However, because the rates of reaction are slower, the only explanation which fits the other dynamic aspects for catalysis in TMADH is that the H172Q mutation has brought about an increase in the width of the reaction barrier that is responsible for the decrease in reaction rate.

Table 4.3: Temperature Dependence Studies on the H172Q TMADH Mutant

pH	$\Delta H^{\ddagger}_{C\text{-}H}$ (kJ·mol^{-1})	$\Delta H^{\ddagger}_{C\text{-}D}$ (kJ·mol^{-1})	$\Delta\Delta H^{\ddagger}$ (kJ·mol^{-1})	A'_H/A'_D
6.5[1]	32.7 ± 2.7	60.1 ± 2.7	27.4 ± 5.4	1.7×10^{-4}
7.0	46.9 ± 1.9	48.13 ± 2.4	1.23 ± 4.3	4.807
8.5[2]	48.7 ± 1.4	48.1 ± 2.4	-0.6 ± 3.8	9.679

[1,2]Data supplied by Dr Jaswir Basran.

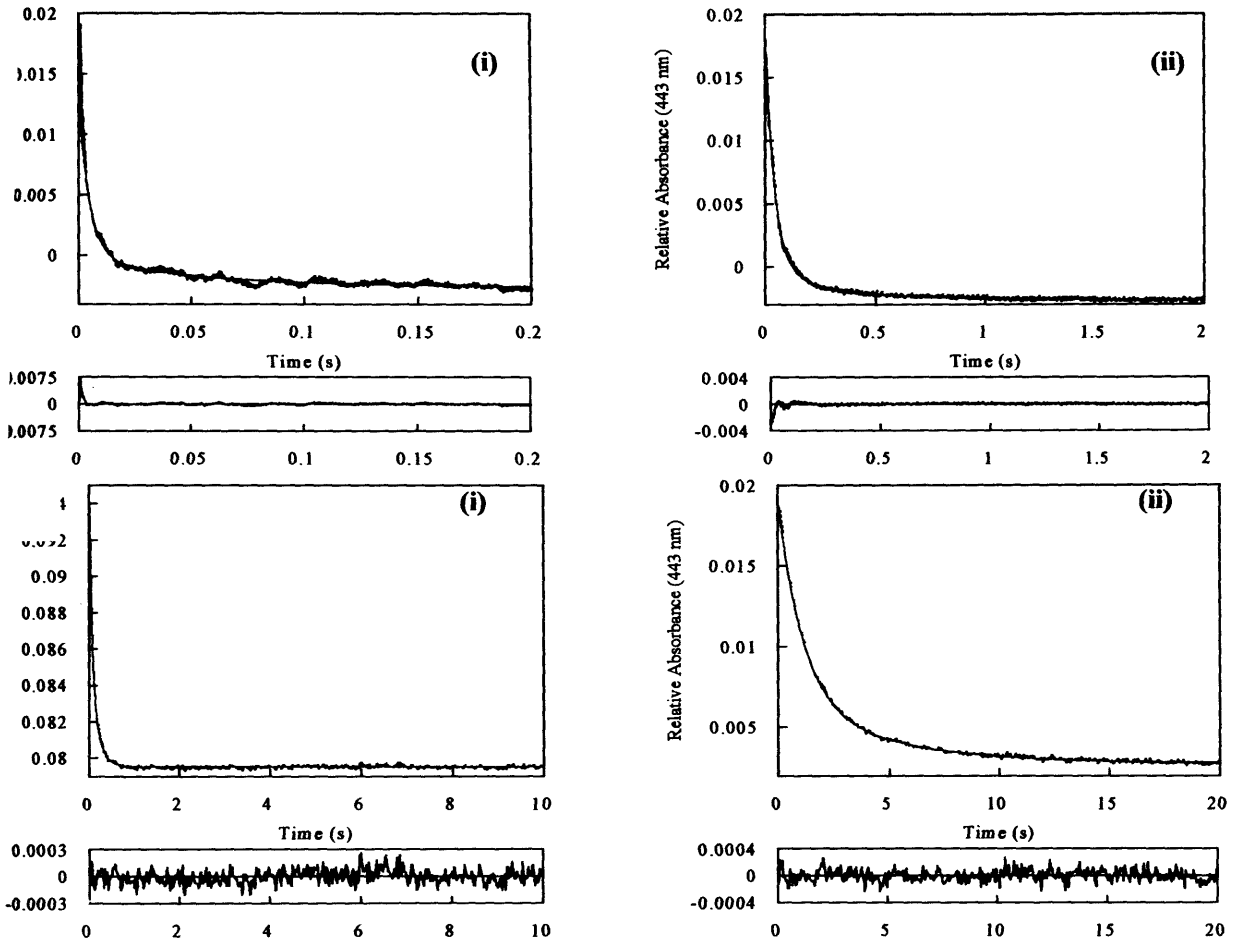

Figure 4.10: Kinetic transients for the reduction of flavin in the H172Q TMADH mutant at pH 7.0, as monitored at 443 nm. For illustrative purposes, the transients shown here were obtained at: A, 5 °C and B, 35 °C, with (i) TMA as substrate and (ii) dTMA as substrate. Substrate concentration was 150 mM in each case. The lower panels show the plots of residuals for fits to a biphasic absorbance change.

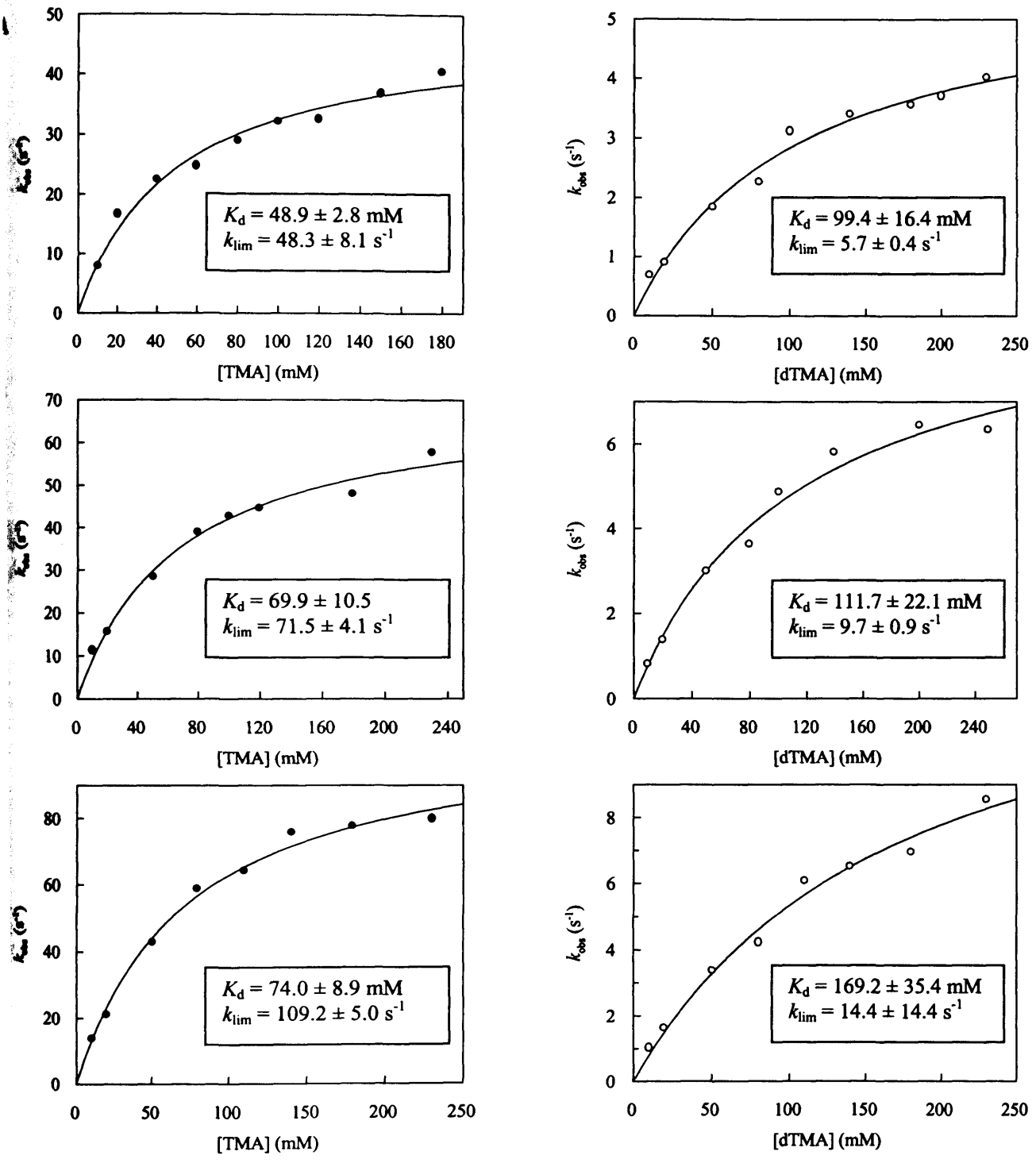

Figure 4.12: Plots of observed rate constants versus substrate concentration for H172Q mutant TMADH at pH 7.0: With TMA (closed circles) and dTMA (open circles) as substrate. Reactions were performed in 20 mM potassium phosphate buffer at A: 5 °C, B: 10 °C and C: 15 °C. Flavin reduction was monitored at 443 nm and data were fitted to Equation 2.4.

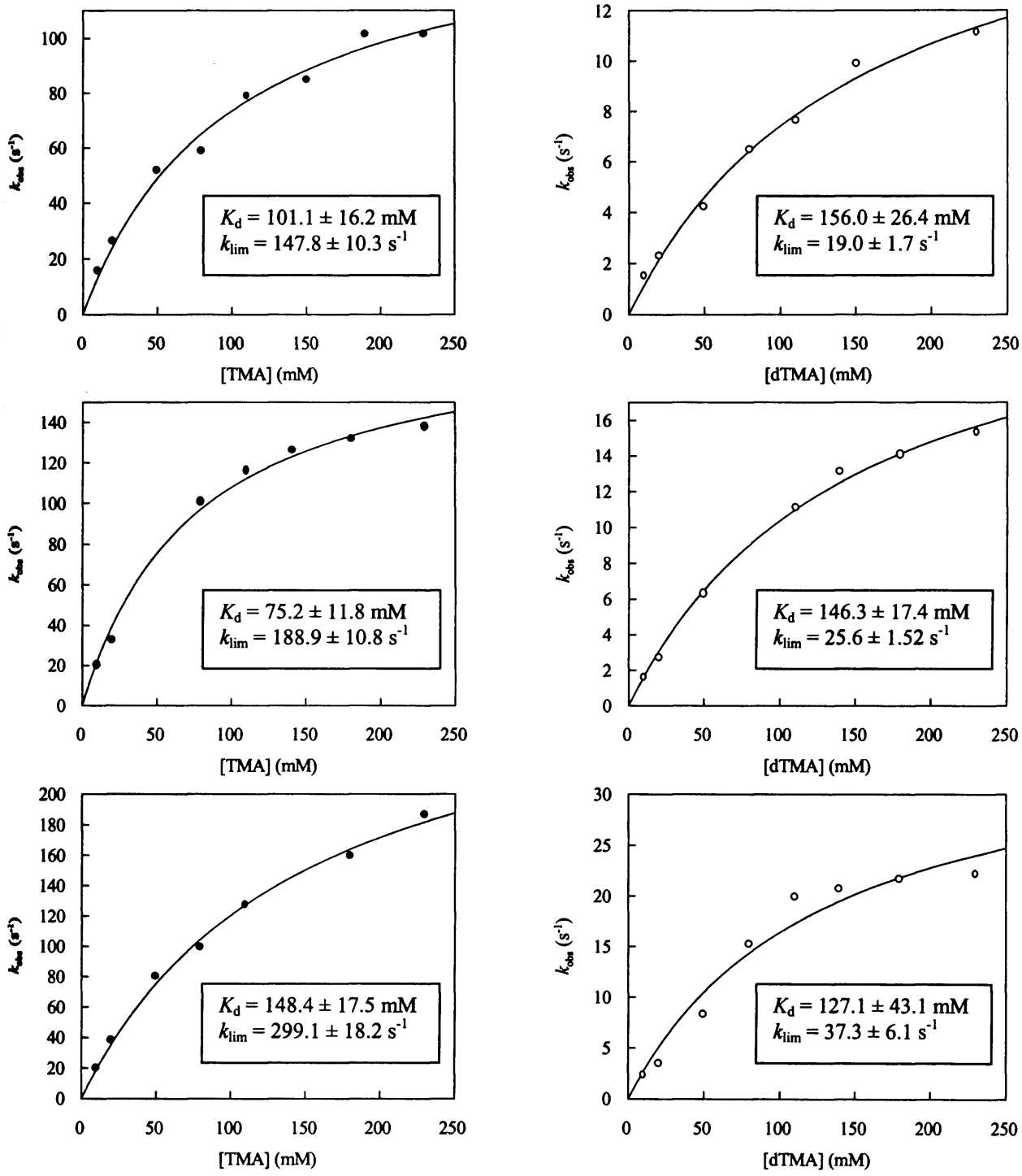

Figure 4.13: Plots of observed rate constants versus substrate concentration for H172Q mutant TMADH at pH 7.0: With TMA (closed circles) and dTMA (open circles) as substrate. Reactions were performed in 20 mM potassium phosphate buffer at A: 20 °C, B: 25 °C and C: 30 °C. Flavin reduction was monitored at 443 nm and data were fitted to Equation 2.4.

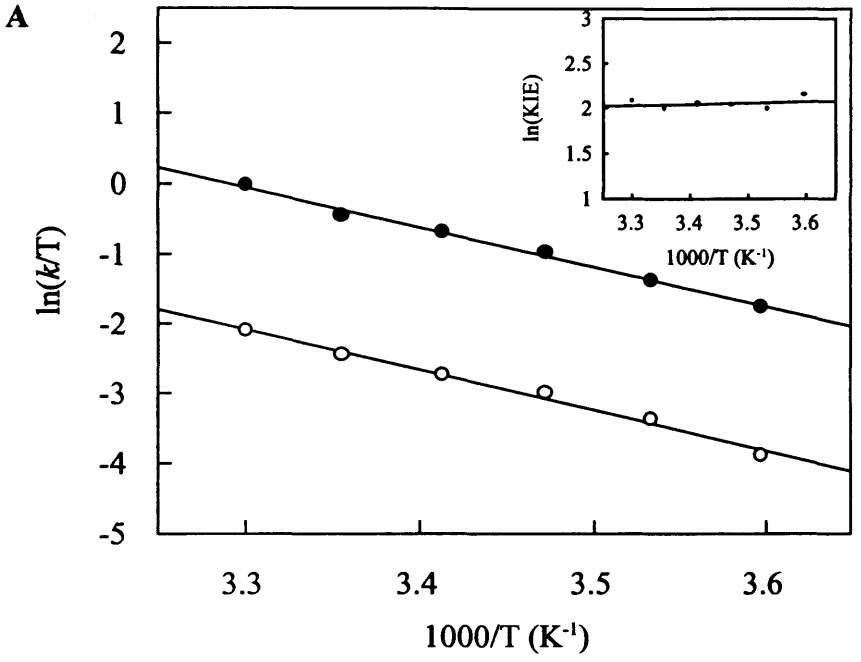

Figure 4.14: Temperature dependence and KIE data for the H172Q TMADH mutant at pH 7.0. Main panel: temperature dependence plots for the Y169F mutant with TMA (closed circles) and dTMA (open circles) as substrates. Inset: plot of KIE versus 1000/T. Data obtained from these data is presented in Table 4.3.

4.3 Discussion

H-tunnelling driven by protein dynamics has now been established for at least three enzyme systems (Basran *et al.*, 1999d; Harris *et al.*, 2000; Kohen *et al.*, 1999). Given that the acceptance of this phenomenon is still in the early stages, this chapter has presented the results of a preliminary study, first into whether TMADH uses H-tunnelling during catalysis, and second, whether changes introduced by pH or by mutations have an effect on this. To investigate this, a series of temperature dependencies for the TMADH reaction was carried out with TMA and dTMA over a range of pH and using native and H172Q and Y169F mutant forms of the enzyme.

At this point, there are encouraging signs that H-tunnelling is the preferred mode of H-transfer following C-H bond cleavage in TMADH: H-tunnelling would address the issue of how an enzyme such as TMADH cleaves stable C-H bonds in its substrate (Scrutton *et al.*, 1999; Sutcliffe & Scrutton, 2000), but a lack of knowledge about the precise mechanism of the TMADH reaction prevents strong confirmation that H-tunnelling driven by protein dynamics occurs. Perhaps the most interesting aspect of these results is that there is an apparent change in the expression of tunnelling that occurs as pH increases, from extensive tunnelling of protium compared to deuterium at pH 6.5, to a state where both protium and deuterium appear close to tunnelling from the ground state at pH 8.5. It is possible that this reflects a pH-dependent change in the rate limiting step for catalysis, such that the reaction at lower pH's is affected by internal commitments. However, an alternative explanation is that a change of pH affects the potential energy surface for the reaction, causing a narrowing of barrier width as pH increases. Because protium is able to tunnel over a greater distance than deuterium, a small increase in the overall width of a dynamic barrier would lead to protium tunnelling more readily than deuterium. This would be expressed as Arrhenius prefactor ratios <1, as is seen for native TMADH at pH 6.5. As barrier width narrows, the differential between protium and deuterium tunnelling decreases, until both are tunnelling through a narrow barrier, essentially from the ground state. This appears to reflect the situation close to pH 8.5

It has been stressed throughout this chapter that the results can only be viewed as an initial study. In this study, KIEs have been measured by stopped-flow techniques at substrate saturation and are therefore interpreted as representing k_3, the rate constant for substrate oxidation (as measured by the loss of the absorbance of the protein bound flavin). However, as explained in the introduction, the rate of substrate oxidation/flavin reduction can reflect several steps, or commitments. Therefore, the

absorbance change measured does not guarantee that a single (C-H bond) cleavage step is fully rate limiting. In addition, there are other factors that indicate that a more thorough knowledge of the TMADH reaction is required. For example, if interpreted through a dynamic theory of catalysis, such as VEGST, it appears that there is an increased tendency for TMADH to operate in a ground state tunnelling regime as pH increases. However, as pH increases, the results for each enzyme show that there is generally an increase in the energy of activation as the pH increases also. This is counterintuitive: as ground state tunnelling increases, there would presumably be less energy required for the enzyme to reach a conformation that is conducive to tunnelling through a potential energy barrier than when some 'activation' of the substrate is required. This is could be a strong indicator that altering pH affects more than barrier width.

With MADH and thermophilic ADH ((Basran *et al.*, 1999d; Kohen *et al.*, 1999), the observed kinetic behaviour was interpreted to indicate ground state tunnelling of hydrogen and deuterium through a fluctuating potential energy barrier; the dynamic nature of the potential energy barrier arises in these cases from the low-frequency thermal motions of the protein molecule. The model that shows the best fit to the data for MADH is that provided by Bruno and Bialek (Bruno & Bialek, 1992), termed VEGST (Scrutton *et al.*, 1999). Importantly, this dynamic barrier model for enzymatic C-H bond cleavage can accommodate KIEs of <7 (i.e., the semi-classical region of the static barrier models). VEGST has been demonstrated experimentally by the work on MADH (Basran *et al.*, 1999d), but there are potential complications arising from these isotope studies with TMADH. Apart from the issue of kinetic complexity, there could be effects due to the magnitude of secondary isotope effects arising from perdeuteration of substrate. As regards commitments, it is possible, with decreasing temperature, that the expected increase in KIE (for semi-classical behaviour) is offset by a decrease in kinetic commitment, leading to an observed KIE that is apparently independent of temperature, as described by the equation

$$\frac{k_{obs}^{H}}{k_{obs}^{D}} = \frac{\left(\frac{k_{int}^{H}}{k_{int}^{D}} + C\right)}{(1+C)} \qquad \textbf{Equation 4.3}$$

where C is a ratio of rate constants reflecting the degree by which C-H bond breakage is rate-determining, k_{obs}^{H}/k_{obs}^{D} is the observed KIE, and k_{int}^{H}/k_{int}^{D} is the intrinsic KIE (Schimerlik *et al.*, 1977). Even in single-turnover experiments, which can sometimes eliminate the effect of commitments (Northrop, 1981), and which focus on 'one-step' of a reaction, the rate of substrate oxidation/flavin reduction might reflect more than

one kinetic step. It could be argued that it is improbable that there could be a perfectly matched compensatory change in intrinsic KIE and internal commitment yielding an observed KIE that is independent of temperature in TMADH as a ground state tunnelling regime is approached. An upper limit for secondary KIEs of 1.36 may complicate analysis if the full secondary KIE is realised. Thus, although stopped-flow provide indications for a VEGST mechanism in TMADH, future studies will need to address these aspects with regard to the TMADH-catalysed oxidation of amines to prove unequivocally a role for VEGST of hydrogen during C-H bond cleavage.

Overall, this study provides very positive indications for the existence of H-tunnelling in TMADH, even given reservations about the effect of commitments. While apparent changes in tunnelling regime might only reflect changes in rate limiting step, it is intriguing to speculate that as TMADH approaches its optimum pH for activity (pH 8.5) that the expression of tunnelling changes from a regime where there is a differential tunnelling of protium and deuterium to one where both isotopes tunnel from the ground state. As more is revealed about the reaction mechanism of TMADH, it is possible that this preliminary study will serve as a good indicator of how tunnelling in TMADH is altered by changes in pH, that reflect differences in barrier width.

Chapter 5

Rational Engineering of Substrate Specificity in TMADH

5.1 Introduction

5.1.1 Producing Enzymes with New Activities

There is a great deal of research effort put into attempts to engineer novel activities into existing proteins for practical applications in industry and medicine (Arnold & Schmidt-Dannert, 1999; Ogawa & Shimizu, 1999). Broadly, biotechnologists would like to create mutant proteins with predetermined enzymatic characteristics such as catalytic efficiencies, pH optima, altered substrate specificity and improved stabilities (Chen, 1999; Shao & Arnold, 1996), using a variety of approaches, involving both 'rational' and 'irrational' design of enzymes (Shao & Arnold, 1996). This is hardly surprising, given the ability of enzymes to carry out complex chemical reactions under mild conditions with virtually no waste products (Arnold, 1996). Against this background, and given some of the properties of TMADH which will be expanded upon later, the work in this chapter presents the results from an attempt to improve the substrate specificity of TMADH for the substrate dimethylamine, DMA, using a rational protein engineering approach to introduce specific mutations into the active site of TMADH.

A literature search will reveal that there are a large number of studies that demonstrate the mutability of enzyme substrate specificity (e.g. Ballinger *et al.*, 1994; Onuffer & Kirsch, 1995; Olsen & Breddam, 1995). In these cases the technique used has been to align sequences of homologous enzymes of known specificity to identify amino acid residues that will allow alteration of specificity in a desired fashion (Shao & Arnold, 1996). Hence, initially such a project can be approached with some hope of success and, prior to the work presented in this chapter, TMADH *was* the subject of an attempt to rationally engineer a change in substrate specificity from TMA to dimethylamine, DMA (Basran *et al.*, 1997), based upon the homology that TMADH has with the enzyme DMADH (Yang, 1997; Yang *et al.*, 1995). Three mutations were introduced into the active site of TMADH, using protein homology modelling as a basis for the introduced mutations. The ability of TMADH to use TMA as substrate was greatly perturbed by these mutations, and led to increased selectivity of the enzyme for DMA, but was not accompanied by any improvement in the intrinsic ability of TMADH to use DMA as a substrate. Hence, the work in this chapter was intended to build upon this earlier work and bring about a meaningful change in substrate specificity so that TMADH could efficiently use DMA as a substrate.

The classical approach to introducing new or altered activities into enzymes, based on structural or sequence homologies, arose out of the development of site-directed mutagenesis in the mid-1980's. Site-directed mutagenesis revolutionised the study of proteins and has gained great importance in studies of gene expression and protein structure-function relationships (Creighton, 1993), bridging the gap between knowledge gained from structural determinations of enzymes and the kinetic information gained from ligand binding studies (Clarke *et al.*, 1989a; Ulmer, 1983). The use of site-directed mutagenesis for the incorporation of structural or chemical changes to specifically alter protein function for a desired end has been termed 'protein engineering' (Fersht & Winter, 1992), and while this rational approach to producing enzymes with new functions has had some notable successes (Bocanegra *et al.*, 1993; Clarke *et al.*, 1989a; Clarke *et al.*, 1989b; Scrutton *et al.*, 1990; Wells & Estell, 1988), it has generally been more successful in simply modifying existing properties or catalytic activities (Shao & Arnold, 1996).

The 'reductionist' approach to producing proteins with desired activities has had some spectacular successes, such as the protein engineering of subtilisin for the detergent industry (Wells & Estell, 1988), but has not been able to consistently deliver enzymes for use in industry (Arnold, 1996). Furthermore, this approach requires that mutants be identified by sequencing and the mutant enzymes purified and their kinetic and functional properties determined after each round of mutagenesis (Arnold, 1996; Chen, 1999). This can be tedious, expensive and impractical for many rounds of mutagenesis (Kuchner & Arnold, 1997; Stemmer, 1994a). Hence, a range of new approaches have been developed for obtaining proteins with novel functions, which can be broadly grouped under the heading of 'irrational design' or 'directed evolution' (Arnold, 1996; Arnold & Schmidt-Dannert, 1999).

Traditionally, directed evolution has been a term that refers to the selection, through the use of many rounds of selection and growth in chemostats, of bacterial species or strains that are able to metabolise a target substrate (Dykhuizen *et al.*, 1987; Hall & Hauer, 1993; Ogawa & Shimizu, 1999; Silman *et al.*, 1991). Now, directed evolution more often refers to the creation of large libraries of mutant enzymes and then screening for desired activities in recombinant bacteria or cell extracts (Arnold & Schmidt-Dannert, 1999; Chen, 1999). There are many choices available for creating mutant protein libraries, such as error-prone PCR (Henke & Bornscheuer, 1999), combinatorial mutagenesis (MacBeath *et al.*, 1998), DNA shuffling (Stemmer, 1994a; Stemmer, 1994b), StEP recombination (Zhao & Arnold, 1999) and *in vitro* recombination (Hartung & KistersWoike, 1998; Schneider *et al.*, 1998). For example, DNA shuffling, involving multiple rounds of *in vitro* recombination and mutation of a

pool of related sequences, followed by selection *in vivo*, has been successfully used to evolve an arsenate resistance operon and to select for an improved form of green fluorescent protein (Crameri *et al.*, 1997; Crameri *et al.*, 1996; Stemmer, 1994a; Stemmer, 1994b). Recently (Altamarino *et al.*, 2000), the alpha/beta barrel structural scaffold has been used as a template which, following *in vitro* mutagenesis and recombination, followed by *in vivo* selection, has resulted in a new phosphoribosylanthranilate isomerase.

It is therefore apparent that there are a number of approaches for developing enzymes with new activities that remove the need for extensive knowledge of structure and mechanism, information that is not available for many proteins (Chen, 1999; Shao & Arnold, 1996). In addition, catalysts can be produced from antibodies (Jacobsen & Schultz, 1995) or in the construction of hybrid proteins incorporating binding and/or catalytic modules from different sources, which can lead to new biosynthetic activities (McDaniel *et al.*, 1995; Sanz *et al.*, 1996). However, there is structural information for TMADH and, given that only a slight modification of the intrinsic DMA activity was required, rational engineering was adopted as the first approach to this problem.

5.1.2 Rationale for Engineering TMADH

There are good reasons for attempting to introduce new substrate specificities into TMADH. The enzyme has the ability to demethylate a number of secondary and tertiary amines, and is even capable of demethylating a substrate such as methamphetamine (Mewies, 1997). Small amines are found as components of many compounds of medical and biochemical interest (Yu *et al.*, 1995). For example, the physiological importance of catecholamines in neurotransmission, and the use of creatinine as a chemical marker of insufficient renal clearance is well established (Mountcastle, 1980; Orten & Neuhaus, 1975); the methylenedioxy derivatives of amphetamine and methamphetamine represent the largest group of designer drugs (Christophersen, 2000). The active site of TMADH, with its fairly promiscuous use of amines, could be seen as a template for the recognition of a number of biologically important amines (Figure 5.1).

The detection and quantitation for most clinically relevant compounds does not present any special problems for a clinical laboratory. For example, there are a number of methods for determining creatinine in blood and urine (Jia *et al.*, 1999;

Kock *et al.*, 1995; Mali & Nicholas, 1987). However, away from the laboratory, for example in the doctors surgery, there would be advantages to developing quick and simple methods for the detection of clinical markers of disease. Being able to detect creatinine in blood or urine samples 'on-site' could be beneficial both in terms of speed of diagnosis and as an initial screen. A single-step method, based around the use of an enzyme such as TMADH, for the detection of abnormal levels of clinically relevant amines such as creatine, creatinine or methamphetamine would be commercially attractive in this regard.

A combination of structural knowledge about TMADH and consideration of electron flow through the enzyme provides good reasons for its use in diagnostic technology. TMADH is robust, and can be purified in large quantities from a recombinant source. The property of the enzyme as an electron transferase is also exploitable; TMADH rapidly reduces artificial electron acceptors such as PMS and Fc^+, reactions that are followed spectrophotometrically and provide the most basic method for detection of any substrate that the enzyme is able to demethylate. However, in addition to observing a change in absorbance there are more commercially attractive proposals for the use of TMADH as a diagnostic enzyme. Whenever electrons are released in a reaction such as during the oxidation of TMA, there is the option of following this reaction as electrons are shuttled to electron surfaces. Electrons can be shuttled to a gold electrode, as has been done for cytochrome *c* (Bain & Evans, 1995) or, as has been accomplished for glucose oxidase (Medisense, UK), electrons generated by a reaction could be coupled by a ferrocene mediator to an electrochemical cell (Lias, 1994; Stenger *et al.*, 1996). Alternatively, if TMADH could be interfaced with existing horseradish peroxidase/chromogenic substrate technology, such as that routinely used in ELISAs (Wilson & Walker, 1994), then the oxidation of a target substrate could be linked to a simple colour change. This would require a 'switching on' of the oxidase activity in TMADH, either by mutagenesis or by siting a solvent accessible, oxygen-sensitive flavin at the surface of TMADH close to where electrons exit the protein, for example at Tyr-442 (N. Scrutton, personal communication). Electrons derived from substrate could then be scavenged by oxygen, and the concomitant generation of hydrogen peroxide would be linked to colorimetric changes.

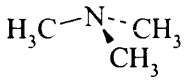

Trimethylamine (TMA)

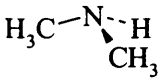

Dimethylamine (DMA)

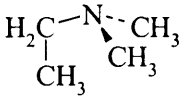

Ethyldimethylamine (EDMA)

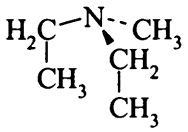

Diethylmethylamine (DEMA)

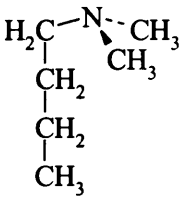

Dimethylbutylamine (DMButA)

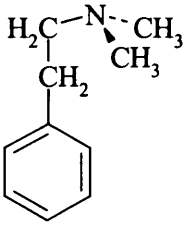

Dimethybenzylamine (DMBenA)

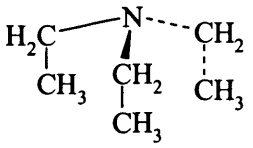

Triethylamine (TEA)

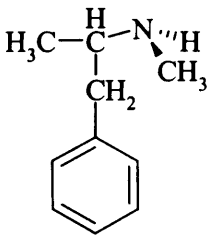

Methamphetamine

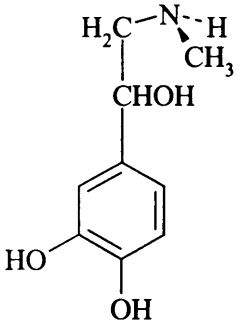

Epinephrine

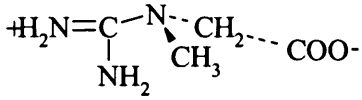

Creatine

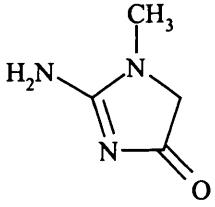

Creatinine

Figure 5.1. Actual and target amine substrates for TMADH. TMADH has been shown to have activity with the substrates DMA, EDMA, DEMA, DMButA, DMBenA and TEA. In addition, the enzyme has activity with methamphetamine, a common drug of abuse. The catalytic framework provided by TMADH might therefore be a basis for recognition of important amines such as epinephrine, creatine and creatinine.

5.1.3 Choosing a Target Substrate

The first part in this development of TMADH as a diagnostic enzyme is to bring about the desired change in substrate specificity. The chosen target molecule for engineering of TMADH was DMA, a substrate which TMADH is already able to use. However, TMADH is relatively insensitive to DMA (K_m for DMA of about 2.3 mM) so it would be advantageous to improve the inherent activity of TMADH with DMA.

There are two main reasons for choosing DMA as a target substrate. Firstly, DMA simply lacks one of the methyl groups possessed by TMADH's natural substrate. Improving DMA specificity appears to present a more straightforward challenge than switching specificity between more disparate substrates. Success would set a basis from which to attempt more ambitious protein engineering projects. Secondly, from a commercial aspect, TMA and DMA are economically relevant to the consumer and fisheries industries (de Koning & Mol, 1992; Malle & Poumeyrol, 1989). DMA is produced during the decomposition of frozen fish with its presence being used as an indicator of deterioration in fish quality during cold storage (MAFF, 1989a; MAFF, 1989b). Hence, specificity for DMA would be commercially attractive if, for example a DMA-sensitive strip was included with all frozen fish sold so that consumers would have a clear indication of the quality of the fish, either 'on the shelf' or after storage. As an important basis for choosing DMA as a target substrate the primary structural data was available for dimethylamine dehydrogenase (DMADH) from *Hyphomicrobium X*, an enzyme that already uses DMA as a substrate (Yang *et al.*, 1995).

Why attempt to engineer specificity for DMA into TMADH when DMADH already exists? This question is answered by consideration of the proposed role of the enzyme. For biotechnological exploitation, DMADH ideally needs to be purified in high quantities, preferably from a recombinant source. DMADH is only yielded in modest quantities from its native source and purification is complicated by its similarity to TMADH (also present in *Hyphomicrobium X*). DMADH from a recombinant source is favoured because its expression can be placed under the influence of a promoter, and proteins present in a recombinant species, such as *E. coli* are unlikely to mimic or mask the activity of the enzyme. Unfortunately, while the gene for DMADH has been successfully cloned (Yang *et al.*, 1995), the enzyme has always been produced in an insoluble state in the expression systems used (*E. coli* and *B. subtilis*) and attempts to solubilise DMADH from these sources have been unsuccessful (Yang, 1997). Conversely, TMADH is produced successfully in

recombinant form and has been studied in great detail. High-resolution structural data exists for TMADH (Lim *et al.*, 1986; Mathews *et al.*, 1999), and the knowledge that this has produced in tandem with mutagenic studies (Wilson *et al.*, 1996), has helped to target possible sites for interface with the electron transfer systems that would be required for its use in a commercially attractive detection system.

5.1.4 A Model Developed from Dimethylamine Dehydrogenase

Amino acid residues that were targetted for mutagenesis in TMADH resulted from the construction of a structural model for the enzyme. DMADH and TMADH are closely related, both being homodimers, with each subunit having covalently attached FMN and a 4Fe-4S centre, with subunit masses of 83 kD and 78 kD for TMADH and DMADH respectively. The FMN of DMADH is attached via a 6-S-cysteinyl linkage and so far it is the only other enzyme besides TMADH found to possess this type of link to the protein-bound flavin.

In addition to the physical similarities between TMADH and DMADH, cloning and sequencing of the *dmd* gene from *Hyphomicrobium X* has revealed a great deal of similarity between the enzymes at the molecular level (Figure 5.2). The amino acid sequence of DMADH is 63 % identical to TMADH, and a number of these similarities are worthy of note; Cys-30 in TMADH is conserved as Cys-30 in DMADH; and the cysteines (345, 349, 351 and 364) and surrounding residues which comprise the 4Fe-4S cluster in TMADH are highly conserved in DMADH (cysteines 350, 353, 356 and 369). Other residues of interest, for example His-172 and Tyr-169 of TMADH (see Chapter 4), has equivalents in DMADH, His-178 and Tyr 175 respectively. However, for the purpose of engineering substrate specificity, the focus of attention naturally falls on the active sites of both enzymes.

```
TMADH   0 MARDPKHDILFEPIQIGPKTLRNRFYQVPHCIGAGSDKPGFQSAHRSVKA  49
DMADH   0 MARDPRFDILFTPLKLGSKTIRNRFYQVPHCNGAGTNSPGMNMAHRGIKA  49

          50 EGGWAALNTEYCSINPESDDTHRLSARIWDEGDVRNLKAMTDEVHKYGAL  99
          50 EGGWGAVNTEQCSIHPECDDTLRITARIWDQGDMRNLRAMVDHVHSHGSL  99

         100 AGVELWYGGAHAPNMESRATPRGPSQYASEFET......LSYCKEMDLSD 143
         100 AGCELFYGGPHAPAIESRTISRGPSQYNSEFATVPGCPGFTYNHEADIDE 149

         144 IAQVQQFYVDAAKRSRDAGFDIVYVYGAHSYLPLQFLNPYYNKRTDKYGG 193
         150 LERLQQQYVDAALRARDTGFDLVNVYGAHAYGPMQWLNPYYNRRTDKYGG 199

         194 SLENRARFWLETLEKVKHAVGSDCAIATRFGVDTVYGPGQIEAEVDGQKF 243
         200 SFDNRARFWIETLEKIRRAVNDDVALVTRCATDTLYGTKGVELTEDGLRF 249

         244 VEMADSLVDMWDITIGDIAEWGEDAGPSRFYQQGHTIPWVKLVKQVSKKP 293
         250 IELASPYLDLWDVNIGDIAEWGEDAGPSRFYPIAHENDWIRHIKQATNKP 299

         294 VLGVGRYTDPEKMIEIVTKGYADIIGCARPSIADPFLPQKVEQGRYDDIR 343
         300 VVGVGRYYDPEKMLQVIKAGIIDIIGAARPSIADPWLPRKIDEGRVDDIR 349

         344 VCIGCNVCISRWEIGGPPMICTQNATAGEEYRRGWHPEKFRQTKNKDSVL 393
         350 TCIGCNVCISRWEMGGVPFICTQNATAGEEYRRGWHPEKFEPKKSDHDVL 399

         394 IVGAGPSGSEAARVLMESGYTVHLTDTAEKIGGHLNQVAALPGLGEWSYH 443
         400 IVGAGPAGSECARVLMERGYTVHLVDTREKTGGYVNDVATLPGLGEWSFH 449

         444 RDYRETQITKLLKKNKESQLALGQKPMTADDVLQYGADKVIIATGARWNT 493
         450 RDYRQTQLEKLLKKNPECQIALKQKPMTADDILQYGASRVVIATGAKWST 499

         494 DGTNCLTHDPIPGADASLPDQLTPEQVMDGKKKIGKRVVILNADTYFMAP 543
         500 TGVNHRTHEPIPGADASLPHVLTPEQVYEGKKAVGKRVMIINYDAYYTAP 549

         544 SLAEKLATAGHEVTIVSGVHLANYMHFTLEYPNMMRRLHELHVEELGDHF 593
         550 SLAEKFARAGHDVTVATVCGLGAYMEYTLEGANMQRLIHELGIKVLGETG 599

         594 CSRIEPGRMEIYNIWGDGSKRTYRGPGVSPRDANTSHRWIEFDSLVLVTG 643
         600 CSRVEQGRVELFNIWGEGYKRSYKGAGQLPRNENTSHEWHECDTVILVTS 649

         644 RHSECTLWNELKARESEWAENDIKGIYLIGDAEAPRLIADATFTGHRVAR 693
         650 RRSEDTLYRELKARKGEWEANGITNVFVIGDAESPRIIADATFDGHRLAR 699

         694 EIEEANPQIAIPYKRETIAWGTPHMPGGNFKIEYKV 729
         700 EIEDADPQHQKPYKREQRAWGTAYNPDENPDLVWRV 735
```

Figure 5.2. Alignment of the amino acid sequence of *M. methylotrophus* TMADH (upper sequence) with the sequence of *Hyphomicrobium X* DMADH (lower sequence). Alignments were performed using GAP of the GCG package (Genetics Computer Group). The gap weight is 3.0 and the length weight is 0.1. The identity is 63.5% and the similarity is 79.3%. (Yang *et al.*, 1995)

5.1.5 Modelling the Active Site of DMADH

The protein structure of DMADH was obtained by homology modelling the primary structural data for the enzyme to the known crystal co-ordinates for TMADH. This work was initially carried out in collaboration with Dr A.R.C. Raine of the Department of Biochemistry, University of Cambridge (Raine *et al.*, 1995). The DMADH model was built using the informatic point mutation tool in the software package QUANTA (Molecular Simulations Inc.). Using this tool, QUANTA preserves the positions of all atoms that are common to the side chains of both enzymes, and new atoms are placed in an extended conformation. Energy minimisation of the model was performed using X-PLOR (Brünger, 1992). A more recent model, containing all the characteristics of the earlier model of Raine. (Raine *et al.*, 1995) has also been constructed, using the internet-based server SWISS-MODEL (Guex *et al.*, 1999).

The DMADH model appeared to reveal why this enzyme has specificity for DMA. Within the active site, identity between DMADH and TMADH is almost perfect (Basran *et al.*, 1997). Sequence conservation is lowest in those residues that comprise the subunit interface of the enzyme dimer (43% identical), possibly reflecting the need for both TMADH and DMADH to recognise 'self' in the cell. The model suggested that a single amino acid change is responsible for the difference in substrate specificity between the two enzymes (Figure 5.3). In TMADH, TMA is held in the active site by cation-π bonding in the 'aromatic bowl' consisting of Trp-264, Trp-355, and Tyr-60. In the model of DMADH it was found that the two tryptophan residues were conserved, but the residue corresponding to Tyr-60 is a glutamine. This appeared to suggest a solution to the question of how these two enzymes distinguish between their very similar substrates. TMA has C-3 rotational symmetry, so in TMADH there is no requirement for specifically orienting the substrate in the active site. However, DMA lacks this symmetry and must be bound in a specific orientation so that a methyl group is correctly presented for oxidation. Modelling DMA into the active site of the DMADH model shows that Gln-60 is ideally positioned to make a hydrogen bond from the side chain amide carbonyl to the N-H hydrogen of DMA, while the remaining methyl groups of DMA make cation-π interactions with two tryptophan residues as in TMADH (Basran *et al.*, 1997).

Just beyond the first solvation shell for substrate, there are two further changes in residue identity between TMADH and DMADH which appeared to be important (Basran *et al.*, 1997). These residues (74 and 105 of TMADH) pack against

position 60 in both enzymes and could be important in placing this residue in the correct context for interaction with DMA. In TMADH, residues 74 and 105 are a serine and tryptophan respectively, while in the DMADH model they are exchanged for Thr-74 and Phe-105.

The production of a model for DMADH therefore initially identified three residues closest to the active site (60, 74 and 105) whose difference from their counterparts in TMADH appears critical for recognition of DMA. These residues were therefore chosen as targets for the first attempt to engineer substrate specificity for DMA into TMADH (Basran *et al.*, 1997).

5.1.6 Engineering Substrate Specificity for DMA into TMADH: The Work of Basran *et al.*(1997)

Basran *et al.* (1997) cumulatively introduced three mutations into the active site of TMADH (Basran *et al.*, 1997). These mutations were an attempt to rectify the differences which modelling had identified between the active sites of TMADH and DMADH. Hence, three TMADH mutants were produced, the Y60Q, Y60Q.S74T and Y60Q.S74T.W105F mutants, referred to as the Single-, Double- and Triple-mutants respectively.

Recombinant wild-type TMADH turns over TMA with a k_{cat} of 15.6 s^{-1}, with a K_m of 13.7 μM. As analysed by steady-state kinetic methods, mutation of Tyr-60 to a glutamine leads to a large increase in the K_m for TMA (to 545 μM), and this is further raised in the double and triple mutants (737 μM and 8.74 mM respectively). There is about a 100-fold fall in k_{cat} for the TMADH Single- and Double-mutants and a 800-fold fall for the Triple-mutant. The data therefore confirmed that Tyr-60 is an important determinant for the binding of TMA in the active site, and the introduction of the other changes had further disrupted the ability of the enzyme to interact with TMA. On the other hand, the intrinsic ability of TMADH to turn over DMA (k_{cat} of 0.67 s^{-1} and a K_m of 2.34 mM) was maintained in all three mutant enzymes and only very modest changes were observed in the steady-state kinetic parameters upon mutation (k_{cat} of 0.42 s^{-1} and a K_m of 7.25 mM in the Triple-mutant). These results are summarised in Table 5.1, Section 5.2.4.

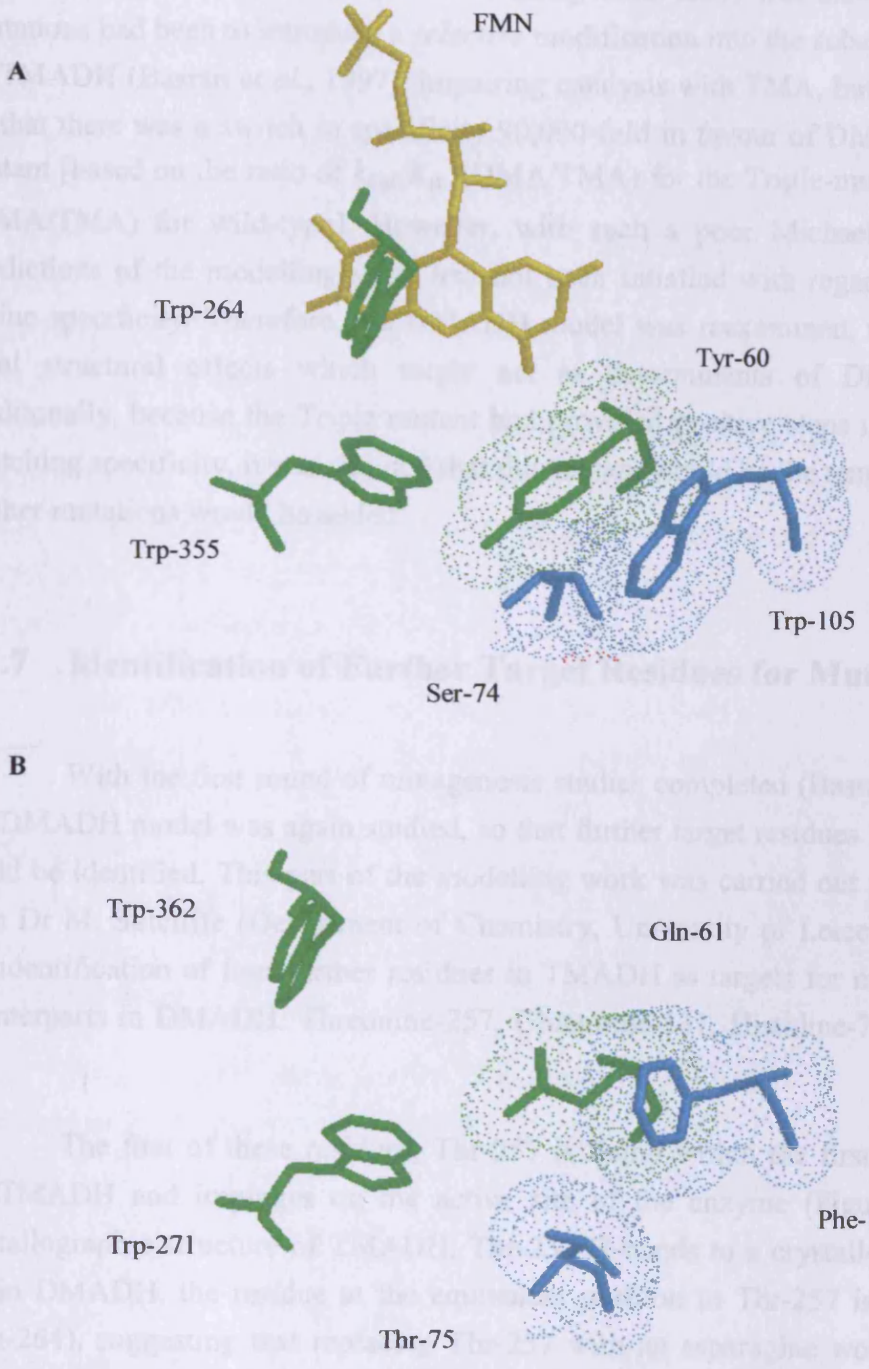

Figure 5.3. Molecular graphics representation of the active site of (A, top) TMADH and the model (B, bottom) DMADH. Details of the model construction are given in the text. A van der Waals surface is displayed around the three active site residues of DMADH and TMADH that are thought to account for the difference in substrate specificity).

The conclusion from the initial mutagenesis study was that the effect of the mutations had been to introduce a *selective* modification into the substrate binding site of TMADH (Basran *et al.*, 1997), impairing catalysis with TMA, but not with DMA, so that there was a switch in specificity 90,000-fold in favour of DMA in the Triple-mutant [based on the ratio of k_{cat}/K_m (DMA/TMA) for the Triple-mutant and k_{cat}/K_m (DMA/TMA) for wild-type]. However, with such a poor Michaelis constant, the predictions of the modelling work had not been satisfied with regards to secondary amine specificity. Therefore, the DMADH model was reexamined, to identify other local structural effects which might act as determinants of DMA specificity. Additonally, because the Triple mutant had provided positive steps in the process of switching specificity, it was decided that this mutant would be the template into which further mutations would be added.

5.1.7 Identification of Further Target Residues for Mutagenesis

With the first round of mutagenesis studies completed (Basran *et al.*, 1997), the DMADH model was again studied, so that further target residues for mutagenesis could be identified. This part of the modelling work was carried out in collaboration with Dr M. Sutcliffe (Department of Chemistry, University of Leicester) and led to the identification of four further residues in TMADH as targets for mutation to their counterparts in DMADH: Threonine-257, Glutamine-131, Histidine-71 and Leucine-73.

The first of these residues, Thr-257 is found within the first substrate shell for TMADH and impinges on the active site of the enzyme (Figure 5.5). In the crystallographic structure of TMADH, Thr-257 H-bonds to a crystallographic water, but in DMADH, the residue at the equivalent position to Thr-257 is an asparagine (Asn-264), suggesting that replacing Thr-257 with an asparagine would lead to the loss of this H-bond to water and replace it with an H-bond between the amide nitrogen of Asn-257 and the $O_{3'}$ atom of the FMN, a H-bonding pattern suggested by the DMADH model. It was conjectured that this could cause a rearrangement of the FMN in TMADH to its conformation in DMADH, leading to increased selectivity with DMA as substrate. Therefore, the mutation T257N was targeted for introduction into the Triple-mutant, to produce the Quad-mutant (Y60Q.S74T.W105F.T257N).

Modelling also identified Glu-131 as a possible target for mutagenesis in TMADH. Glu-131 is part of a H-bonding network linking residues Arg-72, Asp-69

and Tyr-60 (Figure 5.4). In the native structure of TMADH it appears that this H-bonding network keeps Tyr-60 in the correct orientation for interaction with TMA. There are two pieces of evidence which point to the lack of this H-bonding network in DMADH: firstly, in DMADH, the counterpart residue to Glu-131 is an alanine, so there would be no hydrogen-bond between this alanine and Arg-72. Glu-131 of TMADH is also positioned where there is a 6-residue insertion in DMADH (sequence VPGCPG, residues 133-138 Figure 5.2), so it is unlikely that an equivalent H-bonding network maintains Arg-72 in the same position in DMADH as it is in TMADH. Additionally, the DMADH model indicated a different H-bonding network in this enzyme, in which Arg-72 in DMADH is not fixed by a H-bond to Glu-131: it has the ability to rotate so that it can H-bond to Gln-60. It is this H-bond from Arg-72 that is postulated to fix Gln-60 in the correct orientation to interact correctly with DMA. Hence, the replacement of Glu-131 with an alanine, in order to produce the Penta-mutant (Y60Q.S74T.W105F.E131A.T257N), was set as another target for switching the specificity of TMADH for DMA.

The introduction of the mutation E131A into TMADH also presented possibilities for the introduction of additional mutations. The DMADH model shows that Arg-72, implicated in the above hydrogen bonding network, is part of a loop region made up of residues 63 to 74 (Figure 5.4). Within this loop, residues His-71 and Leu-73 were identified as targets for mutagenesis to their equivalents in DMADH (a leucine and isoleucine respectively); it was reasoned that the introduction of these mutations might provide the loop with a more 'DMADH-like' conformation.

To summarise, modelling of the structure of DMADH identified four new mutations to add to the three introduced by Basran *et al.* (1997), which were hoped to complete the switch in specificity from TMA to DMA. In total, the aim of the work was to produce the following four mutants:
Quad-mutant (Y60Q.S74T.W105F.T257N),
Penta-mutant (Y60Q.S74T.W105F.E131A.T257N),
Hexa-mutant (Y60Q.H71L.L73I.S74T.W105F.T257N) and the Hepta-mutant (Y60Q.H71L.L73I.S74T.W105F.E131A.T257N), incorporating all of the extra mutations. For reasons which will become clear in the Results section, the series of introduced mutations did not extend as far as the production of the Hepta-mutant.

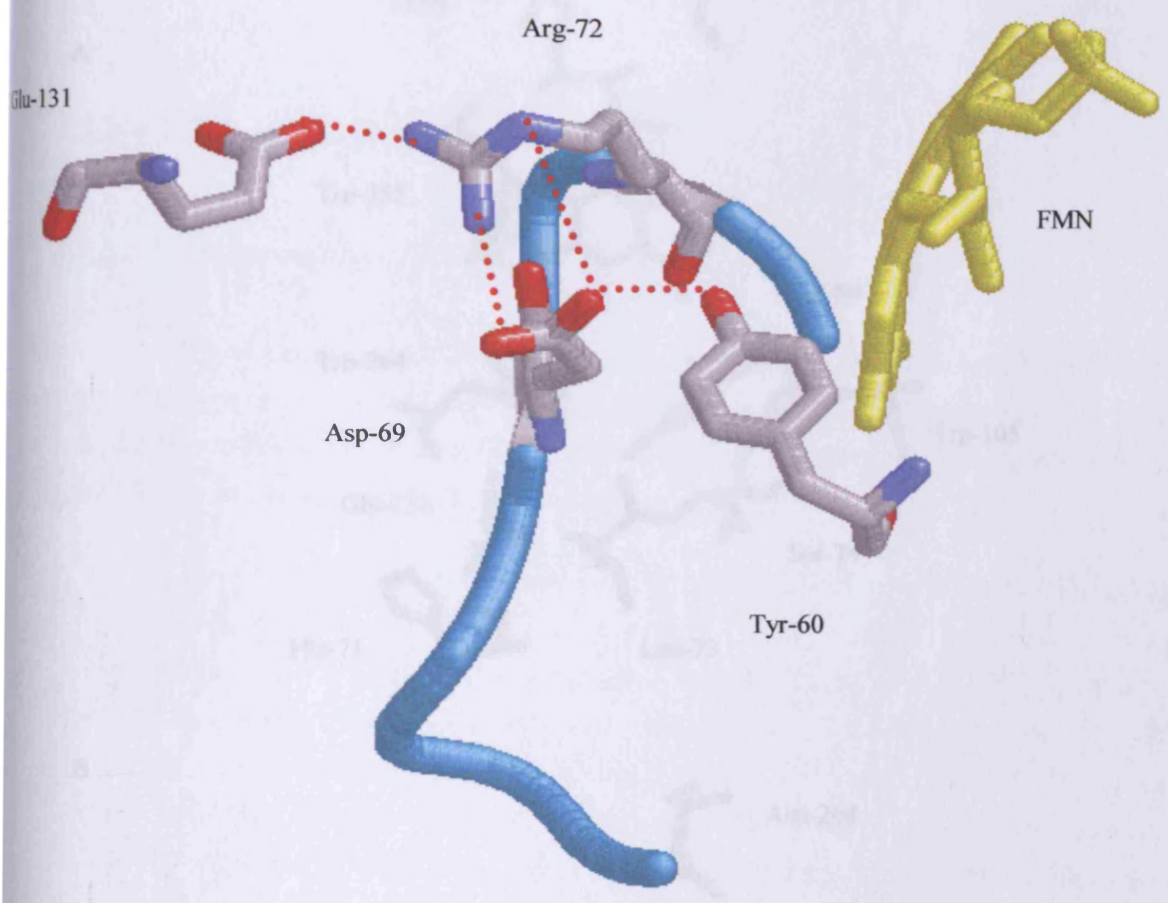

Figure 5.4: H-bonding network holding Tyr-60 in place for interaction with substrate in TMADH. The model of DMADH suggests that there is no equivalent H-bonding network in DMADH. Disrupting the TMADH network by mutating the residues Glu-131 and Arg-72 to their equivalents in DMADH is proposed to free Arg-72 to make an interaction with Gln-60 (in mutated TMADH), thus holding it in place for correct interaction with the target substrate DMA. The loop region consisting of residues 63-74, of which residues His-71 and Leu-73 were also mutagenic targets, is shown in cyan.

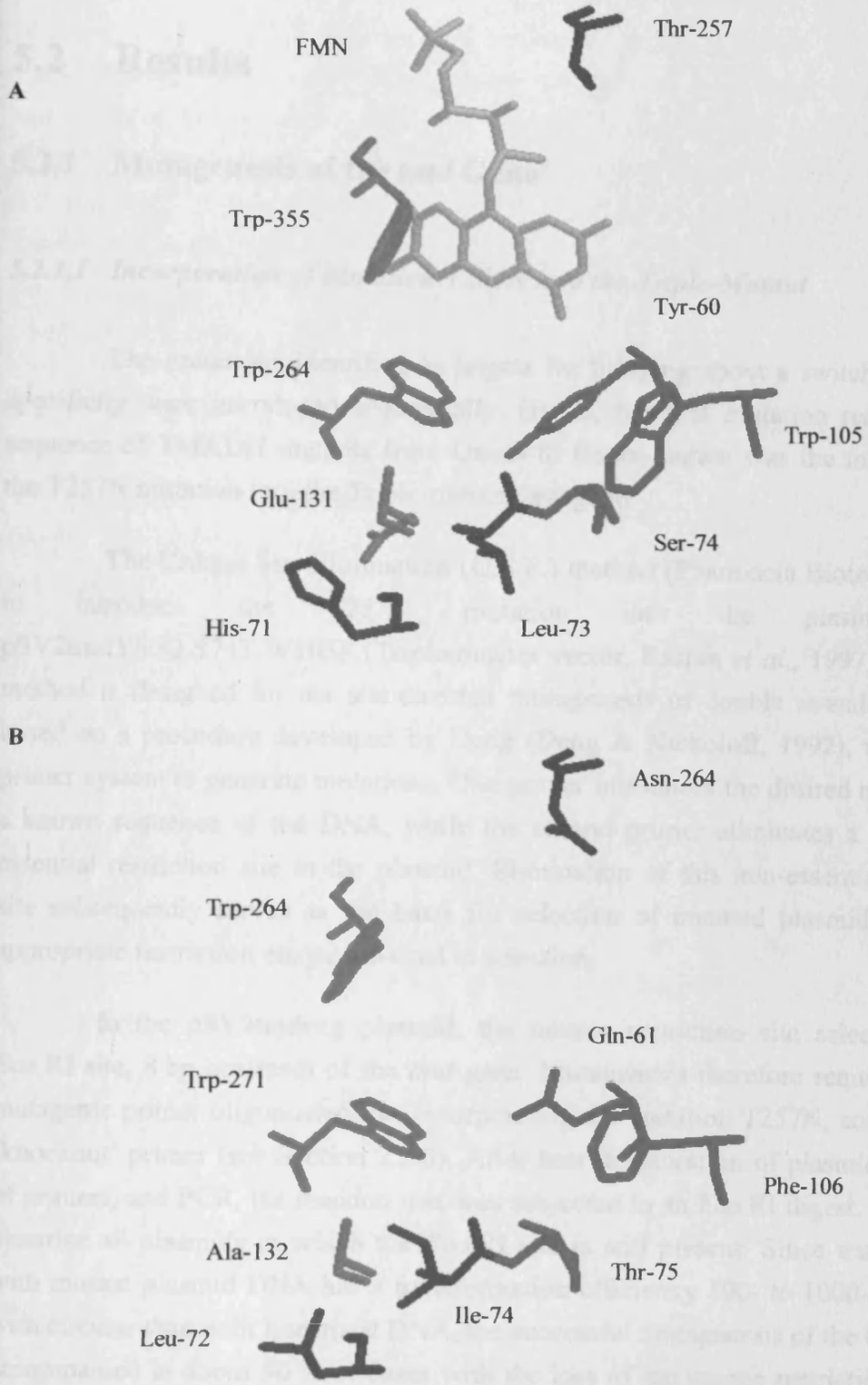

Figure 5.5: Overview of residues in TMADH (A, top) targeted for mutation to their equivalent residues in DMADH (B, bottom) for redesign of substrate specificity. Corresponding residues between TMADH and the DMADH model are identified with the same colour.

5.2 Results

5.2.1 Mutagenesis of the *tmd* Gene

5.2.1.1 Incorporation of Mutation T257N into the Triple-Mutant

The mutations identified as targets for bringing about a switch in substrate specificity were introduced sequentially. Hence, the first mutation required in the sequence of TMADH mutants from Quad- to Hepta-mutant was the introduction of the T257N mutation into the Triple-mutant *tmd* gene.

The Unique Site Elimination (U.S.E.) method (Pharmacia Biotech) was used to introduce the T257N mutation into the plasmid vector pSV2tmdY60Q.S74T.W105F (Triple-mutant vector, Basran *et al.*, 1997). The U.S.E method is designed for the site-directed mutagenesis of double stranded plasmids, based on a procedure developed by Deng (Deng & Nickoloff, 1992), using a two-primer system to generate mutations. One primer introduces the desired mutation into a known sequence of the DNA, while the second primer eliminates a unique non-essential restriction site in the plasmid. Elimination of this non-essential restriction site subsequently serves as the basis for selection of mutated plasmids, when the appropriate restriction enzyme is used in selection.

In the pSV2tmdveg plasmid, the unique restriction site selected was an *Eco* RI site, 8 bp upstream of the *tmd* gene. Mutagenesis therefore required a target mutagenic primer oligonucleotide, incorporating the mutation T257N, and an *Eco* RI 'knockout' primer (see Section 2.2.6). After heat denaturation of plasmid, annealing of primers, and PCR, the reaction mix was subjected to an *Eco* RI digest. This should linearise all plasmids in which the *Eco* RI site is still present. Since transformation with mutant plasmid DNA has a transformation efficiency 100- to 1000-fold greater with circular than with linearised DNA, the successful mutagenesis of the target site is accompanied in about 90 % of cases with the loss of the unique restriction site. The digested mix of mutated and non-mutated DNA was then used to transform a repair-defective (*mutS*) strain of *E. coli*.

Plasmid DNA isolated from transformed *mutS* cells was subjected to a second round of *Eco* RI selection to increase the proportion of mutant plasmids. After this second round of selection, *E. coli* TG1 cells were transformed with the digested plasmid preparation. Following the second round of restriction digest selection

required by the U.S.E mutagenesis protocol, single colonies of *E. coli* TG1 transformants were selected. The plasmid DNA from these cells was subjected to restriction digests, a single digest (either *Eco* RI or *Hin* dIII) and a double digest (*Eco* RI/*Hin* dIII). Putative mutant plasmids produce DNA fragments of a specific size (see Table 2.3) and can be selected by their characteristic banding pattern on an agarose gel, indicating that they have lost their *Eco* RI site. DNA within the target site for mutagenesis was sequenced to confirm that the T257N mutation had been correctly incorporated (Figure 5.6).

5.2.1.2 Subcloning of the Kpn I Fragment from the pSV2tmdQuad Plasmid

To use the pSV2tmdQuad plasmid in further rounds of mutagenesis, the *Eco* RI site removed by mutagenesis during the U.S.E. procedure had to be reintroduced into the plasmid. Rather than undergoing mutagenesis to regenerate the *Eco* RI site, it was an established procedure in the laboratory to subclone part of the *tmd* gene (140 bp) containing the mutations back into a version of the pSV2tmdveg plasmid in which the *Eco* RI site was still present. Hence, a *Kpn* I fragment (size 1.4 kb) was excised from the Quad-mutant *tmd* gene and used to replace the equivalent fragment in the plasmid pSV2tmdY60A. The TMADH Y60A vector contains an additional *Hin* dIII site in the *tmd* gene, as a result of the Y60A mutation at position 180 (Figure 5.7), so that when pSV2tmdY60A is digested with *Hin* dIII, a characteristic banding pattern is seen (Figure 5.8). Restriction digests (Table 2.3) can then be used to check for the correct incorporation into the pSV2tmd vector of the *Kpn* I *tmd* gene fragment.

A 1.4 kb *Kpn* I fragment, containing the mutated portion of the *tmd* gene was excised from the plasmid pSV2tmdQuad and isolated on a low melting point agarose gel. This 1.4 kb *Kpn* I fragment was ligated into *Kpn* I digested pSV2tmdY60A which had previously been digested with *Kpn* I (Figure 5.8). Following ligation, the plasmid DNA was subjected to both a *Hin* dIII and a *Bam* HI/*Hin* dIII digest, and the DNA fragments were separated and visualised on an agarose gel (Figure 5.8). The restriction digests will produce DNA fragments of a characteristic size, depending on whether the 1.4 kb *Kpn* I fragement containing the mutation has successfully replaced the equivalent fragment in the pSV2tmdY60A vector (Table 2.3).

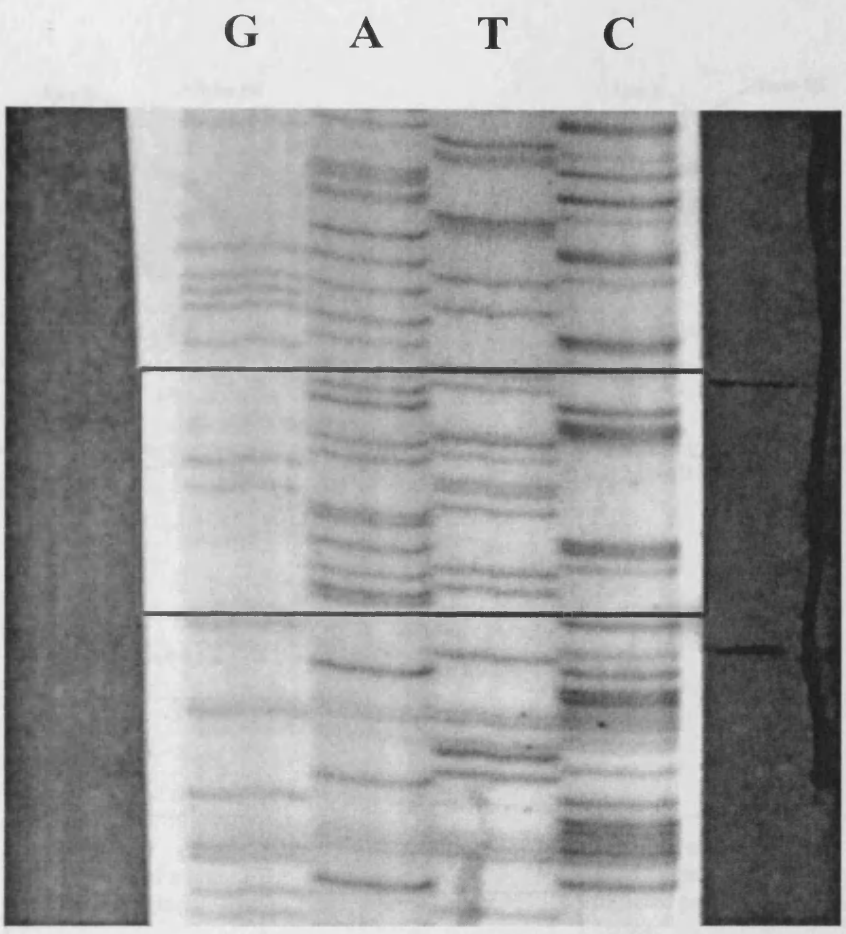

Figure 5.6: DNA sequencing gel showing incorporation of T257N mutation into the *tmd* gene. Reading upwards, boxed sequence reads (introduced mutation in bold): AATATCACCAAT**GTT**GATATCCCACAT.

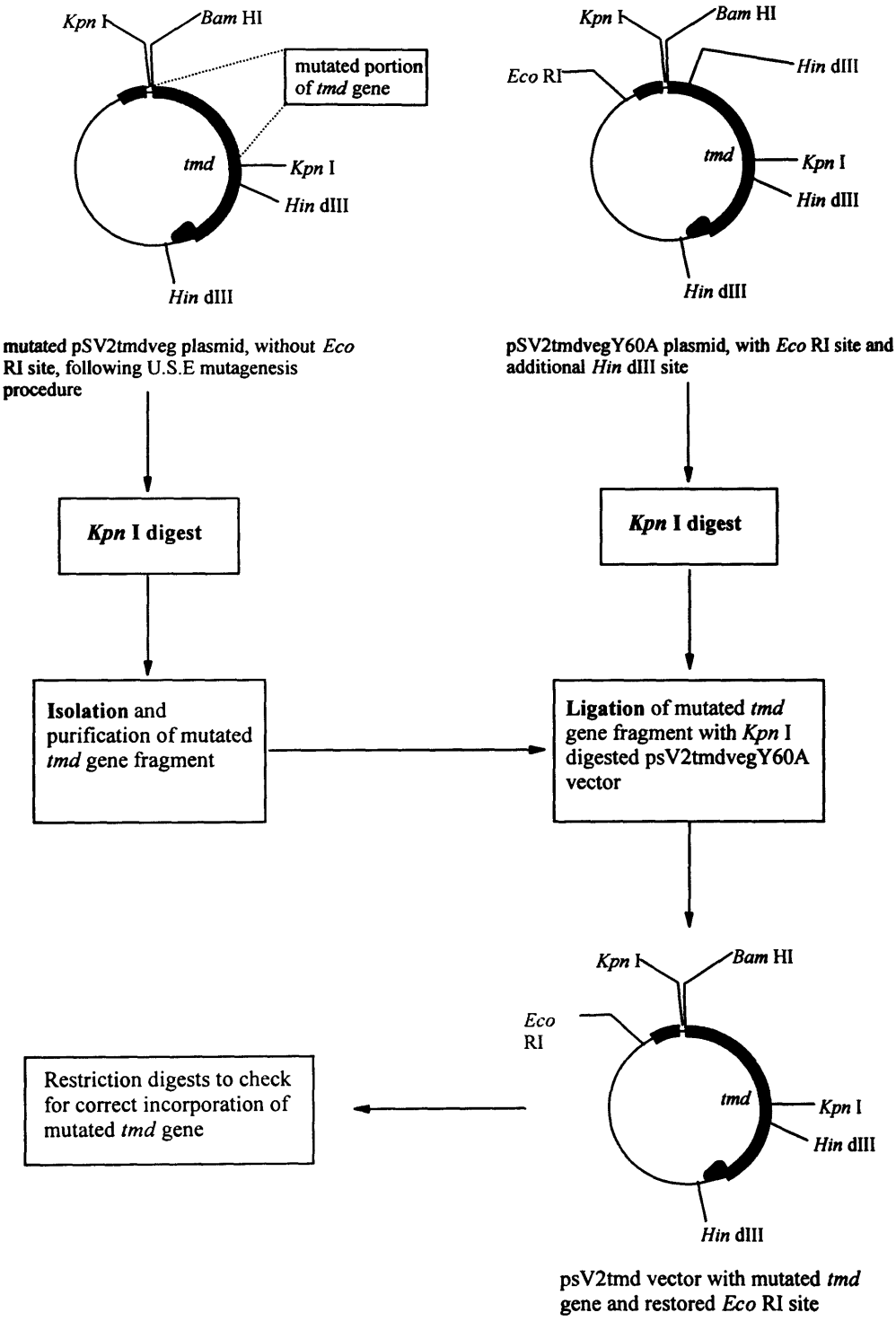

Figure 5.7: Subcloning protocol following U.S.E. mutagenesis procedure. This subcloning method was used to restore the *Eco* RI site upstream of *tmd* gene for use of plasmid in further rounds of U.S.E. mutagenesis.

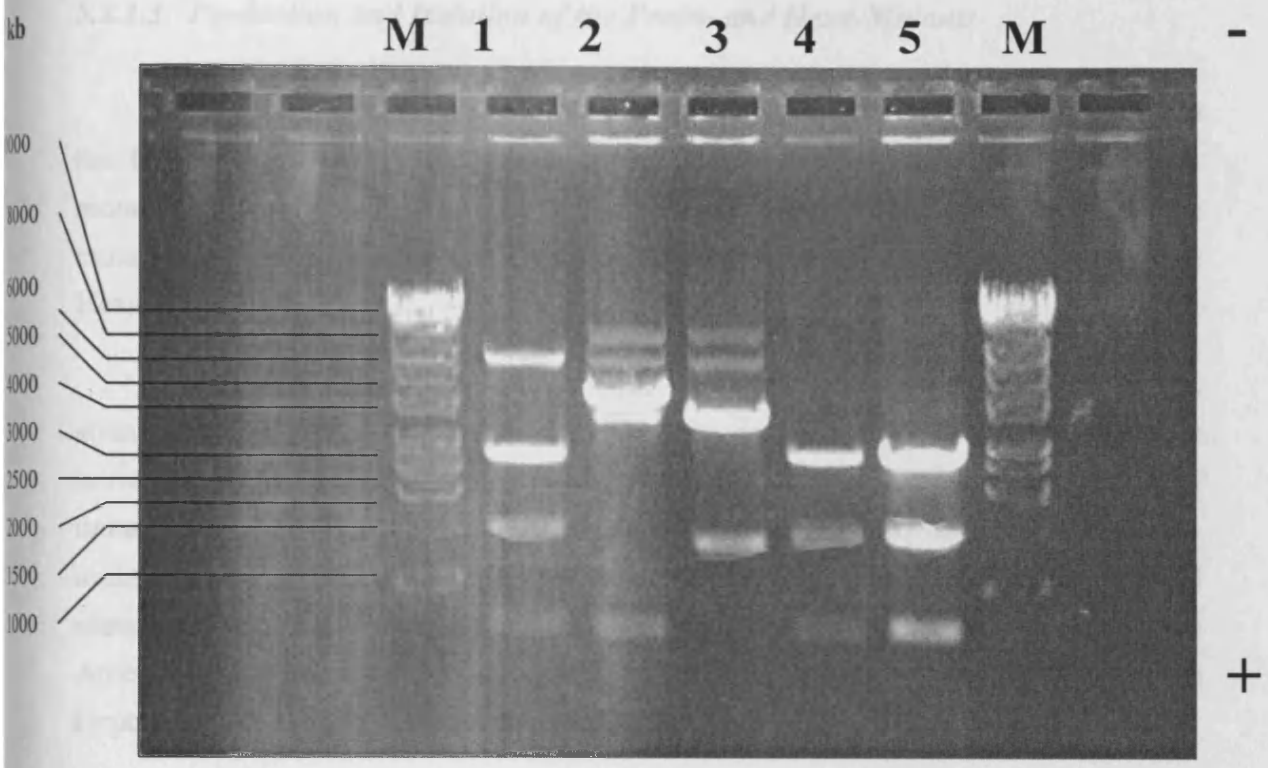

Figure 5.8: Agarose gel of diagnostic digests following subcloning of mutated fraction of *tmd* gene into Y60A plasmid. The approximate sizes of DNA fragments in the marker DNA (M) are indicated on the left hand side.

1: *Bam* HI/*Hin* dIII digest of pSV2tmd plasmid following successful subcloning of 1.4 kb *Kpn* I *tmd* gene fragment, replacing the equivalent *Kpn* I fragment in the pSV2tmdY60A vector. The plasmid is thus cut at three sites, producing DNA fragments of sizes 2.78, 1.47, and 0.72 kb, the same as 'wild-type' pSV2tmdveg plasmid. The fragment with a size of about 5 kb is due to incomplete digest of the psV2tmd plasmid.

2: *Hin* dIII digest of mutated pSV2tmd plasmid following successful subcloning of 1.4 kb *Kpn* I *tmd* gene fragment into the pSV2tmdY60A vector. Plasmid is cut at two sites, producing DNA fragments of sizes 4.25 and 0.72 kb.

3: *Kpn* I cut of mutated plasmid following successful mutation. This *Kpn* I fragment is isolated and ligated into *Kpn* I digested Y60A plasmid. The *Kpn* I digest of the pSV2tmdveg plasmid vector releases a *tmd* gene fragment of 1.4 kb.

4: *Bam* HI/*Hin* dIII digest of Y60A plasmid. In this digest, the presence of an extra *Hin* dIII site in the psV2tmdY60A plasmid produces four DNA bands of sizes 2.61, 1.57, 0.72 and 0.07 kb.

5: *Hind* III digest of Y60A. In this digest, the presence of an extra *Hin* dIII site in the psV2tmdY60A plasmid produces four DNA bands of sizes 2.68, 1.57 and 0.72 kb.

5.2.1.3 Production and Isolation of the Penta- and Hexa-Mutants

Using the Quad-mutant template, the mutation E131A was introduced into the Quad-mutant *tmd* gene, producing the Penta-mutant (Figure 5.9). The Quad-mutant template was also used in a separate mutagenesis reaction to introduce the mutations H71L.L73I into the Quad-mutant *tmd* gene (Figure 5.9), producing the Hexa-mutant.

Although the Quad-, Penta- and Hexa-mutants were successfully made, attempts to produce the Hepta-mutant were unsuccessful. Several attempts to introduce the H71L.L73I and E131A mutations simultaneously in one round of mutagenesis were unsuccessful. Attempts were then made to introduce the E131A mutation into the Hexa-mutant template or alternatively, to introduce the H71L.L73I mutations into the Penta-mutant template using the Quikchange protocol from Amersham, but were again unsuccessful. As will become clear, the generation of the Hepta-mutant was not subsequently required.

5.2.2 Purification of the Quad-, Penta- and Hexa-Mutants

Following successful mutagenesis, the entire *tmd* gene was sequenced in each case to ensure that no spurious mutations had been introduced into the gene during the mutagenesis procedure. Each mutant was purified to homogeneity as described in Materials and Methods (Section 2.4.1). However, to obtain sufficient enzyme for kinetic analyses, the growth of 50 litres of cell culture at 20 °C was required, yielding only about 1 mg of enzyme in each case. Purification of recombinant TMADH usually entails a 10 litre growth culture, giving a TMADH yield of about 25 mg/litre of enzyme (Mewies, 1997). The large decrease in expression of soluble TMADH had been a feature of the series of engineered mutants ever since the Triple-mutant had been generated (Basran *et al.*, 1997), and was attributed, perhaps naively, to the manifestation of 'DMADH-like' properties in the mutants. Growth at 20 °C was used to suppress the formation of inclusion bodies in the *E. coli* cells expressing the mutant forms of TMADH (Basran *et al.*, 1997).

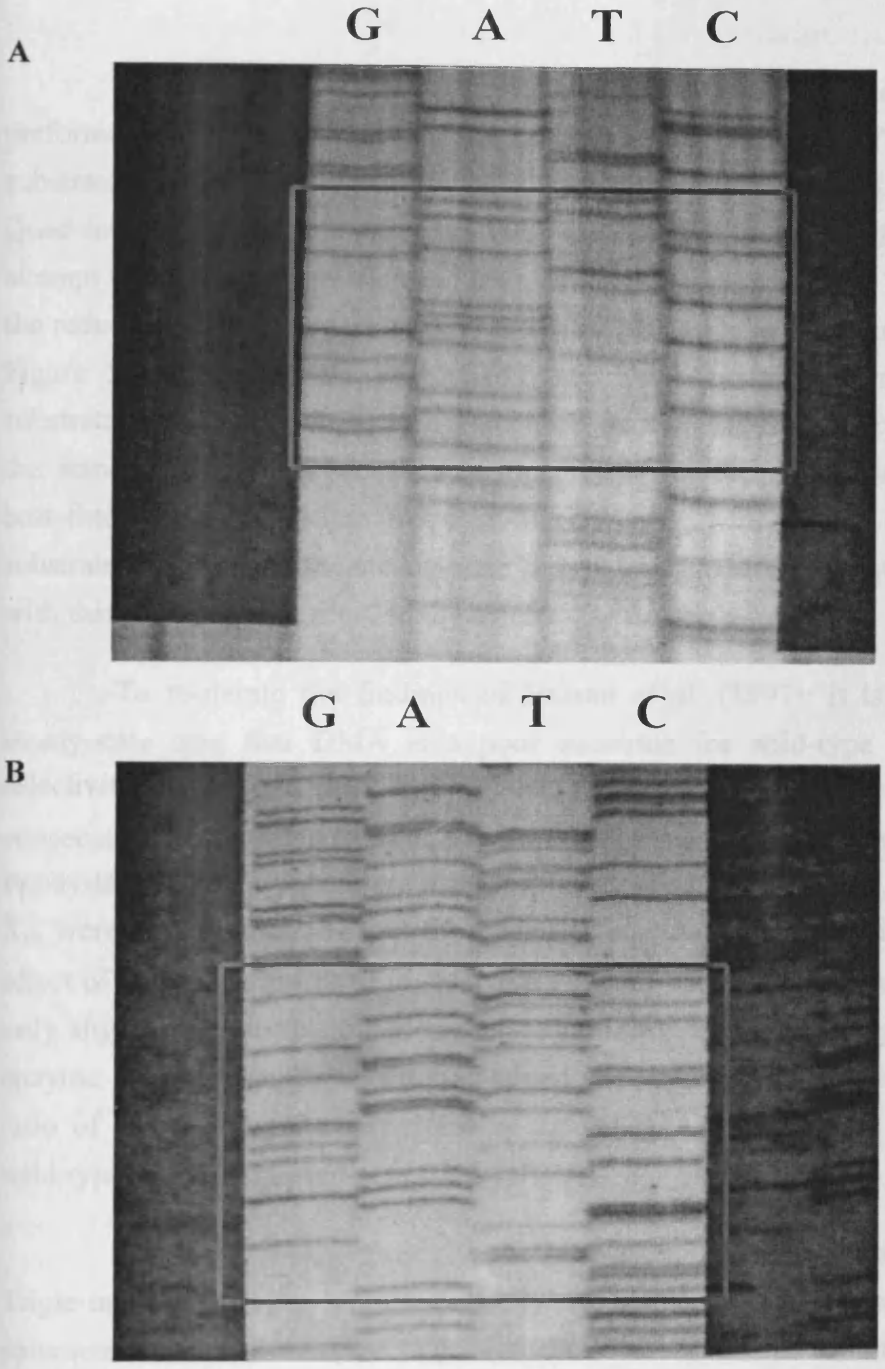

Figure 5.9. DNA sequencing gels showing incorporation of the mutations E131A, and H71L.L73I into the *tmd* gene. A) incorporation of the E131A mutation into the *tmd* gene. Reading upwards, boxed sequence reads (introduced mutation in bold): GTAGGACAGCGT**AGC**AAACTCTGACGCATA. B) Incorporation of the H71L and L73I mutations into the *tmd* gene. Reading upwards, boxed sequence reads: CACCTTCGTCCAGATACGTGC**GGTAAT**ACGCAATGTATCA TCTGACTC. This portion of the *tmd* gene already contains the mutation S74T, introduced in an earlier round of mutagenesis (Basran *et al.*, 1997).

5.2.3 Steady-State Kinetic Analysis of the Quad-mutant

The results of a steady-state kinetic analysis for Quad-mutant TMADH, performed at the optimum pH for activity (pH 8.5), using TMA and DMA as substrates and PMS as electron acceptor are displayed in Table 5.1. The data for the Quad-mutant are alongside the data from the study of Basran *et al.* (1997), the earlier attempt to switch the specificity of TMADH from TMA to DMA. The kinetic data for the reduction of the Quad-mutant with both TMA and DMA as substrate is plotted in Figure 5.10. Neither the Y60Q.S74T nor Triple-mutant enzymes had displayed substrate inhibition with TMA as substrate, so data for these enzymes were fitted to the standard Michaelis-Menten equation. Data for the Quad-mutant were likewise best-fitted to this equation. None of the enzymes, wild-type or mutant, had shown substrate inhibition in the steady-state assays using DMA as substrate, so all data for with this substrate was fitted to the Michaelis-Menten equation.

To re-iterate the findings of Basran *et al.* (1997): it is apparent from the steady-state data that DMA is a poor substrate for wild-type TMADH [ratio of selectivity coefficients (i.e., k_{cat}/K_m) for TMA and DMA is about 4000]. With the consecutive introduction of mutations, only very modest changes were observed in the steady-state kinetic parameters using DMA as substrate. No large increases in k_{cat} or K_m were observed throughout the series of enzymes. In the steady-state, the major effect of mutations has been to *selectively* impair catalysis observed with TMA while only slightly compromising the level of DMA-dependent activity seen in wild-type enzyme. The magnitude of switch in specificity was 90 000-fold, as determined by the ratio of the selectivity coefficients of DMA/TMA, between the Triple-mutant and wild-type enzyme (Basran *et al.*, 1997).

Somewhat disappointingly, the introduction of the mutation T257N into the Triple-mutant brought about virtually no changes in the steady-state kinetic parameters for this enzyme with either TMA or DMA as substrate. The same observations made for the Triple-mutant apply to the Quad-mutant. However, the precise effects of the mutation, cannot be ascertained from a steady-state analysis alone. The Michaelis constant is not equivalent to the dissociation constant for substrate. Additionally, since electron transfer from flavin to the 4Fe-4S centre in TMADH is rate-limiting in wild-type enzyme, k_{cat} values might not report on flavin reduction rates in the mutant enzyme. For these reasons, stopped-flow kinetic analyses were also performed on the Quad-mutant to fully determine the effects of the introduced mutation.

Table 5.1. Steady-State Kinetic Parameters for the Wild-Type and Mutant Forms of TMADH with Trimethylamine and Dimethylamine as Substrate.

Substrate: Trimethylamine			
Enzyme	K_m (μM)	k_{cat} (s^{-1})	k_{cat}/K_m (s^{-1} M^{-1})
wild type[a]	13.7± 1.7	15.6± 2.4	1.14×10^6
Y60Q[a]	545± 280	0.08± 0.01	147
Y60Q.S74T	737± 71	0.13± 0.004	176
Triple-mutant	8470± 2700	0.02± 0.003	2.29
Quad-mutant	10288± 2224	0.02± 0.001	2.38
Substrate: Dimethylamine			
Enzyme	K_m (mM)	k_{cat} (s^{-1})	k_{cat}/K_m (s^{-1} M^{-1})
wild type[a]	2.34± 0.19	0.67± 0.02	286
Y60Q[a]	2.52± 0.47	0.55± 0.03	218
Y60Q.S74T	3.12± 0.45	0.32± 0.015	102
Triple-mutant	7.25± 0.88	0.38± 0.024	52
Quad-mutant	8.18± 1.06	0.42± 0.014	51

[a]Data calculated by fitting to Equation 2.3. $K_i = 1 \pm 0.3$ mM, $b = 0.24 \pm 0.03$ for the wild-type enzyme and $K_i = 2.6 \pm 2.4$ mM, $b = 0.32 \pm 0.1$ for the Y60Q mutant enzyme. k_{cat} values for the wild-type and Y60Q enzymes with TMA as substrate were calculated from the observed V_{max} rather than the theoretical V_{max} that would have been seen in the absence of substrate inhibition. All other data were calculated by fitting to the Michaelis-Menten equation, since no substrate inhibition was apparent over the concentration range used in the assays (up to 80 mM).

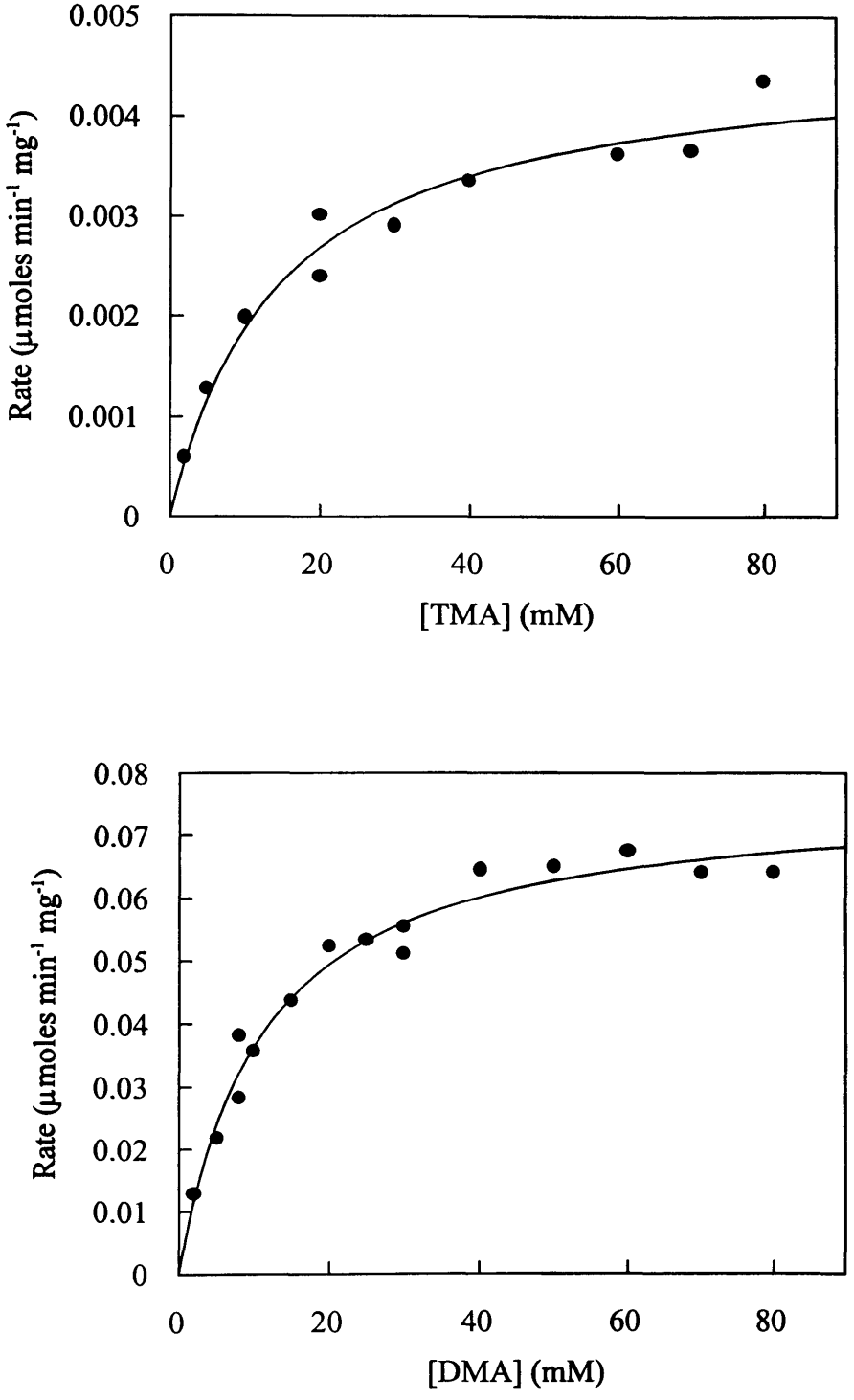

Figure 5.10: Plots of initial velocity versus TMA and DMA concentration for the TMADH Quad-mutant. Reactions were performed in 100 mM sodium pyrophosphate buffer, pH 8.5, 30 °C, using PMS and DCPIP as electron acceptors.

5.2.4 Reductive Half-Reaction of the Quad-Mutant

5.2.4.1 Single Wavelength Studies at 443 nm

In single wavelength stopped-flow studies of the reductive half-reaction were performed at pH 7.5. The study of Basran *et al.* (1997) had shown that this pH was the most convenient at which to examine the kinetics of the reductive half-reaction, since the rates of flavin reduction in wild-type TMADH, with which all the mutants are compared, are sufficiently slow at this pH to be observed by the stopped-flow technique. During the reductive half-reaction, the monophasic changes in absorbance observed at 443 nm (Figure 5.11) predominantly represent reduction of the flavin to produce the hydroquinone, while changes at 365 nm are associated with internal electron transfer from hydroquinone to the 4Fe-4S centre to produce flavin semiquinone and reduced 4Fe-4S centre.

In the monitoring of the reductive half-reaction, the Quad-mutant has similar properties to other TMADH mutants which have slow rates of flavin reduction, in that there is mixing of the first and second kinetic phases, i.e. those monitored at 443 nm and 365 nm respectively (Basran *et al.*, 1997). This is due to a substantial slowing of the first kinetic phase of the reductive half-reaction which can be caused either by mutation, or by the use of slow substrates such as DMA. All kinetic transients at 443 nm were monophasic and the rates of flavin reduction displayed a hyperbolic dependence on substrate concentration, with both TMA and DMA. The data were therefore fitted to the Strickland equation (Equation 2.6) to obtain values of K_d and limiting rates for flavin reduction (Figure 5.12).

As with the three previous mutants of TMADH, the Quad-mutant was found to have an increased dissociation constant for TMA, when compared with wild-type enzyme (Table 5.2). The K_d value for the Quad-mutant shows a larger increase than previous mutants (three-fold increase over the Triple-mutant), although there is a fairly large error on this value (30 %), caused by the large extrapolation to k_{lim} as the result of the hyperbolic fit to the Strickland equation. As with the Triple-mutant, there has been a >4000-fold reduction in rate constant for the Quad-mutant with TMA as substrate. With DMA as substrate, the dissociation constant is increased in the Quad-mutant, whereas previous mutants had shown very little change from the wild-type enzyme. However, this change is only a very small increase, and the large error on the K_d value obtained is more likely an indicator that essentially, the Quad-mutant too has been little changed from the wild-type enzyme.

Table 5.2. Limiting Rate Constants and Dissociation Constants Calculated from Single Wavelength (443 nm) Stopped-Flow Data for Wild-Type and Mutant TMADH Enzymes at pH 7.5.

Substrate: Trimethylamine			
Enzyme	k_{lim} (s^{-1})	K_d (mM)	k_{lim}/K_d ($s^{-1}M^{-1}$)
wild type	706± 15	0.21± 0.06	3.36×10^6
Y60Q	2.15± 0.1	52.5± 5.3	40.9
Y60Q.S74T	1.77± 0.1	76.8± 12	23.0
Triple-mutant	0.16± 0.01	86.6± 9.4	1.85
Quad-mutant	0.18± 0.03	251± 71	0.72
Substrate: Dimethylamine			
Enzyme	k_{lim} (s^{-1})	K_d (mM)	k_{lim}/K_d ($s^{-1}M^{-1}$)
wild type	19.2± 1.2	117± 14	164
Y60Q	1.13± 0.1	100± 24	11.3
Y60Q.S74T	1.0±0.1	119± 13	8.40
Triple-mutant	0.78± 0.03	105± 7.6	7.42
Quad-mutant	0.62± 0.1	343± 95	1.81

5.2.4.2 Single Wavelength Studies at 365 nm

The reaction of the Quad-mutant with TMA as substrate exhibited monophasic absorbance changes at 365 nm (Figure 5.11) that were dependent on substrate concentration. As with the studies at 443 nm, data for the Quad-mutant was fitted to the Strickland equation (Figure 5.12). The limiting rate constants and dissociation constants calculated (Table 5.3) are similar to the results from data collected at 443 nm, which would be expected if the 365 nm transients are closely related to the substrate-dependent rates of flavin reduction. The data therefore demonstrate that the absorbance changes monitored at 365 nm on mixing the mutant with TMA do not report on the *intrinsic* electron-transfer rates from flavin to the 4Fe-

4S centre, but are controlled by the preceding step (i.e. flavin reduction) in the reductive half-reaction.

Table 5.3. Limiting Rate Constants and Apparent Dissociation Constants for the Monophasic Absorbance Changes Occurring at 365 nm for Mutant TMADH Enzymes with Trimethylamine as Substrate.

Enzyme	k_{lim} (s^{-1})	K_d (mM)
Y60Q	2.0± 0.1	31± 6
Y60Q.S74T	2.3± 0.2	73± 10
Triple-mutant	0.2± 0.02	140± 26
Quad-mutant	0.12± 0.01	143± 19

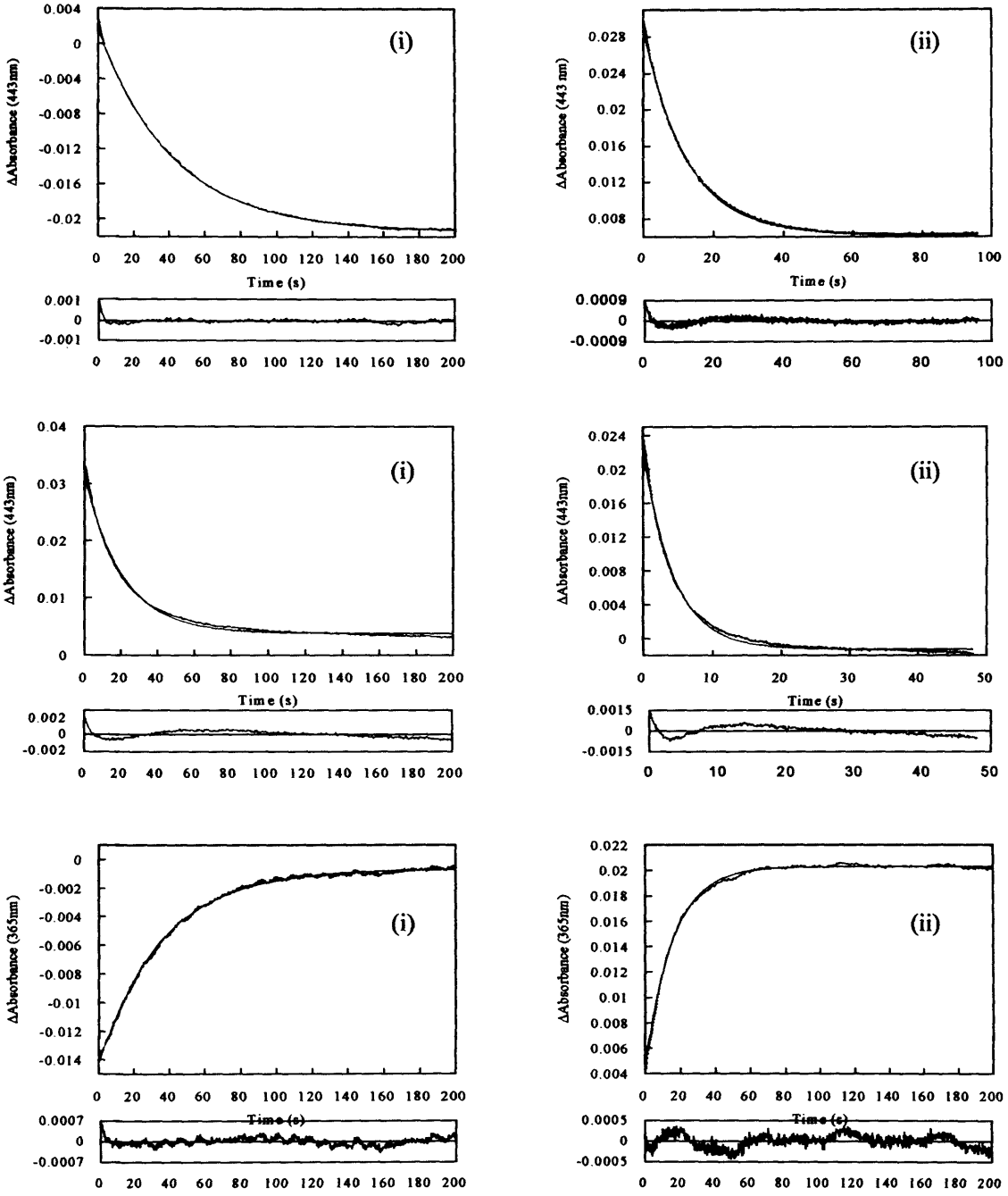

Figure 5.11: Kinetic transients illustrating the monophasic nature of the absorbance change measured at 443 nm and 365 nm for the Quad mutant with TMA and DMA as substrate. Two example traces are shown for each condition at (i) 10 mM and (ii) 80 mM substrate. A. Change in absorbance at 443 nm with TMA as substrate; B. Change in absorbance at 443 nm with DMA as substrate. C. Change in absorbance at 365 nm with TMA as substrate. Reactions were carried out in 100 mM potassium phosphate buffer, pH 7.5 at 25 °C.

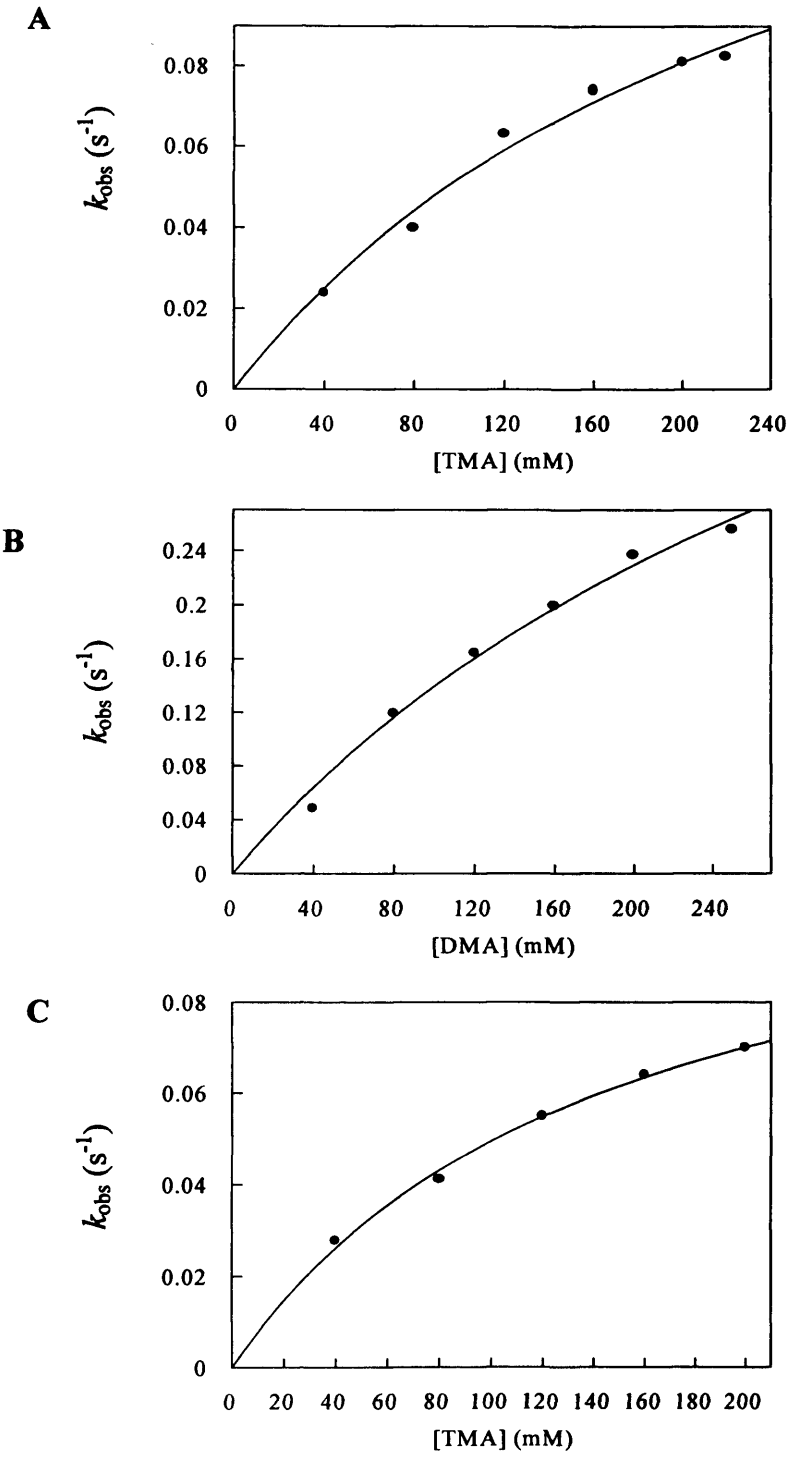

Figure 5.12: Limiting rates of flavin reduction and internal electron transfer for the TMADH Quad-mutant with TMA and DMA as substrate. A. Observed rate of flavin reduction with TMA as substrate. B. Observed rate of flavin reduction with DMA as substrate. C. Observed rate of internal electron transfer as monitored at 365 nm. Reactions were carried out in 100 mM potassium phosphate buffer, pH 7.5 at 25 °C.

5.2.5 Analysis of the TMADH Penta- and Hexa-mutants

An initial steady-state analysis of the TMADH Penta- and Hexa mutants showed that the enzymes displayed extremely low activity (Figure 5.13). Steady-state activity could only be detected with large amounts of both enzyme and substrate. For example, 44 nmoles and 7 nmoles of the Penta- and Hexa-mutants was respectively required per 1 ml assay, to achieve a reaction rate barely above background rates using 180 mM substrate, compared with approximately 0.1 nmoles of native enzyme used in similar assays. A full steady-state analysis of the Penta- and Hexa-mutants was prevented due to the poor yield in the purification of these enzymes. Additionally, the kinetic traces, as measured by the rate in reduction of absorbance at 600 nm (Figure 5.13), exhibited an unusual profile. At the very high concentrations of TMA and DMA used, the kinetic traces would be expected to remain linear (i.e. maintain the same reaction rate) over the recording period of 30 s. However, the kinetic traces clearly show a continual diminution in reaction rate over this period. There are a number of reasons why this type of kinetic trace might be seen:

(i) The data is being collected where substrate concentration is limiting and we are seeing substrate depletion causing a slowing down of reaction velocity: this is unlikely because of the high substrate concentrations used and was unable to be verified because of the limited amounts of enzyme available.

(ii) Product inhibition is occurring: again unlikely, because this has never been seen in any TMADH mutant.

(iii) The enzyme is being inactivated as it turns over substrate: this seem to present the most likely explanation for the following reasons. The kinetic traces are highly reminiscent of steady-state kinetic traces seen for an earlier TMADH mutant, the C30A mutant (Huang *et al.*, 1996). In this mutant the 6-S-cysteinyl linkage to FMN by Cys-30 is disrupted. In the case of the 'as purified' C30A mutant, FMN resides in the active site of the enzyme, although not covalently bound, and is initially capable of taking part in turnover of substrate. However, the FMN quickly becomes derivatised to 6-hydroxy-flavin, and the enzyme rapidly inactivated (Huang *et al.*, 1996). This inactivation produces a steady-state kinetic trace showing a rapid slowing down of substrate turnover resembling the kinetic traces seen for both the Penta- and Hexa-mutants.

An attempt was made to measure the rate of flavin reduction in the Penta- and Hexa-mutants. However, when an attempt was made to reduce either enzyme

with TMA, monitoring flavin reduction at 443 nm, it was clear that there was no measurable reaction (Figure5.13). Previous work has shown that the 4Fe-4S centre and ADP cofactors are stoichiometrically assembled with recombinant TMADH and this assertion is corroborated by the UV-visible absorption spectrum of each enzyme (Figure 5.14). The proportion of flavinylated enzyme was determined for each sample, being calculated using Equation 2.1 and was as follows: Quad-mutant = 50%, Penta-mutant = 3%, Hexa-mutant = 6%. However, a qualitative analysis of the spectral profile for the Penta- and Hexa-mutants, when compared with the usual spectra observed for TMADH, meant that these flavinylation levels were viewed with some scepticism and it was therefore decided to determine the proportion of FMN bound by these enzymes by perchloric acid precipitation (Section 2.4.3). Disappointingly, the absorption spectra for the free and bound flavin contents in samples of each enzyme (Figure 5.13) indicated that the flavin content in both mutants was very low or non-existent. Following perchloric acid precipitation, the spectrum of either protein does not resemble previously published spectra for perchloric acid precipitated, fully-flavinylated TMADH (Mewies *et al.*, 1995). It is likely that the spectrum seen in Figure 5.14 (i) represents the absorbance from the 4Fe-4S centre of the enzyme. Furthermore, no appreciable amount of flavin was released from either mutant enzyme. Hence, although there could be a small amount of enzyme bound FMN, allowing slow substrate turnover, this is so small and might be non-covalently bound. Hence, kinetic analysis of the Penta- and Hexa-mutants could not be carried out.

In summary, the extra mutations that have been introduced into the Quad-mutant have brought about unforeseen structural changes, preventing meaningful kinetic characterisation of further mutants. This was disappointing because the extra mutations that had been introduced were those that the modelling work had identified as being the most suitable to re-create the binding site of DMADH. Also, the adverse effects of introducing these mutations could not be predicted, given that the Quad-mutant was stable and reasonably flavinylated. Given the proposed biotechnological aim of this protein engineering project, further analysis of the Penta- and Hexa-mutant enzymes was deemed to be inappropriate and the production of the Hepta-mutant was therefore also shelved as it is unlikely that an extra mutation would have led to a restoration of activity.

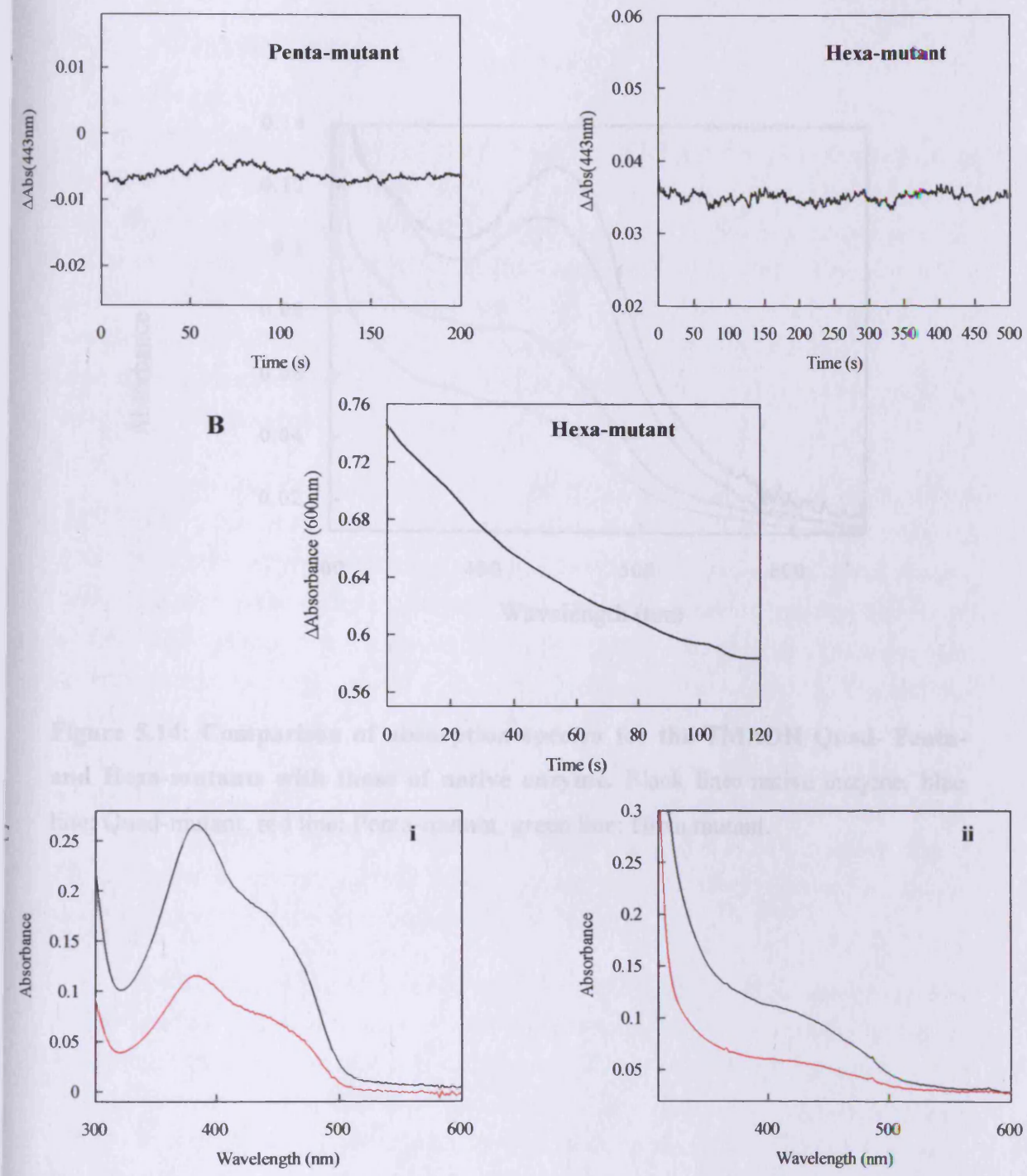

Figure 5.13: Characteristics of the TMADH Penta- and Hexa-mutants. A. Lack of discernible flavin reduction during stopped-flow of either mutant with TMA. B. Steady-state kinetic trace for the reaction of the Hexa-mutant enzyme with TMA. C. (i) spectra of protein and (ii) supernatant spectra for penta (red line) and hexa (black line) mutants, following perchloric acid precipitation.

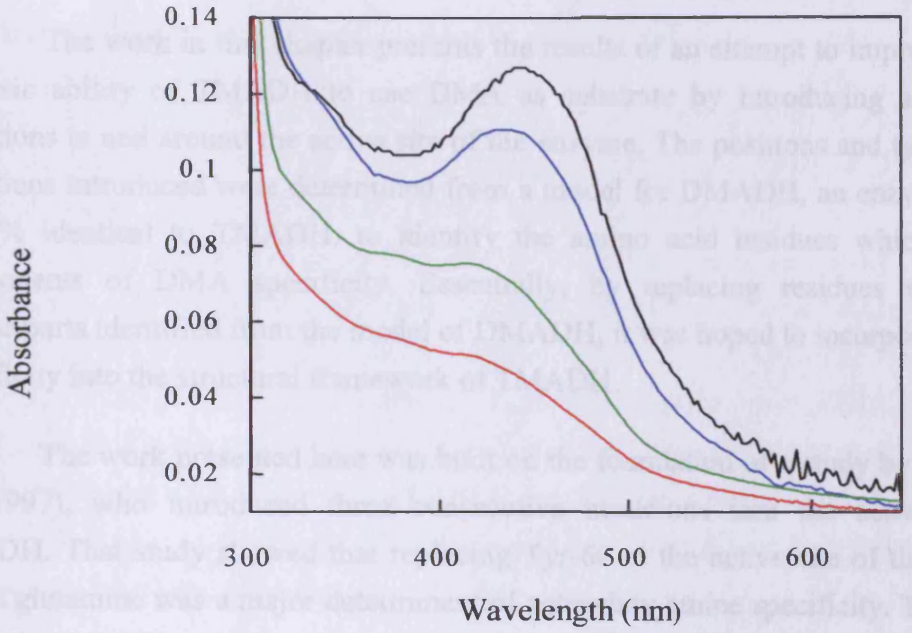

Figure 5.14: Comparison of absorption spectra for the TMADH Quad- Penta- and Hexa-mutants with those of native enzyme. Black line: native enzyme, blue line: Quad-mutant, red line: Penta-mutant, green line: Hexa mutant.

5.3 Discussion

The work in this chapter presents the results of an attempt to improve on the intrinsic ability of TMADH to use DMA as substrate by introducing a series of mutations in and around the active site of the enzyme. The positions and types of the mutations introduced were determined from a model for DMADH, an enzyme which is 63% identical to TMADH, to identify the amino acid residues which are the components of DMA specificity. Essentially, by replacing residues with their counterparts identified from the model of DMADH, it was hoped to incorporate DMA specificity into the structural framework of TMADH.

The work presented here was built on the foundation of a study by Basran *et al.* (1997), who introduced three consecutive mutations into the active site of TMADH. That study showed that replacing Tyr-60 at the active site of the enzyme with a glutamine was a major determinant of secondary amine specificity. The model of DMADH had shown that a glutamine in this position would make a hydrogen bond to the hydrogen that replaces one of the methyl groups of TMA in DMA. The addition of two more mutations, Ser-74 → Thr and Trp-105 → Phe, which appear to influence the position of Glu-60 in the DMADH model, led to a severe impairment in the ability of TMADH to use TMA as substrate, but had little effect on its reaction with DMA. The Triple-mutant TMADH (Y60Q.S74T.W105F) appeared to be a positive step in the process of engineering DMA specificity and was therefore used as the starting point for the additional protein engineering of TMADH.

Modelling at the University of Leicester led to the identification of four further residues that were thought to contribute to secondary amine specificity and the following mutations were to be consecutively added into the Triple-mutant: Thr-257 → Asn, Glu-131 → Ala, His-71 → Leu and Leu-73 → Ile. These last two mutations were to be introduced simultaneously. Overall, four new variants of TMADH were to be generated, but due to problems with mutagenesis, only three variants were successfully made: the Quad-, Penta-, and Hexa-mutants.

The Quad-mutant enzyme (Y60Q.S74T.W105F.T257N) showed essentially the same properties as the Triple-mutant. Under steady-state conditions, the K_m of the Quad-mutant was 10.3 ± 2 mM with TMA as substrate, a 750-fold increase over the wild-type enzyme, so was severely impaired in its ability to use its native substrate. Conversely, with DMA as substrate, the K_m of the Quad-mutant was 8.19 ± 1 mM, representing only a 3.5-fold increase over the wild-type enzyme. Therefore, in the

Quad-mutant, as with the Triple-mutant, the magnitude in the switch in specificity for DMA over TMA was therefore maintained at about 90 000-fold. Therefore, the introduction of the mutation of T257N had brought about virtually no change in the steady-state parameters that were manifest in the Triple-mutant.

The rate of flavin reduction with TMA is diminished in the Quad-mutants to the extent that flavin reduction is now partially rate-limiting in catalysis. These effects are observed as a mixing of phases (flavin reduction and internal electron transfer to 4Fe-4S) observed in the stopped-flow study. The transients observed at 365 nm are monophasic and display an apparent substrate dependence as a result of kinetic mixing with the transients observed at 443 nm. This result is identical with findings observed for the TMADH Triple-mutant. In the Quad-mutant with DMA, the rate of flavin reduction is reduced by about 30-fold, so the rate of internal electron transfer is controlled by rate of flavin reduction, giving rise to monophasic transients at 365 nm. Because there is no attenuation of internal electron transfer the Quad-mutant did not display any substrate inhibition.

The Quad-mutant displayed no improvement in its ability to use DMA as substrate when compared with the Triple-mutant. However, it contained a higher proportion of covalently bound flavin than the Triple-mutant and therefore appeared to be a reasonable mutant from which to carry out further protein engineering. Unfortunately, the incorporation of further mutations, to produce the Penta- and Hexa-mutants, led to enzymes that probably contained no covalently bound flavin and essentially were kinetically inert. It is possible that the introduction of further mutations has led to a distortion of the active site so that covalent attachment of flavin is no longer possible. Therefore the Quad-mutant represented the last point in this attempt to rationally engineer TMADH so that it could use DMA as substrate.

Despite the disappointing outcome of this rational engineering project, it was worth attempting given the hoped-for outcome of producing a commercially usable enzyme. However, could other techniques have been used to bring about the production of a TMADH variant with specificity for DMA? There are a number of approaches for developing new enzyme variants for specific uses that could be more productive for TMADH. At the simplest level, 'directed evolution' of the enzyme in the host organism *M. methylotrophus* by attempted growth on target substrates did not produce any positive results (P. Roberts, unpublished results). There are also other methods for producing new enzyme variants that involve combinatorial approaches to altering target genes and mass screening of potential enzymes, as outlined in the Introduction to this chapter. The most promising approaches for the production of

enzyme appear to be those of *in vitro* molecular evolution involving the random mutagenesis of amino acid residues, followed by selection of enzymes with desired activity (Arnold, 1996; Arnold & Schmidt-Dannert, 1999). There would be some problems to overcome with this approach, such as the development of a suitable screening method; the demethylation of DMA produces formaldehyde, which would be toxic to a host organism such as *E.coli*. However, as an alternative to the rational engineering approach, the 'irrational engineering' of TMADH might be more fruitful.

To conclude, simply switching like-for-like residues between TMADH and DMADH did not bring about the desired switch in substrate specificity. Despite the inherent confidence in a homology model when there is such a high degree of identity as there is between TMADH and DMADH (Guex *et al.*, 1999), perhaps only the production of a crystal model for DMADH will explain what combination of residues is required to bring about DMA specificity. Although a directed evolution approach offers an alternative way for causing the switch, the work could still be developed further as a rational engineering project. For example, there is a 6 residue insertion in the gene for DMADH (Figure 5.1) that could have medium- or long-range effects on the active site of DMADH that are crucial for DMA specificity. Therefore, this 6-residue sequence could be introduced into TMADH to see what effect this has upon the ability of the enzyme to use DMA as substrate. Alternatively, different combinations of the mutations already introduced into TMADH could be attempted, producing a small library of mutant proteins that might show improved DMA activity. Whichever approach is adopted, the long-term goal of developing TMADH for commercial exploitation remains.

Chapter 6

General Discussion

6.1 Discussion

Research on TMADH has proven to be an excellent illustration that there are many different aspects to be considered for a thorough understanding of enzyme function. Early investigations of TMADH demonstrated for the first time that flavin could be covalently bound to an enzyme through the C-6 position of the isoalloxazine ring (Ghisla, 1980; Steenkamp *et al.*, 1978a; Steenkamp *et al.*, 1978b). This prompted research into the flavinylation reaction in TMADH, which in turn has demonstrated that the function of this covalent link in some flavoproteins is to prevent derivitisation of the flavin to the 6-hydroxy form during catalysis (Mewies *et al.*, 1997; Mewies *et al.*, 1996; Mewies *et al.*, 1995; Packman *et al.*, 1995). X-ray crystallographic structural data of TMADH has shown that its substrate is bound within an 'aromatic bowl' of two tryptophans and one tyrosine residue (Bellamy *et al.*, 1989; Lim *et al.*, 1986), serving as a simple model for cation-π binding in proteins (Scrutton & Raine, 1996). The unusually slow rate of internal electron transfer between the covalently bound flavin and 4Fe-4S centre has prompted a number of studies into the causes of substrate inhibition in TMADH (Falzon & Davidson, 1996b; Jang *et al.*, 1999a; Pollock *et al.*, 1988), leading directly to the conclusions presented in Chapter 3 of this thesis. Recently, TMADH has been constructively used to contribute to debate about how flavoproteins oxidise amines (Basran *et al.*, 1999a; Basran *et al.*, 1999c; Jang *et al.*, 1999a) and, in combination with studies on its physiological redox partner, ETF, TMADH has also served as a model to investigate interprotein electron transfer (Basran *et al.*, 1999b; Chohan *et al.*, 1998; Huang *et al.*, 1995; Jones *et al.*, 2000; Wilson *et al.*, 1997a).

Despite this wealth of research concerning TMADH, the work in this thesis demonstrates that there is room for further investigations in developing a more thorough understanding of the enzyme. Clearly, there is a great deal of scope here, and the work of this thesis ranges from a standard protein engineering exercise to 'quantum enzymology'. In Chapter 3 of this thesis, work is presented demonstrating that TMADH cycles through different redox states, depending on the relative amounts of electron acceptor and substrate. During conditions of high substrate concentration, substrate binding to reduced enzyme stabilises the semiquinone form of the 6-S-cysteinyl FMN, effectively preventing further reduction of the enzyme until internal electron transfer to the 4Fe-4S centre has occurred. In common with other flavoproteins which undergo product or substrate inhibition, modulation of redox potentials, by ligand binding to stabilise either the 1- or 2-electron reduced state of the

flavin could provide a means of regulating TMADH (Gutman, 1977; Gutman *et al.*, 1980), in this case preventing over-production of toxic formaldehyde (Falzon & Davidson, 1996b). For the first time, using stopped-flow spectroscopy, the redox state of the enzyme could be monitored as the reaction was occurring. Due to the known spectral properties of the enzyme under different oxidation-reduction states, the redox state of TMADH could be directly monitored throughout the steady-state reaction over a range of different substrate concentrations. Although it had been proposed in the past that the inhibition of TMADH was caused by stabilisation of semiquinone flavin at the active site of the enzyme, this was the first time that a 1-electron reduced form of TMADH was demonstrated to exist outside of spectroelectrochemical studies (Pace & Stankovich, 1991).

In Chapter 4, TMADH was investigated in a preliminary attempt to determine the applicability of recent, exciting evidence that cleavage of stable C-H bonds and subsequent transfer of hydrogen in enzymes is accomplished by H-tunnelling modulated by thermal fluctuations of the protein thermal scaffold (Kohen & Klinman, 1999; Scrutton *et al.*, 1999). Research in this area is at a fairly early stage, both in terms of the volume of evidence and a general acceptance of the concept that *all* enzymatic H-transfer reactions require a dynamic component and tunnelling of hydrogen. However, for the moment it cannot be assumed that the TMADH reaction involves either protein dynamics or H-tunnelling, and it is an unfortunate consequence of kinetic complexity in the TMADH reaction that, although there are promising indications that it might operate using 'vibrationally enhanced tunnelling' (Bruno & Bialek, 1992), the data presented in Chapter 4 requires proper consideration only with the knowledge of the exact mode of C-H bond cleavage. The research effort at the University of Leicester to rectify this lack of knowledge is ongoing. However, there are some positive indications that firstly, H-tunnelling does occur in TMADH, and secondly, that the extent to which tunnelling of both protium and deuterium occurs markedly alters over a small range of pH. These results offer some evidence, consistent with dynamic theories of enzyme catalysis, that barrier width is a more important factor in reaction rate than barrier height; changing barrier width, through the alteration of pH or mutation could be partly to blame for the difference in reaction rates observed with these changes.

Finally, in Chapter 5, TMADH served as the structural framework into which there was an attempt to alter amine specificity, from TMA to DMA. The work was based upon the construction of a model for the enzyme DMADH (Raine *et al.*, 1995). Given the strong sequence homology between TMADH and DMADH (Yang *et al.*, 1995), the final model for DMADH could be viewed with some confidence (Yang *et*

al., 1995). As a result, prior to the work presented in Chapter 5, there was partial success in achieving the hoped-for change in specificity, in that the specificity for TMA was greatly perturbed, without affecting the intrinsic ability of TMADH to use DMA (Basran *et al.*, 1997). However, the introduction of additional mutations into the active site of TMADH either caused no more changes in properties, or produced such structural perturbation of the active site of the enzyme that covalent attachment of FMN, critical for the activity of the enzyme, did not occur. It is possible that there are ways in which a rational approach could bring about the desired change in specificity. However, rational engineering can be tedious if many rounds of mutation are required and is beyond the scope of a PhD project unless positive results occur early on, and perhaps an irrational, directed evolution approach would have offered more success (Arnold, 1996).

There is scope for developing the themes of this thesis furhter. For example, how does substrate binding stabilise semiquinone FMN in reduced TMADH? From a structural viewpoint, it would be interesting to know what differences exist in the relationship between substrate and flavin with the binding of a non-inhibitory substrate such as DMButA, compared to that of TMA. Clearly, the interaction of substrate with flavin is important in TMADH, contributing to the formation of the spin-interacting state (Steenkamp & Beinert, 1982b). Structural work, perhaps with the W264L TMADH mutant, which is not inhibited by TMA, would address the issue of whether active site residues 'push' substrate onto the enzyme-bound FMN, and a loss of active site bulk abolishes inhibition. Another important outcome of the substrate inhibition work was the development of Fc^+ as an electron acceptor for use in directly observing the redox state of TMADH as it underwent steady-state turnover. Perhaps the use of Fc^+ can provide insights to the steady-state turnover of other flavoenzymes for which it acts as an electron acceptor.

The importance of H-tunnelling and thermal motions of proteins to enzyme catalysis will remain an exciting area for some time, as demonstrated by work on aromatic amine dehydrogenase at Leicester University. Whether TMADH is able to contribute to this research will depend upon whether the mechanism for C-H bond cleavage can be elucidated. However, as this phenomenon is unveiled in more enzyme systems, it is clear that the traditional view of enzyme catalysis will have to be changed. In addition, the means by which the whole protein contributes to catalysis will present a major intelluctual challenge for researchers.

Will TMADH one day form part of a 'fish freshness' kit? The proposals for the biotechnological exploitation of the enzyme are ambitious, and there are clearly a

series of obstacles to overcome if the enzyme is to be developed along these lines. Unfortunately, as a start to commercial exploitation, rational engineering of TMADH did not bring about the desired change in substrate specificity. However, there is still scope for developing the enzyme using irrational approaches such as directed molecular evolution and it is possible that this will be the means by which TMADH will serve as the catalytic framework for developing specificities for a range of biogenic amines. Overall, it is clear that research on TMADH can still make important contributions to the field of enzymology and flavoprotein research.

References

Albery, W. J. & Knowles, J. R. (1976). Evolution of enzyme function and the development of catalytic efficiency. *Biochemistry* **25**, 5631-5640.

Alston, W. C., Kanska, M. & Murray, C. J. (1996). Secondary H/T and D/T isotope effects in enzymatic enolization reactions. Coupled motion and tunnelling in the triosephosphate isomerase reaction. *Biochemistry* **35**, 12873-12881.

Altamarino, M. M., Blackburn, J. M., Aguayo, C. & Fersht, A. R. (2000). Directed evolution of new catalytic activity using the alpha/beta barrel scaffold. *Nature* **403**(6770), 617-622.

Anthony, C. (1982). *The biochemistry of methylotrophs*, Academic Press, New York.

Antoniou, D. & Schwartz, S. D. (1997). Large kinetic isotope effects in enzymatic proton transfer and the role of substrate oscillations. *Proceedings of the National Academy Sciences USA* **94**, 12360-12365.

Arnold, F. H. (1996). Directed evolution: creating biocatalysts for the future. *Chemical Engineering News* **51**(23), 5091-5102.

Arnold, F. H. & Schmidt-Dannert, C. (1999). Directed evolution of industrial enzymes. *Trends in Biotechnology* **17**, 135-136.

Atkins, P. W. (1982). *Physical Chemistry*. 2nd edit, Oxford University Press, Oxford.

Bahnson, B. J. & Klinman, J. P. (1995). Hydrogen tunnelling in enzyme catalysis. In *Enzyme Kinetics and Mechanism* (Purich, D. L., ed.), Vol. 249, pp. 373-397. Academic Press, London.

Bahnson, B. J., Park, D.-H., Kim, K., Plapp, B. V. & Klinman, J. P. (1993). Unmasking of hydrogen tunnelling in the horse liver alcohol dehydrogenase reaction by site-directed mutagenesis. *Biochemistry* **32**, 5503-5507.

Bain, C. D. & Evans, S. D. (1995). Laying it on thin. In *Chemistry in Britain*, pp. 46-48.

Bala, P., Grochowski, P., Lesyng, B. & McCammon, J. A. (1996). Quantum-classical molecular dynamics simulations of proton transfer processes in molecular complexes and in enzymes. *Journal of Physical Chemistry* **100**, 2535-2545.

Ballinger, M. D., Tom, J. & Wells, J. A. (1994). Designing subtilisin BPN to cleave substrates containing dibasic residues. *Biochemistry* **35**, 1712-1721.

Barber, M. J., Neame, P. J., Lim, L. W., White, S. & Mathews, F. S. (1992). Correlation of X-Ray deduced and experimental amino-acid-sequences of trimethylamine dehydrogenase. *The Journal of Biological Chemistry* **267**(10), 6611-6619.

Basran, J., Chohan, K. K., Sutcliffe, M. J. & Scrutton, N. S. (2000). *Biochemistry (submitted)*.

Basran, J., Jang, M. H., Sutcliffe, M. J., Hille, R. & Scrutton, N. S. (1999a). The role of Tyr-169 of trimethylamine dehydrogenase in substrate oxidation and magnetic interaction between FMN cofactor and the 4Fe/4S center. *The Journal of Biological Chemistry* **274**(19), 13155-13161.

Basran, J., Mewies, M., Mathews, F. S. & Scrutton, N. S. (1997). Selective modification of alkylammonium ion specificity in trimethylamine dehydrogenase by the rational engineering of cation-pi bonding. *Biochemistry* **36**(8), 1989-1998.

Basran, J., Sutcliffe, M. J., Hille, R. & Scrutton, N. S. (1999b). Differential coupling through Val-344 and Tyr-442 of trimethylamine dehydrogenase in electron transfer reactions with ferricenium ions and electron transferring flavoprotein. *Unpublished.*

Basran, J., Sutcliffe, M. J., Hille, R. & Scrutton, N. S. (1999c). Reductive half-reaction of the H172Q mutant of trimethylamine dehydrogenase: evidence against a carbanion mechanism and assignment of kinetically influential ionizations in the enzyme-substrate complex. *Biochemical Journal* **341**(Pt2), 307-314.

Basran, J., Sutcliffe, M. J. & Scrutton, N. S. (1999d). Enzymatic H-transfer requires vibration-driven extreme tunneling. *Biochemistry* **38**(10), 3218-3222.

Bell, R. P. (1980). *The tunnelling effect in chemistry*, Chapman and Hall, London and New York.

Bellamy, H. D., Lim, L. W., Mathews, F. S. & Dunham, W. R. (1989). Studies of crystalline trimethylamine dehydrogenasein 3 oxidation- states and in the presence of substrate and inhibitor. *The Journal of Biological Chemistry* **264**(20), 11887-11892.

Berry, H., Debat, H. & Larreta-Garde, V. (1997). Excess substrate inhibition of soybean lipoxygenase-1 is mainly oxygen-dependent. *FEBS Letters* **408**, 324-326.

Berti, P. J. (1999). Determining transition states from kinetic isotope effects. *Methods in Enzymology* **308**, 355-397.

Bocanegra, J. A., Scrutton, N. S. & Perham, R. N. (1993). Creation of an Nadp-Dependent Pyruvate-Dehydrogenase Multienzyme Complex By Protein Engineering. *Biochemistry* **32**(11), 2737-2740.

Borgis, D. & Hynes, J. T. (1991). Molecular-dynamics simulation for a model nonadiabatic proton transfer reaction in solution. *The Journal of Chemical Physics* **94**(5), 3619-3628.

Bork, P. J., Gellerich, H., Groth, R., Hooft, A. & Martin, F. (1995). Divergent evolution of a beta/alpha barrel subclass: detection of numerous phosphate-binding sites by motif search. *Protein Science* **4**, 268-274.

Boyd, G., Mathews, F. S., Packman, L. C. & Scrutton, N. S. (1992). Trimethylamine dehydrogenase Of bacterium W_3A_1: Molecular-cloning, sequence determination and over-expression of the gene. *Febs Letters* **308**(3), 271-276.

Boyer, P. D. (1970). *Kinetics and Mechanism.* The Enzymes, II, Academic Press, London.

Brandsch, R. & Bischler, V. (1991). Autoflavinylation of apo 6-hydroxy-D-nicotine oxidase. *The Journal of Biological Chemistry* **266**, 19056-19062.

Brünger, A. T. (1992). *X-Plor, version 3.1. A system for X-ray crystallography and NMR*, Yale University Press, New Haven.

Bruno, W. J. & Bialek, W. (1992). Vibrationally enhanced tunneling as a mechanism for enzymatic hydrogen transfer. *Biophysical Journal* **63**(3), 689-699.

Brunori, M., Cutruzzola, F., Travaglini-Allocatelli, C. & Vallone, B. (1999). Does picosecond protein dynamics have survival? *Trends in Biochemical Sciences* **24**, 253-255.

Brunori, M., Rotilio, G. C. & Antonini, E. (1971). Oxidation-reduction potentials of D-amino acid oxidase. *The Journal of Biological Chemistry* **246**(10), 3140-3144.

Brunton, G., Griller, D., Barclay, L. R. C. & Ingold, K. U. (1976). Kinetic applications of electron paramagnetic resonance spectroscopy. 26. Quantum mechanical tunneling in the isomerization of sterically hindered aryl radicals. *Journal of the Americal Chemical Society* **98**, 6803-6811.

Burton, S. M., Byrom, D., Carver, M., Jones, G. D. D. & Jones, C. W. (1983). The oxidation of methylated amines by the methylotrophic bacterium *Methylophilus methylotrophus*. *FEMS Microbiology Letters* **17**, 185-190.

Cha, Y., Murray, C. J. & Klinman, J. P. (1989). Hydrogen tunnelling in enzyme reactions. *Science* **243**, 1325-1330.

Chen, D. W. & Swenson, R. P. (1994). Cloning, Sequence-Analysis, and Expression Of the Genes Encoding the 2 Subunits Of the Methylotrophic Bacterium W_3A_1 Electron-Transfer Flavoprotein. *The Journal of Biological Chemistry* **269**(51), 32120-32130.

Chen, R. (1999). A general strategy for enzyme engineering. *Trends in Biotechnology* **17**, 344-345.

Chohan, K. K., Scrutton, N. S. & Sutcliffe, M. J. (1998). Major structural reorganisation most likely accompanies the transient formation of a physiological electron transfer complex. *Protein and Peptide Letters* **5**(4), 231-236.

Christophersen, A. S. (2000). Amphetamine designer drugs - an overview and epidemiology. *Toxicology Letters* **112**, 127-131.

Clarke, A. R., Atkinson, T. & Holbrook, J. J. (1989a). From analysis to synthesis: new ligand binding sites on the lactate dehydrogenase framework. Part I. *Trends in Biochemical Sciences* **14**, 101-105.

Clarke, A. R., Atkinson, T. & Holbrook, J. J. (1989b). From analysis to synthesis: new ligand binding sites on the lactate dehydrogenase framework. Part II. *Trends in Biochemical Sciences* **14**, 145-148.

Cleland, W. W. (1979). Substrate inhibition. In *Enzyme Kinetics and Mechanism* (Purich, D. L., ed.), Vol. 63, pp. 500-513. Academic Press, London.

Cleland, W. W. (1982). The use of isotope effects to determine transition-state structure for enzymic reactions. In *Enzyme Kinetics and Mechanism* (Purich, D. L., ed.), Vol. 87, pp. 625-641. Academic Press, New York, London.

Cleland, W. W. & Northrop, D. B. (1999). Energetics of substrate binding, catalysis, and product release. *Methods in Enzymology* **308**, 3-27.

Colby, J. & Zatman, L. J. (1973). Trimethyalmine metabolism in obligate and facultative methylotrophs. *Biochemical Journal* **132**, 101-112.

Colby, J. & Zatman, L. J. (1974). Purification and properties of the trimethylamine dehydrogenase of Bacterium 4B6. *Biochemical Journal* **143**, 555-567.

Colby, J. & Zatman, L. J. (1975a). Enzymological aspects of the pathways for trimethylamine oxidation and C_1 assimilation in obligate methylotrophs and restricted facultative methylotrophs. *Biochemical Journal* **148**, 513-520.

Colby, J. & Zatman, L. J. (1975b). Tricarboxylic acid-cycle and related enzymes and in restricted facultative methylotrophs. *Biochemical Journal* **148**, 505-511.

Colfen, H., Harding, S. E., Wilson, E. K., Packman, L. C. & Scrutton, N. S. (1996). Homodimeric and expanded behaviour of trimethylamine dehydrogenase in solution at different temperatures. *European Biophysics Journal With Biophysics Letters* **24**(3), 159-164.

Cornish-Bowden, A. (1995). *Fundamentals of Enzyme Kinetics*, Portland Press, London.

Cox, M. M. & Jencks, W. P. (1981). Catalysis of the methoxyaminolysis of phenyl acetate by a preassociation mechanism with a solvent isotope maximum. *Journal of the American Chemical Society* **103**, 572-580.

Crameri, A., Dawes, G., Rodriguez, E., Silver, S. & Stemmer, W. P. C. (1997). Molecular evolution of an arsenate detoxification pathway DNA shuffling. *Nature Biotechnology* **15**(5), 436-438.

Crameri, A., Whitehorn, E. A., Tate, E. & Stemmer, W. P. C. (1996). Improved green fluorescent protein by molecular evolution using DNA shuffling. *Nature Biotechnology* **14**(3), 315-319.

Creighton, T. E. (1993). *Proteins: structures and molecular principles*. 2nd edit, W.H. Freeman, New York.

Daff, S. N., Chapman, S. K., Turner, K. L., Holt, R. A., Govindaraj, S., Poulos, T. L. & Munro, A. W. (1997). Redox control of the catalytic cycle of flavocytochrome P-450 BM3. *Biochemistry* **36**, 13816-13823.

de Koning, A. J. & Mol, T. (1992). Quantitative quality tests for frozen fish. Dimethylamine content as a quality criterion for frozen South African hake (*Merluccius capensis* and *Merluccius paradoxus*) fillets and mince stored at -5 °C, -18 °C and -40 °C. *Journal of the Science of Food and Agriculture* **59**, 135-137.

Deng, W. P. & Nickoloff, J. A. (1992). Site-directed mutagenesis of virtually any plasmid by eliminating a unique site. *Analytical Biochemistry* **200**, 81-88.

Dixon, M. & Webb, E. C. (1979). *Enzymes*, Longman, London.

Dognadze, R. R., Kuznetsov, A. M. & Ulstrop, J. (1977). Conformational dynamics in biological electron and atom transfer reactions. *Journal of Theoretical Biology* **69**, 239-263.

Dougherty, D. A. (1996). Cation-π interactions in chemistry and biology: a new view of benzene, phe,tyr and trp. *Science* **271**, 163-167.

DuPlessis, E. R., Rohlfs, R. J., Hille, R. & Thorpe, C. (1994). Electron-transferring flavoprotein from pig and the methylotrophic bacterium W_3A_1 contains AMP as well as FAD. *Biochemistry and Molecular Biology International* **32**(1), 195-199.

Dykhuizen, D. E., Dean, A. M. & Hartl, D. L. (1987). Metabolic flux and fitness. *Genetics* **115**, 25-31.

Edmondson, D. & Ghisla, S. (1999). Flavoenzyme structure and function. In *Flavoprotein Protocols* (Chapman, S. K. & Reid, G. A., eds.), Vol. 131, pp. 157-179. Humana Press Inc., Totowa, NJ.

Edmondson, D. E. & De Francisco, R. (1992). Structure, synthesis and physical properties of covalently bound flavins and 6- and 8-hydroxyflavins. In *Chemistry and Biochemistry of Flavoproteins* (Muller, F., ed.), Vol. 1, pp. 73-103. CRC Press, Boca Raton, Florida.

Ertughrul, O. W. D., Errington, N., Raza, S., Sutcliffe, M. J., Rowe, A. J. & Scrutton, N. S. (1998). Probing the stabilizing role of C-terminal residues in trimethylamine dehydrogenase. *Protein Engineering* **11**(6), 447-455.

Eszes, C. M., Sessions, R. B., Clarke, A. R., Moreton, K. M. & Holbrook, J. J. (1996). Removal of substrate inhibition in a lactate dehydrogenase from human muscle by a single residue change. *FEBS Letters* **399**, 193-197.

Falzon, L. & Davidson, V. L. (1996a). Intramolecular electron transfer in trimethylamine dehydrogenase: A thermodynamic analysis. *Biochemistry* **35**(37), 12111-12118.

Falzon, L. & Davidson, V. L. (1996b). Kinetic model for the regulation by substrate of intramolecular electron transfer in trimethylamine dehydrogenase. *Biochemistry* **35**(7), 2445-2452.

Fersht, A. (1985). *Enzyme Structure and Mechanism.* 2nd edit, W.H. Freeman and Company, New York.

Fersht, A. & Winter, G. (1992). Protein engineering. *Trends in Biochemical Sciences* **17**, 292-294.

Fraaije, M. W., van den Heuvel, R. H. H., van Berkel, W. J. H. & Mattevi, A. (1999). Covalent flavinylation is essential for efficient redox catalysis in vanillyl-alcohol oxidase. *Journal of Biological Chemistry* **274**(50), 35514-35520.

Gavish, B. (1986). Molecular dynamics and the transient strain model of enzyme catalysis. In *The Fluctuating Enzyme* (Welch, G. R., ed.), pp. 263-339. Wiley and Sons, New York.

Gavish, B. & Werber, M. M. (1979). Viscosity-dependent structural fluctuations in enzyme catalysis. *Biochemistry* **18**(7), 1269-1275.

Ghisla, S. (1980). Chemical synthesis and some properties of 6-substituted flavins. *Biochemistry* **19**(12), 2537-2544.

Glasstone, S., Laidler, K. J. & Eyring, H. (1941). *The Theory of Rate Processes*, McGraw-Hill, New York.

Glickman, M. H. & Klinman, J. P. (1995). Nature of rate-limiting steps in the soybean lipoxygenase-1 reaction. *Biochemistry* **34**, 14077-14092.

Goldanskii, V. I. (1979). Facts and hypotheses of molecular chemical tunnelling. *Nature* **279**, 109-115.

Grant, K. L. & Klinman, J. P. (1989). Evidence that both protium an deuterium undergo significant tunnelling in the reaction catalysed by bovine serum amine oxidase. *Biochemistry* **28**, 6597-6605.

Guex, N., Diemand, A. & Peitsch, M. C. (1999). Protein modelling for all. *Trends in Biochemical Sciences* **24**, 364-367.

Gutfreund, H. (1995). *Kinetics for the Life Sciences.* 1st edit, Cambridge University Press, Cambridge.

Gutfreund, J. H. (1965). *An Introduction to the Study of Enzymes*, Blackwell Scientific Publications, Oxford.

Gutman, M. (1977). Regulation of mitochondrial succinate dehydrogenase by substrate type activators. *Biochemistry* **16**(14), 3067-3072.

Gutman, M., Bonomi, F., Pagani, S., Cerletti, P. & Kroneck, P. (1980). Modulation of the flavin redox potential as mode of regulation of succinate dehydrogenase activity. *Biochimica et Biophysica Acta* **591**, 400-408.

Hall, B. G. & Hauer, B. (1993). Acquisition of new metabolic activities by microbial populations. *Methods in Enzymology* **224**, 603-631.

Harris, R. J., Meskys, R., Sutcliffe, M. J. & Scrutton, N. S. (2000). Kinetic studies of the mechanism of carbon-hydrogen bond breakage by the heterotetrameric sarcosine oxidase of *Arthrobacter* sp. 1-IN. *Biochemistry.*

Hartung, M. & KistersWoike, B. (1998). Cre mutants with altered DNA binding properties. *Journal of Biological Chemistry* **273**(36), 22884-22891.

Hasford, J. J., Kemnitzer, W. & Rizzo, C. J. (1997). Conformational effects on flavin redox chemistry. *Journal Of Organic Chemistry* **62**(16), 5244-5245.

Hemmerich, P. & Massey, V. (1982). The role of the apoprotein in directing pathways of flavin catalysis. In *Oxidases and related redox systems* (King, T. E., ed.), pp. 379-405. Pergamon Press, Oxford and New York.

Henke, E. & Bornscheuer, U. T. (1999). Directed evolution of an esterase from *Psuedomonas fluorescens*. Directed evolution by error-prone PCR or a mutator strain and identification of mutants showing enhanced enantioselectivity by a resorufin-based flurorescence assay. *Biological Chemistry* **380**(7-8), 1029-1033.

Hill, C. L., Steenkamp, D. J., Holm, R. H. & Singer, T. P. (1977). Identification of the Iron-Sulfur Center in Trimethylamine Dehydrogenase. *Proceeding of the National Academy of Sciences of the USA* **74**(2), 547-551.

Huang, L. X., Rohlfs, R. J. & Hille, R. (1995). The Reaction Of Trimethylamine Dehydrogenase With Electron Transferring Flavoprotein. *The Journal of Biological Chemistry* **270**(41), 23958-23965.

Huang, L. X., Scrutton, N. S. & Hille, R. (1996). Reaction of the C30A mutant of trimethylamine dehydrogenase with diethylmethylamine. *The Journal of Biological Chemistry* **271**(23), 13401-13406.

Huskey, W. P. & Schowen, R. L. (1983). Reaction-coordinate tunnelling in hydride-transfer reactions. *Journal of the American Chemical Society* **105**, 5704-5706.

Hwang, J.-K., Chu, Z. T., Yadav, A. & Warshel, A. (1991). Simulations of quantum mechanical corrections for rate constants of hydride-transfer reactions in enzymes and solutions. *Journal of Physical Chemistry* **95**, 8445-8448.

Hwang, J.-K. & Warshel, A. (1996). How important are quantum mechanical nuclear motions in enzyme catalysis? *Journal of the American Chemical Society* **118**, 11745-11751.

Iyanagi, T., Watanabe, S. & Anan, K. F. (1984). One-electron oxidation-reduction properties of hepatic NADH-cytochrome b_5 reductase. *Biochemistry* **23**, 1418-1425.

Jacobsen, J. R. & Schultz, P. G. (1995). The scope of antibody catalysis. *Current Opinion in Structural Biology* 5, 818-824.

Jang, M. H., Basran, J., Scrutton, N. S. & Hille, R. (1999a). The reaction of trimethylamine dehydrogenase with trimethylamine. *The Journal of Biological Chemistry* **274**(19), 13147-13154.

Jang, M.-H., Scrutton, N. S. & Hille, R. (1999b). *Journal of Biological Chemistry.*

Jia, L., Chen, X. & Wang, X. (1999). Simultaneous determination of creatinine and uric acid in human urine. *JOURNAL OF LIQUID CHROMATOGRAPHY & RELATED TECHNOLOGIES* **22**(16), 2433-2442.

Jones, M., Basran, J., Sutcliffe, M. J., Grossman, J. G. & Scrutton, N. S. (2000). X-ray scattering studies of *Methylophilus methylotrophus* (sp. W_3A_1) electron transferring flavoprotein: evidence for multiple conformational states and an induced fit mechanism for assembly with trimethylamine dehydrogenase. .

Jonsson, T., Edmondson, D. E. & Klinman, J. P. (1994). Hydrogen tunnelling in the flavoenzyme monoamine oxidase B. *Biochemistry* **33**, 14871-14878.

Jonsson, T., Glickman, M. H., Sun, S. & Klinman, J. P. (1996). Experimental evidence for extensive tunnelling of hydrogen in the lipoxygenase reaction: implications for enzyme catalysis. *Journal of the American Chemical Society* **118**, 10319-10320.

Karpen, M. E. & Brooks, C. L. (1996). Modelling protein conformation by molecular mechanics and dynamics. In *Protein Structure Prediction* (Sternberg, M. J. E., ed.), pp. 229-261. IRL Press, New York.

Karplus, M. & McCammon, J. A. (1986). The dynamics of proteins. *Scientific American* **254**(4), 30-39.

Kasprzak, A. A., Papas, E. J. & Steenkamp, D. J. (1983). Identity Of the Subunits and the Stoichiometry Of Prosthetic Groups In Trimethylamine Dehydrogenase and Dimethylamine Dehydrogenase. *Biochemical Journal* **211**(3), 535-541.

Kasprzak, A. A. & Steenkamp, D. J. (1983). Localization of the major dehydrogenases in two methylotrophs by radiochemical labelling. *Journal of Bacteriology* **156**(1), 358-353.

Kenney, W. C., McIntire, W. & Steenkamp, D. J. (1978). Amino acid sequence of a cofactor peptide from trimethylamine dehydrogenase. *FEBS Letters* **85**(1), 137-140.

Kim, J., Fuller, J. H., Kuusk, V., Cunane, L., Chen, Z. W., Mathews, F. S. & McIntire, W. S. (1995). The cytochrome subunit is necessary for covalent FAD attachment to the flavoprotein subunit of p-cresol methylhydroxylase. *The Journal of Biological Chemistry* **270**(52), 31202-31209.

Klinman, J. P. (1978). Kinetic isotope effects in enzymology. *Advances in Enzymology and Related Areas of Molecular Biology* **46**, 415-494.

Klinman, J. P. (1989). Quantum mechanical effects in enzyme-catalysed hydrogen transfer reactions. *Trends in Biochemical Sciences* **14**, 368-373.

Koch, H. F. & Dahlberg, D. B. (1980). Use of kinetic isotope effects in mechanism studies. Effect of an internal return mechanism on the Arrhenius behaviour of primary hydrogen isotope effects. *The Journal of the American Chemical Society* **102**, 6102-6107.

Kock, R., Seitz, S., Delvoux, B. & Greiling, H. (1995). A Method For the Simultaneous Determination of Creatinine and Uric. *European Journal of Clinical Chemistry and Clinical Biochemistry* **33**(1), 23-29.

Kohen, A., Cannio, R., Bartolucci, S. & Klinman, J. P. (1999). Enzyme dynamics and hydrogen tunnelling in a thermophilic alcohol dehydrogenase. *Nature* **399**, 496-499.

Kohen, A., Jonsson, T. & Klinman, J. P. (1997). Effects of protein glycosylation on catalysis: changes in hydrogen tunnelling and enthalpy of activation in the glucose oxidase reaction. *Biochemistry* **36**, 2603-2611.

Kohen, A. & Klinman, J. P. (1998). Enzyme catalysis: beyond classical paradigms. *Accounts of Chemical Research* **31**, 397-404.

Kohen, A. & Klinman, J. P. (1999). Hydrogen tunnelling in biology. *Chemistry and Biology* **6**, R191-R198.

Kramers, H. A. (1940). Brownian motion in a field of force and the diffusion model of chemical reactions. *Physica (Utrecht)* **7**, 284-304.

Kraut, J. (1988). How do enzymes work? *Science* **242**, 533-540.

Kuchner, O. & Arnold, F. H. (1997). Directed evolution of enzyme catalysis. *Trends in Biotechnology* **15**(12), 523-530.

Kuhl, P. W. (1987). Allochrony- a new concept for understanding non-Michaelian behaviour of enzymes and receptors. *Biological Chemistry Hoppe-Seyler* **368**, 1069.

Kuhl, P. W. (1994). Excess-substrate inhibition in enzymology and high-dose inhibition in pharmacology: a re-interpretation. *Biochemical Journal* **298**, 171-180.

Kyte, J. (1995). *Mechanism in Protein Chemistry*, Garland Publishing Inc., New York.

Laemmli, U. K. (1970). Cleavage of structural proteins during the assembly of the head of bacteriophage T4. *Nature* **227**, 680-685.

Large, P. J. (1983). *Methylotrophy and Methanogenesis*. Aspects of Microbiology 8, Van Nostrand and Rheinhold, Honk Kong.

Leatherbarrow, R. J. (1992). Grafit 3.0 edit. Eritacus Software Ltd., Staines, U.K.

Lehman, T. C., Hale, D. E., Bhala, A. & Thorpe, C. (1990). An acyl-coenzyme A dehydrogenase assay utilising the ferricenium ion. *Analytical Biochemistry* **186**, 280-284.

Lehman, T. C. & Thorpe, C. (1990). Alternate Electron Acceptors for Medium-Chain Acyl-CoA Dehydrogenase: Use of Ferricenium Salts. *Biochemistry* **29**, 10594-10602.

Lehninger, A. L., Nelson, D. L. & Cox, M. M. (1993). *Principles of Biochemistry*, Worth Publishers, New York.

Lias, R. (1994). Laboratory assessment of glucose meters and reliability of clinical-performance. *Laboratory Medicine* **25**(3), 189.

Lim, L. W., Mathews, F. S. & Steenkamp, D. J. (1982). Crystallographic Study Of the Iron-Sulfur Flavoprotein Trimethylamine Dehydrogenase From the Bacterium W_3A_1. *Journal Of Molecular Biology* **162**(4), 869-876.

Lim, L. W., Mathews, F. S. & Steenkamp, D. J. (1988). Identification Of ADP In the Iron-Sulfur Flavoprotein Trimethylamine Dehydrogenase. *The Journal of Biological Chemistry* **263**(7), 3075-3078.

Lim, L. W., Shamala, N., Mathews, F. S. & Steenkamp, D. J. (1984). Molecular-Structure Of Trimethylamine Dehydrogenase From the Bacterium W3a1 At 6.0-a Resolution. *The Journal of Biological Chemistry* **259**(23), 4458-4462.

Lim, L. W., Shamala, N., Mathews, F. S., Steenkamp, D. J., Hamlin, R. & Xuong, N. H. (1986). 3-Dimensional Structure Of the Iron-Sulfur Flavoprotein Trimethylamine

Dehydrogenase At 2.4-a Resolution. *The Journal of Biological Chemistry* **261**(32), 5140-5146.

Lindqvist, Y., Branden, C. I., Mathews, F. S. & Lederer, F. (1991). Spinach Glycolate Oxidase and Yeast Flavocytochrome-B2 Are Structurally Homologous and Evolutionarily Related Enzymes With Distinctly Different Function and Flavin Mononucleotide Binding. *The Journal of Biological Chemistry* **266**(5), 3198-3207.

Loginova, N. V. & Trotsenko, Y. A. (1978). Carbon metabolism in methylotrophic bacteria isolated from activated sludge. *Mikrobiologiya* **47**, 939-946.

MacBeath, G., Kast, P. & Hilvert, D. (1998). Probing enzyme quaternary structure by combinatorial mutagenesis and selection. *Protein Science* **7**(8), 1757-1767.

Macheroux, P. (1999). UV-visible spectroscopy as a tool to study flavoproteins. In *Flavoprotein Protocols* (Chapman, S. K. & Reid, G. A., eds.), Vol. 131, pp. 1-7. Humana Press Inc., Totowa, NJ.

MacRae, I. J. & Segel, I. H. (1999). Adenosine 5'-Phosphosulfate (APS) Kinase: Diagnosing the Mechanism of Substrate Inhibition. *Archives of Biochemistry and Biophysics* **361**(2), 277-282.

Torry Research Station. (1989a). Torry Advisory Note No. 91: Sensory assessment of fish quality. MAFF.

Torry Research Station. (1989b). Torry Advisory Note No. 92: Non-sensory assessment of fish quality. MAFF.

Mali, B. & Nicholas, P. C. (1987). Jaffes Reaction For Creatinine - Spectrophotometric Study of. *Biochemical Society Transactions* **15**(6), 1160-1161.

Malle, P. & Poumeyrol, M. (1989). A new chemical criterion for the quality control of fish: trimethylamine/total volatile base nitrogen (%). *Journal of Food Protection* **52(6)**, 419-423.

Manstein, D. J. & Pai, E. F. (1986). Absolute stereochemistry of flavins in enzyme-catalysed reactions. *Biochemistry* **25**, 6807-6816.

Massey, V. (1995). Flavoprotein structure and mechanism. *The FASEB Journal* **9**, 473-475.

Massey, V. & Hemmerich, P. (1980). Active site probes of flavoproteins. *Biochemical Society Transactions* **8**, 246-257.

Mathews, C. K. & van Holde, K. E. (1990). *Biochemistry*, The Benjamin/Cummings Publishing Company, Redwood City, CA.

Mathews, F. S., Trickey, P., Barton, J. D., Chen, Z.-W., Basran, J., Lian, L.-Y., Sutcliffe, M. J. & Scrutton, N. S. (1999). Structural and biochemical characterization of recombinant wild type and C30A mutant of trimethylamine dehydrogenase from *Methylophilus methylotrophus* (sp. W_3A_1). *Unpublished.*

Mayhew, S. G., Foust, G. P. & Massey, V. (1969). Oxidation-reduction properties of flavodoxin from *Peptostreptococcus elsdenii. The Journal of Biological Chemistry* **244(6)**, 803-810.

McDaniel, R., Ebert-Khosla, S., Hopwood, D. A. & Khosla, C. (1995). Rational redesign of aromatic polyketide natural products by redombinant assembly of enzymatic subunits. *Nature* **375**, 549-554.

McIntire, W. S. (1990). Trimethylamine Dehydrogenase From Bacterium W_3A_1. *Methods In Enzymology* **188**, 250-260.

Meiberg, J. B. M. & Harder, W. (1979). Dimethylamine dehydrogenase from *Hyphomicrobium X*: purification and some properties of a new enzyme that oxidizes secondary amines. *Journal of General Microbiology* **115**, 49-58.

Mewies, M. (1997). Protein Engineering and Mechanistic Studies of Trimethylamine Dehydrogenase, Cambridge.

Mewies, M., Basran, J., Packman, L. C., Hille, R. & Scrutton, N. S. (1997). Involvement of a flavin iminoquinone methide in the formation of 6- hydroxyflavin mononucleotide in trimethylamine dehydrogenase: A rationale for the existence of 8 alpha-methyl and C6-linked covalent flavoproteins. *Biochemistry* **36**(23), 7162-7168.

Mewies, M., McIntire, W. S. & Scrutton, N. S. (1998). Covalent attachment of flavin adenine nucleotide (FAD) and flavin mononucleotide (FMN) to enzymes: the current state of affairs. *Protein Science* 7, 7-20.

Mewies, M., Packman, L. C., Mathews, F. S. & Scrutton, N. S. (1996). Flavinylation in wild-type trimethylamine dehydrogenase and differentially charged mutant enzymes: A study of the protein environment around the N1 of the flavin isoalloxazine. *Biochemical Journal* **317**(Pt1), 267-272.

Mewies, M., Packman, L. C. & Scrutton, N. S. (1995). Dissection of the FMN-binding site in trimethylamine dehydrogenase. *Biochemical Society Transactions* **23**(4), S509.

Miller, W. H. (1986). Semiclassical methods in chemical physics. *Science* **233**, 171-177.

More O'Ferral, R. A. (1975). Substrate isotope effects. In *Isotope Effects in Chemical Reactions*. Chapman and Hall, London.

Mountcastle, V. B., Ed. (1980). Medical Physiology. Vol. II. III vols. St. Louis: The C.V. Mosby Company.

Murataliev, M. B. (1999). Application of electron spin resonance (ESR) for detection and characterisation of flavoprotein semiquinones. In *Flavoprotein Protocols* (Chapman, S. K. & Reid, G. A., eds.), Vol. 131, pp. 97-110. Humana Press Inc., Totowa, NJ.

Nagy, J., Kenney, W. C. & Singer, T. P. (1979). The reaction of phenylhydrazine with trimethylamine dehydrogenase and with free flavins. *Journal of Biological Chemistry* **254**(8), 2684-2688.

Nesheim, J. C. & Lipscomb, J. D. (1996). Large kinetic isotope effects in methane oxidation catalysed by methane monooxygenase: evidence for C-H bond cleavage in a reaction cycle intermediate. *Biochemistry* **35**, 10240-10247.

Northrop, D. B. (1981). The expression of isotope effects on enzyme-catalysed reactions. *Annual Review of Biochemistry* **50**, 103-131.

Northrop, D. B. (1982). Deuterium and tritium kinetic isotope effects on initial rates. In *Enzyme Kinetics and Mechanism* (Purich, D. L., ed.), Vol. 87, pp. 607-625. Academic Press, New York, London.

Ogawa, J. & Shimizu, S. (1999). Microbial enzymes: new industrial applications from traditional screening methods. *Trends in Biotechnology* **17**, 13-21.

O'Leary, M. H. (1988). Transition-state structures in enzyme-catalysed decarboxylations. *Accounts of Chemical Research* **21**, 450-455.

Olsen, K. & Breddam, K. (1995). Increase of the P_1Lys/Leu substrate preference of carboxypeptidase Y by rational design based on known primary and tertiary structures of serine carboxypeptidases. *Biochemistry* **34**, 15689-15699.

Onuffer, J. J. & Kirsch, J. F. (1995). Redesign of the substrate specificity of *Escherichia coli* tyrosine aminotransferase by homology modelling and site-directed mutagenesis. *Protein Science* **4**, 13312-13319.

Orten, J. M. & Neuhaus, O. W. (1975). *Human Biochemistry*. 9th edit, The C.V. Mosby Company.

Pace, C. P. & Stankovich, M. T. (1991). Oxidation Reduction Properties Of Trimethylamine Dehydrogenase - Effect Of Inhibitor Binding. *Archives Of Biochemistry and Biophysics* **287**(1), 97-104.

Packman, L. C., Mewies, M. & Scrutton, N. S. (1995). The Flavinylation Reaction Of Trimethylamine Dehydrogenase - Analysis By Directed Mutagenesis and Electrospray Mass-Spectrometry. *The Journal of Biological Chemistry* **270**(22), 13186-13191.

Palcic, M. M. & Klinman, J. P. (1983). Isotopic probes yield microscopic constants: separation of binding energy from catalytic efficiency in the bovine plasma amine oxidase reaction. *Biochemistry* **22**, 5957-5966.

Palfrey, B. A. & Massey, V. (1998). Flavin-dependent enzymes. In *Radical Reactions and Oxidation/Reduction* (Sinnot, M., ed.), Vol. 3, pp. 83-154. 4 vols. Academic Press, London.

Phillips, D. C., Sternberg, M. J. E., Thornton, J. M. & Wilson, I. A. (1978). Structure of triose phosphate isomerase and its comparison with lactate dehydrogenase. *Journal of Molecular Biology* **119**, 329-351.

Pollock, V., Kempner, J. F., Kay, C. J., Spence, J. T. & Barber, M. J. (1988). Oxidation-Reduction Properties Of Trimethylamine Dehydrogenase. *Faseb Journal* **2**(4), A354.

Price, N. C. & Steven, L. (1982). *Fundamentals of Enzymology*, Oxford University Press, New York.

Raine, A. R. C., Yang, C. C., Packman, L. C., White, S. A., Mathews, F. S. & Scrutton, N. S. (1995). Protein Recognition Of Ammonium Cations Using Side-Chain Aromatics - a Structural Variation For Secondary Ammonium Ligands. *Protein Science* **4**(12), 2625-2628.

Rasmussen, B. F., Stock, A. M., Ringe, D. & Petsko, G. A. (1992). Crystalline ribonuclease A loses function below the dynamical transition at 200 K. *Nature* **357**, 423-424.

Reinsch, J., Katz, A., Wean, J., Aprahamian, G. & McFarland, J. T. (1980). The deuterium isotope effect upon the reaction of fatty acyl-CoA deydrogenase and butyryl-CoA. *The Journal of Biological Chemistry* **255**(19), 9093-9097.

Ringe, D. & Petsko, G. A. (1999). Tunnel vision. *Nature* **399**, 417-418.

Roberts, P. T., Basran, J., Wilson, E. K., Hille, R. & Scrutton, N. S. (1999). Redox cycles in trimethylamine dehydrogenase and mechanism of substrate inhibition. *Biochemistry* **38**(45), 14927-14940.

Rohlfs, R. J. & Hille, R. (1991). Intramolecular Electron-Transfer In Trimethylamine Dehydrogenase From Bacterium W3a1. *The Journal of Biological Chemistry* **266**(23), 15244-15252.

Rohlfs, R. J. & Hille, R. (1992). The Reductive Half Reaction Of Trimethylamine Dehydrogenase. *Faseb Journal* **6**(1), A319.

Rohlfs, R. J. & Hille, R. (1994). The Reaction Of Trimethylamine Dehydrogenase With Diethylmethylamine. *The Journal of Biological Chemistry* **269**(49), 30869-30879.

Rohlfs, R. J., Huang, L. X. & Hille, R. (1995). Prototropic Control Of Intramolecular Electron-Transfer In Trimethylamine Dehydrogenase. *The Journal of Biological Chemistry* **270**(38), 22196-22207.

Rudd, P. M., Joao, H. C., Coghill, E., Fiten, P., Saunders, M. R., Opdenakker, G. & Dwek, R. A. (1994). Glycoforms modify the dynamic stability and functional activity of an enzyme. *Biochemistry* **33**, 17-22.

Sambrook, J. Fritsch, E.F. & Maniatis, T. (1989). *Molecular Cloning; A Laboratory Manual*. 2nd Edition. Cold Spring Harbour Laboratory Press.

Sanger, F., Nicklen, S. & Coulson, A. R. (1977). DNA sequencing with chain terminating inhibitors. *Proceedings of the National Academy of Sciences USA* **74**(12), 5463-5467.

Sanz, J. M., Garcia, P. & Garcia, J. L. (1996). Construction of a multifunctional pneumococcal murein hydrolase by module assembly. *European Journal of Biochemistry* **235**, 601-605.

Saunders, J., W.H. (1985). Calculations of isotope effects in elimination reactions. New experimental criteria for tunnelling in slow proton transfers. *Journal of the American Chemical Society* **107**, 164-169.

Schimerlik, M. I., Grimshaw, C. E. & Cleland, W. W. (1977). Determination of the rate-limiting steps for malic enzyme by the use of isotope effects and other kinetic studies. *Biochemistry* **16**(4), 571-576.

Schneider, A., Stachelhaus, T. & Marahiel, M. A. (1998). Targeted alteration of the substrate specificity of peptide synthetases by rational module swapping. *Molecular and General Genetics* **257**(3), 308-318.

Schneider, M. E. & Stern, M. J. (1972). Arrhenius preexponential factors for primary hydrogen kinetic isotope effects. *Journal of the American Chemical Society* **94**, 1517-1522.

Schowen, K. B. & Schowen, R. L. (1982). Solvent isotope effects on enzyme systems. In *Enzyme Kinetics and Mechanism* (Purich, D. L., ed.), Vol. 87, pp. 551-606. Academic Press, New York, London.

Schramm, V. L. (1999). Enzymatic transition-state analysis and transition state analogs. *Methods in Enzymology* **308**, 301-355.

Schramm, V. L., Horenstein, B. A. & Kline, P. C. (1994). Transition state analysis and inhibitor design for enzymatic reactions. *The Journal of Biological Chemistry* **269**(28), 18259-18262.

Scrutton, N. S. (1993). α/β Barrel evolution and the modular assembly of enzymes: emerging trends in the flavin oxidase/dehydrogenase family. *BioEssays* **16**(2), 115-122.

Scrutton, N. S., Basran, J. & Sutcliffe, M. J. (1999). New insights into enzyme catalysis. Ground state tunnelling driven by protein dynamics. *European Journal of Biochemistry* **264**, 666-671.

Scrutton, N. S., Berry, A. & Perham, R. N. (1990). Redesign of the Coenzyme Specificity of a Dehydrogenase By Protein Engineering. *Nature* **343**(6253), 38-43.

Scrutton, N. S., Packman, L. C., Mathews, F. S., Rohlfs, R. J. & Hille, R. (1994). Assembly Of Redox Centers In the Trimethylamine Dehydrogenase Of Bacterium W_3A_1 - Properties Of the Wild-Type Enzyme and a C30a Mutant Expressed From a Cloned Gene In Escherichia-Coli. *The Journal of Biological Chemistry* **269**(19), 13942-13950.

Scrutton, N. S. & Raine, A. R. C. (1996). Cation-pi bonding and amino-aromatic interactions in the biomolecular recognition of substituted ammonium ligands. *Biochemical Journal* **319**(Pt1), 1-8.

Shao, Z. & Arnold, F. H. (1996). Engineering new functions and altering existing functions. *Current Opinion in Structural Biology* **6**, 513-518.

Shieh, H.-S., Ghisla, S., Hanson, L. K., Ludwig, M. L. & Nordman, C. E. (1981). Molecular complex of lumiflavin and 2-aminobenzoic acid: crystal structure, crystal spectra, and solution properties. *Biochemistry* **20**, 4766-4774.

Siegel, L. M. (1978). Quantitative determination of noncovalently bound flavins: types and methods of analysis. In *Biomembranes* (Fleischer, S. & Packer, L., eds.), Vol. 53, pp. 419-429. Academic Press, London.

Silman, N. J., Carver, M. A. & Jones, C. W. (1991). Directed evolution of amidase in *Methylophilus methylotrophus*; purification and properties of amidases from wild-type and mutant strains. *Journal of General Microbiology* **137**, 169-178.

Singer, T. P. & Edmondson, D. E., Eds. (1978). Flavoproteins (Overview). Vol. 53. Methods in Enzymology. Edited by Fleischer, S. & Packer, L. London: Academic Press.

Sinnot, M., Garner, C. D., First, E. & Davies, G. (1998). *The Lexicon of Terms and Concepts in Mechanistic Enzymology*. Comprehensive Biological Catalysis; A Mechanistic Reference (Sinnot, M., Ed.), IV. IV vols, Academic Press, London and New York.

Sligar, S. G. & Gunsalus, I. C. (1976). A thermodynamic model of regulation: modulation of redox equilibria in camphor monoxygenase. *Proceeding of the National Academy of Sciences of the USA* **73**, 1078-1082.

Steenkamp, D. J. & Beinert, H. (1982a). Mechanistic Studies On the Dehydrogenases Of Methylotrophic Bacteria .1. the Influence Of Substrate Binding to Reduced Trimethylamine Dehydrogenase On the Intramolecular Electron-Transfer Between Its Prosthetic Groups. *Biochemical Journal* **207**(2), 233-239.

Steenkamp, D. J. & Beinert, H. (1982b). Mechanistic Studies On the Dehydrogenases Of Methylotrophic Bacteria. 2. Kinetic Studies on the Intramolecular Electron Transfer in Trimethylamine and Dimethylamine Dehydrogenase. *Biochemical Journal* **207**(2), 241-252.

Steenkamp, D. J. & Gallup, M. (1978). The natural flavoprotein acceptor of trimethylamine dehydrogenase. *The Journal of Biological Chemistry* **253**, 4086-4089.

Steenkamp, D. J., Kenney, W. C. & Singer, T. P. (1978a). A novel type of covalently bound coenzyme in trimethylamine dehydrogenase. *The Journal of Biological Chemistry* **253**(8), 2812-2817.

Steenkamp, D. J. & Mallinson, J. (1976). Trimethylamine Dehydrogenase from a Methylotrophic Bacterium. *Biochimica et Biophysica Acta* **429**, 705-719.

Steenkamp, D. J., McIntire, W. & Kenney, W. C. (1978b). Structure of the covalently bound coenzyme of trimethylamine dehydrogenase. *The Journal of Biological Chemistry* **253**(8), 2818-2824.

Steenkamp, D. J. & Singer, T. P. (1976). On the Presence of a Novel Covalently Bound Oxidation-Reduction Cofactor, Iron and Labile Sulphur in Trimethyalmine Dehydrogenase. *Biochemical and Biophysical Research Communications* **71**(4), 1289-1295.

Steenkamp, D. J., Singer, T. P. & Beinert, H. (1978c). Participation of the iron-sulphur cluster and of covalently bound coenzyme of trimethylamine dehydrogenase in catalysis. *Biochemical Journal* **169**, 361-369.

Stemmer, W. P. C. (1994a). Dna Shuffling By Random Fragmentation and Reassembly - in-Vitro Recombination For Molecular Evolution. *Proceedings of the National Academy of Sciences of the United States of America* **91**(22), 10747-10751.

Stemmer, W. P. C. (1994b). Rapid Evolution of a Protein in-Vitro By Dna Shuffling. *Nature* **370**(6488), 389-391.

Stenger, P., Allen, M. E. & Lisius, L. (1996). Accuracy of the MediSense Precision QID blood glucoes monitor in pregnant subjects diabetes. *Clinical Chemistry* **42**(6), 189.

Stern, M. J. & Weston, R. E., Jr. (1974a). Phenomenological manifestations of quantum-mechanical tunnelling. I. Curvature in Arrhenius plots. *The Journal of Chemical Physics* **60**(7), 2803-2807.

Stern, M. J. & Weston, R. E., Jr. (1974b). Phenomenological manifestations of quantum-mechanical tunnelling. II. Effects on Arrhenius pre-exponential factors for primary hydrogen kinetic isotope effects. *The Journal of Chemical Physics* **60**(7), 2808-2814.

Stevenson, R. C., Dunham, W. R., Sands, R. H., Singer, T. P. & Beinert, H. (1986). Studies on the spin-spin interaction between flavin and iron-sulfur cluster in an iron-sulfur flavoprotein. *Biochimica et Biophysica Acta* **869**, 81-88.

Stryer, L. (1988). *Biochemistry*. 3rd edit, W.H. Freeman and Company, New York.

Suarez, A. & Silbey, R. (1990). Hydrogen tunnelling in condensed media. *The Journal of Chemical Physics* **94**(7), 4809-4816.

Sumi, H. & Ulstrop, A. M. (1988). Dynamics of protein conformational fluctuations in enzyme catalysis with special attention to proton transfers in serine proteases. *Biochemica et Biophysica Acta* **955**, 26-42.

Sutcliffe, M. J. & Scrutton, N. S. (2000). Enzymology takes a quantum leap forward. *Philosophical Transactions of the Royal Society London* **358**, 367-386.

Swain, C. G., Stivers, E. C., Reuwer, J. F. & Schaad, L. J. (1958). Attacking nucleophile in enolisation of ketones. *Journal of the American Chemical Society* **80**, 5885-5890.

Tegoni, M., Janot, J. M. & Labeyrie, F. (1986). Regulation of dehydrogenases/one-electron transferases by modification of flavin redox potentials. Effect of product binding on semiquinone stabilization in yeast cytochrome b_2. *European Journal of Biochemistry* **155**, 491-503.

Tipton, K. F. (1996). Patterns of enzyme inhibition. In *Enzymology* (Engel, P. C., ed.), pp. 144-151. BIOS Scientific Publishers Ltd, Oxford.

Ulmer, K. M. (1983). Protein engineering. *Science* **219**, 666-671.

Ureta, T. (1978). The role of isozymes in metabolism: A model of metabolic pathways as the basis for the biological role of isozymes. *Current Topics in Cell Regulation* **13**, 233-250.

Vaillancourt, F. H., Han, S., Fortin, P. D., Bolin, J. T. & Eltis, L. D. (1998). Molecular basis for the stabilization and inhibition of 2,3-dihydroxybiphenyl 1,2-dioxygenase by *t*-butanol. *The Journal of Biological Chemistry* **273**(52), 34887-34895.

van Bastelaere, P. B. M., Kersters-Hilderson, H. L. M. & Lambeir, A.-M. (1995). Wild-type and mutant D-xylose isomerase from *Actinoplanes missouriensis*: metal-ion dissociation constants, kinetic parameters of deuterated and non-deuterated substrates and solvent-isotope effects. *Biochemical Journal* **307**, 135-142.

Van den Berghe-Snorek, S. & Stankovich, M. T. (1985). Thermodynamic control of D-amino acid oxidase by benzoate binding. *The Journal of Biological Chemistry* **260**(6), 3373-3379.

Van Hook, W. A. (1971). Kinetic isotope effects: introduction and discussion of the theory. In *Isotope Effects in Chemical Reactions*, pp. 1-89. van Nostrand Rheinhold, New York.

Wang, J.-T. & Williams, F. (1972). Hydrogen atom abstraction by methyl radicals in γ-irradiated crystalline methyl isocyanide at 77-125 ^{3}K. *Journal of the American Chemical Society* **94**(9), 2930-2934.

Wells, J. A. & Estell, D. A. (1988). Subtilisin- an enzyme designed to be engineered. *Trends in Biochemical Sciences* 13, 291-297.

Westheimer, F. H. (1961). The magnitude of the primary kinetic isotope effect for compounds of hydrogen and deuterium. *Chemical Reviews* **61**, 265-273.

White, S. A., Mathews, F. S., Rohlfs, R. J. & Hille, R. (1994). Crystallization and Preliminary Crystallographic Investigation Of Electron-Transfer Flavoprotein From the Bacterium Methylophilus W3a1. *Journal Of Molecular Biology* **240**(3), 265-266.

Wilmanns, M., Hyde, C. C., Davies, D. R., Kirschener, K. & Jansonius, J. N. (1991). Structural conservation in parallel beta/alpha barrel enzymes that catalyse three sequential reactions in the pathway of tryptophan synthesis. *Biochemistry* **30**, 9161-9169.

Wilson, E. K., Huang, L. X., Hille, R., Mathews, F. S. & Scrutton, N. S. (1996). Electron transfer in trimethylamine dehydrogenase: Directed mutagenesis of a potential tunneling pathway. *Biochemical Society Transactions* **24**(3), S456.

Wilson, E. K., Huang, L. X., Sutcliffe, M. J., Mathews, F. S., Hille, R. & Scrutton, N. S. (1997a). An exposed tyrosine on the surface of trimethylamine dehydrogenase facilitates electron transfer to electron transferring flavoprotein: Kinetics of transfer in wild-type and mutant complexes. *Biochemistry* **36**(1), 41-48.

Wilson, E. K., Mathews, F. S., Packman, L. C. & Scrutton, N. S. (1995). Electron-Tunneling In Substrate-Reduced Trimethylamine Dehydrogenase - Kinetics Of Electron-Transfer and Analysis Of the Tunneling Pathway. *Biochemistry* **34**(8), 2584-2591.

Wilson, E. K., Scrutton, N. S., Colfen, H., Harding, S. E., Jacobsen, M. P. & Winzor, D. J. (1997b). An ultracentrifugal approach to quantitative characterization of the molecular assembly of a physiological electron-transfer complex - The interaction of electron-transferring flavoprotein with trimethylamine dehydrogenase. *European Journal Of Biochemistry* **243**(1-2), 393-399.

Wilson, K. & Walker, J. (1994). *Principles and Techniques of Practical Biochemistry*, Cambridge University Press, Cambridge.

Windass, J. D., Worsey, M. J., Pioli, E. M., Pioli, D., Barth, P. T., Atherton, K. T., Dart, E. C., Byrom, D., Powell, K. & Senior, P. J. (1980). Improved conversion of methanol to single-cell protein by *Methylophilus methylotrophus*. *Nature* **287**, 396-401.

Xia, Z.-X. & Mathews, F. S. (1990). Molecular structure of flavocytochrome b_2 at 2.4 A resolution. *Journal of Molecular Biology* **212**, 837-836.

Yang, C. C. (1997). Dimethylamine Dehydrogenase and the Recognition of Alkyl Ammonium Ions. Ph.D., University of Cambridge.

Yang, C. C., Packman, L. C. & Scrutton, N. S. (1995). The Primary Structure Of Hyphomicrobium-X Dimethylamine Dehydrogenase - Relationship to

Trimethylamine Dehydrogenase and Implications For Substrate Recognition. *European Journal Of Biochemistry* **232**(1), 264-271.

Yu, P. M., Boulton, A. A. & Tipton, K. F., Eds. (1995). Current neurochemical and neurological aspects of biogenic amines: their function, oxidative deamination, and inhibition. Vol. 106. Progress in Brain Research. Amsterdam: Elsevier.

Zhao, H. M. & Arnold, F. H. (1999). Directed evolution converts subtilisin E into a functional equivalent of thermitase. *Protein Engineering* **12**(1), 47-53.

Redox Cycles in Trimethylamine Dehydrogenase and Mechanism of Substrate Inhibition†

Peter Roberts,‡ Jaswir Basran,‡ Emma K. Wilson,‡ Russ Hille,§ and Nigel S. Scrutton*,‡

Department of Biochemistry, University of Leicester, Adrian Building, University Road, Leicester LE1 7RH, United Kingdom, and Department of Medical Biochemistry, The Ohio State University, Columbus, Ohio 43210

Received June 18, 1999; Revised Manuscript Received August 17, 1999

ABSTRACT: The steady-state reaction of trimethylamine dehydrogenase (TMADH) with the artificial electron acceptor ferricenium hexafluorophosphate (Fc^+) has been studied by stopped-flow spectroscopy, with particular reference to the mechanism of inhibition by trimethylamine (TMA). Previous studies have suggested that the presence of alternate redox cycles is responsible for the inhibition of activity seen in the high-substrate regime. Here, we demonstrate that partitioning between these redox cycles (termed the 0/2 and 1/3 cycles on the basis of the number of reducing equivalents present in the oxidized/reduced enzyme encountered in each cycle) is dependent on both TMA and electron acceptor concentration. The use of Fc^+ as electron acceptor has enabled a study of the major redox forms of TMADH present during steady-state turnover at different concentrations of substrate. Reduction of Fc^+ is found to occur via the 4Fe-4S center of TMADH and not the 6-*S*-cysteinyl flavin mononucleotide: the direction of electron flow is thus analogous to the route of electron transfer to the physiological electron acceptor, an electron-transferring flavoprotein (ETF). In steady-state reactions with Fc^+ as electron acceptor, partitioning between the 0/2 and 1/3 redox cycles is dependent on the concentration of the electron acceptor. In the high-concentration regime, inhibition is less pronounced, consistent with the predicted effects on the proposed branching kinetic scheme. Photodiode array analysis of the absorption spectrum of TMADH during steady-state turnover at high TMA concentrations reveals that one-electron reduced TMADH—possessing the anionic flavin semiquinone—is the predominant species. Conversely, at low concentrations of TMA, the enzyme is predominantly in the oxidized form during steady-state turnover. The data, together with evidence derived from enzyme-monitored turnover experiments performed at different concentrations of TMA, establish the operation of the branched kinetic scheme in steady-state reactions. With dimethylbutylamine (DMButA) as substrate, the partitioning between the 0/2 and 1/3 redox cycles is poised more toward the 0/2 cycle at all DMButA concentrations studied—an observation that is consistent with the inability of DMButA to act as an effective inhibitor of TMADH.

Trimethylamine dehydrogenase (TMADH;[1] EC 1.5.99.7) is an iron−sulfur-containing flavoprotein isolated from the bacterium *Methylophilus methylotrophus* W_3A_1. The enzyme catalyzes the oxidative demethylation of trimethylamine (TMA) to dimethylamine (DMA) and formaldehyde (*1*):

$$(CH_3)_3N + H_2O \rightarrow (CH_3)_2NH + CH_2O + 2H^+ + 2e^-$$

The enzyme is a homodimeric protein having a subunit molecular mass of 83 kDa. Each subunit contains a covalently linked 6-*S*-cysteinyl FMN cofactor and a bacterial ferredoxin-type 4Fe-4S center; each subunit also possesses 1 equiv of tightly bound ADP of unknown function (*1*−*7*) but which probably represents a vestigial remnant of an ancestral dinucleotide-binding domain (*7*, *8*). The physiological electron acceptor for TMADH is an electron-transferring flavoprotein (ETF) (*9*), comprising a $\alpha\beta$ dimer of molecular mass 62 kDa. ETF possesses 1 equiv of FAD and 1 equiv of AMP; the function of AMP remains unclear (*10*). ETF-bound FAD cycles between oxidized and (anionic) semiquinone oxidation states (*9*) and therefore acts physiologically as a one-electron acceptor of TMADH, although two-electron reduction of ETF can be achieved electrochemically (*11*).

Full reduction of TMADH requires three electrons per subunit, two for reduction of the FMN and a third for reduction of the 4Fe-4S center, but only two reducing equivalents are removed from substrate during catalysis. The distribution of reducing equivalents within the two-electron reduced enzyme generated by reduction with excess substrate favors the formation of flavin semiquinone and reduced 4Fe-4S center, with the magnetic moments of the two paramag-

† This work was funded by the Royal Society and the UK Biotechnology and Biological Sciences Research Council. N.S.S. is a Lister Institute Research Fellow.

* Corresponding author: Telephone +44 116 223 1337; Telefax +44 116 252 3369; email nss4@le.ac.uk.

‡ University of Leicester.

§ The Ohio State University.

[1] Abbreviations: TMADH, trimethylamine dehydrogenase; ETF, electron-transferring flavoprotein; PMS, phenazine methosulfate; DCPIP, dichlorophenolindophenol; Fc^+, ferricenium hexafluorophosphate; TMA, trimethylamine; DEMA, diethylmethylamine; EDMA, ethyldimethylamine; DMButA, dimethylbutylamine; DMA, dimethylamine; TMAC, tetramethylammonium chloride; FMN, flavin mononucleotide; FAD, flavin adenine dinucleotide; EPR, electron paramagnetic resonance.

10.1021/bi9914098 CCC: $18.00
Published on Web 10/23/1999

Scheme 1: Proposed Branching Mechanism for TMADH[a]

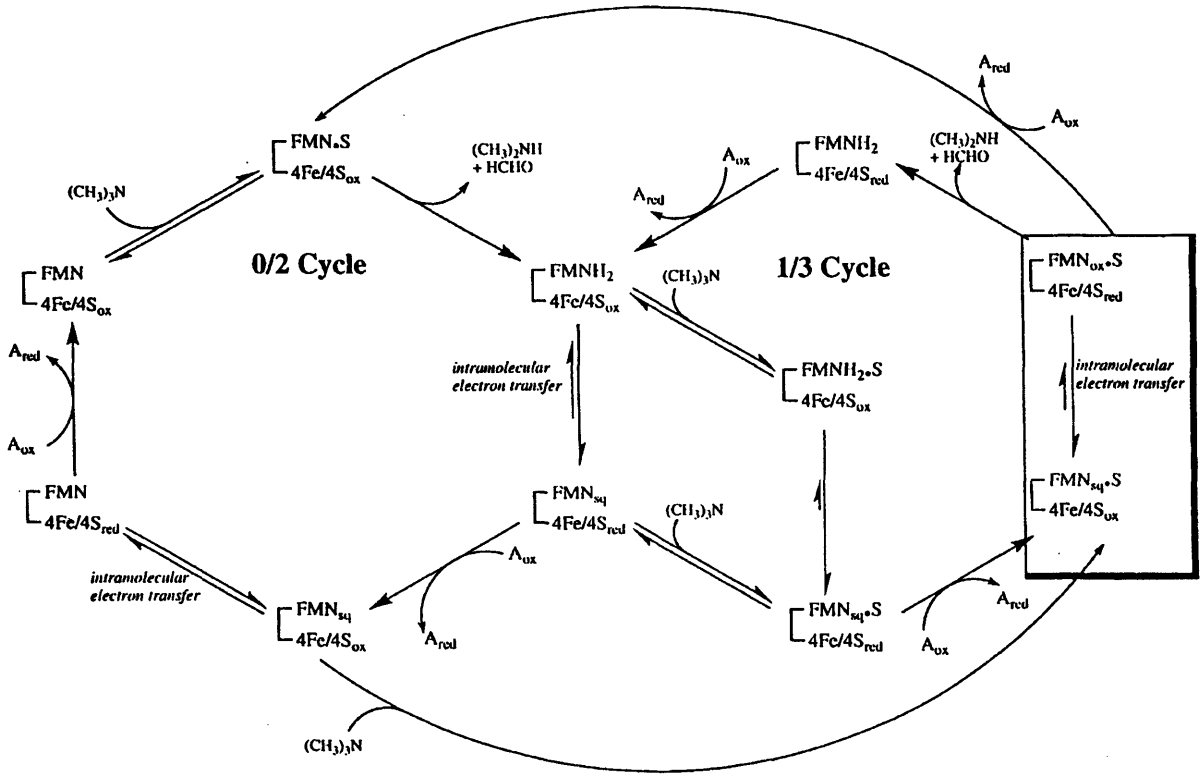

[a] In the 0/2 cycle, enzyme turns over between oxidized and two-electron reduced states; in the 1/3 cycle, enzyme turns over between one- and three-electron reduced states. Population of the 1/3 cycle leads to substrate inhibition of TMADH. The electron acceptor is represented by A.

netic centers interacting strongly to give a spin-interacting state (a triplet state). This triplet state is distinguished by a complex EPR signal centered near $g \sim 2$ and an unusually intense half-field $g \sim 4$ signal (*12*−*16*). Reduction of enzyme with dithionite in the presence of the substrate analogue and inhibitor tetramethylammonium chloride (TMAC) or by titration with dithionite at high pH also generates this characteristic spin-interacting state.

Previous stopped-flow and freeze-quench EPR kinetic studies have demonstrated that the reaction of TMADH with TMA or the slow substrate DEMA consists of three kinetic phases (*12*−*17*). On the basis of this work, an overall reductive half-reaction mechanism for TMADH has been proposed (*17*, *18*). The fast phase represents the two-electron reduction of the flavin cofactor (or, alternatively, formation of a covalent substrate−flavin adduct possessing an absorption spectrum comparable to that of reduced flavin) following cleavage of a C−H bond in one of the substrate methyl groups. The precise mechanism of C−H bond breakage remains unclear, but available evidence favors homolysis of the bond (*19*). The intermediate phase reflects the intramolecular electron transfer from reduced flavin to the 4Fe-4S center, generating flavin semiquinone and reduced iron−sulfur center. The slow phase involves dissociation of product and binding of a second substrate molecule, which perturbs the electron distribution in the partially reduced enzyme to facilitate formation of the spin-interacting state.

TMADH exhibits an unusual dependence on substrate concentration in steady-state reactions (*16*, *20*), being inhibited at high concentrations of TMA with either ETF or phenazine methosulfate (PMS) as electron acceptors. The mechanism of substrate inhibition has been debated. One mechanism posits an inhibitory substrate binding site distinct from the catalytically effective binding site (*20*), although there is no independent evidence for the existence of such an additional substrate binding site (*21*, *22*). Alternatively, we have suggested that TMADH can utilize two alternate catalytic cycles (*23*), cycling between oxidized and two-electron reduced enzyme (a 0/2 cycle) or one- and three-electron reduced enzyme (a 1/3 cycle), as depicted in Scheme 1. This situation arises because substrate donates two electrons, while ETF (or artificial acceptors such as PMS) takes up only one electron, and the enzyme itself can take up as many as three electrons. This model predicts that at low concentrations of TMA and/or high concentrations of oxidizing substrate, the 0/2 cycle predominates, and conversely at high [TMA] and/or low [oxidant], the 1/3 cycle is more important. The key to understanding excess substrate inhibition according to this model lies in the expectation that enzyme turnover in the 1/3 cycle, predominating at high concentrations of TMA, is expected to be slower than that in the 0/2 cycle. This is due to the fact that substrate binding stabilizes the semiquinone form of the flavin in one-electron reduced enzyme (*24*). Thus, binding of substrate to the partially reduced enzyme forms that accumulate in the steady-state under conditions of high substrate concentration must result in a redistribution of reducing equivalents, particularly in the case of $TMADH_{1e}^-$, such that the flavin center becomes reduced (boxed equilibrium, Scheme 1). In this situation, oxidation of the bound substrate cannot occur because the flavin is not able to accept a pair of reducing equivalents from substrate. The kinetic effect is equivalent

to excess substrate inhibition but, significantly, does not involve a second inhibitory substrate-binding site. An analogous mechanism has also been shown to account for the excess substrate inhibition observed with xanthine oxidase (*25*). In this paper, we present spectroscopic and kinetic evidence for the operation of Scheme 1 in steady-state reactions of TMADH and provide a mechanistic framework for understanding substrate inhibition in TMADH.

EXPERIMENTAL PROCEDURES

Enzymes and Materials. Ferricenium hexafluorophosphate was synthesized as described by Lehman et al. (*26*). Wild-type TMADH was purified from *Methylophilus methylotrophus* W_3A_1 as described by Steenkamp and Mallinson (*1*), incorporating the modifications of Wilson et al. (*27*). The concentrations of wild-type TMADH (per subunit) were determined spectrophotometrically at 443 nm (ϵ = 27 300 M^{-1} cm^{-1}; *6*). The Y442G mutant TMADH was isolated and purified as described by Wilson et al. (*28*). The enzyme as isolated possesses its full complement of 4Fe-4S center and ADP, but a significant portion of the enzyme lacks the flavin. By use of spectrophotometric methods reported elsewhere (*29*), the fraction of flavinylated enzyme in the Y442G preparations used in the present study was estimated as approximately 25%. As only the flavinylated portion of the recombinant protein is catalytically active, only this portion of the total enzyme contributes to the absorbance changes seen in the experiments reported here. The concentration of the Y442G mutant of TMADH was determined by use of an effective extinction coefficient (19 000 M^{-1} cm^{-1} at 443 nm) for oxidized enzyme, calculated from the extent of the spectral change elicited by excess substrate (only the flavinylated enzyme is reducible by substrate).

Kinetic Assays. Steady-state kinetic measurements were performed in 20 mM potassium phosphate buffer, pH 7.0, with a 1-cm light path in a final volume of 1 mL. The desired concentrations of TMA and Fc^+ were obtained by making microliter additions from stock solutions to the assay mix. Reactions were initiated by the addition of Fc^+, and the reaction followed by the decrease in absorption at 300 nm due to reduction of Fc^+ (ϵ = 4300 $M^{-1}cm^{-1}$) with a Hewlett-Packard 8452A single-beam diode array spectrophotometer. All data were collected at 30 °C. Some experiments required the use of high concentrations of TMA (>100 mM), which is positively charged at pH 7.0. Control experiments in which the total ionic strength was maintained throughout the concentration range (by the addition of KCl at lower [TMA]) indicated no significant difference in steady-state behavior compared with those reactions performed without the addition of KCl. Data were fitted by the fitting program Grafit (*30*) to the following equation that describes substrate inhibition in TMADH (*20*, *31*):

$$v = \frac{\left(1 + \frac{b[S]}{K_i}\right)V_{max}}{1 + \frac{K_s}{[S]} + \frac{K_s}{K_i} + \frac{[S]}{K_i}} \quad (1)$$

where b is a factor by which the intrinsic maximum velocity is affected. The remaining terms have their usual meanings.

Stopped-Flow Spectroscopy. Stopped-flow experiments were performed on an Applied Photophysics SX.17MV stopped-flow spectrophotometer. Spectral monitoring of the redox-active centers in TMADH during single-turnover and steady-state reactions was performed with a photodiode array detector. Spectral deconvolution was performed by global analysis and numerical integration methods using PROKIN software (Applied Photophysics). For single-wavelength studies, data collected at 443 nm were analyzed by nonlinear least-squares regression on an Archimedes 410-1 microcomputer using Spectrakinetics software (Applied Photophysics). Experiments were performed by mixing TMADH contained in buffer of the desired pH with an equal volume of substrate present at the desired concentration in the same buffer. In single-turnover experiments, the concentration of limiting substrate (Fc^+) was minimally 10-fold greater than that of TMADH, thereby ensuring pseudo-first-order conditions. For each substrate concentration used, at least four replicate measurements were collected and averaged. Substrate-reduced TMADH is quite stable to reoxidation in aerobic environments (half-life about 50 min; *27*), and consequently these stopped-flow experiments were carried out under aerobic conditions. Studies of electron transfer from dithionite-reduced TMADH to Fc^+ were conducted anaerobically. The sample-handling unit of the stopped-flow instrument was contained within a glovebox (Belle Technology Ltd) as described (*32*).

The absorbance change at 443 nm for reduction of TMADH by substrate was essentially monophasic, with a single rate constant obtained from fits of the data to

$$A_{443} = Ce^{-k_{obs}t} + b \quad (2)$$

where C is the amplitude of the phase and b is the final absorbance. As shown previously (*17*, *19*), the observed rate constants were found to exhibit hyperbolic dependence on substrate concentration and the reaction sequence was modeled as shown in the general scheme:

$$TMADH_{ox} + TMA \overset{K_d}{\rightleftharpoons} TMADH_{ox}\cdot TMA \xrightarrow{k_{red}} TMADH_{red} + P \quad (3)$$

Data were then fitted to obtain related K_d and k_{red} values from $k_{obs} = k_{red}[S]/(K_d + [S])$ (*33*). As for reactions performed with ETF, transients for the reoxidation of three-electron reduced TMADH and one-electron reduced, phenylhydrazine-inactivated TMADH by Fc^+ were biphasic. Rate constants were calculated as described previously (*23*).

Selective Inactivation of Redox-Active Centers in TMADH. The 6-*S*-cysteinyl FMN of TMADH was inactivated with phenylhydrazine to produce a redox-inert 6-*S*-cysteinyl FMN C4a phenyl adduct (*6*, *34*). Phenylhydrazine-inactivated TMADH solutions were made anaerobic in a tonometer equipped with a ground joint for the dithionite titration syringe, a sidearm cuvette, and a three-way stopcock valve with a male Luer connector. The sample was alternately evacuated and flushed with oxygen-free argon. Reduced samples were prepared by titration with an anaerobic dithionite solution, and the reaction was followed spectrophotometrically by monitoring the absorbance from 350 to 450 nm. The iron−sulfur center of TMADH was selectively

inactivated by treatment with Fc^+ at pH 10, essentially as described by Huang et al. (*23*). The protein (30 μM) was incubated with Fc^+ (3 mM) contained in 50 mM potassium borate buffer, pH 10, at room temperature for 3 h. Excess oxidant was removed by size-exclusion chromatography using Sephadex G-25 equilibrated in 20 mM potassium phosphate buffer, pH 7. It has been shown that TMADH treated in this way can be reduced by TMA but is unable to pass electrons on to the physiological electron acceptor, ETF (*23*).

RESULTS

Artificial Electron Acceptors and the Direction of Electron Flow in TMADH. In steady-state studies of TMADH, artificial electron acceptors are routinely used in place of the physiological acceptor ETF. This arises because of the constraints in using a protein molecule as a substrate in steady-state reactions—the concentrations of oxidizing substrate required for routine analysis make the use of ETF impracticable and, due to the large absorbance of ETF in the 450 nm region, frequently not feasible. PMS and dichlorophenolindophenol (DCPIP) have been used widely in previous studies of TMADH (*1*, *16*). However, their intense absorption in the visible region makes these acceptors unsuitable for studies in which spectral changes associated with the redox-active centers of TMADH are monitored in the course of an enzyme-monitored turnover experiment. For this reason, we have used Fc^+ as an alternative electron acceptor. This electron acceptor produces less interference than PMS in the informative regions of the visible spectrum (350−450 nm), enabling spectroscopic characterization of the enzyme during steady-state turnover (Figure 1). In using Fc^+, however, it is important to establish that, like ETF, electron transfer occurs via the 4Fe-4S center of TMADH and not the 6-*S*-cysteinyl FMN. In principle, the 6-*S*-cysteinyl-FMN, 4Fe-4S cluster, or both redox centers could donate an electron to Fc^+.

The physiological route of electron transfer in TMADH is from the 6-*S*-cysteinyl FMN to the 4Fe-4S center and then to ETF (*23*, *28*), but the possibility of direct electron transfer from the flavin to Fc^+ must be considered. To determine whether Fc^+ can reoxidize directly the flavin of TMADH, the 4Fe-4S center of TMADH was selectively inactivated as described previously (*23*). Upon reduction by substrate, the flavin center of Fc^+ -inactivated TMADH cannot be oxidized by Fc^+ in either steady-state or stopped-flow single-turnover experiments, indicating that Fc^+ can only accept electrons from the 4Fe-4S center of TMADH. Evidence for competent electron transfer from the 4Fe-4S center to Fc^+ was obtained by inactivating the 6-*S*-cysteinyl FMN by treatment with phenylhydrazine, thereby producing the redox-inert phenyl-4a adduct of the 6-*S*-cysteinyl FMN (see refs *23* and *28*). In this case, it was found that Fc^+ was able to reoxidize dithionite-reduced protein (11.7 μM), as followed at 300 nm by stopped-flow. Under the reaction conditions used (50 mM potassium phosphate buffer, pH 7, 25 °C), reduced phenylhydrazine-inactivated TMADH was able to rapidly reduce Fc^+ (at a concentration of 100 μM), with an observed rate constant for the fast phase of 407 ± 14 s^{-1}. These experiments demonstrate that Fc^+ accepts electrons only from the reduced 4Fe-4S cluster of TMADH and not from the 6-*S*-cysteinyl FMN, and in this regard the flow of

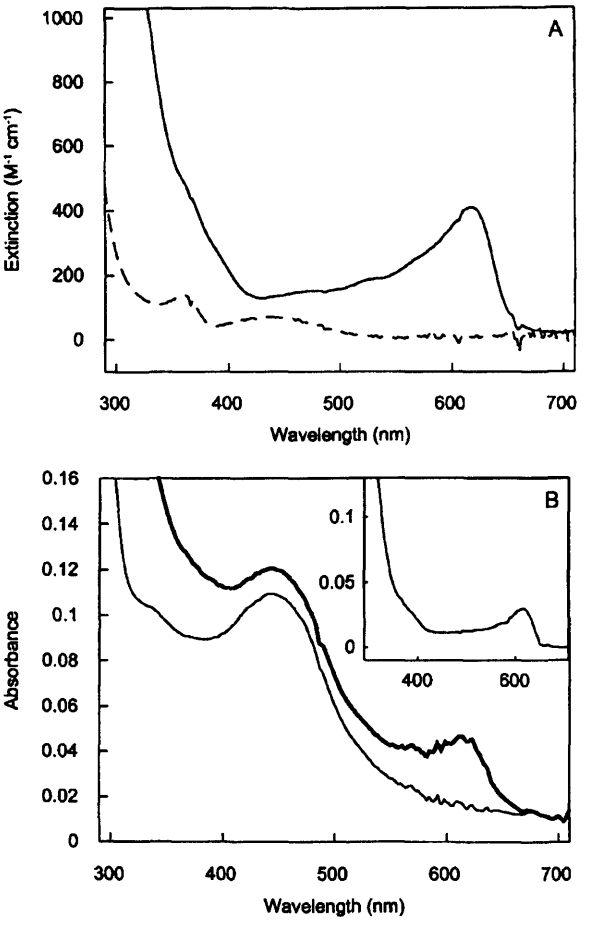

FIGURE 1: Spectra of oxidized and reduced Fc^+ and effects on the spectrum of oxidized TMADH. (A) Oxidized (solid line) and reduced (dashed line) Fc^+ in 20 mM potassium phosphate buffer, pH 7.0. (B) Spectrum of oxidized TMADH (4 μM) and oxidized TMADH (4 μM) plus Fc^+ (100 μM). (Inset) Difference spectrum showing contribution made by Fc^+.

electrons during catalysis is comparable to that seen with the physiological redox acceptor, ETF (*23*).

Replacement of Tyr-442 by glycine on the surface of TMADH has been shown to substantially compromise electron transfer from TMADH to ETF (*28*). The precise role of Tyr-442 in native TMADH remains to be established, but its exchange for glycine both destabilizes the electron-transfer complex formed with ETF (with K_d increasing from 10 to 180 μM) and reduces the limiting rate constant for electron transfer within the TMADH·ETF complex, by about 30-fold (from 170 s^{-1} to 6 s^{-1}). It was of interest to investigate the ability of the Y442G mutant TMADH to reduce Fc^+. Any differential behavior with respect to electron-transfer rate between the wild-type and Y442G TMADH would establish that the productive binding site for Fc^+ is in this region of the protein. Samples of the wild-type and Y442G enzymes were each made anaerobic and fully reduced with dithionite as described (*23*). Each sample was then rapidly mixed with Fc^+ in the stopped-flow apparatus and reoxidation of the enzyme was monitored at 440 nm. This wavelength simultaneously monitors reoxidation of the 4Fe-4S center and the flavin. As expected—and as seen with ETF (*23*) as electron acceptor—the kinetic transients were more complex (approximated to biphasic

behavior), due to the sequential transfer of three electrons to Fc^+. However, the fast phase for each enzyme was clearly resolved from the rest of the absorbance changes. This first phase corresponds to a single electron transfer from the 4Fe-4S center of three-electron reduced TMADH to Fc^+.[2] From plots of the observed rate constant k_{obs} versus Fc^+ concentration, second-order rate constants of $(4.3 \pm 0.1) \times 10^6$ M^{-1} s^{-1} and $(2.3 \pm 0.03) \times 10^6$ M^{-1} s^{-1} were calculated for wild-type and Y442G TMADH, respectively (Figure 2). The data indicate that Tyr-442 plays only a modest role in facilitating electron transfer to Fc^+. The substantially larger effect with ETF (300-fold as compared to Fc^+) most likely reflects the specific role of Tyr-442 in directing specific protein−protein interactions during formation of the TMADH·ETF electron-transfer complex.

Steady-State Assays with Fc^+ as Electron Acceptor. Because prolonged incubation (over several hours) of TMADH with Fc^+ at pH 10 leads to inactivation of the enzyme (*23*), the possibility of enzyme inactivation is a major concern in any experiment that makes use of Fc^+ as electron acceptor. The success of any assay procedure depends on whether inactivation by Fc^+ can be prevented or suppressed on the time scale of the assay. At pH 7.0, preincubation of TMADH and Fc^+ for about 30 s prior to the addition of TMA does indeed reduce the observed initial velocity compared with reactions initiated by addition of Fc^+. Loss of activity increases with incubation time, indicating that preincubation with Fc^+ effects an irreversible inactivation of TMADH. However, when assays are initiated by adding Fc^+ or enzyme, the measured rates are linear over the time course of the experiment (typically between 30 and 60 s), contrary to the curvilinear traces expected for progressive inactivation of TMADH. Moreover, linear traces were obtained irrespective of the Fc^+ concentration, indicating that enzyme inactivation is negligible under the assay conditions employed. In the steady-state analyses described below, all reactions were initiated by the addition of Fc^+ to avoid inactivation of TMADH.

As originally reported by Steenkamp and Beinert (*16*), TMADH is inhibited by high concentrations of the physiological substrate TMA with PMS and DCPIP as electron acceptors. As shown in Figure 3, the same is found to be true when Fc^+ is used as oxidant. As with PMS and DCPIP, the degree of substrate inhibition is also affected by the Fc^+ concentration: at low Fc^+ concentrations, inhibition is more pronounced, whereas at high Fc^+ concentrations, the degree of inhibition is less marked. This observation is consistent with a mechanism in which substrate inhibits enzyme by formation of a catalytically nonproductive complex with partially reduced enzyme (Scheme 1). In this mechanism, high concentrations of Fc^+ will favor partitioning into the 0/2 redox cycle rather than the catalytically compromised 1/3 cycle.

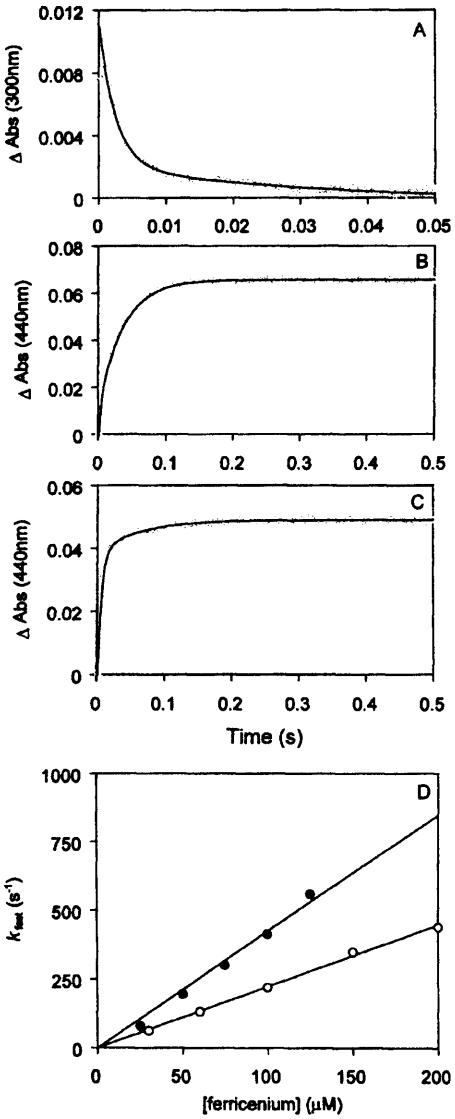

FIGURE 2: Transients and plots of the rate of electron transfer from the 4Fe-4S center of dithionite-reduced TMADH as a function of Fc^+ ion concentration for the wild-type and Y442G enzymes. (A) Transient observed at 300 nm for the reaction of phenylhydrazine-inactivated TMADH (4 μM) and Fc^+ (100 μM), $k_{fast} = 407$ s^{-1}; (B) transient observed at 440 nm for dithionite-reduced (three-electron reduced) TMADH (4 μM) and Fc^+ (100 μM), $k_{fast} = 423$ s^{-1}, $k_{slow} = 28$ s^{-1}; (C) transient observed at 440 nm for dithionite-reduced (fully reduced) Y442G TMADH (4 μM) and Fc^+ (100 μM), $k_{fast} = 220$ s^{-1}, $k_{slow} = 17$ s^{-1}. (D) Rate constants (fast phase) for the electron transfer from dithionite-reduced TMADH (three-electron reduced) and Y442G TMADH (fully reduced) to Fc^+ calculated from the absorbance changes at 440 nm by fitting to a double-exponential process: (●) observed rate constants for the wild-type enzyme; (○) observed rate constants for the Y442G mutant enzyme. The data were used to calculate second-order rate constants of $(4.2 \pm 0.1) \times 10^6$ M^{-1} s^{-1} and $(2.3 \pm 0.03) \times 10^6$ M^{-1} s^{-1} for the wild-type and Y442G mutant TMADH reactions, respectively. For all panels, the reaction components were contained in 50 mM potassium phosphate buffer, pH 7, and reactions were conducted at 25 °C.

Other, nonphysiological substrates for TMADH were also examined for excess substrate inhibition. Of the substrates investigated, ethyldimethylamine (EDMA), diethylmethylamine (DEMA), and triethylamine (TEA) were all found

[2] This phase was assigned to electron transfer from the 4Fe-4S center on the basis of the spectral change associated with this phase of the reaction for the wild-type and mutant protein. The amplitude of this phase contributed about 70% of the total absorbance change for the Y442G mutant and 25% for the wild type. The difference in amplitude is expected because the Y442G mutant is isolated as a mixture of flavinylated (~25%) and deflavo (~75%) enzyme and therefore only a relatively small proportion of the Y442G enzyme sample is reduced at the level of three electrons.

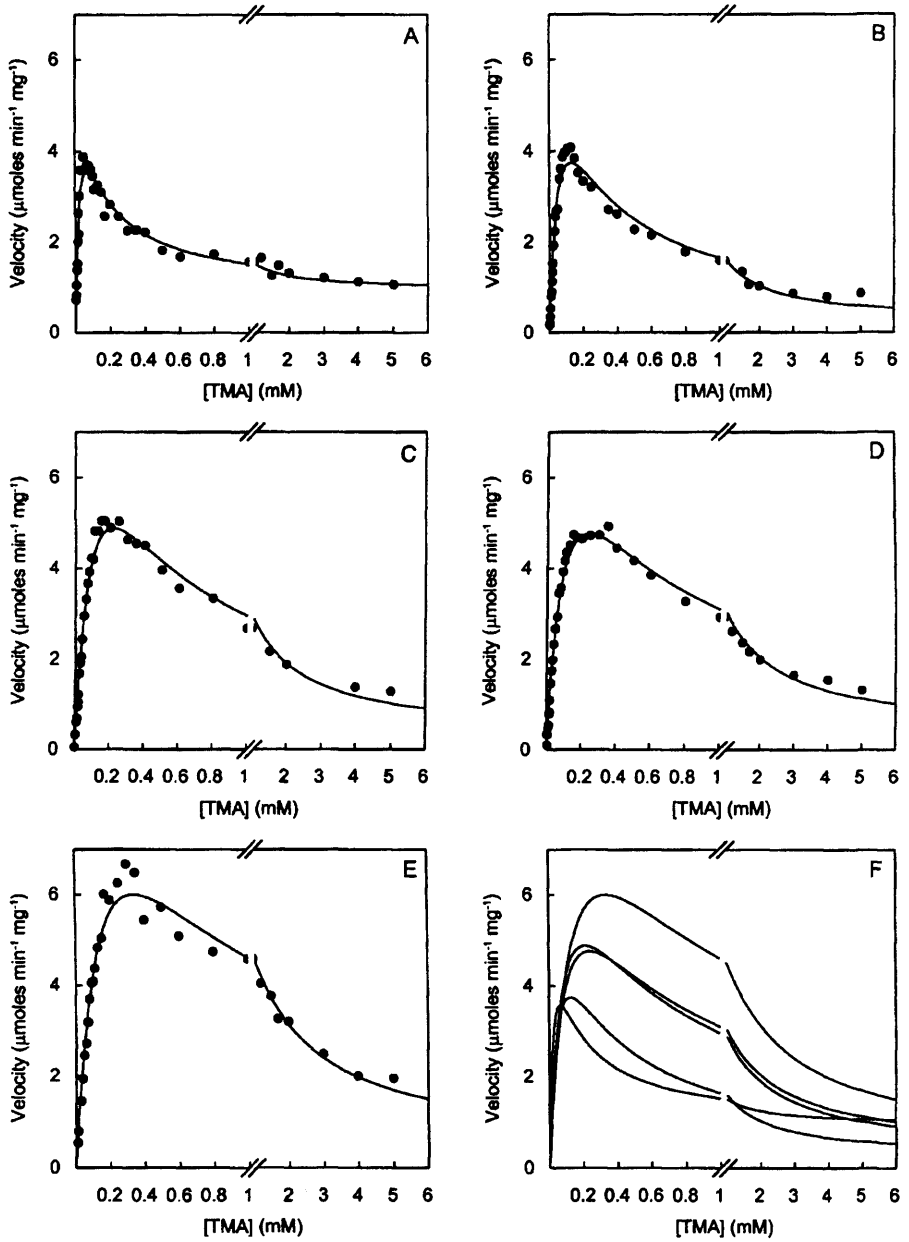

FIGURE 3: Plots of initial velocity against substrate concentration for reactions of TMADH with TMA and Fc^+. Reaction components were contained in 20 mM potassium phosphate buffer, pH 7, and the reactions were initiated by the addition of Fc^+. Assays were performed at 30 °C. Fc^+ concentrations are (A) 50 μM, (B) 100 μM, (C) 200 μM, (D) 300 μM, and (E) 400 μM. (F) Overlay of the fits for each data set shown in panels A–E. Data are fitted with eq 1.

to inhibit TMADH at high concentrations (Figure 4; Table 1); only *n*-butyldimethylamine (DMButA) did not display marked substrate inhibition. DMButA was therefore chosen for further spectroscopic analysis and comparison with the physiological reductant TMA (see below). Single-turnover stopped-flow studies of flavin reduction with DMButA as substrate revealed that flavin reduction is substantially compromised, even though the dissociation constant of the enzyme–substrate complex is reduced (Figure 5; Table 2). The latter finding is important since tight binding of the substrate by TMADH might affect partitioning between the 0/2 and 1/3 cycles of Scheme 1 (see Discussion). A prediction of Scheme 1 is that the rate of flavin reduction is not a factor responsible for partitioning between the two redox cycles. In agreement with this prediction, stopped-flow studies with TEA, for example, revealed it to be a very poor substrate (Figure 5; Table 2) but one that still gives clear steady-state inhibition (Figure 4).

Spectroscopic Analysis of TMADH during Steady-State Reactions with TMA. Stopped-flow studies of the reaction of TMADH with TMA have enabled deconvolution of the spectral forms of intermediates encountered in the reductive half-reaction (Figure 6). Four characteristic spectra are produced: that of the oxidized enzyme, two-electron reduced (dihydroquinone), two-electron reduced (flavin semiquinone and reduced iron-sulfur center), and the so-called spin-interacting state (*12*–*16*). The one- and three-electron reduced forms of TMADH are not observed in single-

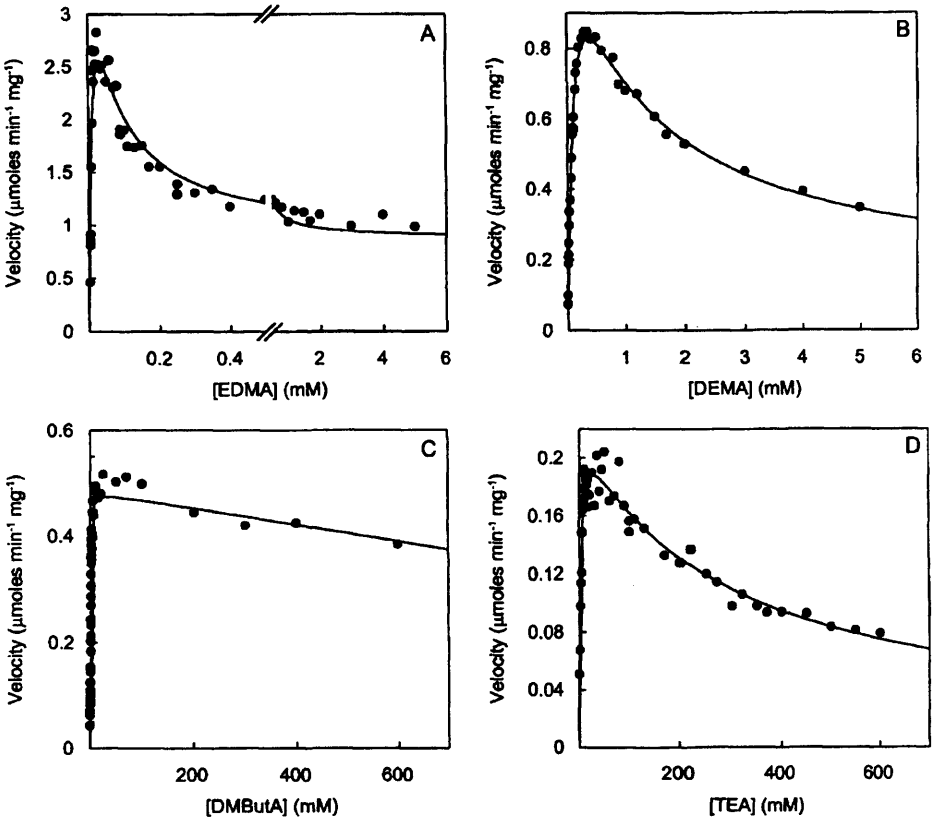

FIGURE 4: Plots of initial velocity against substrate concentration for reactions of TMADH with nonphysiological amines and Fc^+. Reaction conditions were as for Figure 3; Fc^+ concentration was 100 μM. (A) EDMA; (B) DEMA; (C) DMButA; (D) TEA. Data are fitted with eq 1.

Table 1: Steady-State Parameters for the Reaction of TMADH with Various Amine Substrates[a]

substrate	K_m (μM)	K_i (μM)	b	k_{cat} (s^{-1})	k_{cat}/K_m ($\times 10^3$) (M^{-1} s^{-1})
TMA	128 ± 16	120 ± 16	0.14 ± 0.01	40.5 ± 5	317 ± 79
EDMA	23.5 ± 3.8	25.3 ± 3.8	0.10 ± 0.02	23.7 ± 4	1009 ± 310
DEMA	111 ± 17	1009 ± 280	0.1 ± 0.03	3.8 ± 0.4	34.2 ± 8.4
TEA	2614 ± 330	25820 ± 6800	0.05 ± 0.09	0.6 ± 0.02	0.23 ± 0.04
DMButA	382 ± 20	($2 \times 10^{11} \pm 8 \times 10^{12}$)	($7 \times 10^4 \pm 3 \times 10^6$)	0.11 ± 0.01	0.29 ± 0.005

[a] Reactions were performed in 20 mM potassium phosphate buffer, pH 7.0 at 30 °C, and were initiated by the addition of Fc^+. Fc^+ concentration was 100 μM. The poor ability of DMButA to inhibit TMADH in the high-substrate regime prevents meaningful evaluation of K_i and b for this substrate (figures are shown in parentheses). b is a factor that affects the intrinsic maximum velocity that would be obtained if the 1/3 cycle was not populated at saturating levels of substrate. K_m and k_{cat} values are apparent values, since eq 1 does take take into account Fc^+ concentration.

turnover studies, however, although they undoubtedly accumulate in the course of steady-state turnover.

Direct evidence for the operation of alternate redox cycles of the type shown (Scheme 1) was obtained by performing enzyme-monitored turnover experiments (*35*) with diode array detection in which TMADH was reacted in the stopped-flow with a mixture of TMA and Fc^+. In these turnover experiments, the concentration of TMADH was maintained at 4 μM, and Fc^+ was present at 100 μM. The reaction was monitored between 350 and 550 nm, the most informative region of the enzyme spectrum, where Fc^+ contributes little to the observed spectral change (Figure 1); reduction of Fc^+ can be monitored independently in the course of this experiment at 617 nm. Enzyme-monitored turnover experiments were performed over a range of TMA concentrations (20, 55, 100, and 500 μM and 2 mM) at 100 μM Fc^+. Depending on the TMA concentration, the minimum steady-state period observed extended over 5 s. As expected, the concentration of TMA profoundly affects the spectrum obtained during steady-state turnover. At high TMA concentrations (e.g., 500 μM and 2 mM), the spectrum exhibits a high absorption at 365 nm that is characteristic of the anionic flavin semiquinone (Figure 7, panels D and E). However, the relatively large absorption at 440 nm also indicates the iron–sulfur center of TMADH is substantially oxidized (compare with the spectrum of two-electron reduced TMADH with one electron in the flavin and one in the iron–sulfur center; Figure 6). The data therefore indicate that one-electron reduced TMADH (flavin semiquinone/oxidized iron–sulfur center) is the predominant species present during steady-state turnover at high concentrations of TMA. It is this form of TMADH that is predicted to accumulate during steady-state turnover in the 1/3 cycle of Scheme 1, concomitantly with the observation of excess substrate inhibition. In reactions performed at low concentrations of TMA (20 μM), on the other hand, the steady-state spectrum reflects

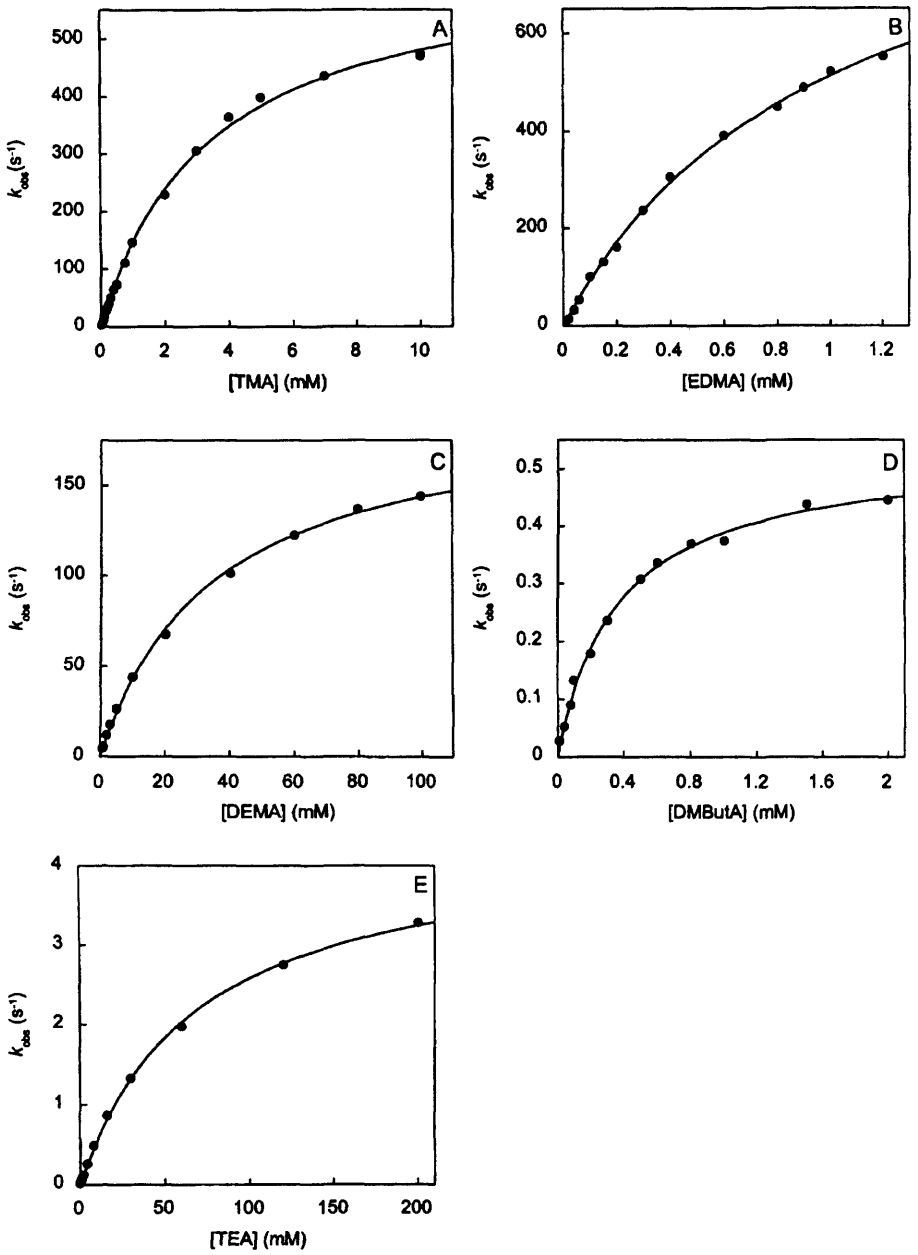

FIGURE 5: Plots of observed rate constants for flavin reduction against substrate concentration for reactions of TMADH with various amine substrates. Reactions were performed in 20 mM potassium phosphate buffer, pH 7.0 at 25 °C. Flavin reduction was monitored at 443 nm and data were fitted to eq 2. Enzyme–substrate dissociation constants and limiting rates for flavin reduction are given in Table 2.

Table 2: Kinetic Parameters for Flavin Reduction Determined by Stopped-Flow Analysis of the Reaction of TMADH with Various Amine Substrates

substrate	K_d (mM)	k_{red} (s^{-1})	k_{red}/K_d ($\times 10^3$) (M^{-1} s^{-1})
TMA	3.4 ± 0.2	643 ± 12	190 ± 12
EDMA	1.0 ± 0.1	1021 ± 35	1031 ± 98
DEMA	35 ± 2	193 ± 4	5.6 ± 0.4
TEA	70 ± 2	4.4 ± 0.1	0.06 ± 0.003
DMButA	0.36 ± 0.02	0.53 ± 0.01	1.5 ± 0.1

only a small quantity of anionic flavin semiquinone. Under these conditions the enhanced absorption at 365 nm seen at high TMA concentrations is lost (Figure 7, A). The steady-state spectrum is similar to that of oxidized TMADH (increased absorption at 443 nm and loss of signature at 365 nm), indicating that oxidized enzyme is the predominant species at low substrate concentrations. Clearly, in this regime, the 1/3 catalytic cycle does not predominate, and the majority of the catalytic throughput is through the 0/2 cycle. At intermediate TMA concentrations (55 and 100 μM) an intermediate situation is observed in which the 365 nm absorption indicative of the 1/3 cycle is present but is much less intense than that seen at high TMA concentrations (Figure 7B,C). Additionally, the 443 nm absorbance is higher than that seen with reactions performed with high concentrations of TMA. In this intermediate regime, therefore, both the 0/2 and 1/3 cycles appear to operate.

Upon reduction of the Fc^+ concentration to 50 μM, the absorbance spectrum of the enzyme indicates that anionic

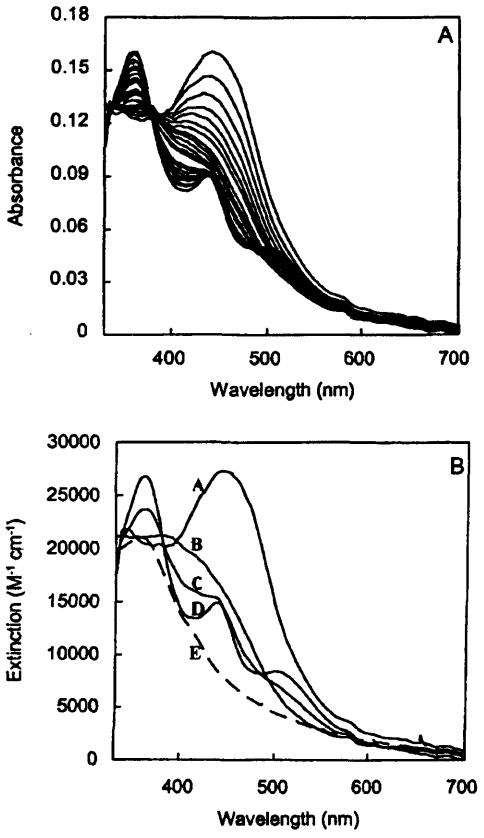

FIGURE 6: Time-dependent spectral changes for TMADH in single-turnover reactions with TMA. TMADH (7.5 μM) was rapidly mixed with TMA (125 μM) at pH 7.5. (A) Time-dependent spectral changes; the first spectrum is recorded 1.28 ms after mixing (for clarity, only selected subsequent spectra are shown). (B) Spectra of the intermediate forms during the course of the reductive half-reaction generated by global analysis and numerical integration methods with ProKin software (Applied Photophysics Ltd). Spectrum A, oxidized enzyme; spectrum B, two-electron reduced enzyme (dihydroflavin); spectrum C, two-electron reduced enzyme (flavin semiquinone and reduced iron–sulfur center); spectrum D, spin-interacting state of TMADH. The spectral changes are shown for a single-turnover reaction at pH 7.5 rather than pH 7.0 because at the latter pH value the flavin reduction and internal electron transfer steps are not fully resolved, leading to kinetic mixing effects (*19*). Under these conditions the spectral forms of the intermediate redox states cannot be deconvoluted. The spectrum of three-electron reduced TMADH (generated under anaerobic conditions by titration with sodium dithionite) is illustrated (dashed spectrum).

flavin semiquinone/oxidized iron–sulfur center are the predominant redox states present in TMADH at all TMA concentrations investigated (20 μM, 500 μM, and 2 mM; Figure 7F). In other words, the switch from the 1/3 cycle to the 0/2 cycle (Scheme 1) that is seen with 100 μM Fc^+ does not occur when the Fc^+ concentration is reduced to 50 μM. The data thus indicate that partitioning between the two redox cycles is critically dependent on both TMA and Fc^+ concentration, as predicted by Scheme 1, and demonstrate that as the ratio of reducing to oxidizing substrate increases, the level of enzyme reduction in the steady-state also increases.

Spectroscopic Analysis of TMADH during Steady-State Reactions with DMButA. Steady-state assays demonstrated that the inhibition seen with DMButA is much less marked than that by other substrates (see above). Enzyme-monitored turnover experiments were therefore of interest, to ascertain whether the 0/2 cycle predominated to a greater extent than is seen with TMA in the experiments above. Reactions were performed with 100 μM Fc^+ and over a range of DMButA concentrations (100 μM, 20 mM, and 200 mM). In all cases, the spectra obtained during steady-state turnover show only incomplete development of the 365 nm absorption of the anionic semiquinone compared to the results obtained with TMA and a 440 nm absorbance similar to that of oxidized TMADH (Figure 8). Clearly, with DMButA as substrate the 1/3 cycle is populated to only a small extent during steady-state turnover and the majority of substrate oxidation occurs exclusively via the 0/2 cycle. This analysis thus provides an explanation for the lack of marked substrate inhibition seen with this nonphysiological substrate in the high-concentration regime.

Single-Wavelength Enzyme-Monitored Turnover Experiments. To more effectively correlate the properties of the enzyme in the steady state, enzyme-monitored turnover experiments were performed in which 4 μM enzyme was reacted with 100 μM Fc^+ and varying concentrations of TMA over the range 250 μM–2.0 mM (all concentrations after mixing). The reaction was followed at three wavelengths: 443 nm, monitoring the net level of enzyme reduction; 365 nm, monitoring the accumulation of the anionic flavin semiquinone in the course of the steady state; and 617 nm, monitoring the enzyme-catalyzed reduction of Fc^+ in the course of the reaction. The data are shown in Figure 9, where several qualitative trends are evident. First, excess substrate inhibition is manifested as a decrease in the slope of the 617 nm transients as the concentration of TMA increases and also in the trend toward longer time excursions as the [TMA] increases—as expected, it takes the enzyme longer to consume the (limiting) 100 μM Fc^+ at the higher concentrations of TMA. Second, an increased accumulation in anionic semiquinone in the steady state as [TMA] increases is evident as a loss of the pronounced bowing in the 365 nm transients in going from 250 μM to 2.0 mM TMA. This is more evident in a comparison of the excursions at 365 nm as a function of [TMA], as shown in Figure 10. The principal observation is that, as the model predicts, there is a substantial increase in the amount of semiquinone that accumulates in the steady state as the [TMA] increases. A comparison of the areas under the curves for the excursions at 365 nm indicates that the amount of semiquinone accumulating and persisting in the steady-state more than doubles in going from 250 μM to 2.0 mM. It is significant that the model in fact predicts this increased accumulation of flavin semiquinone at concentrations of TMA where excess substrate inhibition is observed.

An analysis of the transients at 443 nm at short time intervals permits an examination of the approach of the system to the steady-state. As shown in Figure 11, this approach to the steady state is increasingly rapid as the [TMA] increases, as expected given the known behavior of the fast phase of the reaction of enzyme with both DEMA and TMA (*17*, *19*). A transient "overreduction" of the enzyme is observed at all concentrations of TMA, due to the initial reduction of the flavin in the fast phase of the first turnover. This overshoot of the steady-state level of enzyme reduction increases with [TMA] as the reaction of enzyme with substrate in the first turnover goes increasingly

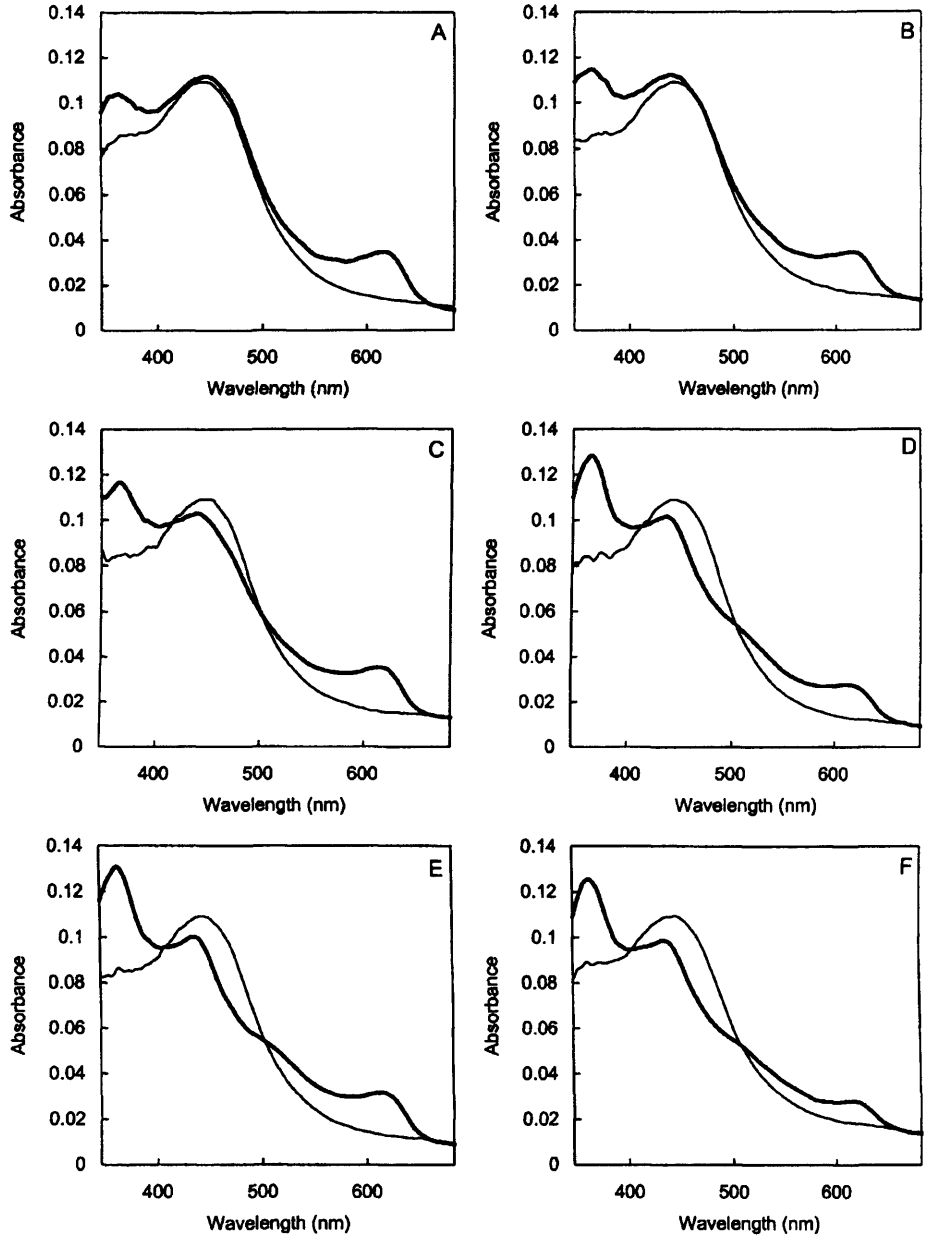

FIGURE 7: Spectral forms of TMADH observed during steady-state turnover with TMA and Fc^+. For reference, in all panels the spectrum of oxidized enzyme is indicated by the thinner line. (A) Steady-state spectrum (thick line) observed in the presence of 20 μM TMA and 100 μM Fc^+; (B) steady-state spectrum (thick line) observed in the presence of 55 μM TMA and 100 μM Fc^+; (C) steady-state spectrum (thick line) observed in the presence of 100 μM TMA and 100 μM Fc^+; (D) steady-state spectrum (thick line) observed in the presence of 500 μM TMA and 100 μM Fc^+; (E) steady-state spectrum (thick line) observed in the presence of 2 mM TMA and 100 μM Fc^+; (F) steady-state spectrum (thick line) observed in the presence of 20 μM TMA and 50 μM Fc^+. All reactions were performed in 20 mM potassium phosphate buffer, pH 7.0 at 25 °C.

to completion prior to entering the steady state, yielding the full absorbance change associated with reduction of the enzyme flavin. The rate constants obtained from this pre-steady-state portion of the 443 nm transients are 50 s^{-1}, 116 s^{-1}, and 286 s^{-1} at 100 μM, 500 μM, and 2 mM TMA, respectively. These values are entirely consistent with the observed rate constants for flavin reduction obtained from single-turnover stopped-flow studies (Figure 5). Once the steady state has been achieved, the absorbance at 443 nm rebounds considerably, reflecting a higher net level of oxidation in the steady state than the initial two-electron reduced form generated in the course of the fast phase of the first turnover.

A major advantage of the enzyme-monitored turnover experiments is that they permit a quantitative comparison of turnover and the status of the enzyme in the course of the steady state, and in particular a comparison of k_{cat} from the ΔA at 617 nm (following Fc^+ reduction explicitly) with that which can be obtained from the transients at 443 nm. Gibson et al. (*35*) have shown that for transients of the type seen at 443 nm in the present experiments, the area under the curve is proportional to the total concentration of limiting substrate

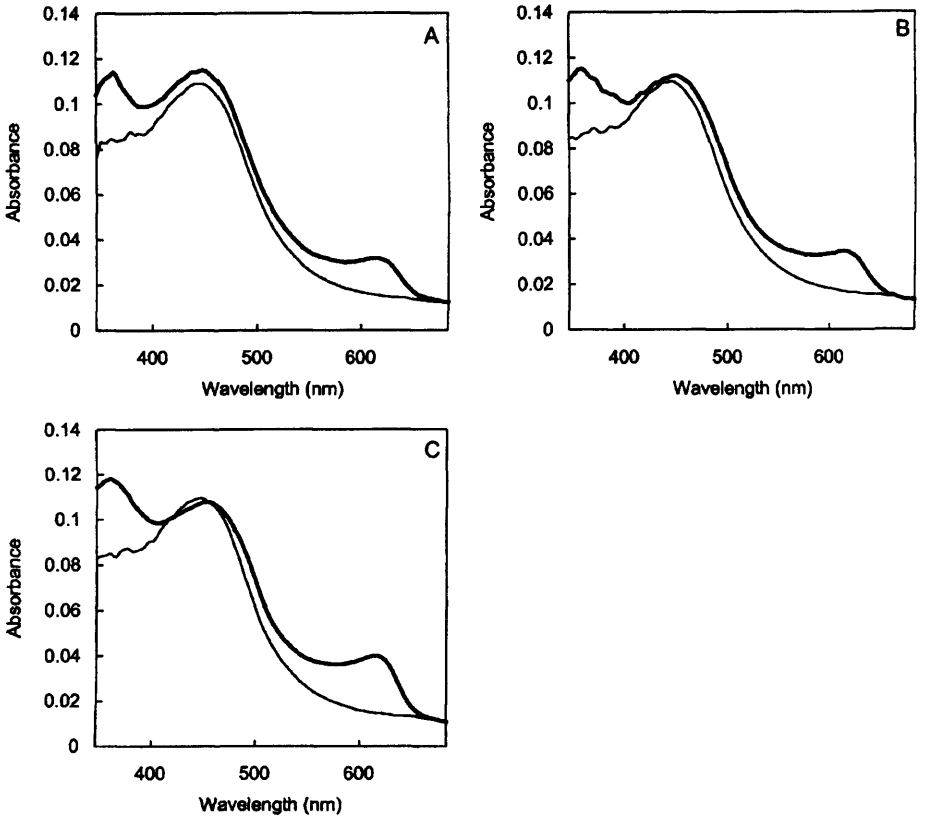

FIGURE 8: Spectral forms of TMADH during steady-state turnover with DMButA. For reference, in all panels the spectrum of oxidized enzyme is indicated by the thinner line. (A) Steady-state spectrum (thick line) observed in the presence of 100 μM DMButA and 100 μM Fc^+; (B) steady-state spectrum (thick line) observed in the presence of 2 mM DMButA and 100 μM Fc^+; (C) steady-state spectrum (thick line) observed in the presence of 200 mM DMButA and 100 μM Fc^+. All reactions were performed in 20 mM potassium phosphate buffer, pH 7.0 at 25 °C.

(in this case, Fc^+, at 100 μM). Turnover numbers at any point in the course of the transient can be obtained from the ratio of the area under the curve over any specific time interval to that of the total curve, yielding the consumption of oxidizing substrate (in the present case) per unit time. Table 3 shows the values for k_{cat} obtained over two time intervals in the transients: between 1 and 2 s and for a 1 s interval in the middle of the steady-state as determined by the 443 nm transient (the initial velocity value from the 617 nm transients over the 0−1 s interval are also given). Interestingly, there is a significant discrepancy between the 617 nm and enzyme-monitored turnover values for k_{cat} for the 1−2 s interval, particularly at the lower [TMA] concentrations (compare the values in columns 3 and 5 of Table 3). This discrepancy largely vanishes by the midpoint of the steady state, however, to within the error of the measurement in all likelihood (columns 4 and 6). This trend is evident in the transients themselves (Figure 9), as the 617 nm transient is distinctly bowed in the steady-state region (particularly at low [TMA]), whereas the absorbance at 443 nm changes relatively little in this region until the Fc^+ has been consumed at the end of the steady state. Again, this bowing in the 617 nm transients becomes significantly less pronounced at higher [TMA]. The 617 nm absorbance change must reflect the actual enzyme turnover, but the 443 nm transients better define the duration of the steady state. What the data indicate quite clearly is that over the course of the steady state, catalytic throughput decreases significantly, particularly at lower [TMA], precisely what the model predicts as the system switches over from the more efficient 0/2 cycle to the less efficient 1/3 cycle.

DISCUSSION

In this paper, we have attempted to correlate the known effects of substrate and inhibitor binding with the mechanism of inhibition of TMADH by substrate under steady-state conditions. Previous studies with TMADH have demonstrated an interaction between the FMN and 4Fe-4S centers that is profoundly influenced by binding of substrate or the substrate analogue TMAC (*13*, *16*). The distribution of the reducing equivalents within two-electron reduced TMADH is known to be influenced strongly by substrate and pH: for dithionite-reduced enzyme at low pH (pH 6), the distribution favors dihydroflavin and oxidized 4Fe-4S center (*18*); at high pH (pH 10), formation of flavin semiquinone and reduced 4Fe-4S center is favored, with the magnetic moments of the two paramagnetic centers interacting strongly to give a spin-interacting state (triplet state), which is distinguished by a complex EPR signal centered near $g \sim 2$ and an unusually intense half-field $g \sim 4$ signal (*12*−*16*, *18*, *36*). In addition, binding of the substrate analogue TMAC is known to perturb the reduction potentials of the flavin center. On binding TMAC, the potential for the quinone/semiquinone couple increases from +44 mV to +240 mV at pH 7.0 (*24*, *37*), while that of the semiquinone/hydroquinone couple decreases from +36 to −50 mV. The effect is not simply to stabilize

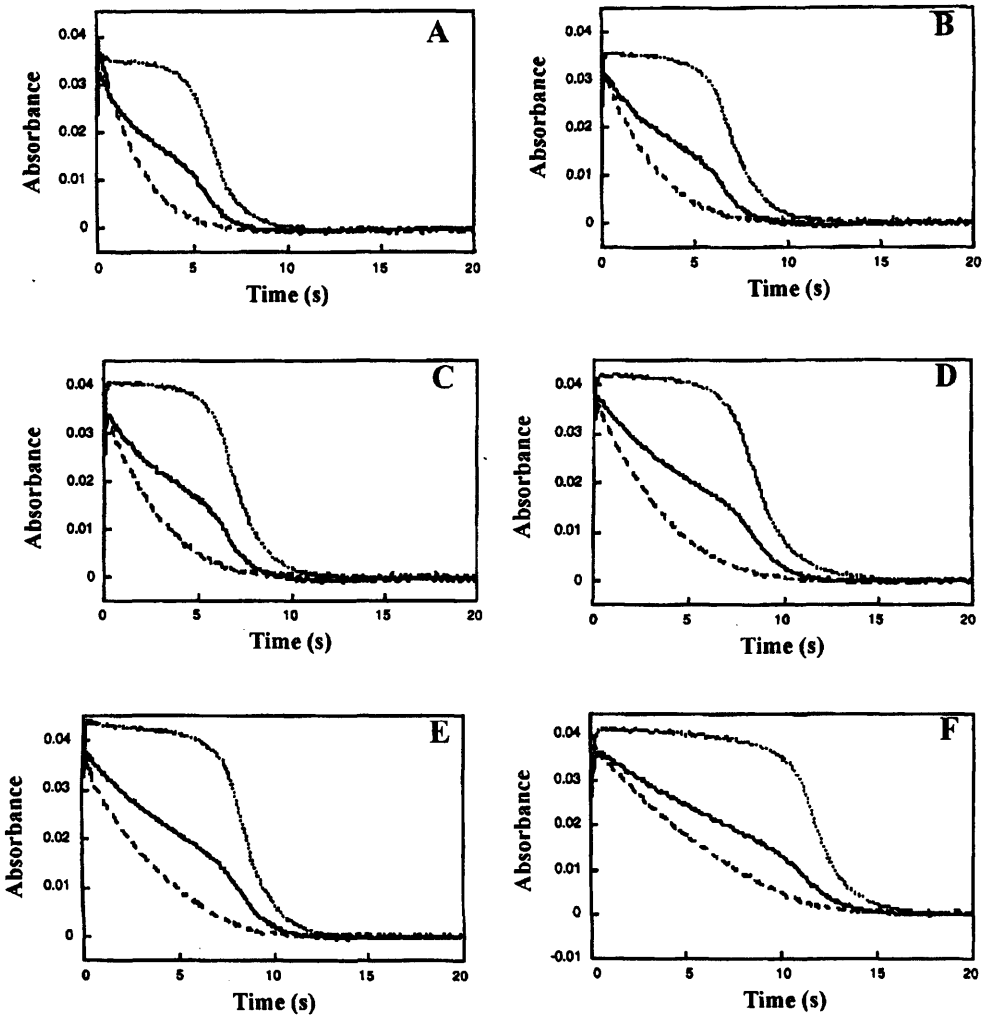

FIGURE 9: Transients obtained from enzyme-monitored turnover experiments. All reactions were performed in 20 mM potassium phosphate buffer, pH 7.0 at 25 °C. TMA concentrations were (A) 250 μM TMA, (B) 300 μM, (C) 400 μM, (D) 500 μM, (E) 1 mM, and (F) 2 mM. In all panels: upper transient, 443 nm; central transient, 365 nm; lower transient, 617 nm.

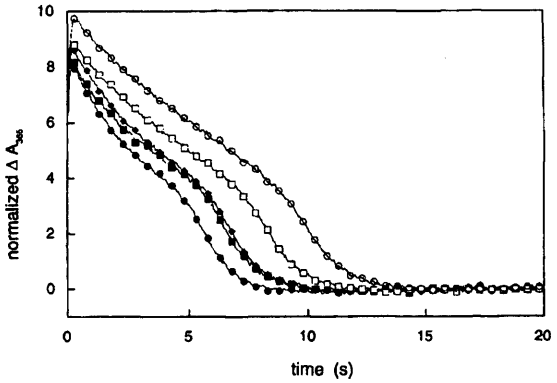

FIGURE 10: Normalized transients seen at 365 nm in the course of turnover. Reaction conditions are the same as in Figure 9. Trimethylamine concentrations were 250 μM (●), 400 μM (■), 500 μM (◆); 1.0 mM (△), and 2.0 mM (○). The increased accumulation of anionic semiquinone at high [TMA] is evident from the larger integrated area under the curves as the concentration of TMA is increased.

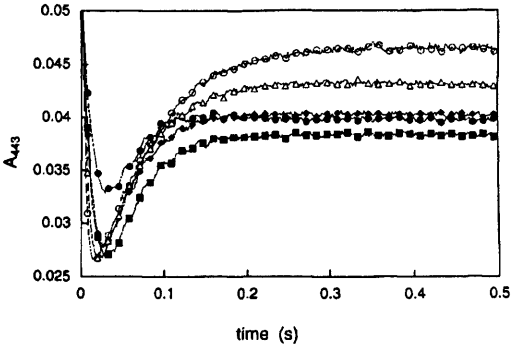

FIGURE 11: Short-time absorbance changes at 443 nm in the course of turnover. Reaction conditions are the same as in Figure 9; trimethylamine concentrations are as in Figure 10. The increased absorbance at 0.5 s in going from 400 μM to 2.0 mM reflects the increasingly oxidized state of the enzyme as the reductive half-reaction slows down in the [TMA] regime where excess substrate inhibition is observed.

the semiquinone oxidation state of the flavin but to alter its value relative to the potential of the iron–sulfur center. At pH 7.0, this potential is +102 mV in the absence of TMAC and +50 mV in its presence. Binding of TMAC (and by inference also TMA) is thus expected to significantly perturb the oxidation–reduction equilibrium between flavin and Fe/S in the one-electron reduced enzyme, shifting the equilibrium

Table 3: Steady-State Kinetic Parameters Determined from Quantitative Analysis of Enzyme-Monitored Turnover Experiments[a]

	turnover number (s^{-1})				
[TMA]	$k_{cat}^{617\ nm_0}$	$k_{cat}^{617\ nm_1}$	$k_{cat}^{617\ nm_2}$	$k_{cat}^{enz_1}$	$k_{cat}^{enz_2}$
250 μM	9.9	5.8	4.0	4.3	4.2
300 μM	7.9	4.9	3.6	4.3	4.0
400 μM	6.3	4.0	3.0	3.5	3.5
500 μM	4.6	3.8	2.5	2.7	2.6
1.0 μM	4.8	3.4	2.5	2.8	2.7
2.0 μM	2.9	2.9	2.0	2.3	2.2

[a] Reactions were performed in 20 mM potassium phosphate buffer, pH 7.0 at 25 °C. TMADH concentration was 4 μM and Fc^+ concentration was 100 μM. $k_{cat}^{617\ nm_0}$, turnover number calculated from the initial velocity of the 617 nm transient in the 0−1 s range; $k_{cat}^{617\ nm_1}$, turnover number calculated for the 617 nm transient in the 1−2 s range; $k_{cat}^{617\ nm_2}$, turnover number calculated for the 617 nm transient from a 1 s interval in the middle of the steady-state period as determined by the 443 nm transient; $k_{cat}^{enz_1}$, enzyme-monitored turnover number calculated from the 443 nm transient in the 1−2 s range; $k_{cat}^{enz_2}$, enzyme-monitored turnover number calculated from the 443 nm transient for a 1 s interval in the middle of the steady-state period.

from a position favoring Fe/S reduction by approximately 10:1 to one favoring essentially quantitative formation of the flavin semiquinone. To the extent that this occurs, the enzyme will not be able to oxidize the bound substrate as the flavin is in the wrong oxidation state. The substrate-bound one-electron reduced intermediate is unique to the 1/3 catalytic cycle, and this effect is thus expected to compromise catalysis by this cycle.

The spectroscopic and potentiometric data for wild-type TMADH provide a framework for rationalizing the observed steady-state behavior of the enzyme. Previous workers have proposed a second substrate binding site in the enzyme whose occupation leads to substrate inhibition by attenuating internal electron transfer from the flavin to the 4Fe-4S center (*20*, *38*). However, the X-ray structure of TMADH in complex with TMAC provides no evidence for a second binding site (*21*, *22*), and studies with ^{14}C TMA reveal that no more than 1 equiv of substrate is bound to the reduced enzyme (*16*). Additionally, and in support of a single TMA-binding site, our recent EPR studies have revealed that only 1 equiv of TMAC is required to generate the spin-interacting state in two-electron reduced TMADH (*19*). An alternative explanation for excess substrate inhibition has been proposed (*23*) in which catalysis occurs via alternate 0/2 and 1/3 catalytic cycles (Scheme 1). Turnover via the 1/3 cycle is expected to predominate at high concentrations and, as discussed above, is expected to be slower because of the unfavorable effect of substrate on flavin reduction potential.

Using Fc^+ as oxidizing substrate, which we have demonstrated to react with TMADH at the Fe/S center (as does ETF), we have examined the reduction levels of the 6-*S*-cysteinyl FMN and 4Fe-4S center in TMADH under steady-state conditions. These studies demonstrate that a one-electron reduced enzyme species containing the anionic semiquinone form of the 6-*S*-cysteinyl FMN and oxidized 4Fe-4S center predominates under steady-state conditions in the presence of high concentrations of substrate, whereas at low substrate concentrations oxidized TMADH is the predominant form. We have also shown that some other substrates for TMADH (e.g., EDMA, DEMA, and TEA) also exhibit excess substrate inhibition. Our stopped-flow studies reveal that the limiting rates for flavin reduction with some of these substrates (e.g., DEMA and particularly TEA) are substantially reduced compared with TMA. Consequently, and as predicted by Scheme 1, the rate of flavin reduction per se does not account for partitioning into the slower 1/3 cycle. Instead, predominance of the 1/3 cycle depends on the ability of substrate to bind to enzyme possessing the flavin semiquinone rather than the oxidized form (as reflected in the perturbation of flavin reduction potential upon binding of substrate). Binding of substrate to enzyme containing the flavin semiquinone perturbs the reduction potential of the oxidized/semiquinone flavin couple (thereby shifting the electron distribution within one-electron reduced enzyme in favor of semiquinone formation). Clearly, over the range of substrate concentrations used in this study, DEMA, EDMA, and TEA are able to bind and perturb the flavin potential of one-electron reduced enzyme. Interestingly, DMButA binds relatively tightly to oxidized TMADH (K_d = 0.36 mM; Table 2) and has the greatest affinity for oxidized TMADH of all the substrates included in this study. However, the lack of marked inhibition seen in the steady state with DMButA suggests this substrate binds less well to reduced forms of the enzyme as compared to TMA. The expectation, therefore, that the anionic flavin semiquinone does not accumulate appreciably during steady-state turnover at all DMButA concentrations studied is consistent with the results of our enzyme-monitored turnover experiments. This situation may be similar to that presumed for the Y169F mutant TMADH, which does not show inhibition with the physiological substrate TMA (*39*). In this latter case, negative charge cannot develop on the side chain of Phe-169 on binding substrate to one-electron reduced enzyme. Thus, the reduction potential of the semiquinone/oxidized flavin couple in the Y169F mutant TMADH should not be perturbed in the manner described for the wild-type enzyme. Work is in progress to determine the reduction potentials of the Y169F mutant TMADH (in the presence and absence of TMAC) to establish further the link between substrate binding, electronic redistribution in the flavin, formation of the spin-interacting state, and enzyme inhibition in the high-substrate regime.

CONCLUSIONS

The steady-state kinetic mechanism of wild-type TMADH comprises two alternating redox cycles and the partitioning between these cycles is dependent on the concentration of reducing substrate and the electron acceptor. This bifurcated kinetic scheme accounts for the observed inhibition of TMADH at high concentrations of substrate without invoking a second, inhibitory substrate binding site. The 1/3 cycle predominating at high [TMA] is catalytically compromised due to the unfavorable position of the equilibrium between the two redox-active centers in the substrate-bound, one-electron reduced enzyme (boxed in Scheme 1). Binding of substrate to one-electron reduced enzyme leads to the accumulation of a flavin semiquinone/oxidized 4Fe-4S intermediate in the so-called 1/3 redox cycle, leading to inhibition in the high substrate regime. Excess substrate inhibition is in fact a necessary consequence of the shift in the reduction potential of the flavin and 4Fe-4S centers in one-electron reduced enzyme upon binding substrate and substrate analogues.

REFERENCES

1. Steenkamp, D. J., and Mallinson, J. (1976) *Biochim. Biophys. Acta 429*, 705−19.
2. Steenkamp, D. J., and Singer, T. P. (1976) *Biochem. Biophys. Res. Commun. 71*, 1289−95.
3. Steenkamp, D. J., McIntire, W., and Kenney, W. C. (1978) *J. Biol. Chem. 253*, 2818−24.
4. Steenkamp, D. J., Kenney, W. C., and Singer, T. P. (1978) *J. Biol. Chem. 253*, 2812−7.
5. Hill, C. L., Steenkamp, D. J., Holm, R. H., and Singer, T. P. (1977) *Proc. Natl. Acad. Sci. U.S.A. 74*, 547−51.
6. Kasprzak, A. A., Papas, E. J., and Steenkamp, D. J. (1983) *Biochem. J. 211*, 535−41.
7. Lim, L. W., Mathews, F. S., and Steenkamp, D. J. (1988) *J. Biol. Chem. 263*, 3075−8.
8. Scrutton, N. S. (1994) *BioEssays 16*, 115−122.
9. Steenkamp, D. J., and Gallup, M. (1978) *J. Biol. Chem. 253*, 4086−9.
10. Duplessis, E. R., Rohlfs, R. J., Hille, R., and Thorpe, C. (1994) *Biochem. Mol. Biol. Int. 32*, 195−199.
11. Byron, C. M., Stankovich, M. T., Husain, M., and Davidson, V. L. (1989) *Biochemistry 28*, 8582−8587.
12. Steenkamp, D. J., Singer, T. P., and Beinert, H. (1978) *Biochem. J. 169*, 361−9.
13. Steenkamp, D. J., Beinert, H., McIntire, W. S., and Singer, T. P. (1978) in *Mechanisms of oxidizing enzymes* (Singer, T. P., and Ondarza, R. N., Eds.) pp 127−141, Elsevier North-Holland Inc, New York.
14. Singer, T. P., Steenkamp, D. J., Kenney, W. I. C., and Beinert, H. (1980) in *Flavins and Flavoproteins* (Yagi, K., and Yamano, T., Eds.) pp 277−287, Japan Scientific Societies Press, Tokyo.
15. Steenkamp, D. J., and Beinert, H. (1982) *Biochem. J. 207*, 241−52.
16. Steenkamp, D. J., and Beinert, H. (1982) *Biochem. J. 207*, 233−9.
17. Rohlfs, R. J., and Hille, R. (1994) *J. Biol. Chem. 269*, 30869−79.
18. Rohlfs, R. J., and Hille, R. (1991) *J. Biol. Chem. 266*, 15244−52.
19. Jang, M.-H., Basran, J., Scrutton, N. S., and Hille, R. (1999) *J. Biol. Chem. 274*, 13147−13154.
20. Falzon, L., and Davidson, V. L. (1996) *Biochemistry 35*, 2445−52.
21. Lim, L. W., Shamala, N., Mathews, F. S., Steenkamp, D. J., Hamlin, R., and Xuong, N. H. (1986) *J. Biol. Chem. 261*, 15140−6.
22. Bellamy, H. D., Lim, L. W., Mathews, F. S., and Dunham, W. R. (1989) *J. Biol. Chem. 264*, 11887−92.
23. Huang, L., Rohlfs, R. J., and Hille, R. (1995) *J. Biol. Chem. 270*, 23958−65.
24. Stankovich, M. T., and Steenkamp, D. J. (1987) in *Flavins and Flavoproteins* (Edmondson, D. E., and McCormick, D. B., Eds.) pp 687−690, Walter de Gruyter, Berlin.
25. Hille, R., and Stewart, R. (1984) *J. Biol. Chem. 259*, 1570−1576.
26. Lehman, T. C., Hale, D. E., Bhala, A., and Thorpe, C. (1990) *Anal. Biochem. 186*, 280−284.
27. Wilson, E. K., Mathews, F. S., Packman, L. C., and Scrutton, N. S. (1995) *Biochemistry 34*, 2584−91.
28. Wilson, E. K., Huang, L., Sutcliffe, M. J., Mathews, F. S., Hille, R., and Scrutton, N. S. (1997) *Biochemistry 36*, 41−8.
29. Scrutton, N. S., Packman, L. C., Mathews, F. S., Rohlfs, R. J., and Hille, R. (1994) *J. Biol. Chem. 269*, 13942−50.
30. Leatherbarrow, R. J. (1992) Grafit v3, Erithacus Software Ltd, Staines, U.K.
31. Segel, I. H. (1975) *Enzyme Kinetics: Behavior and analysis of rapid equilibrium and steady-state enzyme systems*, Wiley-Interscience, New York.
32. Craig, D. H., Moody, P. C. E., Bruce, N. C., and Scrutton, N. S. (1998) *Biochemistry 37*, 7598−607.
33. Strickland, S., Palmer, G., and Massey, V. (1975) *J. Biol. Chem. 250*, 4048−4052.
34. Nagy, J., Kenney, W. C., and Singer, T. P. (1979) *J. Biol. Chem. 254*, 2684−8.
35. Gibson, Q. H., Swoboda, B. E. P., and Massey, V. (1964) *J. Biol. Chem. 239*, 3927−3934.
36. Rohlfs, R. J., Huang, L., and Hille, R. (1995) *J. Biol. Chem. 270*, 22196−207.
37. Pace, C. P., and Stankovich, M. T. (1991) *Arch. Biochem. Biophys. 287*, 97−104.
38. Falzon, L., and Davidson, V. L. (1996) *Biochemistry 35*, 12111−8.
39. Basran, J., Sutcliffe, M. J., Hille, R., and Scrutton, N. S. (1999) *J. Biol. Chem. 274*, 13155−13161.

BI9914098